SP-8
July 1992

Proceedings of the Data Assimilation in Coupled Air-Sea Nowcast/Forecast Systems Workshop

An INO-Sponsored Workshop

Days Inn
Diamondhead, MS

Editor: A. Louise Perkins

February 27 and 28, 1992

The Institute for Naval Oceanography (INO) is operated by the University Corporation for Atmospheric Research (UCAR) under sponsorship of the Naval Research Laboratory (NRL). Any opinions, findings, and conclusions or recommendation expressed in this publication are those of the author(s) and do not necessarily reflect the views of NRL.

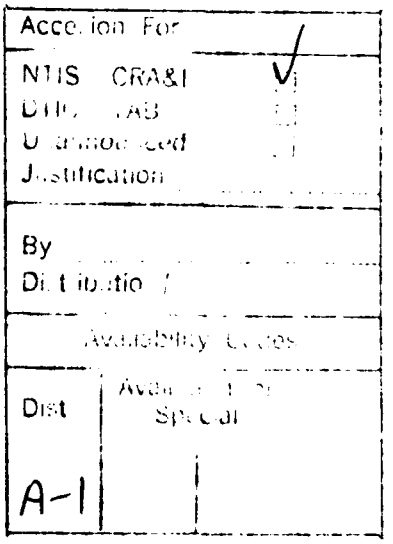

PROCEEDINGS OF THE DATA ASSIMILATION IN COUPLED AIR-SEA NOWCAST/FORECAST SYSTEMS WORKSHOP

An INO-Sponsored
Workshop

Days Inn
Diamondhead, MS

Editor: A. Louise Perkins

February 27 and 28, 1992

ACKNOWLEDGEMENTS

We recognize and thank the two group discussion leaders, George Mellor and Allan Robinson, for their incisive direction. Germana Peggion took notes on the Group I discussions. Bob Willems contributed to the organization of these proceedings. Lydia Harper assisted in the writing of the document. The document was typed by Evelyn Lott and Carolyn Michael.

TABLE OF CONTENTS

INTRODUCTION

The Institute for Naval Oceanography (INO) sponsored Workshop on Data Assimilation in Coupled Air–Sea Nowcast/Forecast Systems was held February 27 and 28, 1992, to promote discussions and develop a strategy for research and development of data assimilation techniques in coupled atmospheric/ocean nowcast/forecast modeling systems for the Mediterranean Sea. The motivation for the workshop, in terms of INO's program, is the changing priority of Navy program sponsors to an emphasis in coastal and semi-enclosed seas research and development efforts. Within this area, the Mediterranean Sea has been specifically identified by the Navy as priority.

The purpose of developing a strategy for air/sea coupling in the Mediterranean is to identify opportunities for collaborative efforts in basic research with regard to data assimilation and for eventual development of coupled nowcast/forecast systems in coastal regions and marginal seas, beginning with the Mediterranean Sea. It is recognized that there has been considerable efforts in gaining a fundamental understanding of the circulation of this region through previous and ongoing observational programs, numerical modeling efforts, and theoretical work, and that there is continuing, strong scientific interest in these topics. There has been progress in applying data assimilation methods to ocean and atmospheric models independent of each other. These uncoupled models can reasonably operate within presently available computing resource environments. Further, some understanding of how to couple air-sea models exists, and there is recognition at this time that an approach could be developed to integrate this knowledge into a design for a coupled air/sea nowcast/forecast system.

OBJECTIVES OF THE WORKSHOP

1. Conduct open forum discussions regarding the fundamental scientific issues in data assimilation in ocean circulation models, in atmospheric models, and in coupled ocean/atmosphere nowcast/forecast systems.

2. Develop a strategy of collaborative research for approaches in addressing data assimilation issues in coupled systems (data types are those "commonly" observed or derived from routine observations).

3. Design a developmental plan to support research efforts such that a research/development coupled nowcast/forecast system for the Mediterranean could reside fully within ECMOP.

4. Produce a manuscript of workshop results/conclusions.

Hence, the participants were charged to propose a strategy for collaborative air–sea interaction research, and to outline a developmental plan for supporting the proposed research. A creative approach to addressing the objectives was motivated through discussions on relevant research issues, that articulated the technical support required, for the design of a coupled nowcast/forecast system in the Mediterranean Sea. To that end, there were presentations on the known existing components that would comprise the coupled system. These were followed by working group and plenary discussions.

WORKING GROUPS

Questions for the working groups to address were posed prior to the workshop. These were not considered to be all inclusive but to serve as a template to aid in meeting the workshop objectives. The questions were:

1. How can one determine the resolution needed to adequately address baroclinic effects with sigma coordinates given Mediterranean topography? How can one determine the maximum bottom slope that can be used in a numerical model and still maintain adequate accuracy for the baroclinic terms at a given resolution and typical Mediterranean buoyancy distribution?

2. What are the physical process scales that must be addressed (i.e., cannot be well represented by present tractable turbulence closure schemes)?

3. What software functionality currently used by this community should be included in future versions of ECMOP?

4. When and where are free-surface effects important in the Mediterranean?

5. What available data and data assimilation schemes are of potential value in a coupled air-sea system? Which of these are applicable for the Mediterranean? How do we validate data assimilation when the model validation uses the same data types for both?

6. Are present mixing and/or instant convective adjustment schemes adequate for addressing Mediterranean water mass transformations? Are there available schemes that are applicable to the two-phase wavy air-sea boundary layer? (NOTE: Observations of weakly stratified "chimneys" in the North

Atlantic suggest that such schemes might not be good for the North Atlantic. Do such phenomena occur as a result of rapid surface cooling through sensible heat exchange or evaporation in the Mediterranean? If so, how important are they? Must we develop new methods to adequately represent them?)

7. Should we use vertical boundary-fitted (sigma) coordinates in order to accurately represent bottom boundary layer effects? (An alternative is to use a separate bottom boundary layer model to determine vertical velocity and momentum, heat, and salinity fluxes from the bottom boundary layer.)

8. What are the important technical issues that need to be addressed to successfully model the interaction between the atmosphere and ocean?

9. Should we apply lateral boundary-fitted coordinates to the Mediterranean? If so, what kind of grid(s) is desirable?

The group discussions, (objective 1 of the workshop), lead to the development of a Strategy for Collaborative Research and a design for the Developmental Plan, fulfilling workshop objectives 2 and 3. This report fulfills objective 4.

CONCLUSIONS AND RECOMMENDATIONS

After the presentations (see Appendix A), two working groups were formed. Each group addressed the questions posed prior to the workshop plus any additions they felt were needed. The original charter was expanded to include fundamental scientific and technical issues to provide a more comprehensive approach. This allowed the groups to also address data–related issues explicitly. Although not all topics were covered as thoroughly as desired, the following conclusions and recommendations were made.

- Subgrid scale process modeling was discussed in detail. "Bulk" methods, such as mixed layers, seem more compatible with layer models, while diffusive-based methods fit more naturally into level models. It was felt that the parameterizations would need to incorporate the findings of non-hydrostatic studies, making them subphysics parameterizations as well. In the Mediterranean, it is most important to let the physical dynamics dictate the parameterizations needed to allow for the episodic nature of the deep convection. That is, there is a need to choose relevant assumptions. Towards this end it was felt that the importance of pre-conditioning

events for the episodic deep convection events be given visibility in the program.

- The physics of the deepening processes, such as those that form the deep water and the Levintine intermediate water, need to be clearly identifiable in the subgrid scale parameterization scheme used. Any such parameterized physics must be consistent throughout all interacting models being used, such as a coupled general circulation model (GCM) and a regional model.

- Twin experiments should be run before beginning the actual data assimilation, or even before beginning to do the data set development and collection, for several reasons: (a) data assimilation schemes need to be thoroughly tested, (b) "value added" determination is needed for various data types, and (c) concerns were voiced regarding the availability of high–quality satellite data. Although the Earth Resources Satellite (ERS–1) is providing data, the errors are still too large, and the data is not widely available. Although existing atmospheric models have water vapor correction algorithms, they are not at sufficient resolution for ocean models. It was suggested that a preliminary study could be made using the Geodetic Earth Orbiting Satellite (GEOSAT) data from 1987–1988, under the known caveat that the available atmospheric model data to complement such a study is not near as good as current model output due to coarser resolution and "bad" wind data.

Other twin experiments can be run.

(1) Previous wind sensitivity studies could be reproduced, accounting for the fact that the ocean needs wind stress rather than the wind field. Research is needed to determine the wave effects, because the stress in a wave model is not the exact same stress for the wind driven ocean circulation. A wave model, such as the WAM, would need to be used to specify the percentage of stress that is successfully transferred into the ocean. WAM is operational in the Mediterranean at coarse resolution.

(2) Tide, expendable bathythermograph (XBT), drifter, and sea–surface temperature (SST) twin experiments need to be run. The relationship between atmospheric and ocean models in terms of consistency, is unknown in both performance and effect. For example, the atmospheric models need sea–surface skin temperature, while ocean models need finite depth sea–surface temperature, and the relationship between the two is not well understood.

(3) There is also a need for three–dimensional (3-D) assimilation, such as can be generated with an objective analysis coupled with a feature model (like the Optimal Thermal Interpolation System [OTIS]), but much more work is needed to develop a product that meets the ocean modeling needs, and no thought has been given to any possible coupled air–sea interaction needs.

- The question of fluxes between the atmospheric and ocean models was also addressed. The different resolution needs of the air and sea probably will not affect the atmospheric models, but probably will affect the coupled ocean model, because it needs higher accuracy. But there are additional existing problems. Flux parameterizations approach zero as the wind speed approaches zero. And in the summer, the Mediterranean can reside in a low wind speed regime for days at a time. During such episodes, the models would be completely uncoupled. Hence, it was suggested that we may need an intermediate step between the two coupled models that first identifies which wind speed regime is active and then switches to an appropriate scheme. It was pointed out that, at the mesoscales, a 1/4°C change in temperature can make the difference between a stable and an unstable atmospheric event; hence, the resolution-feedback interaction may significantly affect the atmospheric forecast.

- A free surface is a necessity because, although the tidal variations overall are of small amplitude, there is a strong tidal effect at Gibraltar (see location of tide guage stations in Figure 1). Further, storm surge winds can play a large dynamic roll in the region. As a side effect it also provides a more elegant way to assimilate altimeter data.

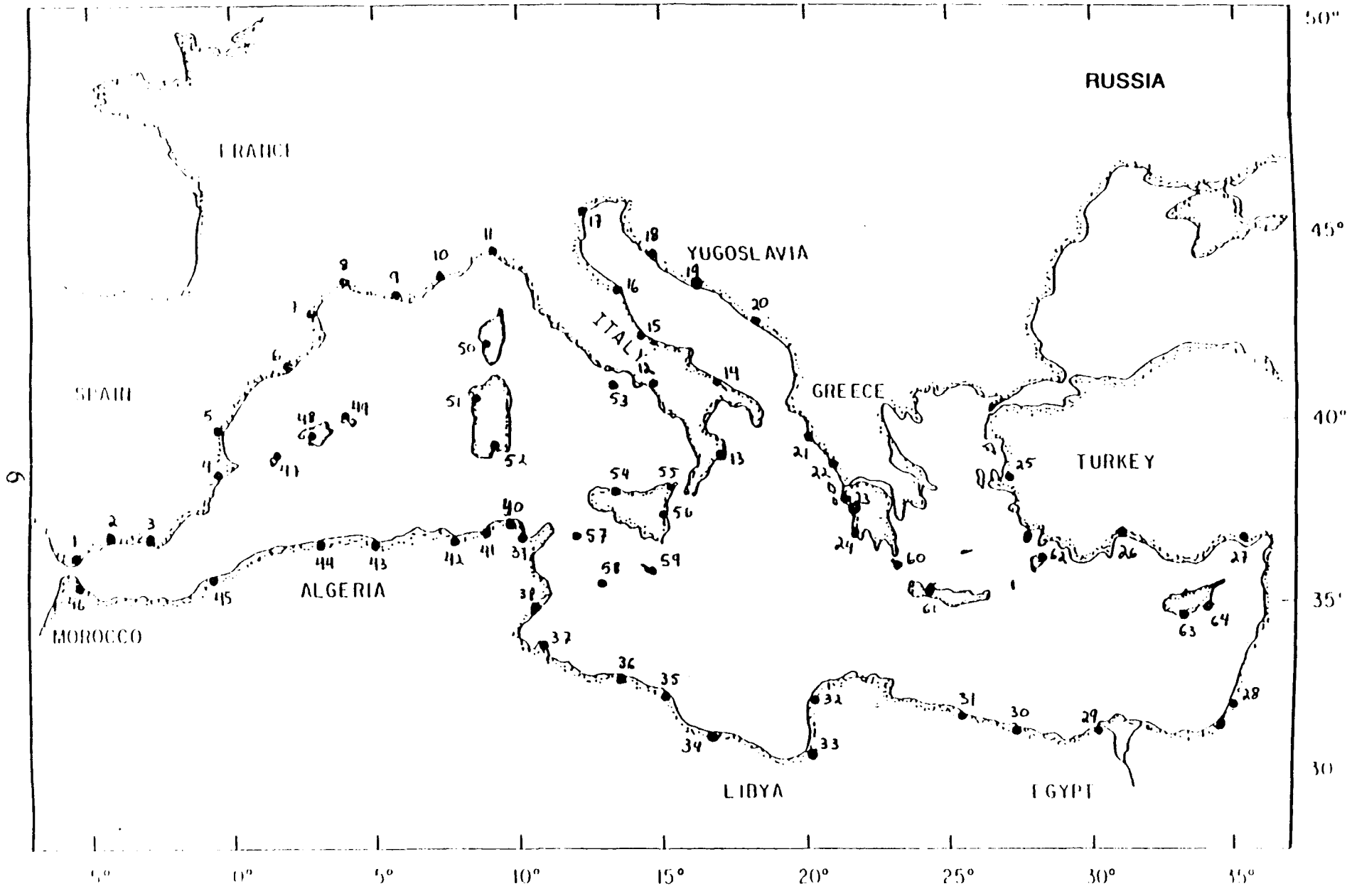

Figure 1. Tidal Effects at Gibraltar

- Fluxes between the atmosphere and ocean seem a more physically compelling medium of exchange than SST, and the choice needs to be investigated indepth. It was recommended that the regional output from the Navy Operational Regional Atmospheric Prediction System (NORAPS), fluxes included, begin to be saved as soon as possible.

- Coupled air-sea models must compute surface fluxes in a "consistent" manner. A caveat was added stating that the coupling studies should start as one-way communication only, reproducing current research in this area.

- Some current atmospheric models average over three hour periods trying to incorporate a diurnal signature, while others try to average out any diurnal variability. Such differences need to be considered when choosing the atmospheric model to use.

- Air-sea interaction consistency would dictate a finite depth SST, but sometimes the atmospheric models may want a true skin temperature.

- A major area of research entails determining the interactive air-sea processes that dictate the feedback coupling mechanisms that occur. Determining the necessity, if any, of additional communication besides SST is a large body of work. The ocean modelers currently believe they need accurate fluxes and wind stress (both magnitude and direction to obtain lines of zero curl) to begin a first order attack. Again, it is unknown if additional information is needed. This is the major fundamental issue around which a strategy for collaboration needs to be constructed.

- An interesting interaction occurs between the atmosphere and the ocean during storms where the ocean sea–surface height (SSH) can vary over a large area, effectively varying z_o.

- Sub-basin to mesoscale interaction is more important in the Mediterranean than in the open ocean, and the data sets must reflect this.

- A resolution study for the Mediterranean was also suggested that would determine a sufficient sampling strategy for the Ekman layer and the other present vertical structures.

- Ocean models will need good correlation functions for the Mediterranean for many reasons, including sparse data and the need for 3-D fields.

- Ocean models need better local wind forcing to resolve coastal upwelling (downwelling). It is unknown what will be a sufficient resolution for the very shallow coastal surf zone forcing.

- Island effects are crucial in the Mediterranean where high mountains can strongly affect the wind field.

- Steep topography in the Mediterranean can be solved by "calibrating" the initial background density field, and should not introduce any new numerical problems.

- A 5 km horizontal resolution combined with 0(30) vertical levels would be desirable, should future computer hardware make this feasible.

- It is recommended that a study be made on the numerical characteristics, including truncation error, associated with different grids including rectilinear, orthogonal curvilinear, and nonorthogonal grids.

- Understand and learn from the existing experience in atmospheric modeling, but at the same time, avoid archaic practices. This recommendation can be taken at many different levels, and INO recommends that one scientist be on the project who has sufficient atmospheric modeling expertise to guide the remaining ocean modelers to the relevant literature. This person does not need to be an INO scientist; they may be a consultant.

- In some regions of the Mediterranean, such as in well defined basins, reduced models have been getting good results (e.g., Harvard quasi–geostrophic model). Although this is a longer term issue, coupling to simplified models for computational efficiency may be considered.

- The need for better planetary boundary layers was considered. It was indicated that there is a need to move from first order closure through one–and–a–half order to second order closure schemes.

- Modeling mixed-layer and convective processes well is a high priority, but this is not a compelling reason to move to "non–hydrostatic" models. Current results in the Mediterranean, with the existing Princeton model turbulence schemes, already reproduce many aspects of convective cells (chimneys); it is unclear whether the evaporation/precipitation process models or the flux parameterization values are responsible for the current discrepancies between models and data. Hence, more measurements are needed.

- Concluding that a Kalman filtering assimilation scheme is inherently limited by its linear nature, it was suggested that both adjoint and optimal interpolation (OI) schemes be pursued concurrently. The OI work would involve an extensive regional effort in the Mediterranean to address the complex, multiscale, inhomogeneous, anisotropic nature of some of the dynamical processes in the region. In the larger group, it was recommended to always let the model define the correlations, but Allan Robinson stressed the need to also consider the data characteristics. While the developed OI scheme would be limited by the research results for the region, it would nonetheless work fairly well for many flow regimes and be relatively efficient. The second adjoint approach would focus on an entirely separate problem: how to simplify the method to make it more efficient and, hence, tractable.

- ECMOP needs more testing and use by the ocean and atmospheric communities before recommendations can be made about choosing it as the Mediterranean platform for future development work. Due to existing limited knowledge, it was not possible to dictate the software facilities needed in ECMOP. On the contrary, it was suggested that ECMOP take on this project as a central application effort instead, which would allow the software support to be put together on an "as needed" basis.

ISSUES NOT ADDRESSED

In workshops many more issues are briefly mentioned than can be addressed by the group at large. These are included here for reference.

- Model Initialization Schemes
  - Very selective set of modes.
- Significance of large scales on mesoscale events.
- Significance of the short atmospheric synoptic time scales that may be responsible for longer time scale ocean phenomena. What coupling is necessary in air-sea interaction to generate El Nino for example.
- Success and failure of bogus feature model data in:
  - Atmospheres.
  - Oceans.
- How better physics parameterizations interact with finer grid resolution.
- Do atmospheric models contain enough correct information to be useful to the ocean and vice versa?
- Are any existing two-way coupling schemes sufficient?
- Is the coupling problem "just computational" or is more theoretical work necessary?
- How much resolution is needed in the different regions of the Mediterranean?
- How important is model climatology in an area where the circulation is strongly dependent on so many interacting rings?
- Significance/impact of higher order advection diffusion differencing.
- Boundary layer characteristics need more theoretical descriptions.
- Need to move away from "it looks good" analysis.
- Topographic vortex stretching and influence on mesoscale events.

- What is dominant time scale of eastern Mediterranean for general circulation?

- What are major features of the POEM data set that we can utilize?

- What is the dominant forcing in each region for each season?

- What is the roll of ambient potential vorticity (PV) in controlling permanent and semi–permanent features?

- Need to develop evaluation tests that exercise different aspects of the coupled systems.

- Grid choices

  - Masking versus boundary–fitted grid.
  - Multiple domain decomposition: coastal ocean not high priority, but sub–basin model coupling may be.

- Navy priority in Mediterranean: Ambient wave noise, surface velocity, and high frequencies.

STRATEGY FOR COLLABORATIVE RESEARCH

The workshop charter called for the development of a strategic plan that outlines the significant research issues that must be addressed. The following list contains the agreed upon needed research.

Develop consistent (air-sea) parameterization of:

- Deepening convective processes, including preconditioning, that adequately models the formation of the Levintine Basin intermediate water and the Ionian deep water.

- Quantify the separate atmospheric/ocean modeling needs for air-sea fluxes including the SST definitions.

- Improve the "matching" of the atmospheric and ocean boundary layers with the air-sea-wave layer physics. Determine which air-sea–wave layer interaction processes dictate the coupling mechanisms that occur between the respective boundary layers. Examine the

utility, for coupling, of the available data "types." Couple the 0(1) SSH "z_o". Determine the resolution needed for the respective coupled models. Improve our modeling capabilities for planetary boundary layers.

- Collaborate with both experimentalists and modelers to collect appropriate air-sea interaction data in the region, including evaporation and precipitation data and better (denser) wind data.

- Develop an OI assimilation scheme for the Mediterranean that addresses the complex covariance structure of region and the complex physics that is multiscale, anisotropic, and inhomogeneous. Then produce and evaluate the model covariance structure and compare with the analytic theory and with data.

- Examine ways to make adjoint methods computationally feasible.

- Determine the effect of multiple scale interactions, in both space and time, on the dynamics of the region and investigate their impact on the numerical approximations. The dominant scales, as well as the important intermittent scales, need to be identified.

DEVELOPMENTAL PLAN

The workshop charter did not stop at a strategic plan, but also called for an outline of a developmental plan. This section outlines the proposed plan.

- Survey existing atmospheric modeling

  - Identify archaic parts.
  - Identify parts that need to be consistent for (air-sea) coupling.
  - Identify work that should be carried over to ocean models.

- Explore anticipated hardware architectures to estimate maximum amount of horizontal and vertical resolution that will be available at the end of the project.

- Compare studies on the Mediterranean Basin.

- Study findings of non-hydrostatic research and, where possible, incorporate into our "subphysics" parameterizations.

- Conduct preliminary studies on basin scales.

- Conduct a resolution study to determine sampling strategies for:

  - Ekman layer.
  - Deep convecting chimneys.
  - Data sets.

- Reproduce previous wind sensitivity studies.

- Conduct twin experiments.

  - Test assimilation schemes, tide, XBT, SST, "OTIS" type objective analysis (OA) data.
  - Determine value added.

- Conduct a preliminary study of assimilation using GEOSAT 1987-1988.

- Study numerical characteristics (truncation error, resolution needs, related analytic problem solved, cell Reynolds instabilities, convergence order, etc.) associated with various gridding strategies, (rectilinear, orthogonal curvilinear, etc.).

  - σ versus z levels.
  - Topographic effects: numerical versus analytical.
  - Island representations and their effects.
  - Boundary fitting effects.

APPENDIX A

Individual Reports

Jim Goerss gave a briefing on the existing Navy Operational Global Atmospheric Prediction System (NOGAPS). He stressed the importance of data quality in sparse data coverage regions. During his talk, discussion about the relative advantages and disadvantages of periodic model reinitialization compared to continuous data assimilation was lively (only one large forecast center uses a continuous assimilation scheme). The atmospheric forecasters present suggested that reinitialization, every six hours for example, allowed better quality control because it rejects fewer good data points, and provides more control of model statistics. His write-up is on pages A-4 to A-6.

Richard Hodur introduced the Navy Operational Regional Atmospheric Prediction System (NORAPS), and the Coupled Ocean/Atmosphere Mesoscale Prediction System (COAMPS). He stressed that the regional boundary conditions (taken from the global model, interpolated in space using bilinear interpolation every twelve hours, and smoothed linearly over five grid points) can seriously impact the regional small-scale noise over monthly time scales. Allan Robinson pointed out that, for assimilation into a local model, finer resolution is a bonus. Subsequent discussion included the observation that the finer scales produced better resolved topography, and these topographic effects exacerbate small-scale noise (the same kind of small–scale noise introduced by the coupled boundary conditions). His write-up is on pages A-7 to A-8.

Pat Phoebus spoke on Westerly Wind Bursts, which are zonal, organized winds that can extend over 20° in length. Her work is in the equatorial Pacific. The hypothesis was that air-sea coupling may work as follows: westerly atmospheric wind bursts may generate Kelvin waves in the underlying ocean leading to upper ocean warming, possibly El Nino. She showed several examples of westerly wind bursts interacting with tropical storms. Paola Rizzoli asked if counter- and contrapositive examples to the stated hypothesis had been searched for, but they had not been. Pat suggested that atmospheric, synoptic–scale wind forcing may be necessary for ocean models to reproduce El Nino. She suggested that wind forcing on these scales can be generated using an atmospheric model to produce denser wind coverage in both space and time than is currently available from data products. Her write-up is on pages A-9 to A-18.

Tom Rosmond introduced an ongoing project, sponsored by Lawrence Livermore National Laboratory, to compare atmospheric models forced with sea surface temperature (SST) data that is updated every model time step. The models use prescribed initial conditions. The aim is to produce homogeneous data sets. He stressed the need to "practice walking before we learn to run." He posed the question "Are atmospheric models good enough" (i.e., do they contain sufficient correct information)? He also reminded us that currently all two-way coupled models still use a flux correction method, which Allan Robinson agreed was "abhorrent." His write-up is on pages A-19 to A-22.

Le Ly spoke about an ocean model coupled to a wave layer model where ocean waves, the ocean, and the atmosphere interact. The model was developed to use an "E-ε" turbulence scheme. Based on a scaled analysis of this parameterized "E-ε" turbulent energy scheme he solves a reduced ε equation analytically. The major issue here is matching the parameterization scheme to the data.

Allan Robinson gave an excellent overview talk on the Physical Oceanography in the Eastern Mediterranean (POEM) project. Their results to date show that the general circulation of the eastern Mediterranean is a multiple–scale problem in both space and time. The basin-scale circulation appears to be a series of interacting mesoscale events of both quasi-permanent and transient rings. They appear to be the "building blocks" of the general circulation.

George Mellor presented runs of the Princeton primitive equation (PE) model in the Mediterranean. He estimated that perhaps 25 to 30 vertical levels will be needed. He stressed that further convective studies to model the episode chimneys are needed.

George Heburn also presented some model runs. He has multiple year simulations of the Mediterranean. He pointed out that strong vertical sheer in too shallow a region, such as occurs in straits, is highly baroclinically unstable.

Paola Rizzoli presented results from her large-scale forcing study. She showed that the impact of the externally forced mesoscale features on the general circulation can be modeled without sufficient resolution to resolve the mesoscale features, provided you have good external forcing in your model. She also discussed an adjoint assimilation method, stressing that it was an assimilation technique that was consistent with both the model and the data.

Ziv Sirkes discussed his ideas for an extension of the steady state Kalran Filter developed by Ichiro Fukumori, Jérôme Benveniste, Carl Wunsch, and Dale B. Haidvogel that would make the Kalman filter more cost effective. These include separating the model time step from the assimilation time step, and using the doubling algorithm to speed up calculations.

Jim Corbin reviewed the status of the Experimental Center for Mesoscale Ocean Prediction (ECMOP), stressing that functional development support is available.

David Dietrich presented results in the Gulf of Mexico and pointed out that some of the terms in the equations contribute dominant errors and should be discretized more carefully. He also suggested the vertical resolution can seriously affect the vorticity evolution. His summary of the Plenary group discussion is on pages A-153 to A-154.

Joe Thompson has provided us with an overview of block structured grids and general curvilinear coordinate systems. He is the Director of the Engineering Research Center at Mississippi State University, and is anxious to assist individual modelers with grid problems. His write-up is on pages A-89 to A-155.

ATMOSPHERIC DATA ASSIMILATION

Jim Goerss
NRL Monterey

The major elements of atmospheric data assimilation systems run by the world's forecast centers are quality control of data, analysis, initialization, and a prediction model. Data quality control is vital to the success of a data assimilation system and is normally performed prior to analysis and within the analysis itself (where observations can be readily compared with other observations as well as with the analysis background or first-guess). The analysis combines information contained in the observational data and in the background fields (a forecast made by the prediction model valid at analysis time) to produce a set of initial fields for the prediction model. The initialization makes adjustments to these fields so that the prediction model can begin its integration with very little noise. In order to have a successful data assimilation system, the analysis must be such that it effectively includes the information contained in the observations to produce fields which are changed very little by the initialization step. Furthermore, the prediction model must be capable of explaining most of the variance of the changes in the atmosphere since the previous analysis so that the current analysis is only required to make relatively small changes. For global data assimilation systems, atmospheric forecast models have reached the state where the error variance in the analysis background fields is comparable to that for the observational data. However, the global assimilation problem is the easiest one for the atmosphere. As the domain of an atmospheric data assimilation system gets smaller, the assimilation problem becomes more difficult. The global domain is relatively rich in observational data, but small mesoscale domains can be data poor. While atmospheric forecast models are quite skillful at predicting the features which dominate the atmosphere on the global scale, a mesoscale domain can be dominated by small-scale features which are not well depicted by today's models (fronts, convective complexes, etc.). Furthermore, as the size of the domain shrinks so does the length of "useful" forecasts by the prediction model. While global models are capable of making skillful forecasts of the atmosphere 7-10 days in the future, the length of skillful forecasts for successful mesoscale models will be measured in hours not days.

Operational Global Data Assimilation

The Navy Operational Global Atmospheric Prediction System (NOGAPS) is the Navy's global data assimilation system. It consists of pre-processing quality

control of observational data (with special emphasis on radiosonde data), a multivariate optimum interpolation (MVOI) analysis, non-linear normal mode initialization, and a spectral forecast model. The MVOI analysis is performed at 16 pressure levels from 1000 mb to 10 mb upon the 1.5 degree resolution Gaussian grid of the forecast model. In order to maximize the use of observational data at each analysis grid point, the globe is divided into over 800 volumes. The volumes have been chosen so that, given normal receipt of observational data, about 300 observations are available for each volume. The global analysis is produced by assembling the individual volume analyses. The MVOI analysis is a statistical analysis scheme in which the weights applied to the observational data are such that analysis error is minimized. The weights are a function of the error properties of the observational data and the analysis background, a 6-hour forecast from the spectral forecast model. In data rich areas (like Northern Hemisphere continental areas) the background errors and observation errors are comparable in size, while in data poor areas (like the Southern Hemisphere) the observation errors are smaller and more weight is put upon the observational data by the analysis. The T79 spectral forecast model (79 waves, triangular truncation) has 18 levels from the surface to approximately 8 mb and parameterizations of all major diabatic processes (radiation, convection, shallow convection, clouds, etc.). At the end of each watch at FNOC the data assimilation cycle is continued by the performance of a re-analysis for the synoptic time (00Z or 12Z), a 6-hour model forecast, an off-time analysis (06Z or 18Z), and a second 6-hour model forecast. Because of the temperature soundings derived from 4 polar orbiting satellites, the global data coverage every 6 hours is good. Unfortunately, the observation errors for these data are double those for conventional soundings (radiosondes). The conventional data are still the best quality data received and are primarily confined to the continental areas of the globe. Therefore, there is a need to supplement the database with synthetic observations in certain areas of the world (the Southern Hemisphere, the tropics, and the North Pacific and Atlantic). Synthetic surface pressure observations have long been produced for the Southern Hemisphere and disseminated by the Australian Bureau of Meterology. These observations are assimilated into NOGAPS along with synthetic "ship" reports which can be generated by the watch at FNOC in the vicinity of extra-tropical cyclones in the North Pacific and Atlantic. The impact of the latter is to improve NOGAPS analysis and short-term forecasts for these cyclones. Because of the forecast skill of the NOGAPS spectral model in the tropics, we have been able to successfully assimilate synthetic tropical wind soundings in the vicinity of tropical cyclones. These soundings are automatically generated using information contained in the warnings issued by the Joint Typhoon Warning Center (JTWC), Guam and by the National Hurricane Center, Miami. With the assimilation of these soundings it

was found that for the 1991 typhoon season NOGAPS produced tropical cyclone track forecasts that were significantly better than those produced by any of the track forecast aids used by JTWC.

MESOSCALE MODELING AT NRL MONTEREY

Richard M. Hodur

I. INTRODUCTION

Many types of mesoscale weather events can adversely affect military operations. These events include flow over and around steep terrain, land and sea breezes and organized convection, such as that found in tropical cyclones and squall lines. Even with the recent, rapid advances in computer hardware, global models are still unable to adequately resolve many of these types of phenomena. This can only be accomplished using mesoscale models with sufficient horizontal and vertical resolutions.

Two models have been developed to examine these forecasting problems. First, the Navy Operational Regional Atmospheric Prediction System (NORAPS) is used operationally to produce 3-dimensional atmospheric simulations over limited-areas with a grid resolution about 3 times higher than the Navy global model (NOGAPS; Navy Operational Global Atmospheric Prediction System). Second, the Coupled Ocean/Atmosphere Mesoscale Prediction System (COAMPS) features a nonhydrostatic atmospheric model and a hydrostatic ocean model. COAMPS is used for 3-dimensional atmospheric and oceanic simulations of mesoscale phenomena such as arctic leads, convective storms, and air-sea fluxes.

II. NORAPS

NORAPS has been used operationally at the Fleet Numerical Oceanography Center since 1982 to provide 12 to 48 hour forecasts for limited areas of the world. NORAPS uses a globally relocatable grid, variable resolutions in the horizontal and vertical and can be used for providing mid-latitude forecasts and tropical forecasts, including the path of tropical cyclones. NORAPS features a 12 h data assimilation cycle, a multivariate optimum interpolation analysis, nonlinear vertical mode initialization, a state-of-the-art mesoscale prediction model and post-processing software. NORAPS is currently used operationally over four areas of the world: Mediterranean, western Pacific, western Atlantic, and the Persian Gulf, with resolutions ranging from 40 to 100 km.

Several forecasts have been made recently that demonstrate the usefulness of the high resolution of NORAPS for mesoscale events. Using 80 km resolution, NORAPS was able to correctly forecast a mistral of approximately 50 knots while NOGAPS, using a resolution of about 150 km forecast maximum wind

speeds of only 20-25 knots. In another case of 55 knot winds near Sicily, a 40 km version of NORAPS forecast maximum winds of 45 knots, an 80 km version of NORAPS forecast maximum winds of 35 knots, and a version of NOGAPS using approximately 125 km resolution forecast maximum winds of about 30 knots. These forecasts indicate that NORAPS can serve as a model which is capable of predicting mesoscale events, particularly in areas such as the Mediterranean, where small-scale forcing from terrain and detailed coastlines are important.

III. COAMPS

COAMPS is being developed as a community R&D model for mesoscale studies. COAMPS features a nonhydrostatic, compressible atmospheric model coupled to a hydrostatic, incompressible ocean model. The atmospheric model uses 1-1/2 order turbulence closure and explicit moist physics, while the ocean model uses first-order turbulence closure and a free surface. COAMPS is appropriate for studying mesoscale phenomena such as convection, tropical cyclones, arctic leads, and coastal and mountain flows with horizontal resolutions ranging from 20 km down to 1 m.

COAMPS has been used to simulate hurricane Gilbert (September 1988) which attained a minimum central pressure of approximately 888 mb with maximum wind speeds of approximately 160 kts. Using only the atmospheric model, with idealized initial conditions, COAMPS forecast the storm to intensify from 1000 mb to 890 mb in 66 hours with peak winds of 163 kts. When the ocean model is used (i.e., the sea surface temperature is allowed to vary in time), the model storm intensifies at a slower rate due to the lower sea surface temperature caused by the upwelling created by the storm circulation. Presently, the coupled experiment has only been run to 48 h, and the forecast intensity is about 10 mb higher than the fixed sea surface temperature case at the same time.

IV. CONCLUSION

NRL-Monterey is aggressively pursuing the development of mesoscale modeling for optimum use by the Navy. NORAPS has been developed and is being continually improved to serve as the central site mesoscale model for 12 to 48 h guidance in coastal areas. COAMPS is being developed as a community research model to study mesoscale phenomena that cannot be resolved by NORAPS for the goals of better understanding these phenomena, as well as for improving physical parameterizations for the larger-scale models.

COUPLED ATMOSPHERE/OCEAN MODELING IN THE TROPICAL PACIFIC

Patricia A. Phoebus
Naval Research Laboratory, Monterey

1. Introduction

Keen (1982) suggested that ocean Kelvin waves moving from west to east in the equatorial Pacific waveguide may be at least partially responsible for the appearance of extremely warm water in the central and eastern Pacific, a phenomena that is commonly referred to as El Niño. These waves may be triggered by short episodes of westerly wind anomalies near the equator in the western part of the basin. These westerly wind anomalies are particularly strong when there is a tropical cyclone couplet present in the western Pacific. Because this area is devoid of radiosonde stations (Fig. 1), previous studies to detect westerly wind events have concentrated on analyzing data from island stations (Harrison and Giese, 1991) and from shipping lane traffic (Morrissey, 1990). For the same reason, attempts to model the ocean's response to this anomalous forcing have relied upon specified wind patches rather than actual observed wind anomalies (McPhaden et al., 1987).

This study proposes that a four-dimensional atmospheric data assimilation system can provide the best estimate of the structure of the atmosphere in data void areas. This statement is particularly valid in areas such as the western equatorial Pacific, where there are ample observations available surrounding the area of interest. A data assimilation system can use these observations to produce three-dimensional wind and mass fields that are consistent with known dynamical and physical properties of the atmosphere. While modeling the tropical atmosphere presents a great challenge, the Navy Operational Global Atmospheric Prediction System (NOGAPS) has performed admirably in the western Pacific since mid-1990 (Goerss et al., 1991). Thus, the NOGAPS low-level wind fields may provide additional information about the temporal and spatial scales of westerly wind events in the equatorial Pacific.

NOGAPS contains four components – data quality control, data analysis, model initialization, and model forecast (see Goerss, this report) – and is run with a 6-hr update cycle. That is, the 6-hr model forecast is used as the first guess for the next analysis, which in turn uses the newest observations to make incremental changes to the first-guess fields. Conventional observations are available from radiosondes, pilot balloons, aircraft, ships, and buoys. Remotely sensed observations include temperature soundings from the polar-orbiting satellites, cloud-tracked wind vectors from the geostationary satellites, and SSM/I wind speed observations from the DMSP polar orbiters (a data source uniquely used by the Navy). NOGAPS also makes use of synthetically generated observations to better depict the strength of oceanic extratropical and tropical cyclones (Phoebus and Goerss, 1992). NOGAPS is provided a real-time sea surface temperature field from an operational ocean data assimilation system that includes a three-dimensional ocean thermal analysis coupled to a mixed-layer forecast model (Clancy et al., 1991) that is forced with NOGAPS wind stresses and surface fluxes.

Since the tropical ocean responds very rapidly to large-scale changes in the surface winds, the Naval Research Laboratory (NRL) is also investigating the impact of modeled westerly wind events on an ocean circulation model (John Kindle, NRL, Mississippi). While the model is not operational at this

time, it is being run in research mode with strictly a one-way coupling. That is, there is no feedback from the ocean circulation model to any other component of the operational ocean/atmosphere data assimilation systems. Most of the experiments are being conducted with a 1.5 layer global model that includes highly parameterized thermodynamics. The model resolution is 0.5° latitude by 0.7° longitude, and it is forced with the 12-hourly NOGAPS surface wind stresses. By studying the ocean model's response to the westerly wind forcing, we hope to distinguish which wind events are significant and what impact ocean Kelvin waves have on sea level changes in the eastern equatorial Pacific.

2. Results

Figure 2 shows a times series of the NOGAPS 10-m zonal wind stress component compared to the zonal wind stress computed from moored buoy observations at 165E, 2N. Westerly wind events are noted by a strong positive peak in wind speed (light wind speeds are indicative of either variable or more meridional wind directions and are not of interest here). Overall, there is very good agreement between the model and the observations, even though data from this buoy was only sporadically available to NOGAPS. The strongest westerlies were observed in mid-to-late November 1990, and were associated with developing storms Page and Owen, both of which became super-typhoons (Fig. 3). But, even though the westerlies are very strong at 2N, there is a much less organized flow along the equator, so the ocean response might be somewhat less than expected.

The peak in December 1990, while weaker at 2N than the previous case, was actually stronger along the equator (Fig. 4). This westerly event was associated with coupled northern (Russ) and southern hemisphere tropical storms (Fig. 5), much like those described by Keen (1982). However, where Keen relied on the relative positions and timing of the storms to define a couplet, by using the model output, we can clearly see that the circulations defining these two storms are dynamically coupled. Another couplet (Kelvin/Sharon) developed in early March 1991. Although strong zonal winds were present along the equator (Fig. 6), there was little evidence of the event at 165E, 2N (Fig. 2). These situations clearly illustrate the potential hazards involved with using isolated ship and island observations to draw conclusions about the strengths and locations of westerly wind events.

Without showing figures for each of these events, I will note that the westerly peak in mid-March 1991 was associated with Typhoon Tim, which developed very near the equator. In early May 1991, another couplet formed (Walt/Lisa) around 155E, concentrating the westerly winds between them. A monsoon depression formed along the monsoon trough in June 1991, while July 1991 had a series of tropical storms in the northern hemisphere (Amy, Brendan, Caitlin). The westerlies in early September 1991 were associated with Typhoon Ivy, and in late September the early signatures of Orchid and Pat were evident near the equator, with westerlies along the southern boundaries of these circulations. The same type of pattern was evident throughout the remainder of 1991, with major westerly wind events appearing in conjunction with tropical storms developing near the equator in one or both hemispheres.

Finally, Figure 7 shows the observed sea level variation at Baltra (90W, 0.5S), one of the Galapagos Islands. Given that it takes around two months for an ocean Kelvin wave to transverse the equa-

torial Pacific, the rise in sea level in February 1991 is likely due to an ocean Kelvin wave generated by the strong westerlies along the equator in December 1990. Similarly, the rises beginning in late April on into May would be expected if the early March (Sharon/Kelvin) westerly event triggered a Kelvin wave, followed shortly thereafter by another wave generated by the westerlies associated with Typhoon Tim in mid-March. Similar results have been seen in the ocean circulation model, which lends further support to this theory.

3. Summary

In almost every case of westerly winds along the equator, there has been a tropical storm developing, which lends further support to Keen's original observation, although not every case involves a couplet. Furthermore, in most cases, the westerlies appear in the very early stages of the storm's development, usually before it reaches tropical storm strength. Thus, there is some question as to whether the westerlies are causing the storm's development, or vice versa. These types of cause/effect questions are at the heart of the El Nino/Southern Oscillation question, and there is still much to be learned about what role is played by each of the pieces. While observed and modeled changes in sea level due to individual ocean Kelvin waves are not large enough to fully explain the El Nino phenomena, it is reasonable that an appropriately timed series of such events could result in larger overall changes in the eastern Pacific. Global data assimilation systems and coupled ocean/atmosphere models may eventually be able to provide some of the answers.

4. References

Clancy, R., J. Harding, K. Pollak, and P. May (1992). Quantification of Improvements in an Operational Global-Scale Ocean Thermal Analysis System. *J. Atmos. Ocean. Tech.*, Vol. 9, pp. 55-66.

Goerss, J., L. Brody, and R. Jeffries (1991). Assimilation of tropical cyclone observations into the Navy Operational Global Atmospheric Prediction System. *Proceedings, Ninth Conference on Numerical Weather Prediction*, Denver, CO, pp. 638-641. American Meteorological Society, Boston, MA.

Harrison, D. and B. Giese (1991). Episodes of surface westerly winds as observed from islands in the western tropical Pacific. *J. Geo. Res.*, Vol. 96, pp. 3221-3237.

Keen, R. (1982). The role of cross-equatorial tropical cyclone pairs in the Southern Oscillation. *Mon. Wea. Rev.*, Vol. 110, pp. 1405-1416.

McPhaden, M., H. Freitag, S. Hayes, and B. Taft (1987). The response of the equatorial Pacific Ocean to a westerly wind burst in May 1986. *J. Geo. Res.*, Vol. 93, pp. 10589-10603.

Morrissey, M. (1990). An evaluation of ship data in the equatorial western Pacific. *J. Clim.*, Vol. 3, pp. 99-112.

Phoebus, P. and J. Goerss (1992). The assimilation of marine surface data in the Navy Global Atmospheric Prediction System. To appear in *J. Marine Tech. Soc.*, June, 1992.

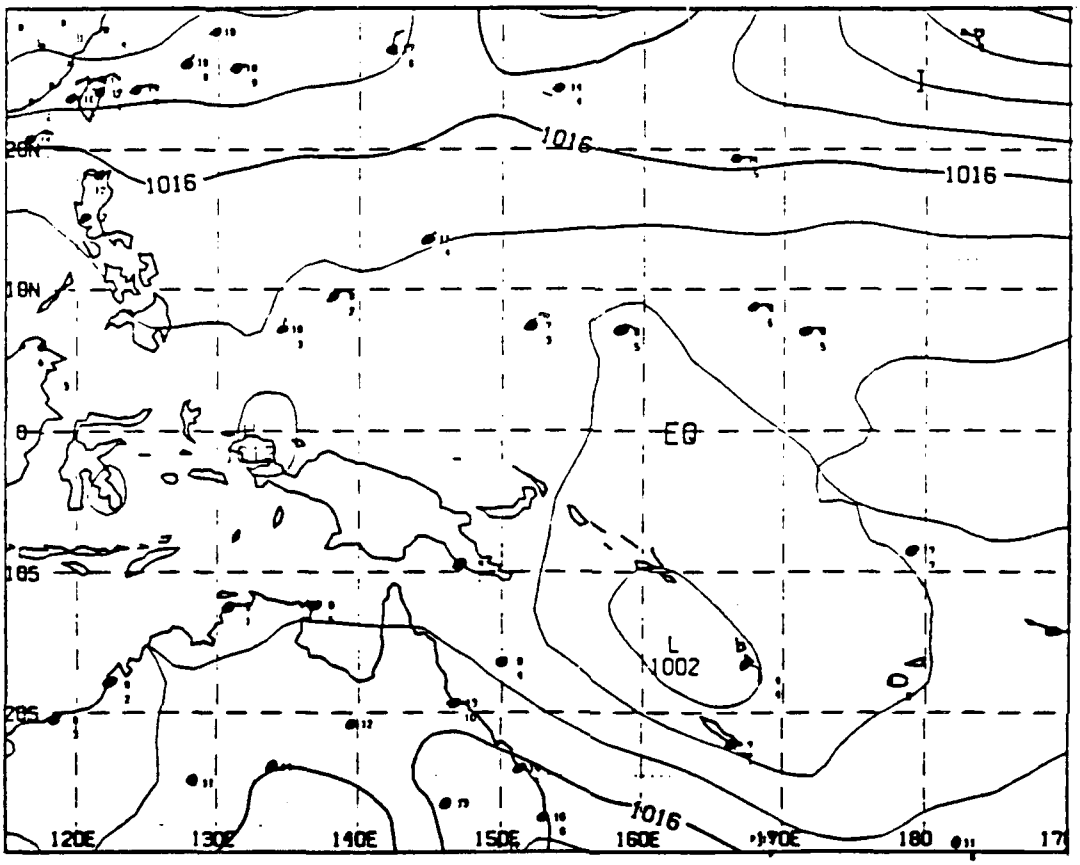

Fig. 1. Locations of radiosonde stations in the western tropical Pacific.

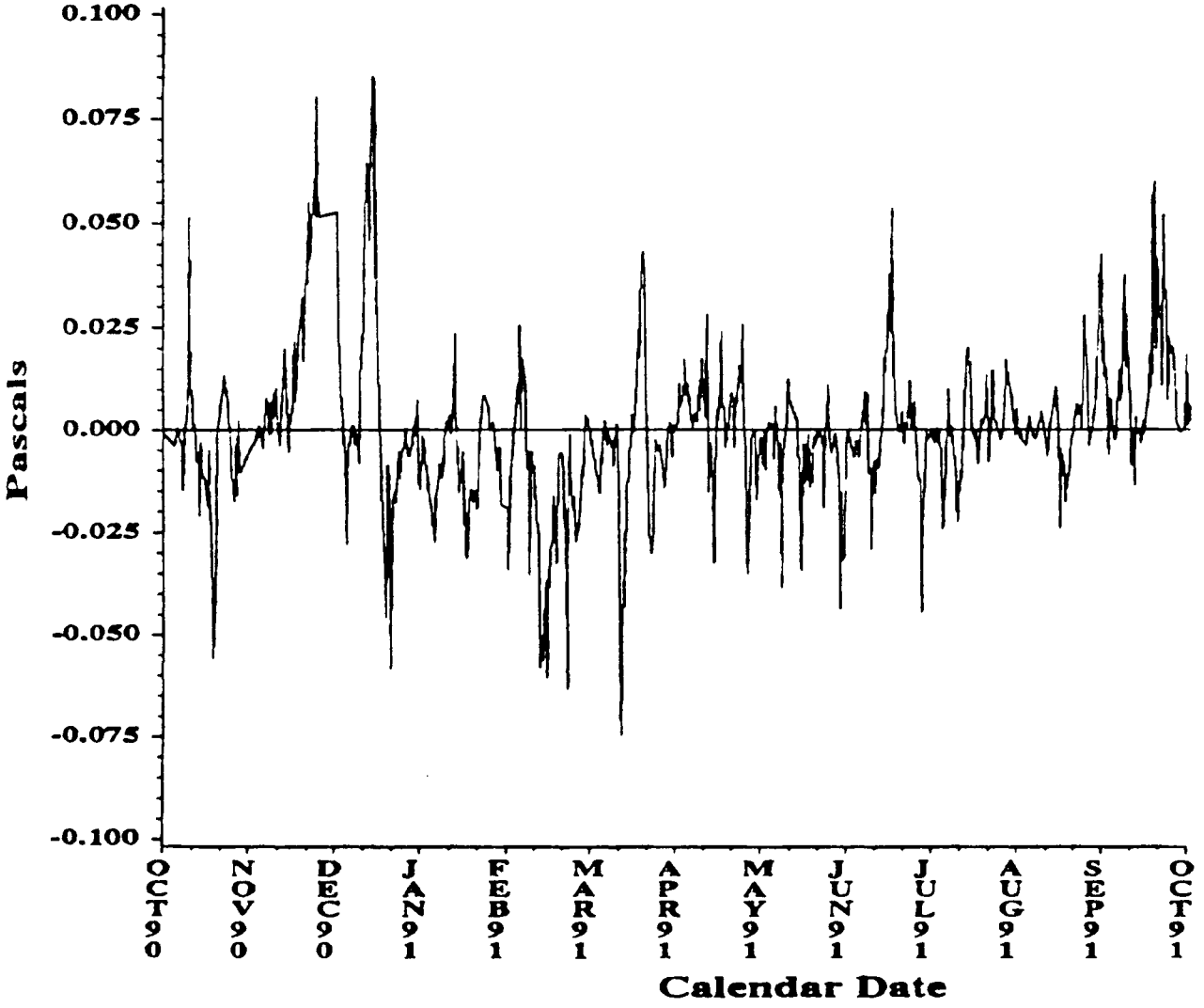

Fig. 2. Time series of NOGAPS 10-m zonal wind stress (solid) compared to buoy observed zonal wind stress (dashed) at 165° E, 2° N. Units are Pascals, and a 5-day filter has been applied to the 12-hourly data.

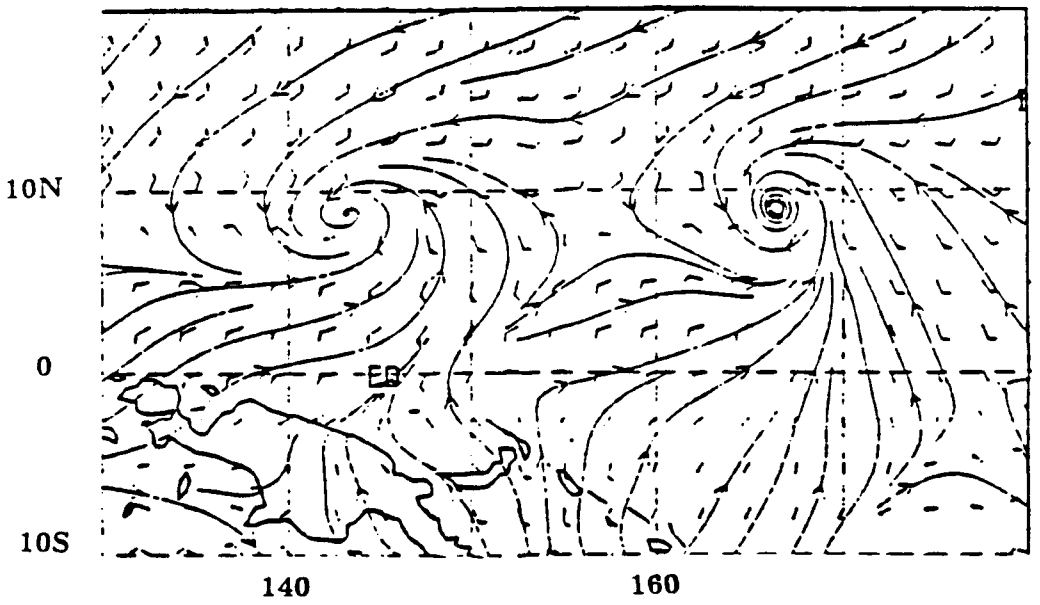

Fig. 3. NOGAPS 1000 mb streamline/wind analysis, 00Z 21 November 1990. The early circulations associated with Supertyphoon Page (142° E) and Supertyphoon Owen (167° E) are clearly developed by the model before any synthetic observations are inserted.

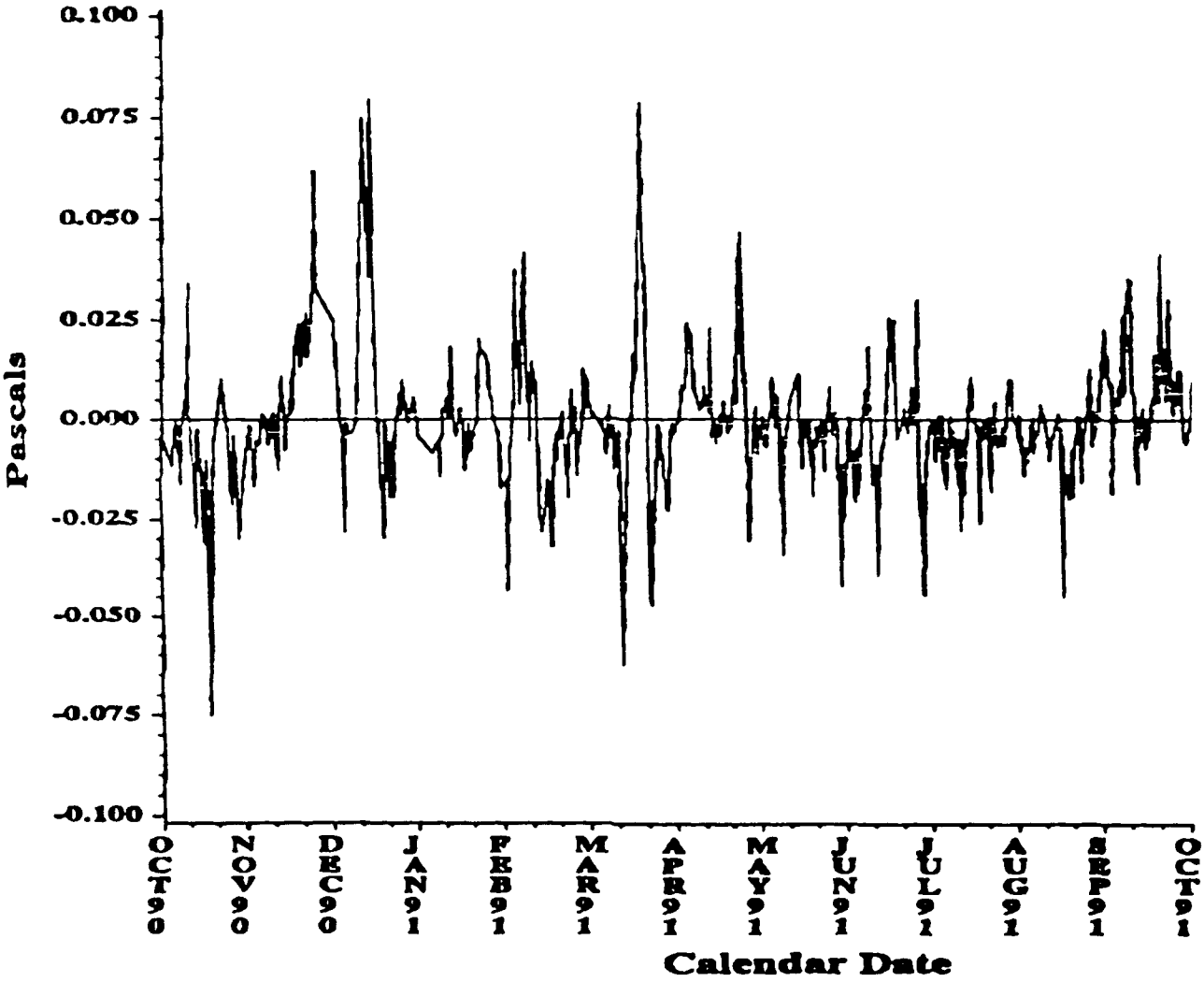

Fig. 4. Time series of NOGAPS 10-m zonal wind stress (solid) compared to buoy observed zonal wind stress (dashed) at 165° E, 0°. Units are Pascals, and a 5-day filter has been applied to the 12-hourly data.

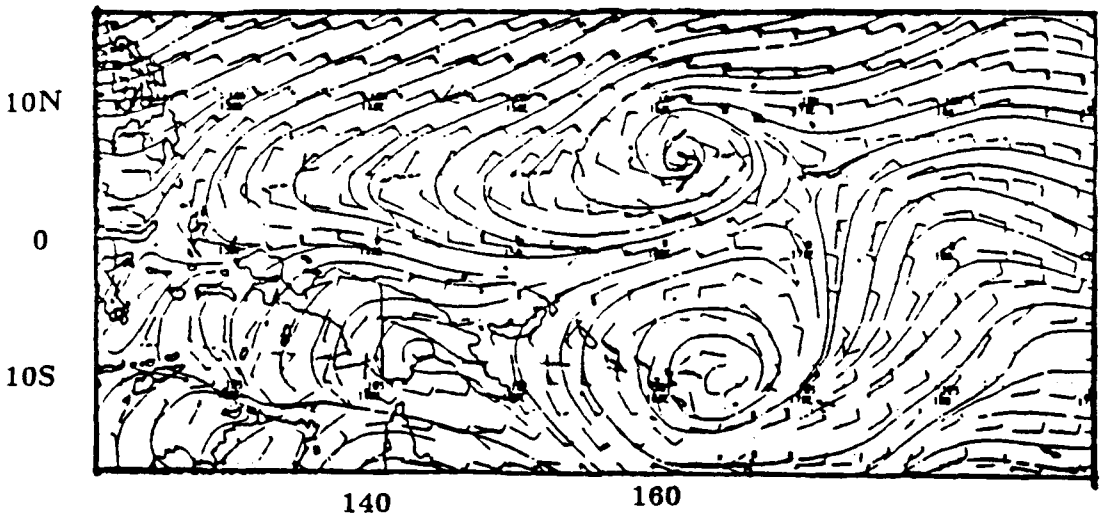

Fig. 5. NOGAPS 925 mb streamline/wind analysis, 00Z, 16 December 1990. Strong westerly winds (25 kt) are concentrated between the two tropical storms.

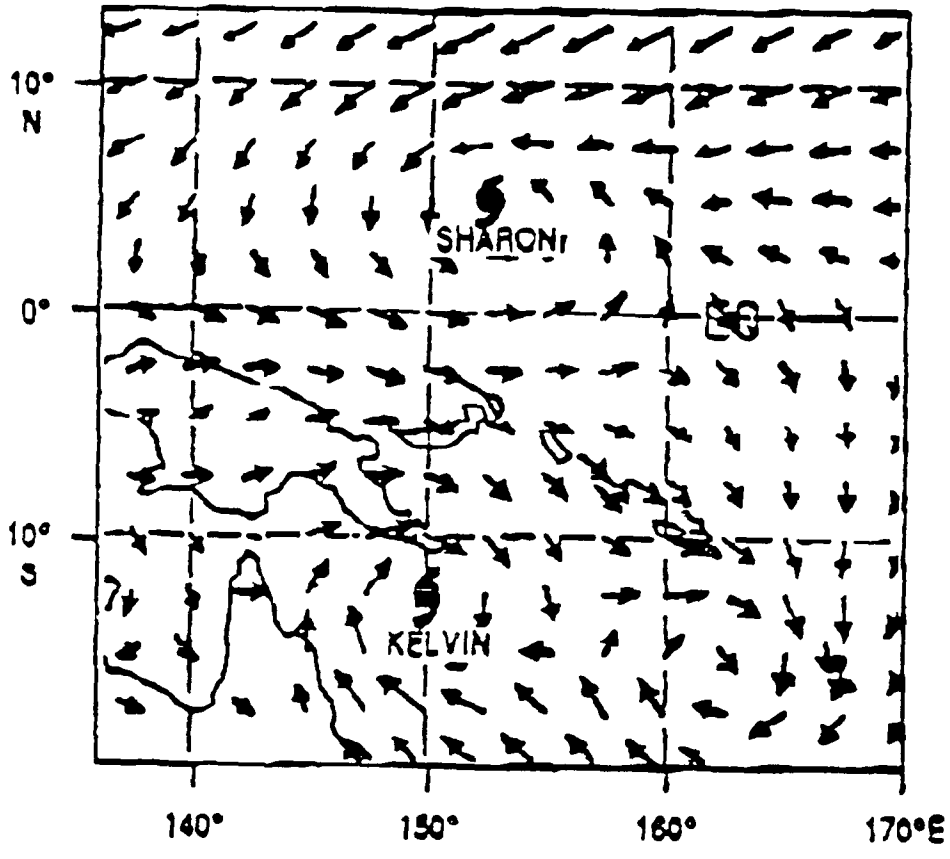

Fig. 6. NOGAPS 1000 mb wind analysis, 00Z 5 March 1991. Winds along the equator between Tropical Storm Kelvin and tropical depression Sharon are almost due westerly at 25 kt.

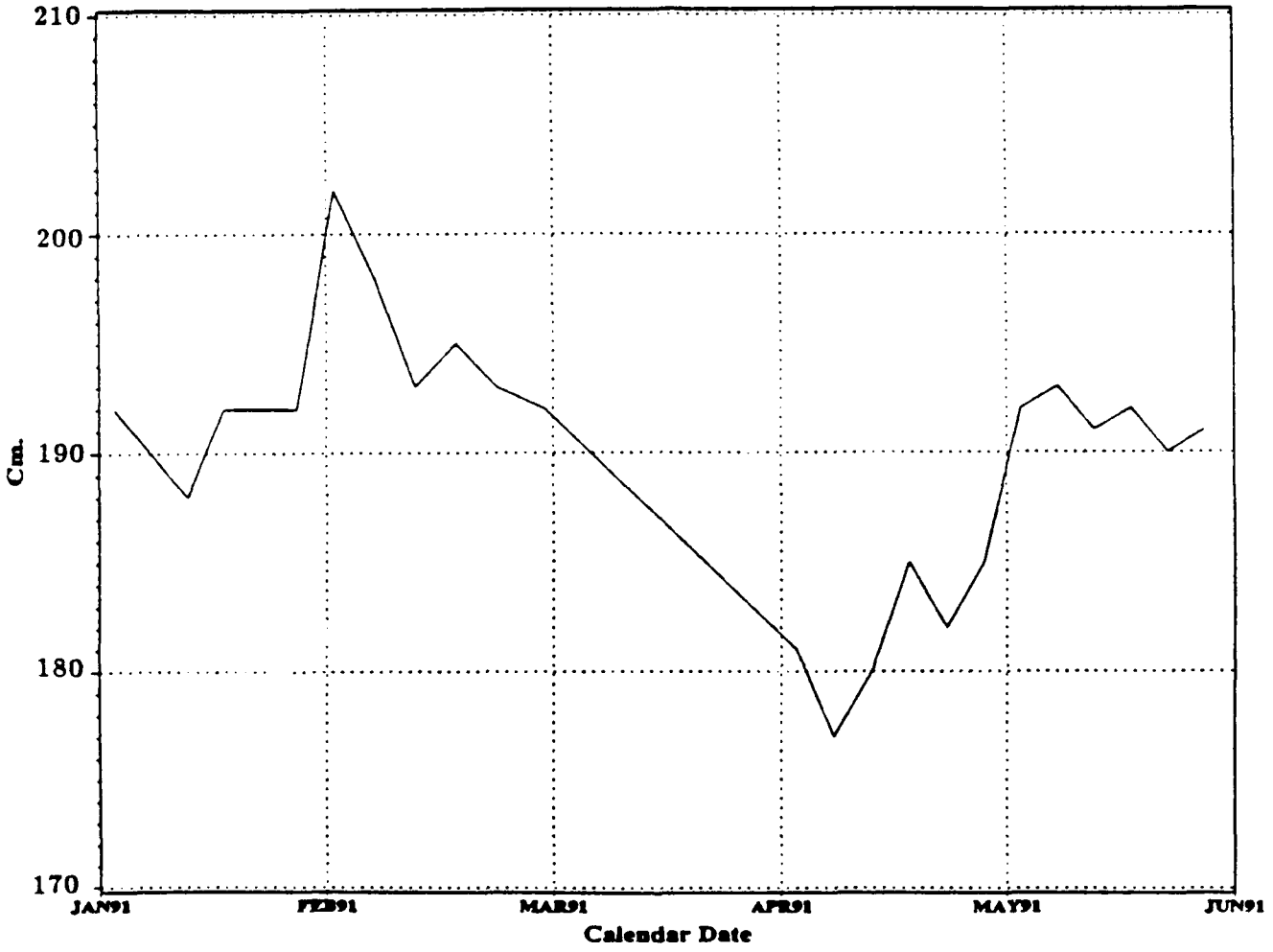

Fig. 7. Observed sea level deviations (cm) at Baltra, Galápagos (90° W, 0.5° S) during the first half of 1991.

NOGAPS DEVELOPEMENT IN SUPPORT OF COUPLED ATMOSPHERE/OCEAN MODELING

Tom Rosmond

NRL-Monterey

1. INTRODUCTION

High priority Navy ocean model research has stimulated the development effort of the Navy Operational Global Atmospheric Prediction System (NOGAPS) in support of this effort. The most significant areas of NOGAPS research are (1) reduction of model systematic error, particularly of the surface fluxes, and (2) development of a fully coupled NOGAPS/TOPS prediction system. The Thermodynamic Ocean Prediction System (TOPS) is the Navy's ocean mixed layer model run operationally by Fleet Numerical Oceanography Center (FNOC).

Systematic or bias error reduction is an ongoing priority for NOGAPS development time because of its importance not only for the coupled model problem, but also because it is a major obstacle to successful medium range forecasts and climate related model research. A useful tool for diagnosing bias is extended integration with prescribed boundary conditions. This report describes a current project of this type, NOGAPS participation in a DOE sponsored Atmosphere Model Intercomparison Program (AMIP).

A fully coupled NOGAPS/TOPS global forecast system has been under development at NRL Monterey for some time. A practical problem with any coupled atmosphere/ocean model is the mismatch of time and space scales between the atmosphere and ocean. The Navy's interests in ocean modeling ultimately require high resolution both in the vertical and horizontal to resolve oceanic eddys and fronts. The computational requirements of this are formidable, even exceeding the capabilties of class VII computers. In this report a coupled NOGAPS/TOPS system with TOPS covering only the Mediterranean and Black Seas is described. This system is a prototype for other more elaborate coupled atmosphere/ocean systems that could satisfy Navy needs without prohibitive computational cost.

2. NOGAPS AMIP PARTICIPATION

Recent national interest in global climate change has stimulated extra effort in the global modeling commmunity to improve the models. The most glaring

deficiency in all global general circulation models (GCM's) is the systematic error or bias, which makes application of these models to the problems of climate change or even extended range forecasting questionable. Nowhere is bias error more critical than in interactive atmosphere/ocean model systems, where the prediction or simulation of realistic sea surface temperature (SST) is central to the entire concept of coupled model research. To date efforts to run fully interactive coupled systems without any constraints on the predicted SST show unacceptable 'climate drift'. Clearly we must improve the GCM's before practical coupled atmosphere/ocean models that satisfy Navy requirements are possible.

The DOE AMIP experiment is an ambitious effort to address these common deficiencies of all GCM's. The Lawrence Livermore National Laboratory (LLNL) has provided a 10 year history (1979-1988) of SST and sea ice boundary conditions to all interested participants. Over 30 global modeling groups from around the world are running their models over this period. The list is a who's who of these modeling groups. NOGAPS is a natural participant because the Navy has much to gain from the knowledge gained not only from NOGAPS results, but also the results from all the other models as well. LLNL will archive the models history files, including special diagnostics used to compare the models systematic errors.

NRL Monterey has completed the first 5 years of the AMIP integration (1979-1983). Note that this period includes the 1982-83 El Nino episode. Preliminary examination of NOGAPS results show dramatically different interannual patterns of surface fluxes, cloud cover, and other important atmospheric parameters over the entire Pacific basin. After completing the full 10 years of the control integration, selective rerunning of interesting periods is planned. Of particular interest will be running the coupled NOGAPS/TOPS to see how well the observed SST patterns can be reproduced with the predictive SST. Careful analysis and comparison of surface energy budgets between the coupled and fixed SST cases will give insight into the reasons for NOGAPS systematic errors. The NOGAPS AMIP data base will be documented and made available to all interested parties. It will provide a unique data set of long term, homogeneous atmospheric fields which have relatively high resolution in both time and space. Ocean modelers in particular should benefit from this data set, both because their own modeling needs are met and also because they can provide valuable feedback to NOGAPS model development.

Anything we can do to improve NOGAPS will benefit the Navy in many important ways. Reduced NOGAPS systematic error will have benefits from better short range tactical weather forecast to better climate

change simulations, all of which are in the Navy's operational and research interests.

3. COUPLED NOGAPS/REGIONAL TOPS

The full global NOGAPS/TOPS is a useful research tool for studying many aspects of atmosphere/ocean interaction. However, the global system has horizontal resolutions limited by the computational costs of running an atmospheric GCM. Typically this resolution is 100 to 200 kilometers both in NOGAPS and TOPS. For modeling the direct response of the ocean mixed layer to atmospheric forcing, this resolution is adequate, but in areas where ocean fronts and eddies are present it is far too coarse. Typical horizontal scales for oceanic fronts and eddies are 10's of kilometers, to TOPS must have horizontal grid spacing fine enough to resolve these features.

The Mediterranean Sea provides an excellent test bed for a regional NOGAPS/TOPS model. Complex small scale circulation patterns dominate the basin, and intense atmospheric forcing is typical in many of the important observed features. The NOGAPS/TOPS model was modified to include only a regional TOPS which covered the Mediterranean and Black Seas. The horizontal grid of the regional TOPS was about 20 kilometers, 1/10 the NOGAPS resolution. Every time step NOGAPS surface fluxes are interpolated to the TOPS fine grid and the fine grid TOPS predicted SST is averaged over the grid area corresponding to the coarse NOGAPS grid. The model has been integrated for 20 days for a January case with no apparent problems. Predicted TOPS SST's show realistic patterns when driven by the NOGAPS surface fluxes. This is in spite of the fact that the initial SST distribution was derived from a coarse mesh climatological SST. There are two serious deficiencies still to be overcome for a successful coupled regional NOGAPS/TOPS, however. First, no thermohaline circulation currents were available to add to the TOPS generated Ekman currents. These will have to eventually come from a 3-dimensional circulation model for the Mediterranean and Black Seas. Second, the thermodynamic fluxes produced by NOGAPS are not sensitive to the high resolution SST from TOPS, since to NOGAPS the details of the TOPS SST are sub-grid scale. A possible solution is as follows: (1) interpolate the NOGAPS fluxes to the TOPS fine mesh. (2) Assume that air/sea temperature difference variations over the TOPS grid are dominated by SST variations, i.e., the NOGAPS predicted surface air temperature is constant over a NOGAPS grid square. (3) Define a linear parametric model for the variation of a reference surface flux as a function of the variation from a reference air/sea temperature difference. In this case the references are the fluxes and temperature difference at the NOGAPS coarse mesh grid point. (4) Use the constraint that the

area integrated surface fluxes over the TOPS fine mesh points must equal the area integrated fluxes for the NOGAPS grid point that corresponds to the TOPS points to determine coefficients and parameters of the surface flux variation model. Other constraints may also be possible and desirable, but the approach will be similar. The benefit of such an adjustment model will be energetically consistent high resolution surface fluxes that will provide realistic high resolution air/sea feedback between the atmosphere and ocean mixed layer.

The principal appeal of the coupled regional NOGAPS/TOPS is the ability to realistically model high vertical and horizontal resolution in the mixed layer without excessive computational cost. The Mediterranean and Black Sea system is especially attractive because of its closed nature, only the Strait of Gibralter requiring inflow/outflow information which is relatively well known. This is in contrast to open ocean regional domains where lateral boundary information is poorly measured and understood. Circulation models of the Mediterranean combined with a regional NOGAPS/TOPS can be an important tool for studying general problems of atmosphere/ocean interaction which will have general application to other coupled model applications.

A Coupled Model for Studying Surface Wave Effects and Its Development Using the E-ε Turbulence Scheme

Le Ngoc Ly
Institute for Naval Oceanography
Stennis Space Center , MS 39529

1 Introduction

The study of air-sea-wave interaction is one of the most important problems of physics of the atmosphere and ocean. This problem is very important not only in the theoretical study of the mechanism of energy transfer in an air-sea-wave system, but also in parameterization of the atmospheric and oceanic boundary-layer processes in ocean circulation and the atmospheric climate modeling. The transport of momentum, heat, humidity and salt always occurs at the air-sea interface and is affected by the ocean surface waves. The character of the transport is regulated by the atmospheric and oceanic turbulent boundary layers (AOBL). The influence of the ocean surface waves on the atmospheric and oceanic surface layers has been well noted by Geernaert et al. (1988), Dubov (1974), Kitaigorodski (1973), Lai and Shemdim (1971), Roll (1965), and others. This process is very complex and still poorly understood.

The difficult problem in modeling air-sea interaction is how to describe the ocean surface wave layer (order of wave height). We don't have sufficient data to specify influences of ocean surface waves on AOBL structure, and don't know yet how to write hydrodynamic equations for this wave layer (WL). The WL effects are expressed through a roughness length, z_0, in traditional physical oceanography. The WL should not be considered as a plane surface. Discontinuity of various physical characteristics are expected across the air-sea interface.

A coupled model is developed to study surface wave effects and variation of the atmospheric stratification on structure of AOBL. This is a part of developing an air-sea-wave interaction model. Both E-ℓ (ℓ is length scale, E is turbulence kinetic energy) and E-ε turbulence schemes are used in this coupled model.

2 The Model

The model consists of a set of equations for: (1) momentum, (2) turbulent kinetic energy (TKE), (3) length scale (E-ℓ turbulence scheme), (4) energy-dissipation (ε), (5) turbulent exchange coefficient (TEC) expressed in terms of TKE, ℓ (E-ℓ turbulence scheme), and ε (E-ε turbulence scheme), and (6) stratifications in the atmosphere and ocean. These equations are written in the same form for both the atmospheric and oceanic boundary layers (Ly, 1986, 1990, 1991). Vertical profiles of air temperature and seawater density are approximated with functions to represent observations. Stratification in the atmosphere is parameterized by the nondimensional surface heat flux. The model includes equations for WL describing the transport of mean energy and TKE fluxes across the air-sea interface. The equation for turbulent kinetic energy flux can be written (Ly, 1990)

$$(K_a\rho_a\frac{dE_a}{dz_a})\mid_{z_{0a}} + (K_s\rho_s\frac{dE_s}{dz_s})\mid_{z_{0s}} = C_1\rho_a u_{*ax}^3 \tag{1}$$

The equation for the mean energy fluxes are written (Ly, 1992):

$$(K_a\rho_a\frac{du_a}{dz_a}u_a)\mid_{z_{0a}} + (K_s\rho_s\frac{du_s}{dz_s}u_s)\mid_{z_{0s}} = C_1\rho_a u_{*ax}^3 \tag{2}$$

$$(K_a\rho_a\frac{dv_a}{dz_a}v_a)\mid_{z_{0a}} + (K_s\rho_s\frac{dv_s}{dz_s}v_s)\mid_{z_{0s}} = C_2\rho_1 u_{*ay}^3 \tag{3}$$

where C_1 and a companion C_2 are nondimensional parameters representing the surface wind wave effect. Subscript a refers to air and s to seawater. The roughness lengths at the upper and lower boundaries of the wave layer are z_{0a} and z_{0s}, the air and seawater densities are ρ_a and ρ_s, and the velocity components of both fluids are u and v.

3 An E-ε Turbulence Scheme And Ocean Breaking Wave Effects

The theory of length scale has had great success in modeling geophysical flows over flat terrain. It is not always obvious how to apply a length scale to flows over complex terrain (ocean surface waves) and in the middle and upper (lower) parts of AOBL. The E–ε closure method makes use of an ε– equation instead of a length scale equation. A few applications of the E-ε method have been made for the atmospheric boundary layer (Lee and Kao, 1979; Detering and Etling, 1985; Stubley and Rooney, 1986), the ocean boundary layer (Marchuck et al., 1977; Svensson, 1979), and both AOBL (Ly, 1991). The advantage of the E-ε method is that it is a new tool for studying turbulence structure, especially since ε can be measured directly in the ocean (Monin and Ozmidov, 1985). It is easier to include the breaking wave effect into a model. The disadvantage of this method is that the ε-equation introduces a new set of constants. The E–ε turbulence scheme includes TKE, ε, and Kolmogorov equations.

The TKE for the atmosphere and ocean is determined from the budget equation

$$\frac{\partial E_i}{\partial t} = \alpha_{1i} K_i [(\frac{du_i}{dz_i})^2 + (\frac{dv_i}{dz_i})^2 - \frac{\alpha_{3i}}{\alpha_{1i}} \frac{g}{S_{0i}} \frac{dS_i}{dz_i}] + \alpha_{4i} \frac{d}{dz_i} K_i \frac{dE_i}{dz_i} - \alpha_{2i} \frac{E_i^2}{K_i} \qquad (4)$$

where subscript $i = a$ for the atmosphere and $i = s$ for the ocean; S_{0a} and S_a are the mean and local values of potential temperature, θ_a or of seawater density; S_{0s} and S_s are the mean and local values of density, ρ_s.

Energy-dissipation, ε_i, for both the atmosphere and ocean is determined from the following equation.

$$\frac{\partial \varepsilon_i}{\partial t} = \beta_{1i} K_i \frac{\varepsilon_i}{E_i} [(\frac{du_i}{dz_i})^2 + (\frac{dv_i}{dz_i})^2 - \frac{\beta_{3i}}{\beta_{1i}} \frac{g}{S_{0i}} \frac{dS_i}{dz_i}] + \beta_{4i} \frac{d}{dz_i} K_i \frac{d\varepsilon_i}{dz_i} - \beta_{2i} \frac{\varepsilon_i^2}{E_i} \qquad (5)$$

The Kolmogorov equation in which the TEC is expressed in terms of the TKE and energy-dissipation is

$$K_i = \alpha_{ki} E_i^2 / \varepsilon_i \qquad (6)$$

where $\alpha_{ki} = 0.046$ determined from experimental data in the surface layer for both the atmospheric and oceanic equations. The constants α_i, β_i and others constants, and more details on equations (4)-(6) can be found in Ly (1991).

3.1 Boundary Conditions

3.1.1 At the air-sea interface

The surface boundary conditions for the turbulent kinetic energy can be written in the traditional form for the atmospheric boundary layer over land (Monin and Yaglom, 1971) and for the air-sea boundary layer problem (Ly, 1986), as follows

$$E_i(z_i) \mid_{z_{0i}} = \alpha_{2i}^{-1/2} u_{*i}^2 \tag{7}$$

where u_{*i} is the friction velocity of the air and water; and z_{0i} is the roughness length for both air ($i = a$) and water ($i = s$).

By ignoring the buoyancy terms, Ly (1991) solved the ε–equation (5) analytically at the air-sea interface and obtained boundary conditions for ε at surface in the form:

$$\varepsilon_a(z_a) \mid_{z_{0a}} = \frac{u_{*a}^3}{k z_{0a}} [q_{1a} + (1 - q_{1a}) \exp(-q_{2a})] \tag{8}$$

for the atmosphere ($i = a$) where

$$q_{1a} = \frac{\beta_{1a}}{\beta_{2a}} \; ; \; q_{2a} = (\frac{\alpha_{2a}^{1/2} \beta_{2a}}{k^2 \beta_{4a}})^{1/2} \tag{9}$$

and

$$\varepsilon_s(z_s) \mid_{z_{0s}} = \frac{u_{*s}^3}{k z_{0s}} [q_{1s} + (1 - q_{1s}) \exp(-q_{2s})] \tag{10}$$

for the ocean ($i = s$) where

$$q_{1s} = \frac{\beta_{1s}}{\beta_{2s}} \; ; \; q_{2s} = \left(\frac{\alpha_{2s}^{1/2}\beta_{2s}}{k^2\beta_{4s}}\right)^{1/2} \tag{11}$$

3.1.2 Ocean Breaking Wave Effect

Ocean wave breaking is another important source of turbulent energy dissipation besides the dissipation of shear production. The ocean turbulent energy dissipation of shear production at the air-sea interface is shown in (10) and (11). In the case where the breaking wave effect is taken into account, the turbulent energy dissipation ε at the ocean surface has the form:

$$\varepsilon_s(z_s)\,|_{z_{0s}} = \frac{u_{*s}^3}{kz_{0s}}\left[q_{1s} + (1 - q_{1s})\exp\left(-q_{2s}\right)\right] + \varepsilon_{0w} \tag{12}$$

where q_{1s} and q_{2s} are the same as in (11), and ε_{0w} is the turbulent energy dissipation of the wave breaking at the air-sea interface. Following Benilov (1973), and Monin and Ozmidov (1986), the energy dissipation ε_{0w} can be expressed in term of ocean surface wave elements:

$$\varepsilon_{0w} = \gamma\,\frac{v_{ph}}{\lambda}\left(\frac{h}{\lambda}\right)^3 \tag{13}$$

where v_{ph}, h, and λ are the wave phase velocity, height, and length, respectively, and γ is a dimensionless constant. It is noted that in the case of no surface waves, equation (12) reduces to equation (10) and we have a situation described by Ly (1991). This is the first attempt ever to model breaking wave effect.

3.1.3 Away from the interface

Away from the air-sea interface the turbulent kinetic energy and dissipation (ε) tend toward zero. The procedure and algorithm for solving the E-ε problem are similar to the one for the E-ℓ model (see Ly, 1989).

4 Simulation and Comparison

The basic coupled model has been developed to study: (1) the baroclinic effects in the atmosphere and ocean on boundary layer structures, (2) the surface wave effects on the upper turbulent layer in the ocean, (3) E-ε turbulence scheme in a coupled model, and (4) the effects of the angle between wind stress and wind velocity vectors on the aerodynamic drag coefficient. Several numerical experiments were carried out to study the ocean surface effect and E–ε turbulence scheme in a coupled model. The numerical results are compared with available data. The results of previous studies (Ly, 1986, 1990, 1991) are summarized here. An example of the model output on the neutral drag coefficient, C_D, in comparison with published drag coefficients is shown in Fig. 1. Curve 10 is the model C_D for $C_1 = 4$ and $C_2 = 0$ (with ocean wave effect). The study shows that the model which takes the wave effect into account gives better C_D in comparison with observed data. Model results are in good agreement with the few available observations of TKE budget, friction velocity, drag coefficient, roughness length and the accepted understanding of the influence of the WL.

The geostrophic drag coefficient (C_{Dg}) and wind speed at 10-m height (U_{10}) determined by the E-ε method agree very well with observations. The E-ε method gives even better neutral C_D than the ℓ-method in comparison with observations for all wind speeds greater than 5 $m\ s^{-1}$. The u_* obtained by the E-ε method agrees very well with observations for winds less than 15 $m\ s^{-1}$. Roughness length z_0 also agrees well with observations and the mixing-length method results.

5 Summary

WL strongly influences turbulent and air-sea interaction characteristics. WL is an additional source of TKE for the lower/upper parts of AOBL. As expected, the atmospheric and oceanic

turbulence properties, more than the air-sea interaction characteristics, are sensitive to the turbulence scheme used. The E-ε turbulence scheme with appropriate constants can give good results in modeling coupled air-sea boundary-layer flows. It must be noted that the effect of surface waves on energy transfer at the air-sea interface is extremely complex and requires additional study. The next effort is the modeling of the ocean breaking wave effect by using E–ε turbulence scheme in a coupled model.

6 References

Amorocho, J., and DeVries, J. J.: 1981. Reply. *J. Geophys. Rev.*, **86**, 4308.

Benilov, A. Yu.: 1973. Generation of ocean turbulence by surface wave. *Atm. Ocean. Phys.*, **9**, 160–164.

Detering, H. W. and Etling, D.: 1985. Application of the E-ε turbulence model to the atmospheric boundary layer. *Boundary-Layer Meteorol.*, **33**, 113–133.

Donelan, M. A.: 1982. The dependence of aerodynamic drag coefficient on wave parameters. In *Proceeding of the First International Conference on Meteorology and Coast Zone*. Boston, MA, Amer. Meteorol. Soc., 381–387.

Dubov, A. S.: 1974: *Process of transfer near the air-sea interface.* Leningrad. Hydromet. Publ. House, 239 pp. (in Russian).

Garratt, J. R.: 1977. Review of drag coefficients over oceans and continents. *Mon. Wea. Rev.*, **105**, 915–929.

Geernaert, G. L., Davidson K. L., Larsen S. E., and Mikkelsen T., 1988: Wind stress measurements during the Tower Ocean Wave and Radar Dependence Experiment. *J.*

Geophys. Res., **93**, 13913–13923.

Geernaert, G. L., Katsaros K., and Richter, K.: 1986. Variation of the drag coefficient and its dependence on sea state. *J. Geophys. Res.*, **91**, 7667–7679.

Hellerman, S. and Rosenstein M.: 1983. Normal monthly wind stress over the world ocean with error estimates. *J. Phys. Oceanogr.*, **17**, 1093–1104.

Hsu, S. A.: 1986. A mechanism for the increase of wind stress (drag) coefficient with wind speed over water surfaces: A parametric mode. *J. Phys. Oceanogr.*, **16**, 144–150.

Kitaigorodski, S. A.: 1973. *The Physics of air–sea Interaction.*, Israel Prog. Scient. Transl., Jerusalem, 236pp.

Kondo, J.: 1985. Air-sea bulk transfer coefficients in diabatic conditions. *Boundary-Layer Meteorol.*, **9**, 91–112.

Lai, R. J. and Shemdim O. H., 1971: Laboratory investigation of air turbulence above simple water waves. *J. Geophys. Res.*, **30**, 7334–7350.

Large, W. G. and Pond, S.: 1981. Open ocean momentum flux measurements in moderate to strong winds. *J. Phys. Oceanogr.*, **11**, 324–336.

Lee, N. H. and Kao, S. U.: 1979. Finite-element numerical modeling of atmospheric turbulent boundary layer. *J. Appl. Meteorol.*, **18**, 1287–1295.

Ly, N. L.: 1992. The effect of the angle between wind stress and wind velocity vectors on the aerodynamic drag coefficient at the air-sea interface. *J. Phys. Oceanogr.*, (In press).

Ly, N. L.: 1991. An application of the E-ε turbulence model for studying coupled air-sea boundary layer structure. *Boundary-Layer Meteor.*, **54**, 327–346.

Ly, N. L.: 1990. Numerical studies of the surface wave effects on the upper turbulent layer in the ocean. *Tellus*, **42A**, 557–567.

Ly, N. L.: 1986. Modeling the interaction between atmospheric and oceanic boundary layers, including a surface wave layer. *J. Phys. Oceanogr.*, **16**, 1430–1443.

Ly, N. L. Kindle, J. C., Thompson, J. D., and Youtsey, J. W.: 1992. Wind stress analysis over the Western Equatorial Pacific and North Atlantic Ocean based on ECMWF operational wind products 1985–1989. *INO Technical Report*, (to be submitted).

Marchuck, G. I., Kochergin, V. P., Klimok, V. I., and Sukhorukov, V. A. : 1977. On the dynamics of the ocean surface mixed layer. *J. Phys. Oceanogr.*, **7**, 865–875.

Monin, A. S. and Ozmidov, R. V.: 1985. *Turbulence in the Ocean.* Reidel Pub. Comp., 247 pp.

Monin, A. S. and Yaglom, A. M.: 1971. *Statistical Fluid Mechanics: Mechanisms of Turbulence*, MIT Press, Cambridge, 769pp.

Roll, H. U.: 1965. *Physics of the Marine Atmosphere.* New York/London, Academic Press, 426 pp.

Smith, S. D.: 1980. Wind stress and heat flux over the ocean in gale force winds. *J. Phys. Oceanogr.*, **10**, 709–726.

Stubley, G. D. and Rooney, D. R.: 1986. The sensitivity of k-ε model computations of the neutral planetary boundary layer to baroclinicity. *Boundary-Layer Meteorol.*, **37**, 53–70.

Svensson, U.: 1979. The structure of the turbulent Ekman layer. *Tellus*, **31**, 340–350.

Wu, J.: 1982. Wind-stress coefficients over sea surface from breeze to hurricane. *J. Geophys. Res.*, **87**, 9704–9706.

7 Figure Captions

Fig. 1 The published neutral drag coefficient, C_D, as a function of wind speed at 10-m height, U_{10} (after Ly et al., 1992). Curve 10 shows C_D from the model taking surface waves into account with $C_1 = 4$ and $C_2 = 0$.

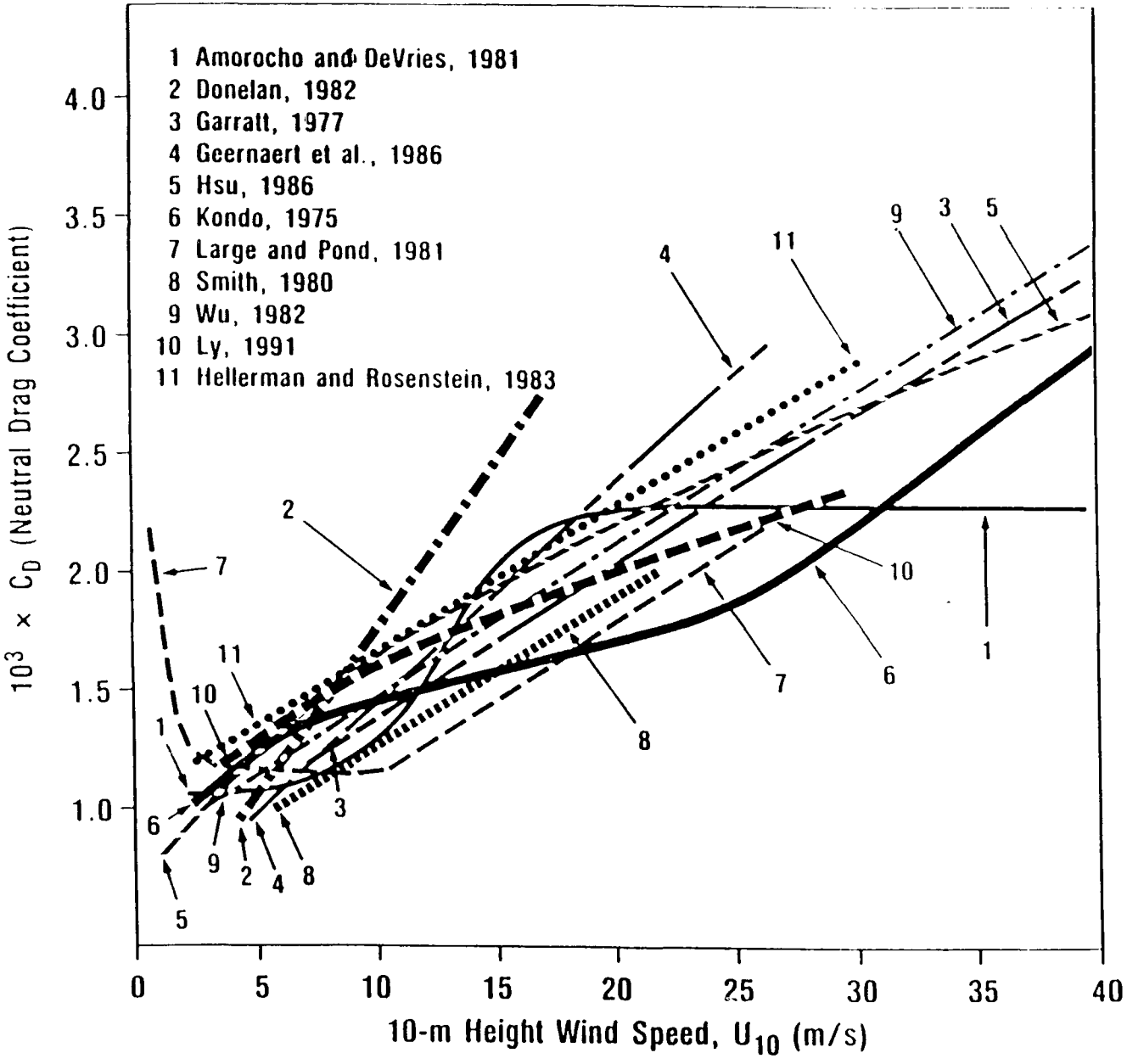

Fig. 1 The published neutral drag coefficient, C_D, as a function of wind speed at 10-m height, U_{10} (after Ly et al., 1992). Curve 10 shows C_D from the model taking surface waves into account with $C_1 = 4$ and $C_2 = 0$.

PROGRESS IN THE UNDERSTANDING OF THE EASTERN MEDITERRANEAN SEA

Allan R. Robinson and Maryam Golnaraghi

Harvard University, Division of Applied Sciences and Dept. of Earth and Planetary Sciences
Cambridge, MA 02138 USA

Recent concentrated research in the Eastern Mediterranean involving both observational and modeling efforts has led to substantial new information and understanding of the general circulation and its variabilities. A new conceptual picture is emerging. As part of phase I of the international research program for Physical Oceanography of the Eastern Mediterranean (POEM) (Malanotte-Rizzoli and Robinson, 1988), a comprehensive pooled hydrographic data base was collected during 1985-1987 by scientists from several institutions and nations. Multi spatial and temporal scales are associated with the general circulation and its variabilites (POEM group, 1991). Three dominant and interactive spatial scales have been identified: full basin scale, sub-basin scale and mesoscale. It has been confirmed that a single slow deep vertical thermohaline cell circulates throughout the Ionian and Levantine basins (Roether, *et al.*, 1991). (Quasi)-permanent sub-basin scales gyres are interconnected by jets and currents to form the basin scale horizontal general circulation of the main thermocline (Robinson, *et al.*, 1991). An energetic mesoscale eddy field exists and interacts with the sub-basin scale features with variability occurring on many time scales (Robinson, *et al.*, 1987). In this paper we will briefly overview novel experimental results on the three dominant scales and introduce the data assimilative local and basinwide dynamical studies underway at Harvard for the Eastern Mediterranean.

Figure 1 shows the data coverage of the POEM coordinated dataset in summer of 1987, which is comprised of coordinated CTD surveys with nominal 1/2 ° latitudinal and longitudinal spacing, each carried out within a few weeks. In conjunction with this quasisynoptic general circulation survey, two basinwide surveys related to both the large, long time deep thermohaline circulation and to the synoptic/mesoscale variability were carried out. A deep transient tracer experiment was carried out by the F/S Meteor. Consistent with the small Rossby deformation radius of about 12 km, 620 XBTs were taken every 10 km along the ship track to provide a uniformly sampled mesoscale dataset throughout the basin.

The basinwide thermohaline circulation involves deep water formation in the Adriatic, which then spills through the Straits of Otranto. An E-W section(section A-B in figure 1) of F-12 concentration is displayed in figure 2. Deep water convective renewal rate has been estimated to be $0.29 \pm .09$ m^3/sec, approximately 15 to 25 % of the exchange through the straits of Sicily. The single coherent convective cell which connects the two basins has a turn over time of 126 years below 1200 meters (Roether, *et al.*, 1991).

The general circulation is shown on figures 3a and 3b, respectively, by the dynamic height anomaly of the upper thermocline layer (30m relative to 450m) and the associated relative geostrophic flow pattern (Robinson, *et al.*, 1991). In general the flow is quite complex and variable. Figure 3a shows a jet of Atlantic water entering through the Straits of Sicily, meandering through the interior of the Ionian sea, which we believe feeds the Mid-Mediterranean Jet, flowing through the central Levantine. The Mid-Mediterranean Jet bifurcates, one branch flows towards Cyprus and then northward to feed the Asia Minor Current, and a second branch separates, flows eastward and then southward. Important sub-basin features are: the Rhodes cyclonic gyre; the Mersa Matruh anticyclonic gyre; and the southeastern Levantine system of anticyclonic eddies, among which is the recurrent Shikmona eddy south of Cyprus. Flow in the upper thermocline is of the order 10-20

cm/sec as shown in figure 3b. A synthesis of the features and their variabilities is shown in figure 4. In summary, the general circulation consists of sub-basin scale gyres and eddies interconnected by jets and filaments. Important variabilities include: 1) shape, position and strength of permanent sub-basin gyres and their unstable lobes, multi centers, mesoscale meanders and swirls, 2) meander pattern, bifurcation structure and strength of permanent jets, 3) occurrence of transient eddies and aperiodic eddies, jets and filaments.

It was found by Robinson et.al. (1987) that a mesoscale existed in the Levantine basin consisting of energetic eddies, jets and filaments. This result was confirmed by the 1987 mesoscale experiment and extended throughout both the Levantine and Ionian basins. Figure 5 is a sample mesoscale vertical temperature section (section CBDE in figure 1). This figure reveals both mesoscale structure in sub-basin scale features and an energetic eddy field dynamically interacting with the general circulation. Mesoscale eddies occur with diameters on the order of 40-80 km and notable features include energetic sub-basin/mesoscale interaction in the Levantine basin and a remarkable thermostad in the Ionian.

In a dedicated modeling effort at Harvard University, the POEM coordinated datasets are assimilated into dynamical models. The Harvard modeling hierarchy consists of an eddy resolving Quasi-Geostrophic dynamic model(Robinson and Walstad, 1987) with attached surface boundary layer (Walstad and Robinson, 1991), and coastal (Milliff, 1990; Milliff and Robinson, 1991) and island (Ozsoy, Lozano and Robinson, 1991) constraints and a primitive equation dynamics option (Spall and Robinson, 1989).

Assimilation of the hydrographic data into the dynamical models is carried out in order to perform dynamical adjustment, dynamical interpolation of fields into data gaps, and to achieve physical process and realistic simulations. Detailed parameter and sensitivity studies are carried out and thorough energy and vorticity balances of dynamically

filtered data reveal dynamical processes which are occurring. Basinwide and (embedded) subregional assimilations and simulations are carried out. Figure 6 shows the complex topography of the Eastern Mediterranean and the domains of two examples, to be discussed here, namely the Mersa Matruh gyre region and the full Levantine basin.

Studies have been carried out in the region of the Mersa Matruh anticyclonic gyre in order to determine the barotropic mode, to fill in a datagap, and to study the local dynamics. Figures 7a and 7b show the streamfunction field at 40 meters and the corresponding error field using the data available in the region from the October/November 1985 (ON85) . Figure 7c is the simulated field of stream function at 40 meters after 14 days. Extended parameter and sensitivity studies indicate deep barotropic flow of 2-3 cm/sec, and successful dynamical interpolation and robustness of data.

A series of simulations have been performed to investigate robustness of features in the data, to determine the distribution of the barotropic mode amplitude and stability and variability of the fields in the Levantine basin. Figures 8a and 8b are simulated fields of streamfunction at 30 meters after 14 days of dynamical interpolation for the October/November 1985 and the March/April 1986 datsets, respectively. Quasi-permanent features, namely the Rhodes Gyre, Mersa Matruh gyre and the southeastern Levantine system of anticyclonic eddies are notable in both figures 8 and 9. However, variabilities in the quasi-permanent gyres and jets do occur. Our studies to date have yielded dynamically adjusted absolute flow and indicated robustness and stability of the sub-basin scale features. This provides the basis for internal dynamical process studies and the investigation for their competition with directly forced responses.

In summary, circulation and variability of the Eastern Mediterranean is now known to be comprised of three dominant interactive scales. A single deep convective cell connects the Levantine and Ionian basins, with an estimated turnover time of 126 years below 1200

meters. The thermocline horizontal general circulation is comprised of sub-basin scale features, gyres and interconnecting jets with variabilities, and fluctuations consisting of recurrent and transient structures. Mesoscale eddies, meanders and oscillations exist and interact with the sub-basin scale, more energetically in the Levantine than the Ionian basin. Assimilation of POEM hydrographic data into Harvard models and a series of numerical simulations indicate robust and stable sub-basin scale features and provide the basis for dynamical process studies including local dynamical processes and sub-basin/mesoscale interactions. Internal dynamical processes, cross-scale interactions, multiple and variable forcing functions, topographic, coastal and air-sea interactions are among the factors to be investigated in terms of these assimilated fields. Such assimilated data will also provide the best estimates of transport fields for chemical, biological and management studies and applications.

Acknowledgements

It is a pleasure to acknowledge many fruitful scientific interactions with POEM colleagues. We are especially grateful to Mr. Wayne G. Leslie for his contribution to the collection and analysis of the XBT data. This research was supported by grants to Harvard University from the National Science Foundation (OCE-9012821) and the Office of Naval Research (N00014-90-J-1593).

Bibliography

1. Malanotte-Rizzoli, P. and A.R. Robinson (1988). POEM: Physical Oceanography of the Eastern Mediterranean, EOS *The Oceanography Report* 69 (14), 194-203.

2. Milliff, R.F. (1990). A Modified Capacitance Matrix Method to Implement Coastal Boundaries in the Harvard Open Ocean Model, *Mathematics and Computers in Simulations* **31** 541-564.

3. Milliff, R.F. and A.R. Robinson (1991). Structure and Dynamics of the Rodes Gyre System and its Dynamical Interpolation for Estimates of the Mesoscale Variability, *Journal of Physical Oceanography*, in press.

4. Ozsoy, E., Lozano, C.J. and Robinson, A.R.(1991). A Baroclinic Quasigeostrophic Model for Closed Basins or Semi-Enclosed Seas with Islands, in preparation.

5. Robinson, A.R., M. Golnaraghi, W.G. Leslie, A. Artegiani, A. Hecht, E. Lazzoni, A. Michelato, E. Sansone, A. Theocharis and U. Unluata (1991). Structure and Variability of the Eastern Mediterranean General Circulation, *Dynamics of Atmospheres and Oceans* **15** (3-5), 215-240.

6. Robinson, A.R., A. Hecht, N. Pinardi, J. Bishop, W.G. Leslie, Y. Rosentroub, A.J. Mariano and S. Brenner (1987). Small Synoptic/Mesoscale Eddies: The Energetic Variability of the Eastern Levantine Basin, *Nature* **327** (6118), 131-134.

7. Robinson, A.R., P. Malanotte-Rizzoli and the POEM group (1991). General Circulation of the Eastern Mediterranean, submitted Manuscript.

8. Robinson, A.R. and Walstad L.J. (1987). The Harvard Open Ocean Model: Calibration and Application to Dynamical Process, Forcasting, and Data Assimilation Studies, *Applied Numerical Mathematics* **3** (1-2), 89-131.

9. Roether, W. and R. Schlitzer (1991). Eastern Mediterranean Deep Water Renewal on the Basis of Chlorofluoromethane and Tritium Data, *Dynamics of Atmospheres and Oceans* **15** (3-5), 333-354.

10. Spall, M.A. and A.R. Robinson (1989). A New Open Ocean, Hybrid Coordinate Primitive Equation Model, *Mathematics and Computers in Simulations* **31** 241-269.

11. Walstad, L.J. and A.R. Robinson (1991). A Coupled Surface Boundary Layer Quasigeostrophic Model for Mesoscale Mixed Layer Dynamics, submitted Manuscript.

Figure Captions

Fig. 1 Station locations, August-September 1987(AS 87). The line of the deep stations obtained from the F/S Meteor starting at **A** and running to **B** at almost constant latitude. **CBDE** is the shortest path along the connected Meteor track through the annotated points.

Fig. 2 A Freon-12 vertical cross section, in the Ionian Sea.

Fig. 3 a) Dynamic height anomaly (dm), upper thermocline (30/450) with coastal constraint, AS 87. b) Horizontal flow vectors at 30 m, AS 87.

Fig. 4 Schematic general circulation. Dashed features are recurrent or transient, upper thermocline.

Fig. 5 A vertical temperature cross section from the mesoscale XBT experiment.

Fig. 6 The bottom topography of the Eastern Mediterranean Sea (contour interval is 500 meters), two subregions of interest, namely the Mersa Matruh gyre region and the Levantine basin are shown.

Fig. 7 a) Initial field of Stream Function at 40 meters using data from October-November 1985 (ON 85). b) Associated error field. c) Simulated stream function at 40 meters after 14 days.

Fig. 8 Simulated field of stream function at 30 meters after 14 days, a) for ON 85, b) for March-April 1986.

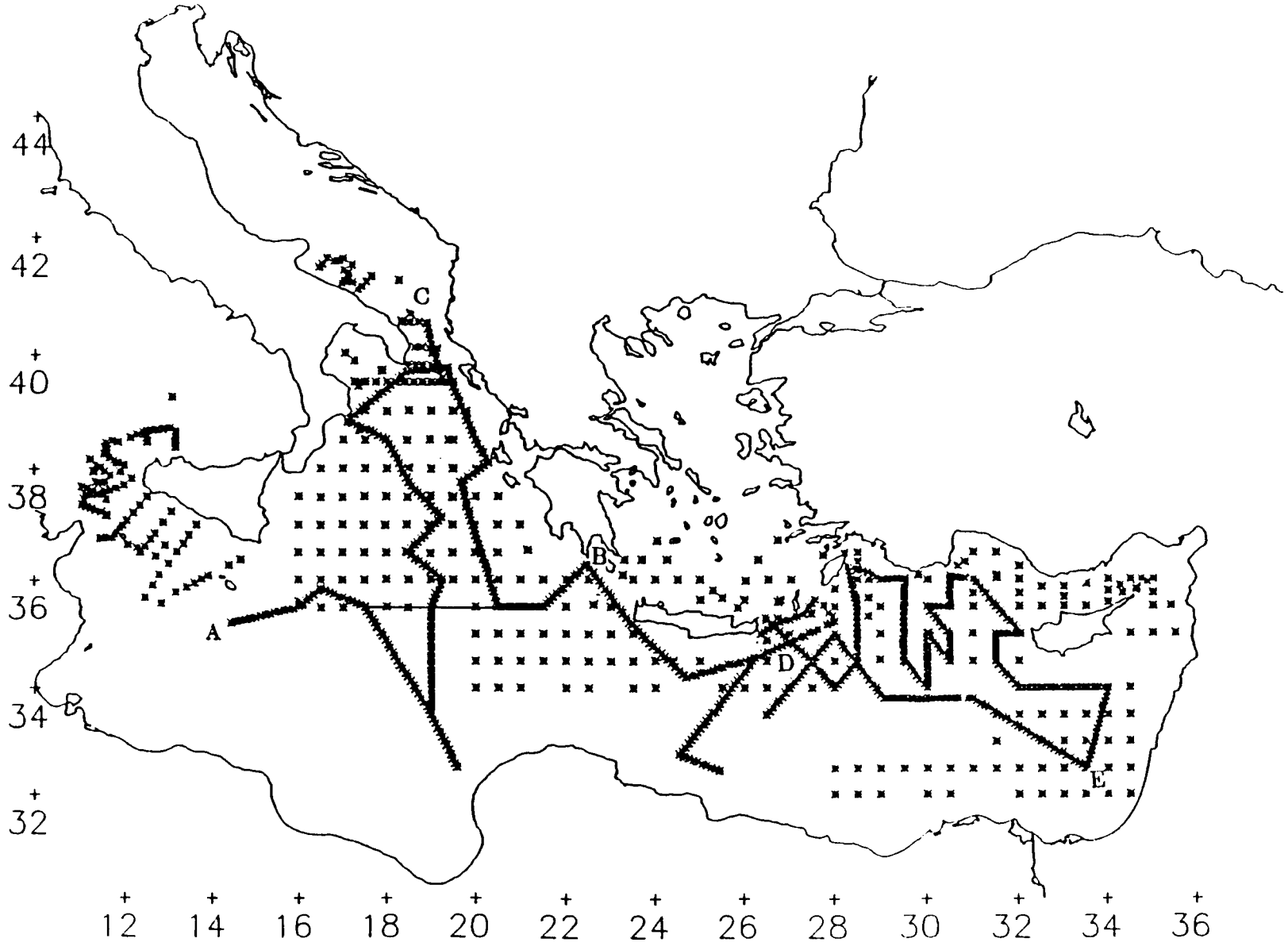

Figure 1

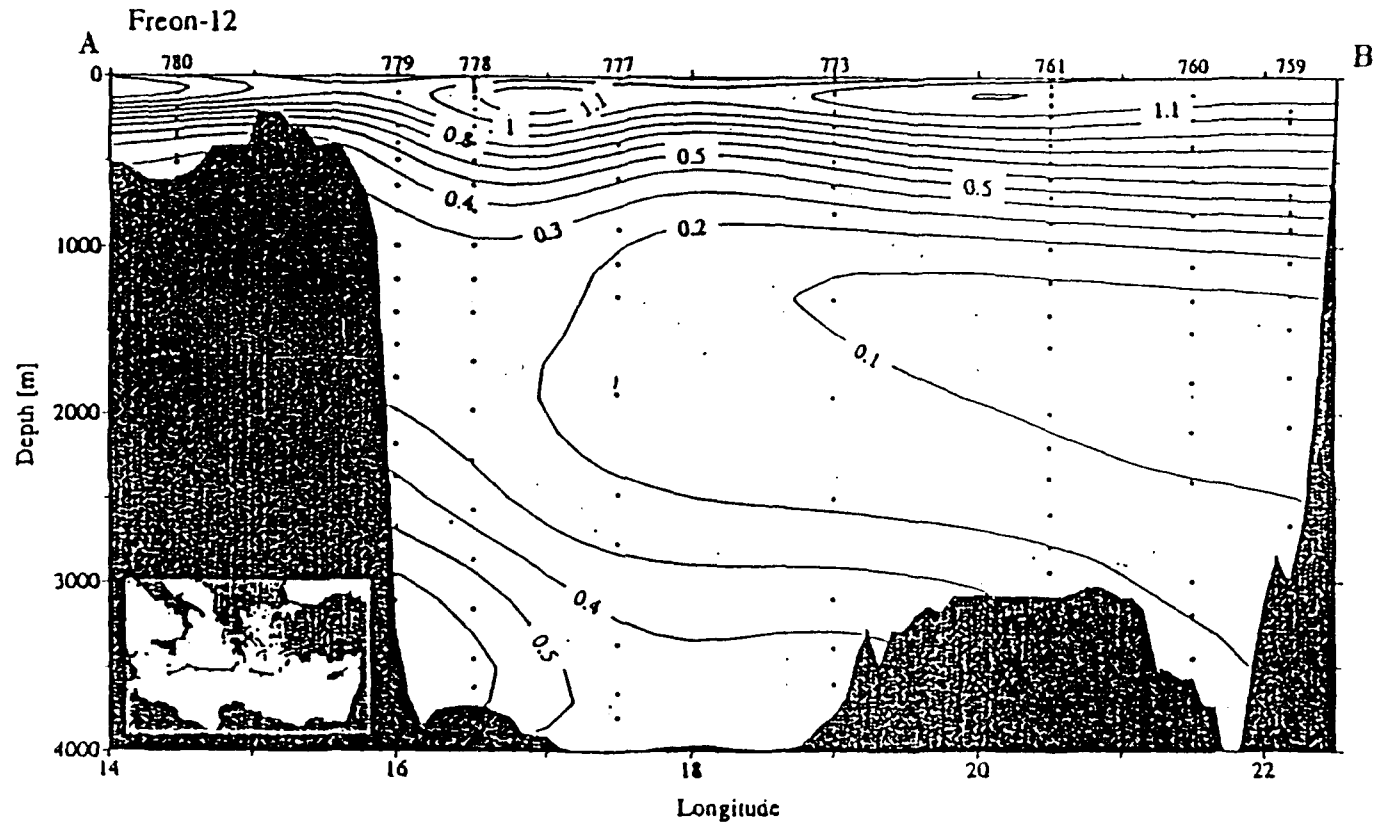
Freon-12
A
B
780
779
778
777
773
761
760
759
0
1000
2000
3000
4000
Depth [m]
1.1
1
0.8
0.5
0.4
0.3
0.2
0.1
14
16
18
20
22
Longitude

Figure 2

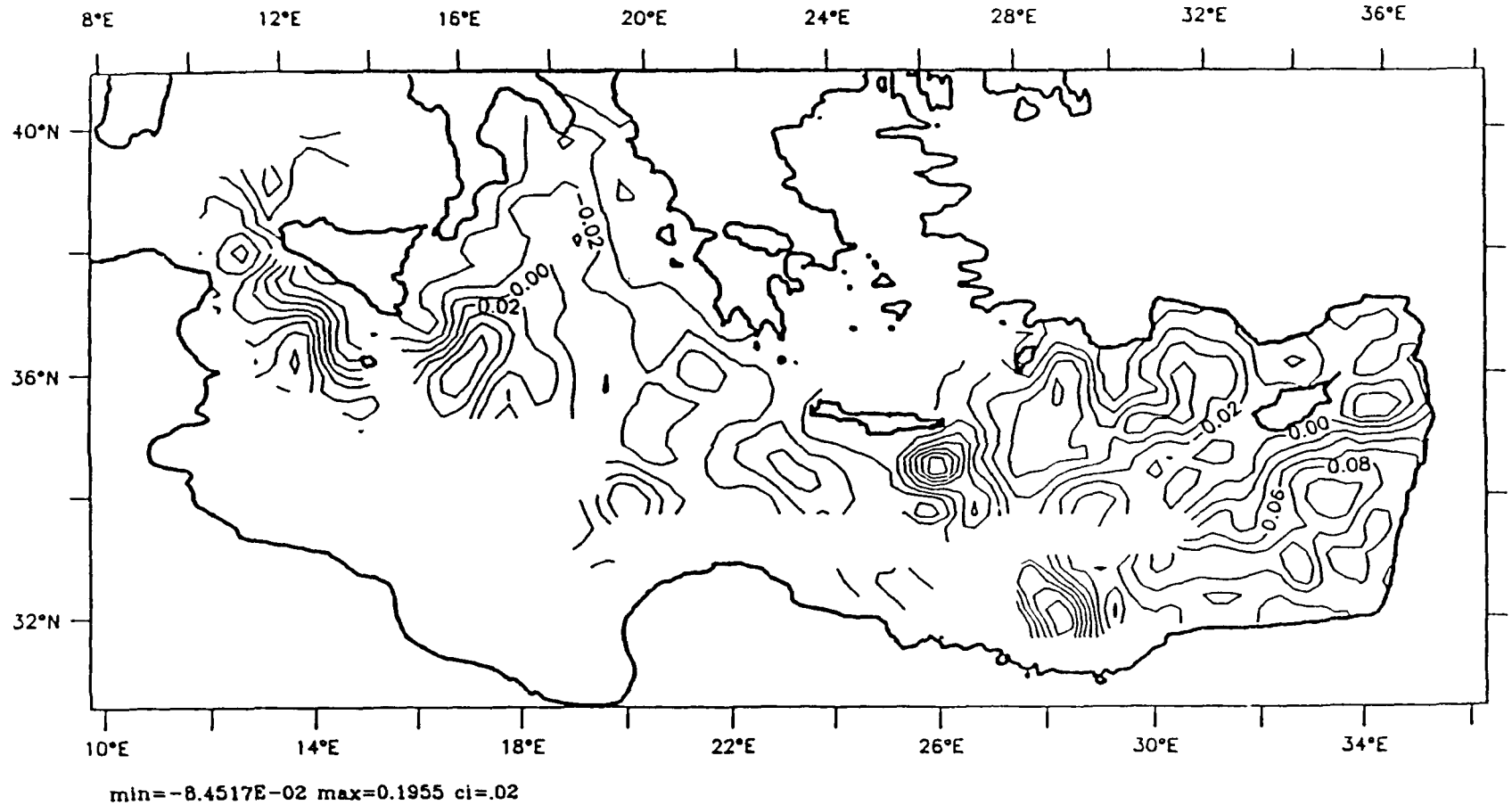
8°E
12°E
16°E
20°E
24°E
28°E
32°E
36°E
40°N
36°N
32°N
10°E
14°E
18°E
22°E
26°E
30°E
34°E
-0.02
0.00
0.02
0.02
0.00
0.08
0.06
min=-8.4517E-02 max=0.1955 ci=.02

Figure 3a

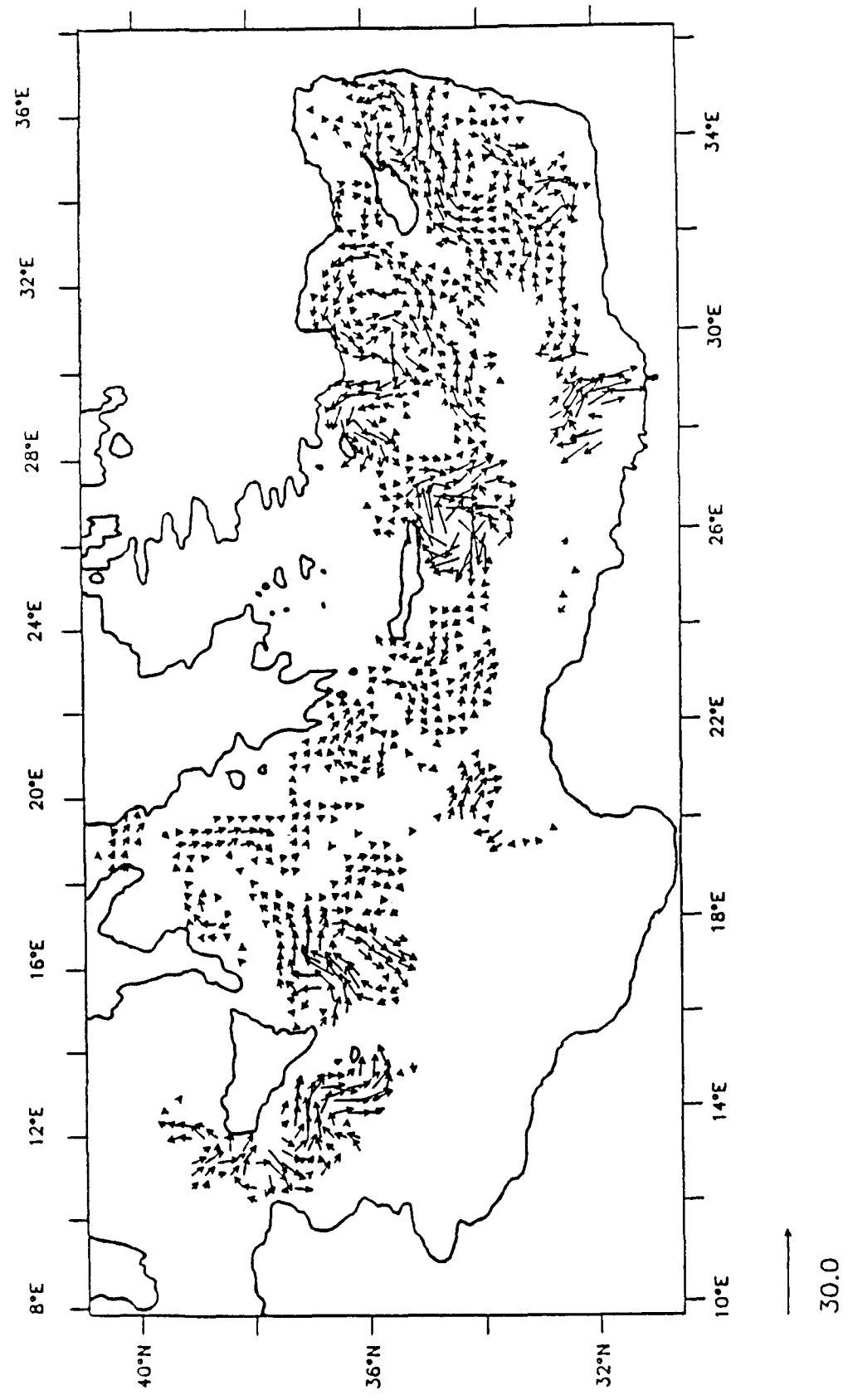
8°E
12°E
16°E
20°E
24°E
28°E
32°E
36°E
10°E
14°E
18°E
22°E
26°E
30°E
34°E
40°N
36°N
32°N
30.0

Figure 3 b

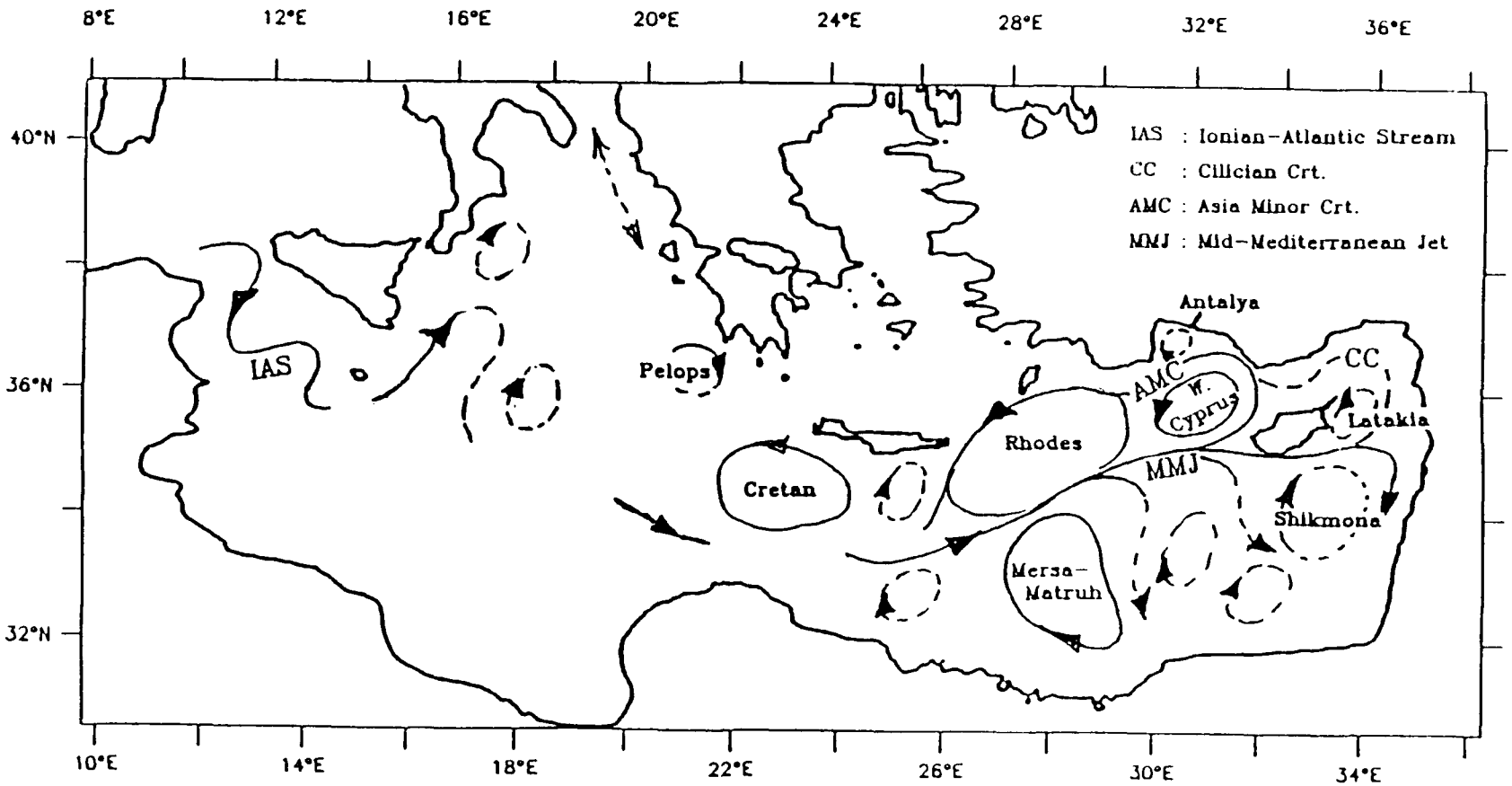
8°E
12°E
16°E
20°E
24°E
28°E
32°E
36°E
40°N
36°N
32°N
10°E
14°E
18°E
22°E
26°E
30°E
34°E
IAS : Ionian-Atlantic Stream
CC : Cilician Crt.
AMC : Asia Minor Crt.
MMJ : Mid-Mediterranean Jet
IAS
Pelops
Antalya
AMC
W. Cyprus
CC
Latakia
Rhodes
MMJ
Cretan
Shikmona
Mersa-Matruh

Figure 4

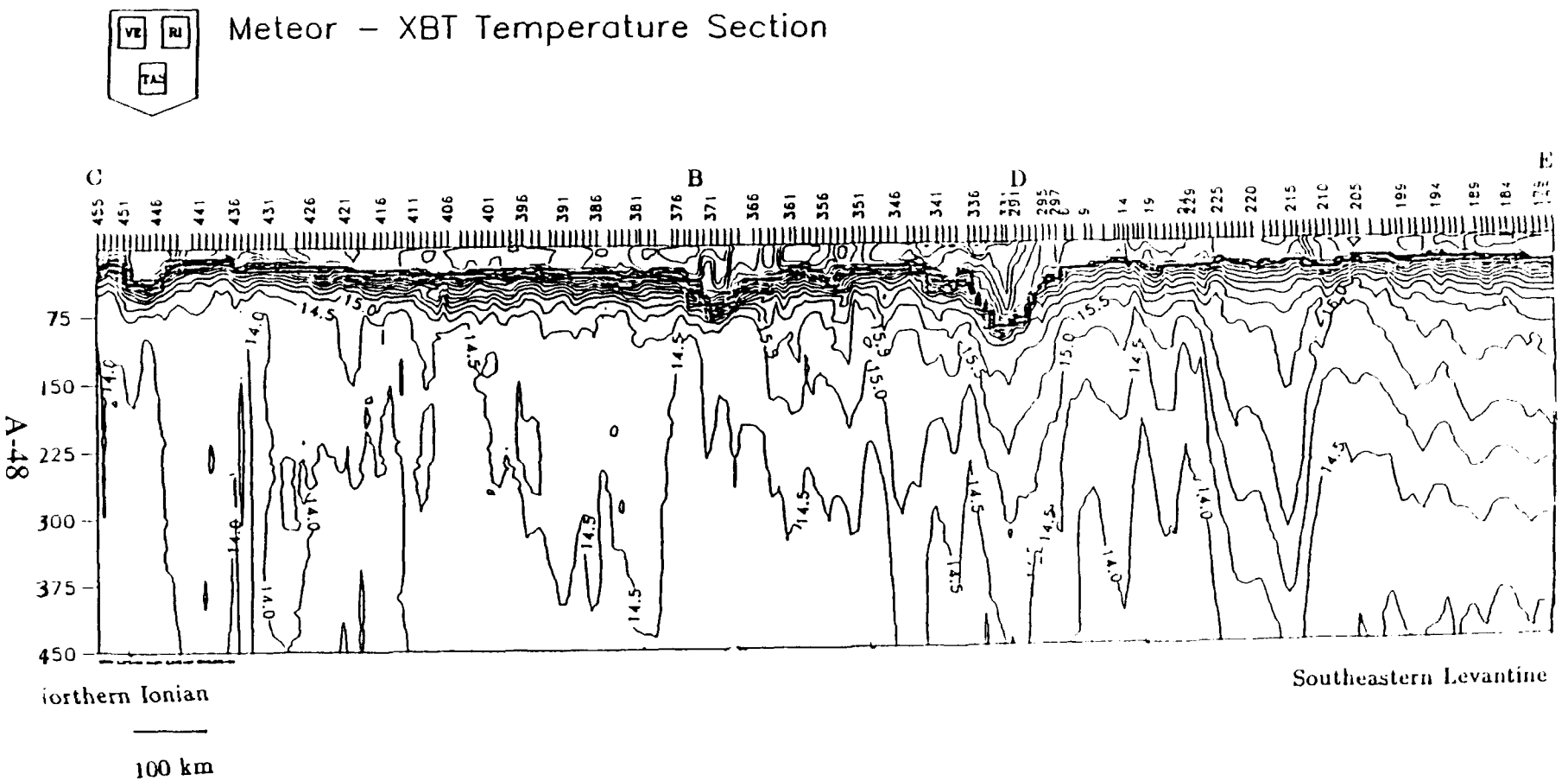
Meteor – XBT Temperature Section
C
B
D
E
A-48
75
150
225
300
375
450
Northern Ionian
Southeastern Levantine
100 km

Figure 5

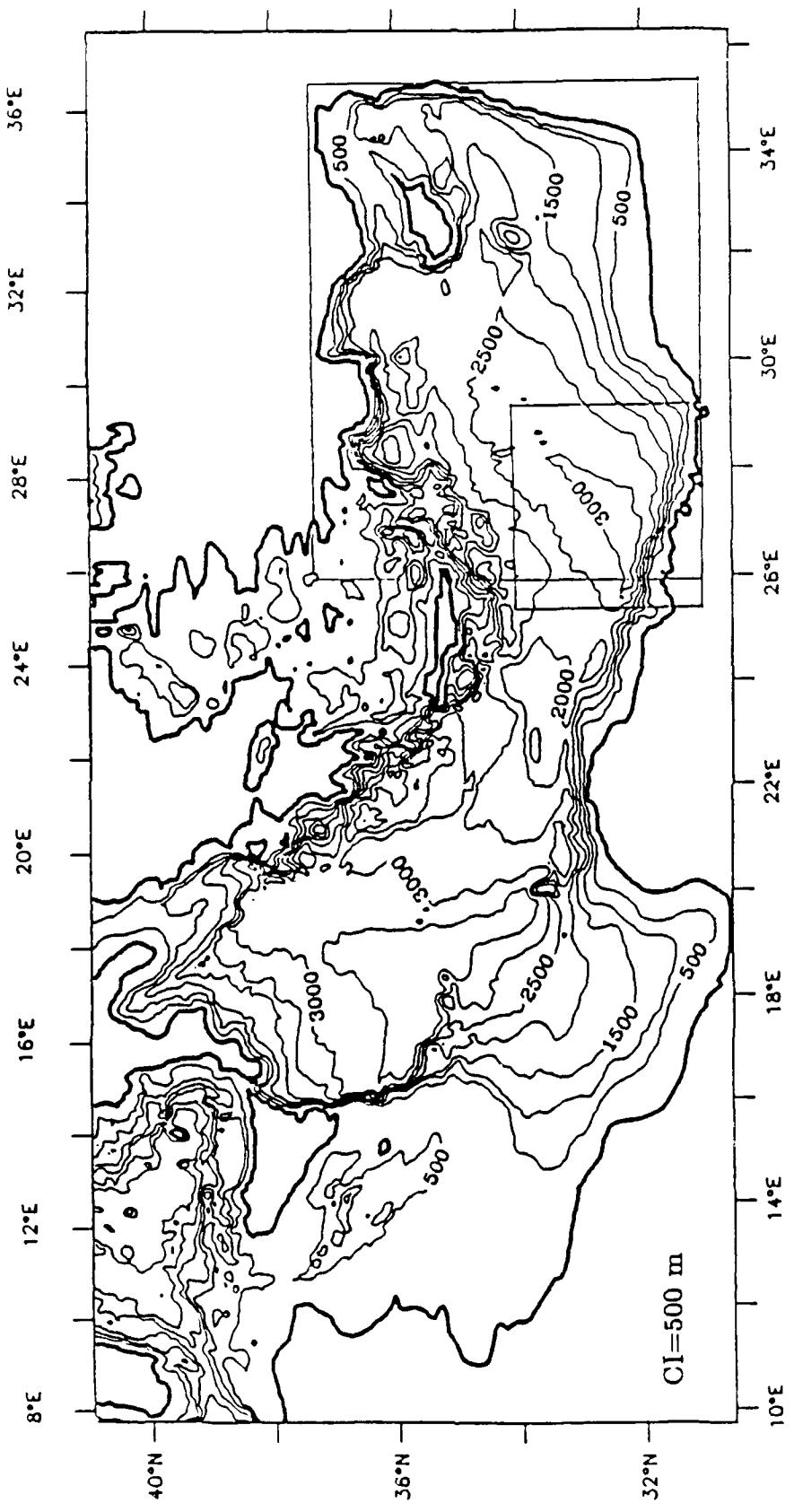
8°E
10°E
12°E
14°E
16°E
18°E
20°E
22°E
24°E
26°E
28°E
30°E
32°E
34°E
36°E
40°N
36°N
32°N
500
1500
2500
3000
2000
CI=500 m

Figure 6

a)

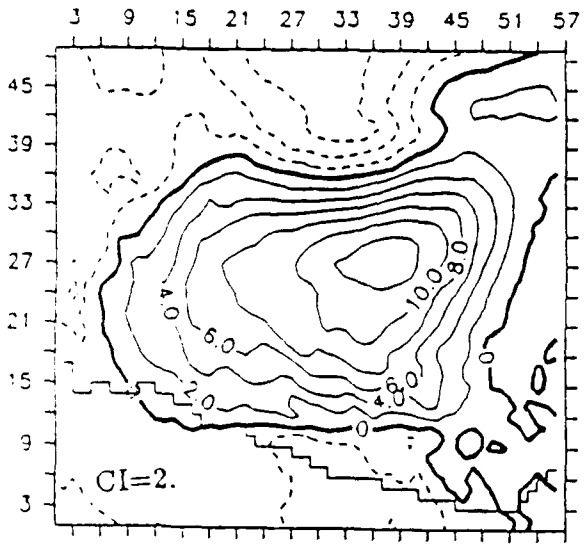
3 9 15 21 27 33 39 45 51 57
45 39 33 27 21 15 9 3
4.0
6.0
2.0
8.0
10.0
0
CI=2.

c)

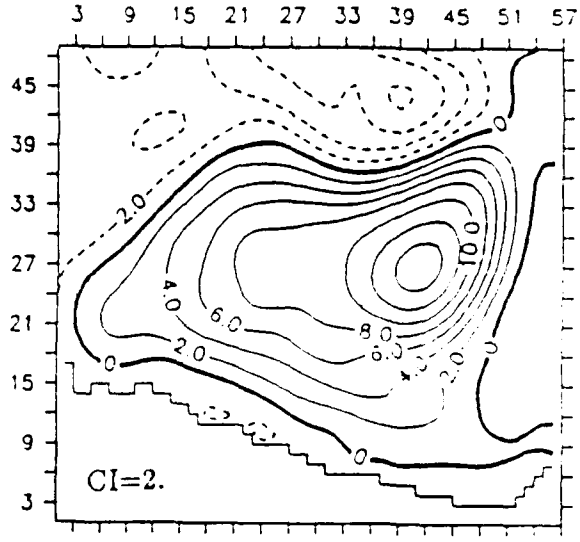
3 9 15 21 27 33 39 45 51 57
45 39 33 27 21 15 9 3
2.0
0
4.0
6.0
8.0
10.0
CI=2.

b)

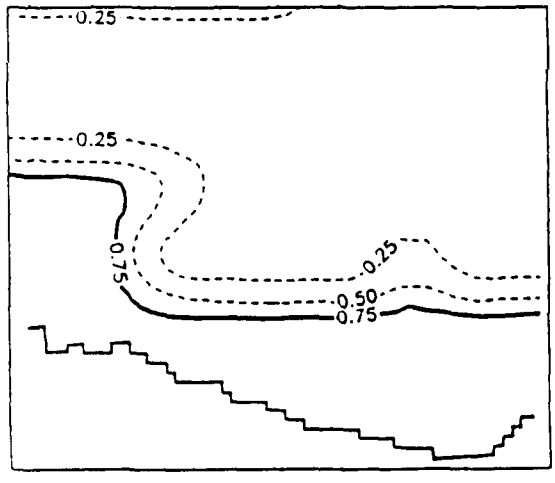
0.25
0.25
0.75
0.25
0.50
0.75

Figure 7

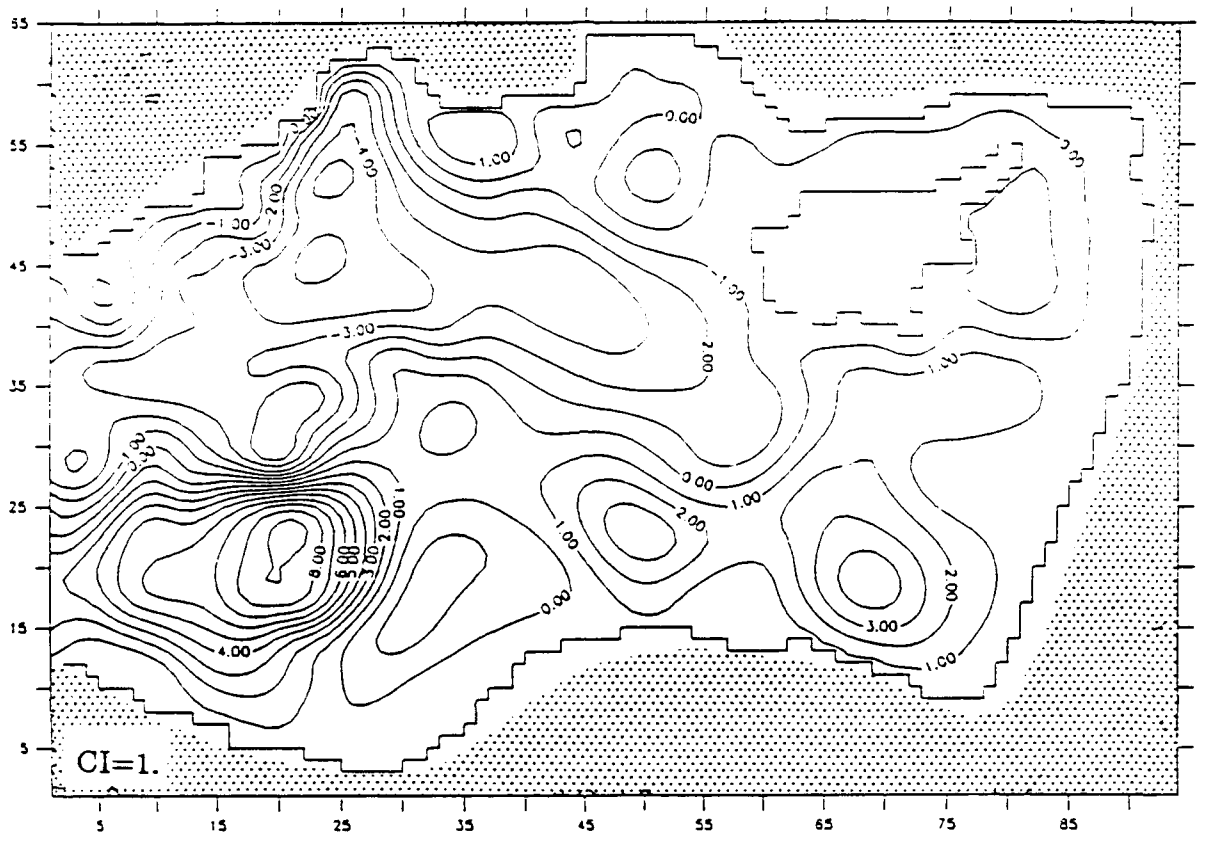

Figure 8a

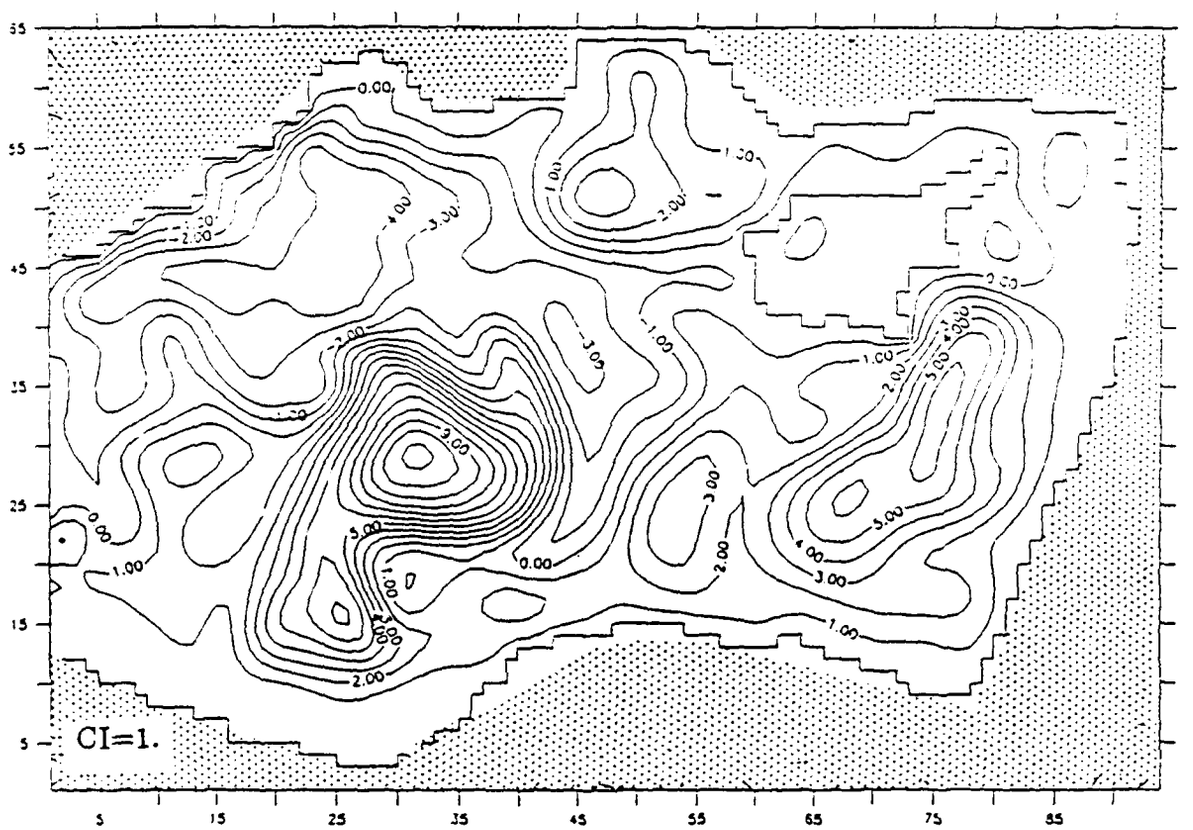

Figure 8b

THE EASTERN MEDITERRANEAN AS A LABORATORY FOR OCEAN CLIMATE PROCESSES

ALLAN R. ROBINSON

Gordon McKay Professor of Geophysical Fluid Dynamics

Division of Applied Sciences and

Department of Earth and Planetary Sciences

Harvard University

1. INTRODUCTION

The Mediterranean Sea, although relatively small, is of sufficient size for its circulation to be governed by large-scale ocean dynamics. It is among the most interesting of our planet's semi-encloseed seas because of the great range of processes and interactions which occur within it (Robinson and Golnaraghi, 1991, hereafter RG91). Most physical processes which characterize the global general ocean circulation, many of which are not well known or understood, occur directly or analogously in the Mediterranean. All major forcing mechanisms, surface wind and buoyancy fluxes and lateral mass exchange, are present. Air-sea interaction is vigorous and both deep water masses and intermediate water masses are formed. Increased density due to saltiness caused by intense surface evaporation is important. The analogy to the global ocean process is that, where deep water masses form in polar regions, dense brine is present as the result of ice formation. Freezing sea water produces fresh ice and salt.

The Mediterranean, connected to the Atlantic by the shallow Straits of Gibraltar, is composed of two similar size basins separated by the shallow and narrow Straits of Sicily. The Eastern Mediterranean is thus itself an isolated basin with multiple forcings and water

mass formations driving the processes and interactions of global interest. Logistically the basin is convenient for operations. Resource-wise, it is both observationally and computationally feasible to conduct basin-wide research in the Eastern Mediterranean with grids of fine enough resolution to define the physical processes of interest. These factors provide a unique opportunity for oceanographic research of general interest. Such research has been underway now for several years, coordinated by the international POEM (Physical Oceanography of the Eastern Mediterranean) program (Malanotte-Rizzoli and Robinson, 1988; The POEM Group, 1991). There has resulted recent rapid progress in knowledge and understanding. Although certain aspects of the circulation have been known generally or speculatively for some time, locations, rates and dynamics of water mass formations and transformations are beginning to emerge. Furthermore, a new picture of the scales, structures and dynamics of the horizontal general circulation and its variabilities is becoming apparent. Thus the basis now exists for research in understanding climate related dynamical processes of global relevance, in detail and in a basin-wide context.

Modeling, of course, plays a significant role in modern ocean scientific research. Multiple and interacting scales and processes require a multi-faceted modeling approach. Furthermore, the assimilation of data into models, the construction of melded estimates from models and observations, and data-based simulations now provide efficient mechanisms for exploiting observations. Data assimilative models are not only useful research tools. They also provide the best mechanism for estimating the four-dimensional fields required for transport estimates for heat, chemicals, particles, etc. necessary for climate related research and other interdisciplinary marine science and technology. A realistic set of high resolution multiscale basin-wide management models can be based upon the research models developed for general circulation and climate change research.

The following sections will discuss processes, describe the multiscale circulation, and illustrate data assimilation for the Eastern Mediterranean Sea.

2. PROCESSES

Processes of global relevance for ocean climate dynamics include aspects of the thermohaline circulations, water mass formations and transformations, dispersion and mixing. Processes are sketched schematically on Figure 1. Fresh water of Atlantic origin (AW) enters through the Straits of Sicily. As it circulates, driven by the wind (τ) and other forces, evaporation (E) much exceeds precipitation at the surface and the water becomes more saline and dense. Net heating (Q) occurs in summer and cooling in winter. In the Levantine basin, predominantly in March, Levantine Intermediate Water (LIW) is formed during storm events. the newly formed water mass circulates and disperses at depths down to a few hundred meters. Some LIW recirculates within the basin and some exits beneath the AW through the Sicily Straits. The ratio of recirculation to eflux is not well known but the net inflow and outflow transports through the Sicily Straits are estimated between 1-1.5 Sverdrup (10^6 m^3/sec). LIW is the predominant source of the Mediterranean water masses in the Atlantic.

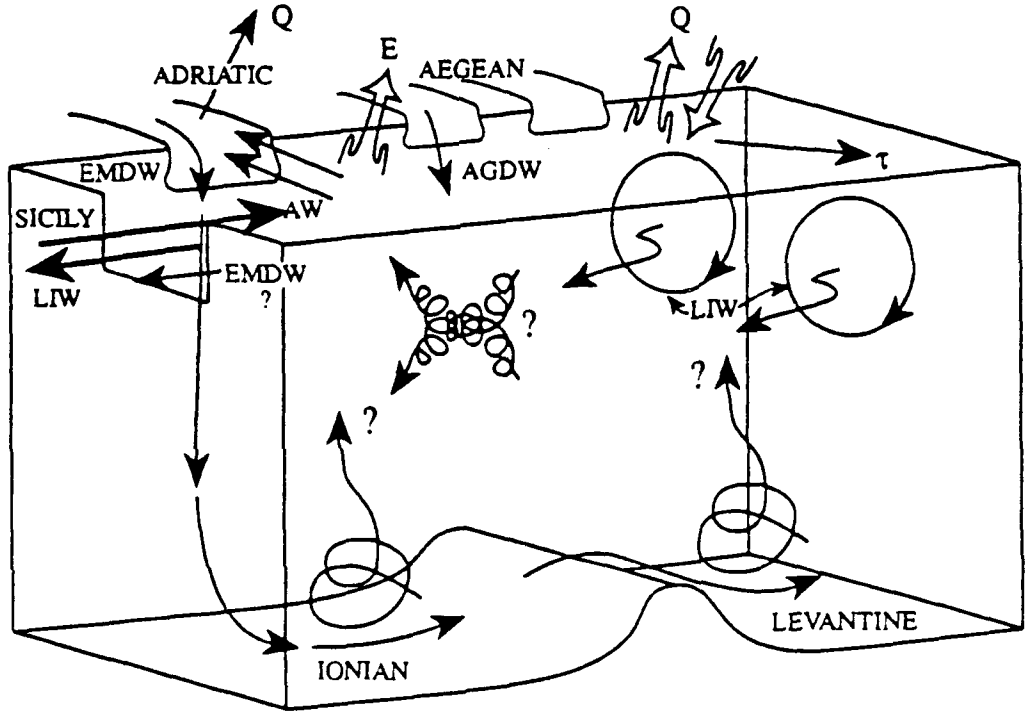

Figure 1. Processes of water mass formations, dispersions and transformations.

Deep water formation occurs primarily in the Adriatic Sea which produces bottom water, the Eastern Mediterranean Deep Water (EMDW). However, Aegean Deep Water (AGDW) also forms which sinks to depths somewhere in the middle of the water column. The site of EMDW formation in winter is the southern Adriatic which is several hundred meters deep. Very cold and dry air storms apparently cause deep convection throughout the water column. The detailed formation process is not well known but it involves surface water admixed with LIW which has entered from the Mediterranean. The newly formed EMDW then exits the Adriatic through the Straits of Otranto, plunges to the bottom, and moves off along the deep western boundary of the Ionian basin. A single vertical thermohaline cell exists for the whole Eastern Mediterranean, although the partitioning of the rising motion between the Ionian and Levantine basins is not known. Other essential unknowns are the locations and rates of mixing between waters of LIW and EMDW origins. This is symbolized by the crossed corkscrew arrows on Figure 1. There is also no observationally based quantitative estimate at present of the amount of (mixed) EMDW which exits at the base of the LIW flow through the Straits of Sicily.

The thermohaline circulations, which are included on Figure 1 are redrawn for clarity on Figure 2. For simplicity the schematic mixing of EMDW and LIW has been omitted. There is an internal cell, a single vertical cell encompassing both the Ionian and Levantine basins, and an external cell. The external thermohaline cell involves an exchange of water through the Straits of Sicily. The remote excursions of EMDW and the return paths in the Western Mediterranean and Atlantic Ocean are not known.

There is special interest attached to the internal cell in that it is a closed thermohaline cell in which the deep water formation involves a preconditioning process of density increase due to saltiness. Thus it is to some extent an analog of the global scale "conveyor belt" thermohaline cell whose deep water forms in the North Atlantic (Gordon, 1986; Broeker, 1987). A detailed understanding of the Eastern Mediterranean cell should be achievable

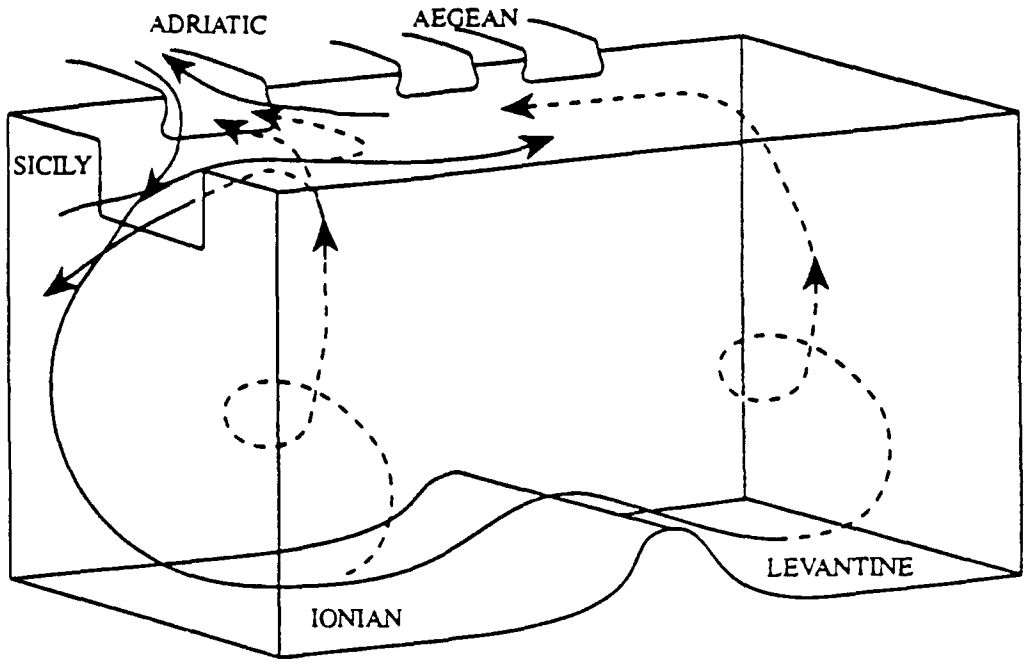

Figure 2. The thermohaline cells.

in the near future which should be expected to contribute insights into globally relevant processes.

3. THE MULTISCALED CIRCULATION

It is now known that the general circulation and its variabilities consists of three predominant spatial scales which must be understood together with their nonlinear interactions. This concept is depicted schematically in Figure 3. The slow (vertical) thermohaline cell is ***basin*** scale. The basin scale general circulation of the main thermocline of the upper ocean is composed of ***subbasin*** scale gyres linked by subbasin scale jets. There are a variety of subbasin scale variabilities which will be described below. The energetic ***mesoscale*** which is present is illustrated in Figure 3 on one of the subbasin scale gyres by a field of internal eddies and a meandering of the outer swirl flow, and as the meandering of a jet segment.

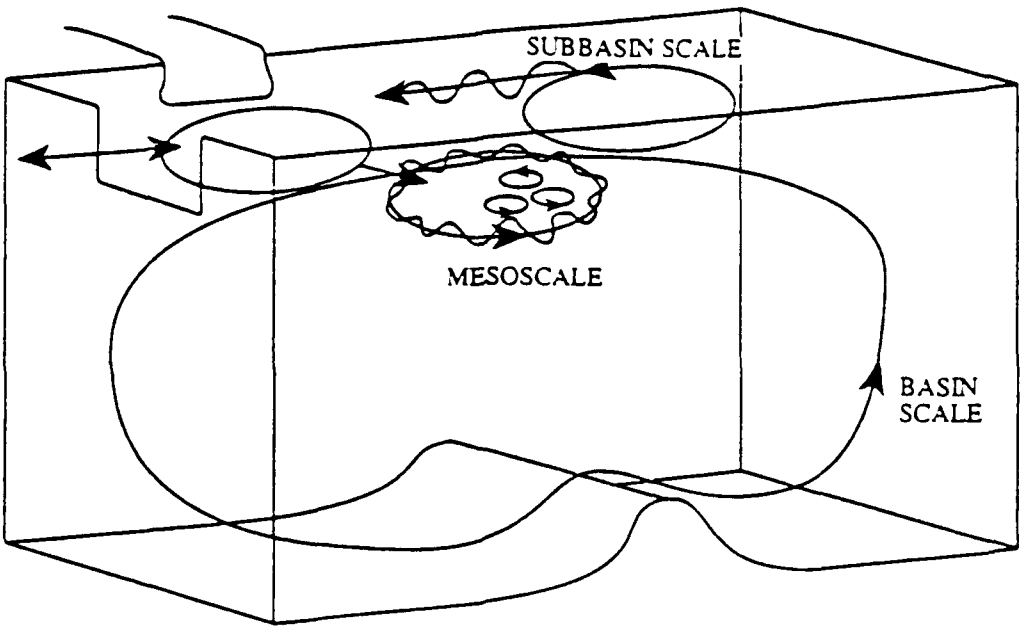

Figure 3. Scales of circulation variabilities and interactions.

The POEM program conducted five quasi-synoptic nominally basin-wide hydrographic surveys from 1985 through 1987 (Robinson *et al.*, 1991). The sampling patterns were grids with nominal spacings of one half degrees of latitude and longitude, which provides fine general circulation (subbasin) scale and coarse mesoscale resolutions (Robinson *et al.*, 1987). The best coverage, achieved with six ships during August-September, 1987, is shown in Figure 4. A basin-wide multiscale experiment was conducted simultaneously from the ***F/S Meteor***, whose track is superimposed over the survey grid on Figure 4. Transient tracer measurements were made to investigate the deep thermohaline circulation and XBTs were taken uniformly every ten kilometers along the ship track to explore the characteristics of mesoscale phenomena throughout the basin. CTD stations were also carried out.

3.1 The Basin Scale Thermohaline Cell

The transient tracer experiment consisted of 62 stations where chlorofluoromethane (CFM) and tritium were measured (Schlitzer *et al.*, 1991). The CFM Freon 12 distribution

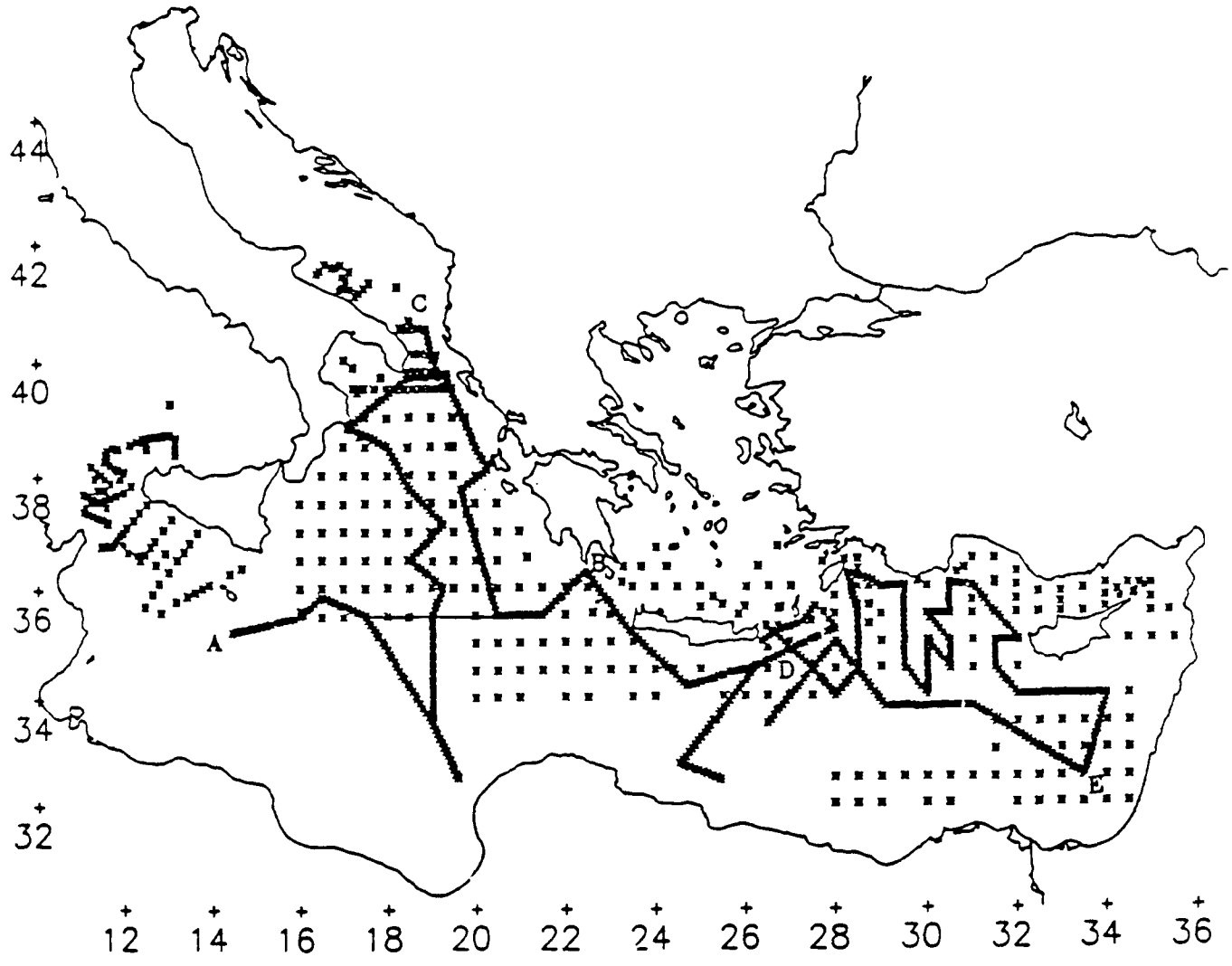

Figure 4. Multiscale survey data sampling map (from RG91 Figure 1).

along the east-west section AB shown on Figure 4 is presented on Figure 5. The source of Freon 12 is the atmosphere, and there is of course a large concentration in the upper ocean. But there is also a maximum in the Freon distribution in the deepest water in the western basin (off the Malta escarpment) which is clear evidence for the presence of recently formed deep water of Adriatic origin. The minimum concentration is at mid-depths in the eastern Ionian basin.

In order to obtain quantitative information about the deep water renewal rate from this data set, Roether and Schlitzer (1991) have constructed a 22 box model with compartments for the Ionian and Levantine deep water below 1000 m depths. They find that the water

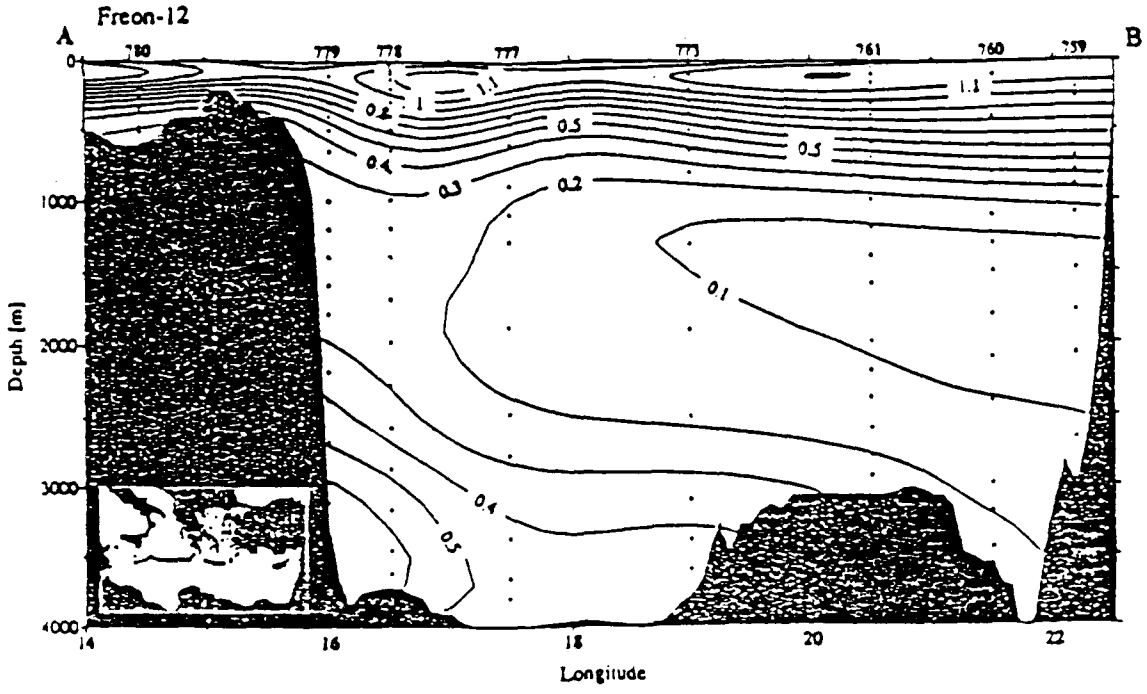

Figure 5. Freon 12 section across the Ionian basin (pmd kg^{-1}) (from Roether and Schlitzer, 1991 Figure 2).

formed in the Adriatic is a mixture of surface water (AW) and intermediate water (LIW) from the Mediterranean which therefore has also previously been subject to surface fluxes. Their results indicate unambiguously that the thermohaline circulation consists of a single vertical cell throughout the entire Eastern Mediterranean, flowing coherently throughout both the Ionian and Levantine basins. The turnover time for the deep water is 126 years.

The rate of deep water supply is 0.29 ± .09 Sverdrups (10^6 m^3/s). This is about one third of the inflow or outflow rate of all waters through the Sicily Straits. There is some qualitative evidence observationally, from transient tracer measurements (Roether and Schlitzer, 1991) that some EMDW does exit through the Straits of Sicily. The only quantitative information comes from a numerical general circulation model for the Eastern Mediterranean which has active thermodynamics (Malanotte-Rizzoli and Bergamasco, 1991). The results must be regarded as tentative: the stratification is imposed and the deep convective process is not modeled. The interesting result however, is that about one third of the water efluxing through the Straits of Sicily is deep water which has upwelled in

the southern Ionian basin. At this time it would seem reasonable to assume that internal and external thermohaline cells are of comparable magnitude.

3.2 The Subbasin Scale Components of the General Circulation

The currents and circulation of the upper ocean thermocline are shown on the objectively analyzed dynamic height (30 m relative to 450 m) and current vector maps of Figures 6a and 6b, respectively. The complex pattern of cyclonic and anticyclonic gyres linked by jets and current segments is real: no contours are plotted where the expected error of the objective analysis is less than fifty percent. A synthetical study has been carried out for the five independent quasisynoptic realizations contained in the pooled data set of POEM (Robinson *et al.*, 1991). The results for the circulation and variabilities are summarized in the schematic of Figure 7 and the companion Table 1.

There are a number of permanent albeit variable, features. Other features are recurrent, i.e. disappear but reappear similarly. Transient gyres and jets also occur randomly throughout the basin. Variabilities characterizing the permanent and recurrent structures include: the center, size and strength of gyres and their multilobe mesoscale instabilities; the axis location, meander pattern and bifurcation structure of jets. The time scales associated with the subbasin scale variabilities and mesoscale interactions are not yet well defined but appear to range from years (e.g., recurrence time of the Shikmona gyre) to days (mesoscale interactions). General circulation modeling studies indicate that subbasin scale structures are the form of the Eastern Mediterranean's response to the large-scale forcing functions (Malanotte-Rizzoli and Bergamasco, 1991) due to factors including topographic effects and the seasonal power in the wind-stress forcing (Pinardi and Navarro, 1991).

3.3 Levantine Intermediate Water

The formation of Levantine Intermediate water was for many years believed to occur

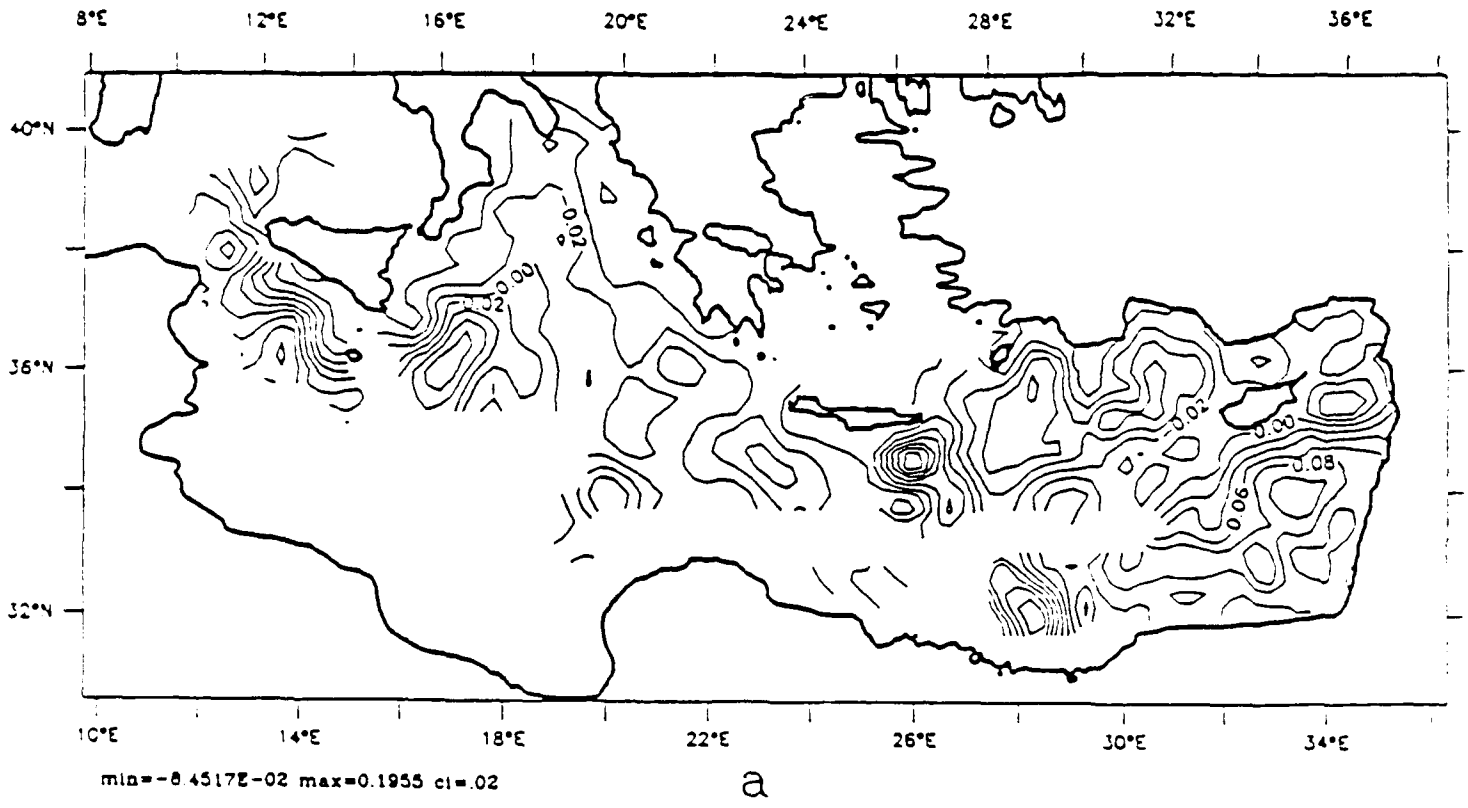

Figure 6. a) Dynamic height anomaly in the upper thermocline, 30 m relative to 450 m (dynamic meters) August-September 1987. b) Associated horizontal geostrophic flow vectors (scale vector cm sec−1) (from Robinson *et al.* 1991 Figure 7).

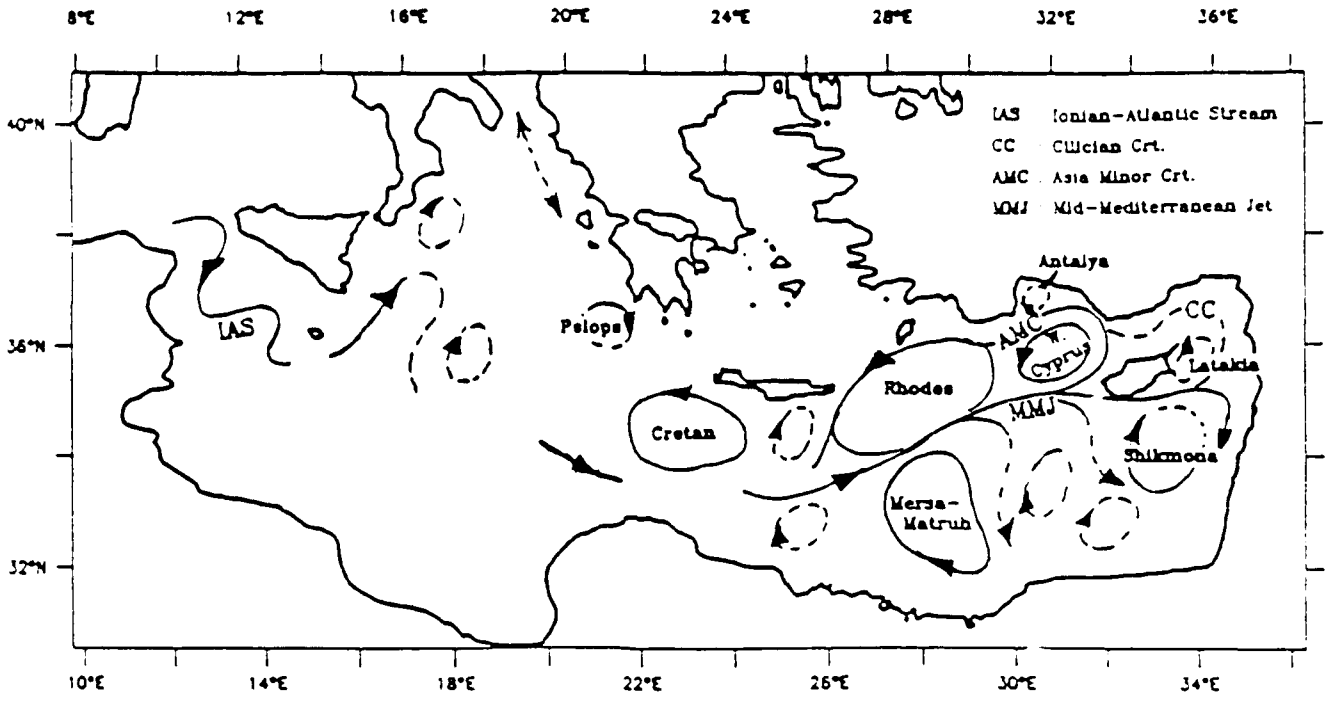

Figure 7. General circulation schematic (from Robinson *et al.* 1991 Figure 2).

TABLE 1 - Upper Thermocline Features
(from Robinson *et al.* 1991 Table 1)

Features	Type	ON 85	MA 86	MA 87	AS 87
Ionian Atlantic Stream	P	-	-	Y	Y
Mid Med. Current	P	Y	Y	-	Y
Asia Minor Current	P	Y	N	Y	N
Cilician Current	R	Y	Y	-	Y
Southeast Levantine Jets	T	Y	Y	-	Y
Rhodes C	P	Y	Y	-	Y
West Cyprus C	P	Y	Y	-	Y
Mersa Matruh AC	P	Y	Y	-	Y
Cretan Sea C	P	Y	?	-	Y
Shikmona AC	R	Y	Y	-	Y
Latakia C	R	Y	N	N	Y
Antalya AC	R	?	Y	-	N
Pelops AC	?	-	Y	?	Y
Ionian eddies AC	T	-	-	-	Y
SE Levantine eddies AC	T	Y	Y	-	Y
Cretan Sea eddies	T	Y	Y	-	Y

Definitions: P=Permanent, R=Recurrent, T=Transient, ?=Not enough information to classify, C=Cyclone, AC=Anticyclone.

predominantly in a limited region between Rhodes, Cypress and the Turkish coast and to involve a preconditioning process afforded by the domed pycnocline characteristic of the Rhodes gyre. Recent evidence, however, indicates that formation occurs over a much larger domain which could include the centers of anticyclonic gyres (Oguz, 1991) via a process related to thermocline deepening in warm core Gulf-Stream rings (Dewar, 1986). The horizontal circulation structures and pattern observed and analyzed by Ozsoy *et al.* (1989) for the upper thermocline of the Levantine basin in October of 1985 is shown in Figure 8a. A composite vertical salinity section around the basin (ABCD on Figure 8a) is shown on Figure 8b with LIW (salinity greater than 38.95 ppm) shaded. LIW is prevalent and ubiquitous throughout the basin including the southern sector.

3.4 Mesoscale Variability

The internal Rossby radius of deformation is the horizontal scale which characterizes mesoscale instabilities, meandering and eddying. It is essentially the vertical scale (e.g. thermocline depth) of the phenomenon amplified by the ratio of the Brunt-Väisälä buoyancy frequency to the Coriolis parameter. Since this length scale is only $\sim$ 10–12 km in the Eastern Mediterranean, four times smaller than typical values for much of the worlds ocean, mesoscale phenomena were not defined in observations until recently when dedicated high resolution sampling was undertaken (Robinson *et al.*, 1987).

The mesoscale experiment conducted in 1987 by A.R. Robinson, W.G. Leslie and N. Pinardi took 620 XBT samples at nominal 10 km spacing along the entire *FS Meteor* ship track. A composite section across the basin from the mouth of the Adriatic Sea to the southeastern Levantine corner (CBDE on Figure 4) is shown on Figure 9. A number of interesting features are present which characterize the highly resolved structures of the subbasin scale gyres and jets (e.g. the Rhodes gyre in the vicinity of D). Mesoscale eddies exist in the open sea (e.g. northwest of E) and interactively with the subbasin scale

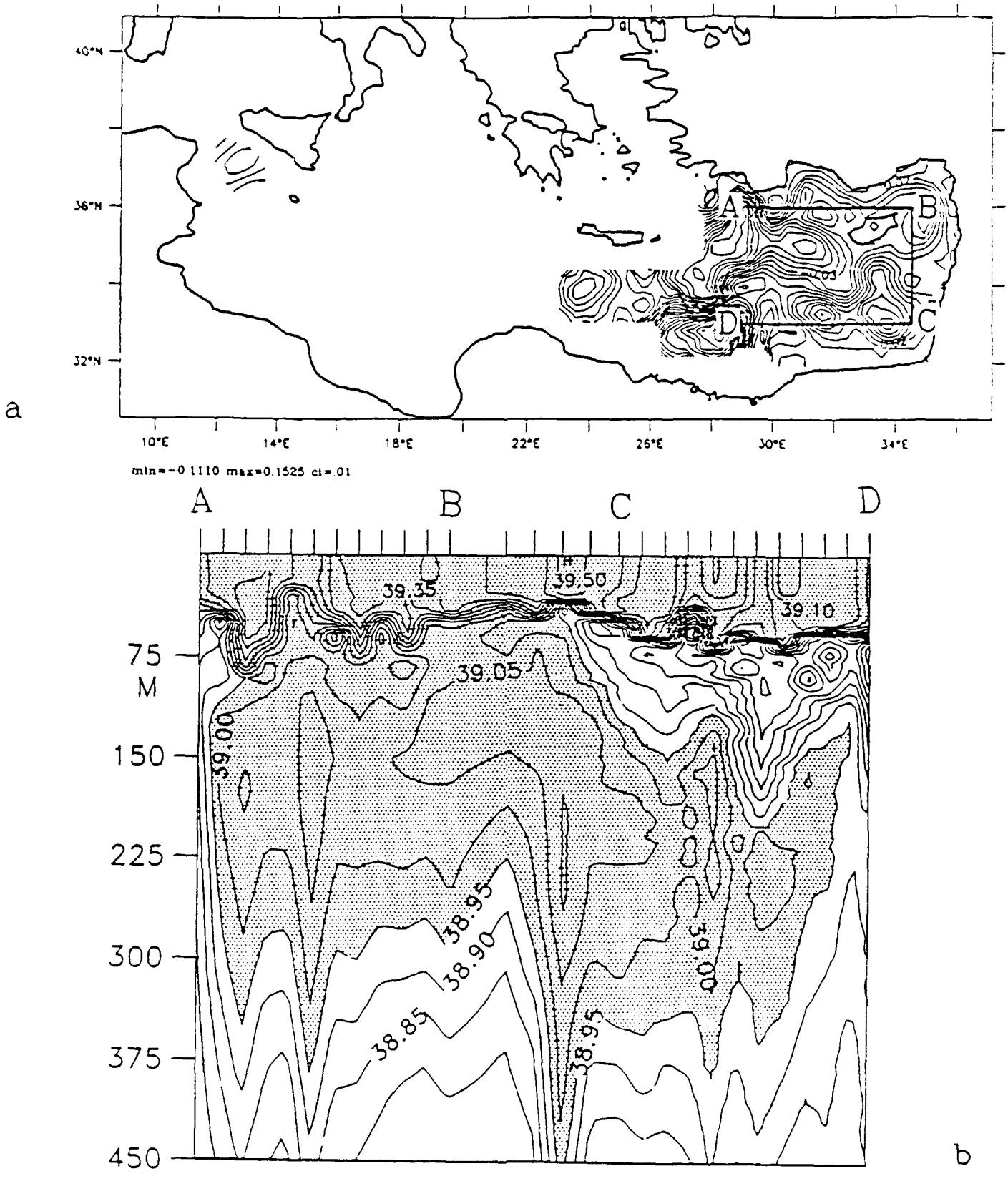

Figure 8. a) Dynamic height as in Figure 6 but for October 1985. b) Vertical salinity (ppm) section along ABCD of Figure 8a with LIW shaded (after POEM group 1991 Figure 3).

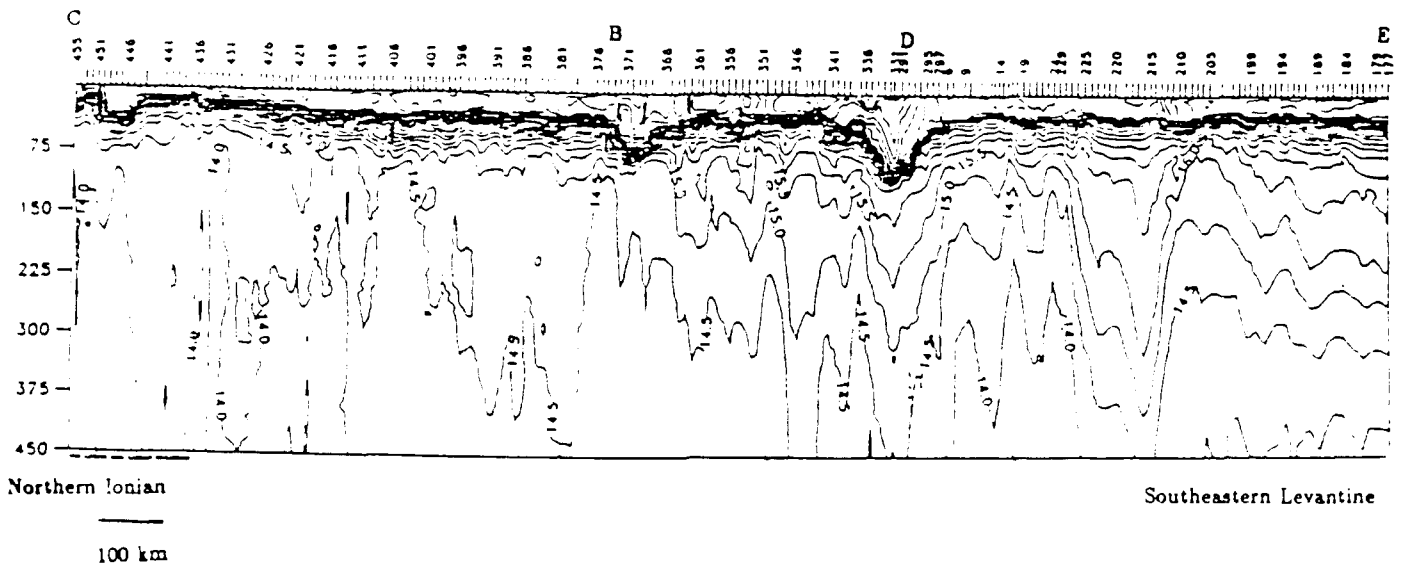

Figure 9. Composite XBT derived temperature section along track CBDE of Figure 4 (from RG91 Figure 5).

features. The Levantine basin appears more energetic in the mesoscale, with the Ionian (C–B) characterized by a remarkable thermostad at 14.0–14.5°C from 75 to 450m.

4. DATA ASSIMILATION INTO DYNAMICAL MODELS

4.1 Methodology

The Harvard dynamical model hierarchy consists of a set of compatible and intercomparable numerical dynamical ocean models constructed under physical assumptions suitable for various regions and phenomena in the oceans. Domains and geometries are general, ranging from an arbitrary piece of open ocean (water-water boundaries) to an entire basin scale. The model hierarchy approach was adopted in order: to achieve the closest possible relationships of modeling to experimental data bases; to allow the focus of computing resources and scientific effort on regions of special interest; and to facilitate the physical interpretation of results via utilization of the simplest physical model required for a simulation of specified accuracy.

The present model hierarchy consists of a quasigeostrophic model for a block of open ocean (Robinson and Walstad, 1987) or for a region (partially) bounded by an arbitrary coastline (Milliff, 1990) which contains islands (Ozsoy, *et al.*, 1991). A surface boundary layer may be attached (Walstad and Robinson, 1991). More general primitive equation dynamics may be utilized with arbitrary open boundary conditions (Spall and Robinson, 1989).

The POEM data sets have been assimilated into the dynamical models and studies are ongoing. Initialization of the dynamical model with a real ocean data set serves to dynamically adjust the data and generally improves the field estimates. Data gaps can be interpolated dynamically. Dynamics together with hydrography yields absolute flow estimates; dynamics provides the consistent barotropic mode. Four dimensional field estimates best suitable for the transport flows necessary as input to interdisciplinary and applied studies are provided. Furthermore, the results of simulations based on real data sets can be analyzed in detail qualitatively and quantitatively in order to reveal real physical processes operative in the ocean. Four examples of the Eastern Mediterranean will be briefly described for the regions shown on Figure 10: the full basin, the eastern Levantine basin, and the Mersa Matruh and Rhodes gyres.

4.2 Results

Figure 11 shows the stream-function field (proportional to upper thermocline dynamic high) for the winter 1986 POEM quasisynoptic survey after fourteen days of dynamical adjustment. The assimilation is remarkably robust. Overall, the features resemble the objective analysis initialization (not shown). There has been dynamical smoothing and natural variabilities (meandering of the mid-Mediterranean jet) are underway. The remarkable robustness of the subbasin scale features to dynamical assimilation in this data set is characteristic of all the data sets.

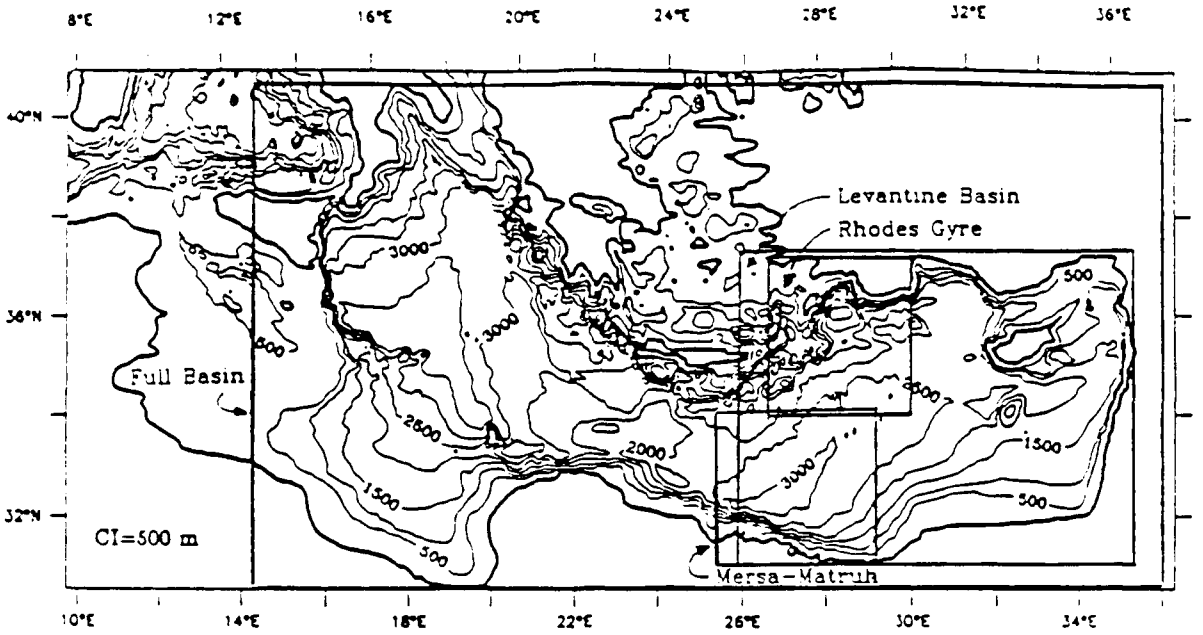

Figure 10. Modeling domains and bottom typography.

Dynamical interpolation is illustrated for the Mersa Matruh gyre in the region indicated in Figure 11 (which is to appear in the doctoral dissertation of Ms. M. Golnaraghi of Harvard University). The objective analysis initialization of Figure 12a can be seen from the expected error maps of Figure 12b to suffer from an absence of data in approximately

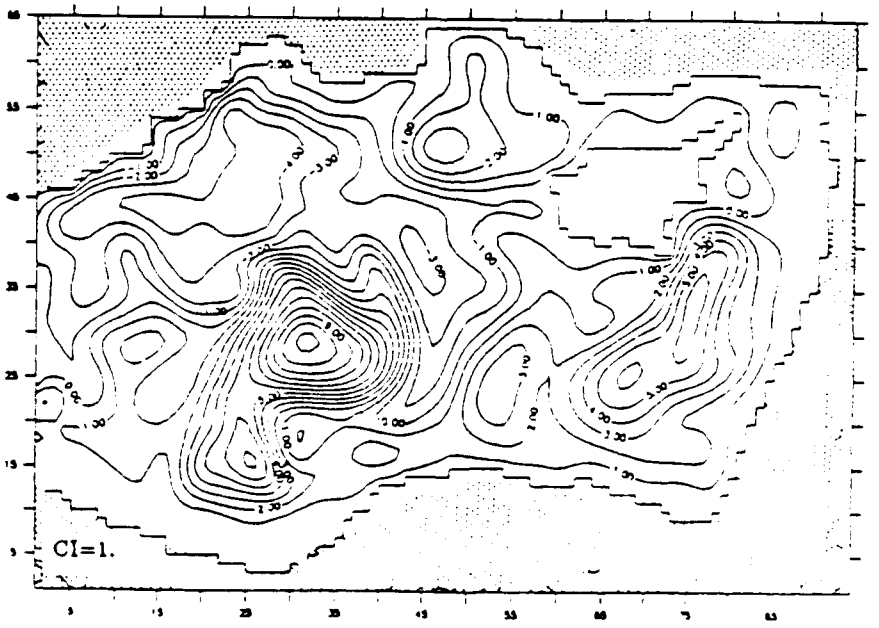

Figure 11. Streamfunction field at 40 m depth 14 days after initialization. The stream function is proportional to dynamic height (nondimensional units) (from RG91 Figure 8).

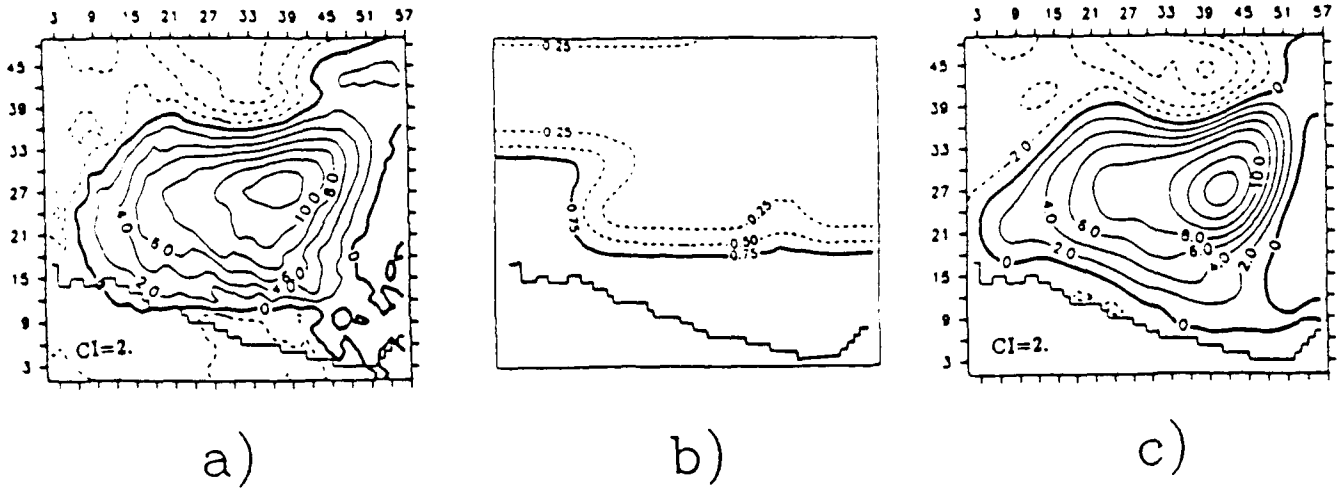

Figure 12. a) Messah Matruh stream function at 40 m objective analysis map. b) Associated expected error map. c) As (a) after 14 days of dynamical run (from RG91 Figure 7).

one third of the domain of interest north of the Egyptian coastline. After fourteen days (Figure 12c) dynamics provides a consistent complete gyre circulation.

The 1987 mesoscale experiment accomplished a mapping pattern in the region of the Rhodes gyre as evidenced by the zig-zag ship track in that region on Figure 4. This served as the basis of a simulation and dynamical process study of mesoscale-subbasin scale interactions for the gyre system (Milliff and Robinson, 1991). The main thermocline stream-function for three, seven and ten days into the simulation are shown in Figure 13. There is a four-lobed oscillation of the gyre center with a period of about a week. This appears to be driven by intermittent bursts of baroclinic instability associated with the tightening of the jet between the cyclonic Rhodes gyre and the anticyclonic gyre to its northeast, which can be seen most intensively on Figure 12c.

A full basin assimilation of the summer 1987 data shown on Figure 6 is presented in Figure 14. Dynamical interpolation and wind forcing have filled in the large data gap in the southern Ionian and also the gaps south of Crete and in the mid-Levantine basin. The flow depicted is forty-five days into a dynamical run initialized with the objective analysis

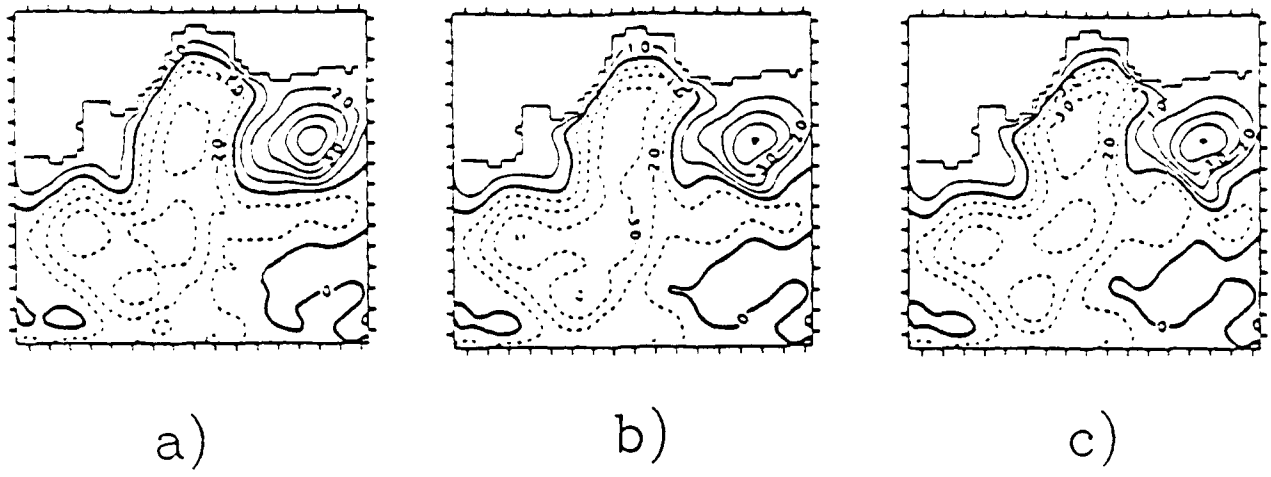

Figure 13. Mesoscale simulation of Rhodes gyre system after a) 3 days, b) 7 days, c) 10 days (after Milliff and Robinson 1991 Figure 6).

of Figure 6a and also driven by the August-September mean winds. The Atlantic Ionian Stream which projects to the northeast into the Ionian threads its way across the basin continuously to the Mid-Mediterranean Jet. This is, to our knowledge, the first time that observations and dynamics have been combined to produce a quasisynoptic realization of a full basin circulation with subbasin scale resolution.

5. SUMMARY AND CONCLUSIONS

The Eastern Mediterranean Sea is an open but isolated basin of interest as a laboratory basin for global ocean general circulation processes including oceanic climate dynamical processes. The circulation and variabilities of the Eastern Mediterranean Sea are known to be constituted from multiple and interactive space and time scales. A single full basin scale thermohaline cell exists with a turnover time of one and one quarter centuries. The main thermoclinic general circulation is built up from subbasin scale features, cyclonic and anticyclonic gyres linked by interconnecting jets. Variabilities include fluctuations in the characteristics of the permanent features as well as the occurrence of recurrent and

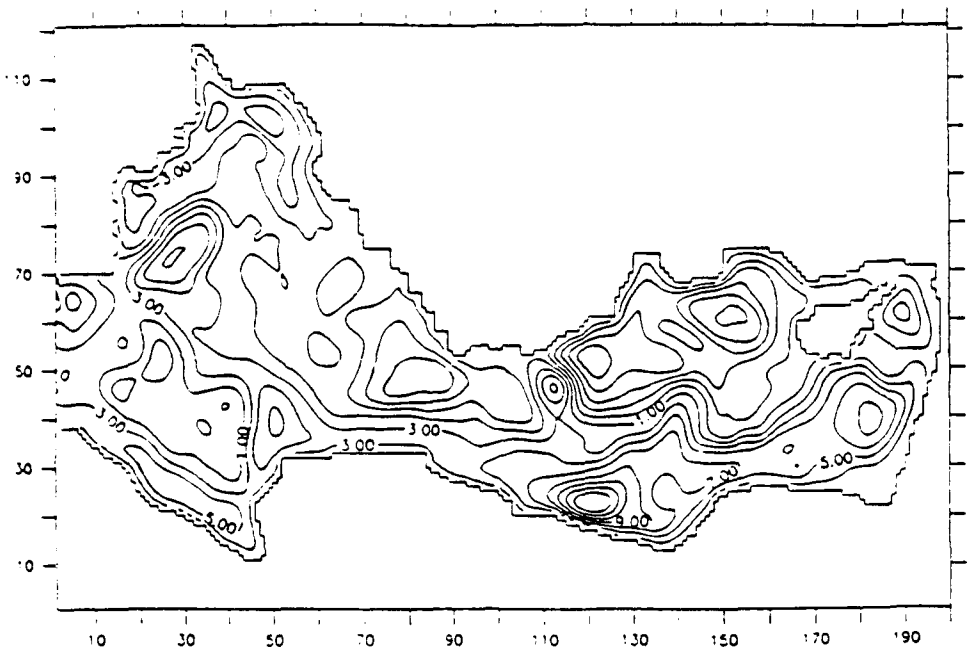

Figure 14. Full basin simulation 45 days after initialization. Upper thermocline function.

transient features. Mesoscale eddies, meanders and oscillations occur and interact with the subbasin scale circulation, most energetically in the Levantine basin (in the summer 1987 data set).

Important climate processes include the formation, dispersion, transformation, mixing and circulation of both intermediate and deep water masses. The basin wide deep thermohaline circulation has both an internal cell, confined to the Eastern Mediterranean, and an external cell which communicates with the world ocean through the Western Mediterranean. The internal cell, whose deep water formation involves preconditioning via salt concentration, may present interesting analogies to the global conveyor belt.

The assimilation of the new data sets into models provides absolute flow from hydrographic data plus dynamics, and improves the data via processes of dynamical adjustment and dynamical interpolation. The subbasin scale general circulation features are stable and robust under assimilation. Data driven extended simulations and process studies for both internal dynamics, general circulation forcings and multiscale nonlinear interactions

are in progress. The realistic synoptic time series of fields estimates, provided regionally or basin wide by such models, also provide best estimate transport fields for biological, chemical and management studies and applications.

ACKNOWLEDGEMENTS

It is a pleasure to acknowledge the help of Ms. Maryam Golnaraghi in the preparation of the scientific material for this review and overview and in carrying out the simulations for the Mersa Matruh gyre and the full and Levantine basins. Thanks are due to Dr. Carlos J. Lozano for help in model set up and to Mr. Wayne G. Leslie for XBT acquisition and data analysis and for figure preparation. I have profited from scientific exchanges with many POEM colleagues, especially Professor Paola Malanotte-Rizzoli of the Massachusetts Institute of Technology. This research was supported by the National Science Foundation and by the Office of Naval Research under grant numbers OCE-90-12812 and N00014-90-J-1593 to Harvard University.

BIBLIOGRAPHY

1. Broecker, W.S. (1987). The Biggest Chill, *Natural History Magazine*, October 74-82.
2. Dewar, W.K. (1986). Mixed Layers in Gulf Stream Rings, *Dynamics of Atmospheres and Oceans* **10**, 1-29.
3. Gordon, A. (1986). Interocean Exchange of Thermocline Water, *Journal of Geophysical Research* **91**, 5037-5046.
4. Malanotte-Rizzoli, P. and A. Bergamasco (1991). The Wind and Thermally Driven Circulation of the Eastern Mediterranean Sea *Dynamics of Atmospheres and Oceans* **15**, 355-420.
5. Malanotte-Rizzoli, P. and A.R. Robinson (1988). POEM: Physical Oceanography of the Eastern Mediterranean, EOS *The Oceanography Report* **69** (14), 194-203.
6. Milliff, R.F. (1990). A Modified Capacitance Matrix Method to Implement Coastal Boundaries in the Harvard Open Ocean Model, *Mathematics and Computers in Simulations* **31**, 541-564.
7. Milliff, R.F. and A.R. Robinson (1991). Structure and Dynamics of the Rhodes Gyre System and its Dynamical Interpolation for Estimates of the Mesoscale Variability, ***Journal of Physical Oceanography***, in press.
8. Oguz, T. (1991). private communication.
9. Özsoy, E., A. Hecht and U. Unluata (1989). Circulation and Hydrography of the Levantine Basin: Results of POEM Coordinated Experiments 1985-1986, ***Progress in Oceanography* 22**, 125-170.
10. Özsoy, E., Lozano, C.J. and Robinson, A.R. (1991). A Baroclinic Quasigeostrophic Model for Closed Basins or Semi-Enclosed Seas with Islands, ***Mathematics and Computers in Simulations***, in press.
11. Pinardi, N. and A. Navarro (1991). Baroclinic Wind Adjustment Processes in the Mediterranean Sea, submitted manuscript.
12. The POEM Group (1991). General Circulation of the Eastern Mediterranean, submitted manuscript.
13. Robinson, A.R. and M. Golnaraghi (1991). Progress in Understanding the Eastern Mediterranean Sea, *ICSEM Proceedings*, Perpingon, France 1990.
14. Robinson, A.R., M. Golnaraghi, W.G. Leslie, A. Artegiani, A. Hecht, E. Lazzoni, A. Michelato, E. Sansone, A. Theocharis and U. Unluata (1991). Structure and Variability of the Eastern Mediterranean General Circulation, *Dynamics of Atmospheres and Oceans* **15** (3-5), 215-240.
15. Robinson, A.R., A. Hecht, N. Pinardi, J. Bishop, W.G. Leslie, Y. Rosentroub, A.J. Mariano and S. Brenner (1987). Small Synoptic/Mesoscale Eddies: The Energetic

Variability of the Eastern Levantine Basin. *Nature* **327** (6118), 131–134.

16. Robinson, A.R. and L.J. Walstad (1987). The Harvard Open Ocean Model: Calibration and Application to Dynamical Process, Forecasting, and Data Assimilation Studies. *Applied Numerical Mathematics* **3** (1–2), 89–131.

17. Roether, W. and R. Schlitzer (1991). Eastern Mediterranean Deep Water Renewal on the Basis of Chlorofluoromethane and Trituim Data. *Dynamics of Atmospheres and Oceans* **15** (3–5), 333–354.

18. Schlitzer, R., W. Roether H. Oster, H-G. Junghans, M. Hausmann, H. Hohannsen and A. Michelato (1991). Chlorofluoromethane and Oxygen in the Eastern Mediterranean. submitted manuscript.

19. Spall, M.A. and A.R. Robinson (1989). A New Open Ocean, Hybrid Coordinate Primitive Equation Model. *Mathematics and Computers in Simulations* **31** 241–269.

20. Walstad, L.J. and A.R. Robinson (1991). A Coupled Surface Boundary Layer Quasi-geostrophic Model for Mesoscale Mixed Layer Dynamics, submitted manuscript.

A NUMERICAL STUDY OF THE CIRCULATION IN THE MEDITERRANEAN SEA

Marco Zavatarelli and George L. Mellor
Princeton University
Program in Atmospheric and Oceanic Sciences
Princeton NJ 08544-0710
USA

February 1992

ABSTRACT

A primitive equation ocean model which makes use of a curvilinear orthogonal grid and of a sigma-coordinate system was used to study the general circulation of the Mediterranean Sea. The model was forced with monthly values of wind stress, heat and salinity flux values. In one experiment, the fresh-water river discharge of the Rhône, Ebro and Po rivers was also used.

The model simulates the circulation reasonably well and the results indicate that, in the western Mediterranean, the wind stress is very important in establishing the summer northward shift of the Atlantic inflow. The lateral boundary forcing, the surface heat and salinity flux are necessary to the maintenance of the cyclonic circulation in the northern Balearic Basin and enhance the summer reversal of the circulation in the Tyrrhenian Sea. A particularly interesting result is the existence of a seasonal variation in the Levantine Intermediate Water path .

In the Ionian Sea , the dynamic consequence of the wind-stress and the surface buoyancy flux tend to offset each other and the path of the Ionian Atlantic stream is seasonally invariant. In the Levantine Sea the dominant forcing mechanism is probably linked to the buoyancy fluxes, but we do not consider our results conclusive because it is probable that the climatological buoyancy fluxes are underestimated.

The Levantine Intermediate water formation in the north-central Levantine Sea (Rhodes gyre) and the deep water formation in the southern Adriatic Sea are reproduced quite well. However, deep water formation in the western Mediterranean is not produced by the model.

1. INTRODUCTION

This paper deals with the simulation of the general circulation of the Mediterranean Sea and augments previous basin-scale and regional modeling efforts. On a basin scale, modeling with primitive equation models were carried out by *Menzin and Moskalenko (1982)*, who studied the barotropic wind driven circulation. *Stanev et al. (1989)* utilized a coarse resolution model to investigate the response of the circulation to annual and seasonal forcing while the recent work of *Pinardi and Navarra (1991)* focused on the baroclinic wind driven circulation in a basin with simplified bathymetry. An inverse model was used by *Tziperman and Malanotte-Rizzoli (1991)* to calculate the seasonal climatological circulation from hydrological data.

Regional circulation studies were carried out by *Heburn (1987)* with a one-layer reduced gravity model of the western Mediterranean and by *Malanotte-Rizzoli and Bergamasco (1989; 1991)* who performed an extensive set of experiments with a primitive equation model to study the barotropic and baroclinic seasonal circulation of the eastern Mediterranean. *Preller (1986)* carried out a regional study for the Alboran Sea and *Malanotte-Rizzoli and Bergamasco (1982)* for the Adriatic Sea.

In this study, we focused on the seasonal variability of the circulation and on water mass formation processes to identify the most important forcing functions and the areas and mechanisms involved in the water mass transformation processes.

The following section is devoted to a description of the Mediterranean Sea, hydrological and oceanographical characteristics in the light of the most recent observational findings. Sections 3, 4 and 5 describe the model, the bathymetry, grid and the surface forcings respectively. Section 6 and 7 describe the characteristics of the numerical experiments and the calculated results. Finally in section 8 we offer discussion and conclusions.

2: BACKGROUND

The Mediterranean Sea (Fig. 1) is an enclosed Basin connected to the Atlantic Ocean by the narrow (width ~ 13 km) and shallow (sill depth ~ 300 m) Strait of Gibraltar and the Black Sea is connected by the Dardanelles - Marmara Sea - Bosphorus system. It lies between 30° and 46° N and between -4° and 36° E and is essentially formed by two sub-basins, the western (WMED) and the eastern (EMED) Mediterranean, connected by the Strait of Sicily whose sill depth is ~ 300 m, and width ~ 35 km.

The WMED has a triangular shape with the Strait of Gibraltar, the island of Sicily and the Ligurian Sea at its apexes. Excepting the Gulf of Lions, the continental shelves are narrow. The Tyrrhenian Sea, between the Italian peninsula and the islands of Sardinia and Corsica, is the easternmost and deepest (depth ~ 3500 m) part of the Basin and joins the rest of the WMED to the south in a wide opening between Sardinia and Sicily. The Balearic Sea (depth ~ 2500 m) occupies the central part of the Basin and extends northeast to the Ligurian Sea and west, toward Gibraltar, to the Alboran Sea.

The EMED has a more complicated structure than the WMED. Four sub-basins can be defined: the Ionian, the Levantine, the Adriatic and the Aegean Seas. The Ionian Sea lies between southern Italy and Greece to the north and Lybia and Tunisia to the South, has a depth of about 3500 - 4000 m, with a maximum of 5000 m south of Greece. The Gulf of Sirte is the southernmost area of the Mediterranean Sea. The Levantine Sea has a roughly rectangular shape with depths of about 2500 - 3000 m in the center of the Basin and a maximum depth of about 4500 m in a depression located southeast of the island of Rhodes. It merges with the Ionian Sea through the Cretan Passage (depth > 1500 m), between Crete and the Lybian coast. The Adriatic Sea is connected with the Ionian by the Strait of Otranto (width ~ 75 km, sill depth ~ 800m); its topography is characterized by an extended continental shelf to the north and by a relatively deep southern section. The northern end of the Adriatic (Gulf of Venice) is the northernmost area of the Mediterranean Sea. The Aegean Sea joins the Levantine Sea through several passages and straits, located between the Greek

and Turkish coast and the islands of Crete and Rhodes, with depths and widths ranging from 300 to 700 m and from 15 to 60 km respectively. It has very irregular coastlines and topography with many islands; its maximum depth is about 1500 m.

The hydrology and the circulation of the Mediterranean Sea waters are strongly affected by the surface energy and mass exchange with the atmosphere; the fresh-water budget is negative; i.e., the loss by evaporation exceeds the input by precipitation and river run-off. The estimated fresh-water deficit amounts to about 2100 km^3/year, corresponding to a sea level drop of about 1 m/year and to a residence time of about 75 - 100 years (*Hopkins, 1978*; *Bethoux, 1979*; *Tchernia, 1980*). The fresh-water deficit (about 5.5% of the total inflowing volume) is mainly replenished by the Atlantic surface waters flowing into the Mediterranean having a salinity of 36.25‰. The excess of salt is balanced by a deep outgoing flow of high salinity, 38.40‰.

The existence of the two superposed flows in the Strait of Gibraltar requires a transformation of the inflowing Atlantic waters and vertical movement which provide the link between the two flows and which determines the formation of three distinct water masses whose vertical distribution is schematized in Fig. 2. The surface waters flowing into the Mediterranean are subject to evaporation and mixing with the underlying waters, causing a progressive increase of the salinity; the surface value rises from 36.25‰ in the Gibraltar area to 37.25‰ in the Strait of Sicily and to values higher than 38.50‰ in the Levantine Sea. Such water forms the Modified Atlantic Water (MAW). Its west to east path across the Mediterranean can be tracked by a subsurface salinity minimum (*Lacombe and Tchernia, 1960*) progressively deepening from 20 to 50 m depth, representing the signature of their Atlantic origin.

The MAW overlies the Levantine Intermediate Water (LIW). Their depth range is 300 - 700 m in the WMED and 200 - 400 m in the EMED. They are the result of convection processes in the EMED occurring in the Rhodes - Cyprus area, and probably in other sectors of the Levantine Sea in winter (*Morcos, 1972*). At their source the LIW have a salinity of

about 39.10‰ and spreads to the whole Mediterranean (S = 38.70‰ at the Strait of Sicily), reaching Gibraltar where they form the Mediterranean outflow into the Atlantic Ocean.

The deep waters of the WMED and of the EMED are the result of intensive, deep convection processes, but their sources are distinct and separate. Moreover their interface depth with the LIW is deeper than the depth of the sill of Sicily, preventing any direct exchange between them. The source of the western Mediterranean deep water is located in the Gulf of Lions area and the water mass formation, the so-called MEDOC deep water formation, takes place in winter (*MEDOC Group, 1969; Sankey, 1973; Leaman and Schott, 1991*). There, intensive convective movements occur under the influence of cold and dry winds, causing the sinking and mixing of the relatively cold and salty surface waters to depths of about 1200 - 1500 m. The resulting water mass has a potential temperature, θ, of about 12.70° C and a salinity of 38.40‰. Such water mass can enter the Mediterranean outflow at Gibraltar without mixing with the LIW (*Kinder and Parrilla, 1987*). The source of the eastern Mediterranean deep waters is the Adriatic Sea (*Pollak, 1951*), where a water mass with θ = 13.60° C and S = 38.70‰ is formed in winter, again under the influence of wind, and spreads to the whole EMED deep Basin. The traditional interpretation of the deep water formation in the Adriatic Sea assigns a key role to the cooling and evaporative processes acting on the shelf waters of the northern Adriatic, causing their sinking along the continental slope. However, *Ovchinnikov et al. (1987)* observed a MEDOC-like deep water formation in the southern Adriatic producing dense waters flowing into the Ionian Sea over the Otranto sill, while the dense water formed in the northern Adriatic were not involved in the exchange.

Recent international research projects, such as the "Western Mediterranean Circulation experiment", WMCE (*La Violette, 1990*), "Mediprod 5" (*Millot, 1991*) and the "Physical Oceanography of the Eastern Mediterranean", POEM (*Robinson et al., 1991*), provide new and important information about the general circulation of the Mediterranean Sea, revealing

general patterns more complex than those depicted by earlier studies (*Lacombe and Tchernia, 1960; Ovchinnikov and Fedoseyev, 1965; Ovchinnikov, 1966*).

The surface and intermediate circulation of the WMED is illustrated in Fig 3, according to *Millot (1987a; b; 1991)*. At the surface the Atlantic water entering the Basin forms, in the Alboran Sea, two anticyclonic gyres (*Heburn and La Violette, 1990*). The eastern side of the eastern Alboran gyre constitutes the Almeria-Oran front (*Tintore et al., 1988; Arnone et al., 1990*), a strong density front (representing the contact between the inflowing Atlantic water and the resident water of the Mediterranean) which deflects the MAW flow toward the African coast and originates the Algerian current flowing along the Algerian coast between 0° and 2° E. The current becomes progressively unstable and generates mesoscale eddies both cyclonic and anticyclonic. Observations (*Millot, 1985*) showed that only the anticyclonic eddies survive, increase in size, propagate eastward and can leave the coast and drift into the Balearic Basin. Thus the MAW do not only flow eastward toward the Strait of Sicily, but can be advected northward by the eddies, finally coming in contact with more modified MAW in the northern Balearic Basin, giving rise to the north Balearic front. Such a pattern also implies that the MAW flow into the EMED is controlled by "eddy shaped sporadic events" (*Millot, 1987a*).

The LIW circulation in the WMED has been the subject of many studies and speculations. It is accepted that at the exit of the Strait of Sicily The LIW turns around the western tip of Sicily into the Tyrrhenian Sea where it cyclonically flows along the Italian coast. Before entering the Ligurian Sea, the LIW current originates a branch flowing south and subsequently turning north around Sardinia. According to *Wust (1961)* and *Ovchinnikov (1966)*, the LIW exiting the Tyrrhenian Sea originates a further branch proceeding directly westward to the Strait of Gibraltar, explaining the presence of a LIW layer off the North-African coasts. This view has been questioned by *Katz (1972)* and *Millot (1985)* on the basis of field studies and simple theory. The LIW presence in the Algerian Basin is now

assumed to result from sporadic erosion of the LIW current by the mesoscale eddies originating from instability of the Algerian current.

The circulation of the EMED, relative to the upper thermocline, is shown in Fig. 4. The general circulation appears to be dominated by sub-basin gyres interconnected by jets. The MAW enters the EMED and flows through the Ionian Sea (Ionian-Atlantic Stream) into the Levantine Sea (Mid-Mediterranean Jet), where the following gyres are present throughout the year (*Ozsoy et. al., 1989; 1991*): a cyclonic gyre between Rhodes and Cyprus (Rhodes gyre) and one south of Crete (Cretan gyre), an anticyclonic gyre off the coast of Egypt (Mersa -Matruh gyre) and a wide anticyclonic area in the north-eastern Levantine Basin (Shikmona eddy). The Mid-Mediterranean jet flows between the Rhodes and the Mersa-Matruh gyres and then bifurcates twice, east and west of Cyprus. The northward branch originating west of Cyprus feeds the Asia-Minor current, while the southward branch enters the south-eastern Levantine anticyclonic region. Although not shown in Fig. 4, another permanent feature in the EMED circulation is the southern Adriatic cyclonic gyre (*Malanotte-Rizzoli and Hecht, 1988*).

3: THE OCEAN MODEL AND THE GRID.

The ocean model is the Princeton ocean model, described in detail by *Blumberg and Mellor (1987)*. The description of the model computer code can be found in *Mellor (1991a)*. It has been applied to the South Atlantic Bight (*Blumberg and Mellor, 1983*), Delaware Bay (*Galperin and Mellor 1990a, b*), the Hudson-Raritan Estuary (*Oey et al., 1985a, b, c*), the Gulf of Mexico (*Blumberg and Mellor, 1985*), and the Gulf Stream (*Ezer and Mellor, 1991*) and some thirty or more additional oceanic regions. It is a primitive equation model with a free surface, a split mode time step and solves the following equations for the ocean velocity $U_i = (U,V,W)$, potential temperature θ and salinity S:

$$\frac{\partial U_i}{\partial x_i} = 0 \qquad (1)$$

$$\frac{\partial}{\partial t}(U, V) + \frac{\partial}{\partial x_i}[U_i\,(U, V)] + f(-V, U) = \frac{1}{\rho_o}[\frac{\partial p}{\partial x}, \frac{\partial p}{\partial y}] + \frac{\partial}{\partial z}[K_M \frac{\partial}{\partial z}(U, V)] + (F_U, F_V) \qquad (2)$$

$$\frac{\partial \theta}{\partial t} + \frac{\partial}{\partial x_i}(U_i \theta) = \frac{\partial}{\partial z}[K_H \frac{\partial \theta}{\partial z}] + F_\theta + \frac{\partial R}{\partial z} \qquad (3)$$

$$\frac{\partial S}{\partial t} + \frac{\partial}{\partial x_i}(U_i\, S) = \frac{\partial}{\partial z}[K_H \frac{\partial S}{\partial z}] + F_S \qquad (4)$$

The vertical mixing coefficients K_M and K_H in (2), (3) and (4) are calculated using the *Mellor and Yamada (1982)* turbulence closure scheme, while the horizontal diffusion terms (F_U, F_V), F_θ and F_S in (2), (3) and (4) are calculated using a Smagorinsky horizontal diffusion formulation (*Mellor and Blumberg, 1985*). The term R in (3) is the portion of the short-wave radiation which penetrates the sea surface.

The hydrostatic approximation yelds:

$$\frac{p}{\rho_o} = g(\eta - z) + \int_z^\eta \frac{\rho' - \rho_o}{\rho_o}\, dz' \qquad (5)$$

where $\eta\,(x,y)$ is the free surface elevation, ρ_o the reference density and $\rho = \rho\,(\theta, S, P)$ is the density calculated by an adaptation of the UNESCO equation of state by *Mellor (1991b)* which is computationally simpler and which has potential temperature rather than *in situ* temperature as its argument.

The model uses a bottom-following sigma coordinate system ($\sigma = (z - \eta)/(H + \eta)$ where $H(x, y)$ is the bottom topography). The transformed equations can be found in the papers cited above. In the present study the model has 16 vertical layers, corresponding to the following sigma coordinates: 0.000, -0.003, -0.006, -0.012, -0.025, -0.050, -0.100,

-0.200, -0.300, -0.400, -0.500, -0.600, -0.700, -0.800, -0.900, -1.000.

The model grid is the curvilinear orthogonal grid shown in Fig. 5 and contains 113 x 39 points. The grid resolution ranges from a minimum of 8 to 15 km in the Alboran Sea region to a maximum of 50 to 60 km in the northernmost part of the Basin.

The model has one open boundary in the Atlantic Ocean about 200 km west of the Strait of Gibraltar. The normal velocities are governed by a Sommerfeld radiation condition. Temperature, salinity and tangential velocities on the boundary are upwinded: when the flow is into the model domain they are prescribed from the observed climatology and the boundary values are advected into the model domain.

4: THE MODEL BATHYMETRY AND THE INITIAL CONDITIONS

The model bathymetry was obtained from the U.S. Navy bathymetric data base, DBDB5, by bilinear interpolation of the depth data into the model grid. The resulting topography is illustrated in Fig. 6 and shows the major features of the basin's geometry, which retains the island of Sardinia, Corsica, Sicily, Mallorca, Crete, Cyprus and Rhodes. The connections with The Black Sea is closed.

The model has been initialized with the temperature and salinity annual climatological averages prepared by the National Institute for Oceanography and Fisheries at Alexandria (Egypt), using the NODC (National Oceanographic Data Center) and the WDC (World Data Center) data-bases. The annual averages are mapped on a 1/4° x 1/4° grid at the following 27 depth layers: 0, 10, 20, 30, 50, 75, 100, 125, 150, 200, 250, 300, 400, 500, 600, 700, 800, 900, 1000, 1100, 1200, 1300, 1400, 1500, 2000, 2500, 3000 m depth. The grid points with missing data were filled by interpolation of the surrounding values. The surface temperature and salinity annual averages are shown in Fig. 7.

5: THE SURFACE BOUNDARY CONDITIONS

The surface boundary conditions are surface heat flux, surface salinity flux and wind-stress. The monthly surface heat flux and wind-stress averages were obtained by *May (1982; 1986)*. These climatologies are mapped on a 1° x 1° grid. The surface heat flux is: short wave radiation, Q_s, long-wave back radiation, Q_l, sensible heat flux, Q_h, and latent heat flux, Q_e; the total heat flux, Q_t , is then given by:

$$Q_t = Q_s - Q_l + Q_h + Q_e \qquad (6)$$

In the model $Q_l + Q_h + Q_e$ plus a portion of the short-wave radiation is absorbed at the surface where the boundary condition is:

$$(K_H \frac{\partial \theta}{\partial z})_{z=0} = (1\text{-}Tr)Q_s + Q_l + Q_h + Q_e \qquad (7)$$

the remainder is directly added to the heat equation (3) as $\partial R/\partial z$, where:

$$R = Q_s Tr \exp(\lambda z) \qquad (8)$$

The transmission coefficient Tr = 0.31 and the attenuation coefficient $\lambda = 0.042\ m^{-1}$ are chosen to fit *Jerlov's (1976)* tabulated attenuation functions for "clear" water type.

The total heat flux fields for the months of February and August, calculated according to (6), are shown in Fig. 8. The February field shows a large cooling area over the Gulf of Lions (WMED), while the EMED is characterized by a zonal pattern with the largest negative values in the northern part of the Basin (around Rhodes). In August, the heat flux is positive everywhere but again the minimum values are found in the Northern Balearic Basin and in the Rhodes region.

The wind-stress fields for the same months are illustrated in Fig. 9 and exemplify the wind regime over the Mediterranean throughout the year. One sees evidence of the gaps between the mountain ranges bordering the northern Mediterranean coasts. The most prominent winter feature characterizing the WMED is the occurrence of a strong northerly wind, the Mistral, blowing from the Rhône river valley through the opening between the Alps and the Pyrenees. In the EMED the wind-stress is mostly zonal. In the northern Adriatic there occurs an easterly wind, the Bora, blowing over the sea from the opening between the Alps and the Dynaric Alps; this wind can be very strong but it is not as frequent as the Mistral and, climatologically, it results in only a slightly larger stress. In August, the Mistral still affects the WMED although with reduced stress. In the EMED, the dominant winds are the Etesians, blowing from the opening between the Balkans and the Anatolian mountains over the Levantine Sea with a cyclonic curvature. The wind-stress direction over the Adriatic and the Ionian Sea is mainly meridional.

The monthly evaporation rate (E) was calculated from *May's* latent heat flux data according to:

$$E = \frac{Q_e}{L_v} \tag{9}$$

where L_v is the latent heat of condensation. The monthly precipitation rate (P) was obtained from *Jaeger (1976)*, whose data are mapped on a 5° x 2.5° grid. Finally the fresh-water surface flux (W_S) was calculated according to:

$$W_S = E - P \tag{10}$$

and the surface boundary condition for salinity is:

$$\left(K_H \frac{\partial S}{\partial z}\right)_{z=0} = W_S S_0 \tag{11}$$

The calculated total annual fresh-water loss amounts to 92.0 cm/year (a value which agrees reasonably well with the results of many budget calculations) and the monthly averages range between a minimum of 3.6 cm/month (May) and a maximum of 10.5 cm/month (August). The W_S fields for the months of February and August are shown in Fig. 10 and are very similar to the total heat flux fields of Fig 8., the reason for which is the dominant influence of the latent heat flux component over both fields, as pointed out by *Malanotte-Rizzoli and Bergamasco (1991)* in their analysis of surface flux fields.

All the surface boundary conditions were applied to the model by interpolating linearly between adiacent monthly values.

In one numerical experiment (see below), the annually averaged fresh-water river discharge for the Rhône, Ebro (WMED) and Po (Adriatic Sea) rivers were added to the model. The averages values (Rhône = 1712 m^3/s, Ebro = 550 m^3/s, Po = 1550 m^3/s) are those reported in *UNEP (1984)*.

6: THE NUMERICAL EXPERIMENTS

We give here a brief description of the numerical experiments performed using different kinds of surface forcings. Their characteristics are summarized in Table 1.

Table 1: Characteristics of the numerical experiments.

EXPERIMENT	WIND-STRESS	THERMAL SURF. CONDITION	SALINITY SURF. CONDITION	RIVER RUNOFF
MED-1	Monthly	Surf. temperature equal to initial conditions	Surf. salinity equal to initial conditions	no
MED-2	Monthly	Monthly heat flux	Constant salinity flux	no
MED-3	Monthly	Monthly heat flux	Surf. salinity equal to initial conditions	no
MED-4	Monthly	Monthly heat flux	Monthly salinity flux	Annual

Experiment MED-1: In this experiment the model was forced with the monthly wind-stress averages, while the surface temperature and salinity were prescribed to be equal to the annual averages (initial conditions) in order to simulate perpetual annual average conditions.

Experiment MED-2: The forcing were the monthly averaged wind stress and the monthly surface heat flux. The surface salinity flux was constant in time and space and was obtained by prescribing a surface fresh-water flux of 1 m/year, corresponding to the estimated annual W_S average for the whole Mediterranean Sea (*Bethoux, 1979*).

Experiment MED-3: The wind-stress and surface heat forcing were analogous to Experiment MED-2, but the surface salinity value was prescribed to be equal to the annual averages.

Experiment MED-4 (the central experiment): the monthly climatological averages were used for all the surface fluxes and the fresh-water inputs, described above, were introduced.

The integration time was 5 years for experiments MED-1, MED-2, MED-3 and 6 years for experiment MED-4, but we show here the results relative to the fifth year of integration in order to be consistent with the other experiments; the results relative to the sixth year results do no show significant differences with those of the fifth year.

7: RESULTS

Experiment MED-1

In experiment MED-1, we examine the effects of the seasonal wind-stress forcing by eliminating any seasonality in the surface heat and salinity fluxes. The surface elevation fields and the velocity field at 50 m depth for the months of February and August are shown in Figs. 11 and 12 respectively. The surface circulation in the WMED is dominated by the MAW inflow along the North African coast and by the cyclonic circulation in the northern Balearic Basin and in the Tyrrhenian Sea. The water incoming from the Atlantic Ocean flows in the Alboran Sea along the coast of Spain and bend southward at the exit of the Sea, forming a front resembling the Almeria-Oran front, from which, in winter, originates a

current moving along the African coast. In summer the circulation in the southern Balearic Basin undergoes a major change: the flow along the African coast is reversed and two anticyclonic gyres are formed. Throughout the year, the flow from the Atlantic Ocean feeds both the cyclonic circulation in the Tyrrhenian Sea and the flow into the EMED. In winter, the MAW Ionian-Atlantic Stream enters the Basin via the Strait of Sicily, bends south and subsequently bifurcates into two branches, one closely following the African coast and directly entering the Levantine Sea, the other meandering in the Ionian Sea and becoming entrained in the large cyclonic gyre developed in the northern Ionian Sea. In summer, the Ionian-Atlantic Stream shifts northward along the eastern coast of Sicily and is entrained into a broad anticyclonic gyre, occupying the whole central part of the Basin. The jet is blocked from flowing into the Levantine Sea by a cyclonic gyre comparable with the Cretan gyre described by the POEM data (Fig.4). The coastal following branch of the winter jet reverses its direction in summer. In the Levantine Sea, the circulation along the coast is cyclonic throughout the year and appears, in winter, directly connected to the Ionian-Atlantic stream, while in summer the current weakens and originates from the Cretan gyre. In the interior of the Basin a meandering jet comparable with the Mid-Mediterranean jet flows eastward, bordering a wide cyclonic gyre whose location and shape correspond to the Rhodes gyre. In summer other anticyclonic gyres develop: one south-east of Crete, one south of the Rhodes gyre similar to the Mersa-Matruh gyre and one south of Cyprus, similar to the Shikmona gyre. Furthermore two interconnected cyclonic gyres close to the Egyptian coast that appear as in the POEM maps of *Ozsoy et al. (1989)* and in the geostrophic calculations by *El-Din and Karam (1976)*.

The circulation at intermediate depth in February and August is shown in Fig. 13. In the WMED the LIW circulation look very similar to the pattern proposed by *Millot (1985)* and described in section 2. The return flow from the EMED in winter crosses the Strait of Sicily and turns around Sicily entering the cyclonic circulation of the Tyrrhenian Sea, from which the LIW exits, then flows around Sardinia, circulates into the cyclonic gyre in the

Balearic Basin and reaches the Alboran Sea moving along the French and Spanish coasts. In summer, the cyclonic circulation in the Tyrrhenian Sea becomes very weak and the LIW bypasses this Basin and flows directly into the Balearic Basin along the coast of Sardinia.

In the EMED, more precisely in the Ionian Sea, there are seasonal differences in the origin of the LIW flow into the WMED. In winter, two currents, coming from the Southern and the Northern Ionian, join south of Sicily to form the outflow and there is no direct contribution from the Levantine Sea. In summer, the flow along the eastern coast of Sicily weakens and the flow toward the WMED is formed mainly by the current from the southern Ionian, which is also partially fed by a flow exiting the Levantine Basin and recirculating into the cyclonic gyre developed in the Gulf of Sirte. Except for this current, the circulation of the Levantine Sea is more or less constant throughout the year and is mainly characterized by a cyclonic gyre with a SW-NE elongation in the center of the Basin centered over the area of maximum depth and by the same anticyclonic gyres observed at the surface.

The deep circulation (Fig. 14) does not show a pronounced seasonal variation. In the WMED the flow in the northern Balearic Basin and in the Tyrrhenian Sea is reversed with respect to the surface and intermediate layers, while in the southern part of the Basin the flow is still directed eastward.

In the EMED The Ionian Sea is fed by water coming from the Adriatic Sea: part of it moves toward the Strait of Sicily and part recirculates into the cyclone in the southern Ionian and enters the Levantine Sea, where the circulation is dominated by a large cyclonic gyre, occupying the greater part of the Basin, whose shape and position are clearly influenced by the bottom topography (Figs. 1 and 6).

Experiments MED-2 and MED-3

As a second step in our study we performed an experiment forcing the model with the monthly surface heat flux and with a constant salinity flux obtained by prescribing a fresh-water flux of 1 m/year. Despite the utilization of a more realistic seasonal forcing the results

of the experiment MED-2 were not entirely satisfactory. The major problem was that, after 5 years of integration, the cyclonic circulation in the northern Balearic Basin almost disappears: i.e. it is very weak in winter and practically non existent in summer (Fig. 15); furthermore the anticyclonic area developing in summer in the meridional part of the Basin is ill defined. The circulation features in the EMED are more satisfactory and comparable with the results of experiment MED-1.

In order to understand if the problems in the northwestern Basin were caused by the surface heat flux or by the surface salinity flux, experiment MED-3 (property fields not shown) was carried out, whereby the model was driven with monthly averaged wind-stress and surface heat flux, but the surface salinity was mantained equal to the annual average. This experiment gave a more satisfactory result, indicating that the choice of a constant salinity flux is probably incorrect; this led us to the experiment which is described below.

Experiment MED-4

Monthly averaged surface salinity fluxes, according to equation (11) and river runoff in the north-western Basin were introduced and improved the performance of the model. The Basin averaged temperature and salinity time history is shown in Fig. 16 and indicates that the model acquires a periodical seasonal cycle. The free surface elevation and velocity surface fields for the months of February and August are shown in Figs. 17 and 18 respectively. The cyclonic gyre in the northern Balearic Basin, although weak in summer, is mantained throughout the year, demonstrating the importance of the salinity surface flux and lateral boundary runoff in this area. With respect to the results of experiment MED-1 a major difference arises in the Alboran Sea region in winter, where two small anticyclonic eddies are formed close to the Moroccan coast, while the main flow of Atlantic water is in the north. Immediately west of the Alboran Sea, the model generates a large and intense (particularly in summer) anticyclonic eddy. In the scientific literature there is no strong evidence of the existence of such a gyre. The only indication comes from the work of *Green and Price*

1991) who tracked buoys deployed in the Alboran Sea and in the Southern Balearic Basin. Their results show that the buoys were occasionally entrained into an anticyclonic eddy which they associate with the Almeria-Oran front. It is interesting to note that, as in the summer of experiment MED-1, the surface flow in the Southern Balearic Basin is characterized by the development of anticyclonic eddies, which in this experiment appear to originate from the described eddy/frontal feature and to propagate eastward. Thus it seems that the model is attempting to reproduce some features of the instability processes of the Algerian current leading to the formation of anticyclonic eddies observed in the southern Balearic Basin.

Another important difference between this experiment and experiment MED-1 occurs in the Tyrrhenian Sea, where, in experiment MED-4, and in agreement with the results of *Tait (1984)* and *Krivosheya and Ovchinnikov (1973)*, in the interior of the Basin the circulation exhibits a strong winter to summer variability, reversing from cyclonic to anticyclonic, while a northward flow along the Italian coast persists throughout the year. A consequence of such reversal is the reduced summer inflow of the MAW in the Tyrrhenian Sea.

In the EMED, the seasonal variability induced by wind stress, seen in experiment MED-1, now seems to be offset by the surface heat and buoyancy fluxes. In this experiment the summer formation of the large anticyclonic gyre in the central Ionian Sea does not occur and the path of the stream simply shifts northward forming a wide anticyclonic meander extending from Sicily almost to the eastern coast of the Gulf of Sirte. Subsequently the stream turns north forming a narrow cyclonic meander and enters the Levantine Sea. The northern portion of the Ionian Sea is occupied by a cyclonic gyre, more intense in winter and weaker in summer, during which it exchanges water with the permanent cyclonic gyre located in the southern Adriatic Sea (*Malanotte-Rizzoli and Hecht, 1988*). The persistence of the cyclonic gyre in this area of the Ionian Sea constitutes one of the major differences between the results of our model and the seasonal maps of the Mediterranean climatological circulation obtained by *Tziperman and Malanotte-Rizzoli (1991)* utilizing an inverse model:

their results show a seasonal reversal of the circulation, being cyclonic in winter and anticyclonic in summer. In The Levantine Sea the most prominent permanent feature is, as in experiment MED-1, the Rhodes gyre. In the Cretan Passage the Mid-Mediterranean jet forms a cyclonic meander, but a clear development of an anticyclonic gyre, comparable to the Mersa-Matruh gyre, does not occur. Another absent feature that is the Shikmona gyre which developed (weakly) in experiment MED-1; in this experiment only a small anticyclonic meander appears in front of the Israeli coast. The eastern Mediterranean model developed by *Malanotte-Rizzoli and Bergamasco (1991)* exhibits the same behaviour. They attributed this model deficiency to the *May (1982)* surface heat flux data, whose magnitude they thought to be underestimated. This may be the case, but the Shikmona eddy may also be controlled by bottom topography and particularly by the Eratosthenes sea-mount, rising from the sea bottom (~2000 m) to ~600 m depth, *(Brenner et. al., 1991)*. Our model barely resolves such topographical feature.

Despite these possible discrepancies, other surface features are represented reasonably well, in particular the northward branching of the Mid-Mediterranean jet west and east of Cyprus, both branches feeding the Asia-Minor Current flowing westward along the Turkish coast and becoming the northern side of the Rhodes gyre.

At intermediate depth, Fig. 19, the circulation pattern in the WMED substantially reproduce the patterns obtained in experiment MED-1, with the important, exception of the Tyrrhenian Sea. In particular, it is noted again that no direct LIW flow from the Strait of Sicily to the Alboran Sea develops, the path being blocked by an anticyclonic gyre. The LIW, once again, reaches the Strait of Gibraltar by flowing along the northwestern Mediterranean coast, transiting by the Tyrrhenian Sea in winter and bypassing it in summer. The entrance of the LIW into the Tyrrhenian Sea appears controlled by the flow reversal occurring between winter and summer and which was not observed in experiment MED-1.

In the EMED the LIW outflow through the Strait of Sicily is formed, similarly to experiment MED-1, by two currents coming from the Northern and Southern Ionian, but no

weakening of the northern current occurs in summer. The central Ionian and the Cretan Passage are permanently occupied by two anticyclonic gyres. In winter the LIW recirculates into the gyre located south of Crete; in summer the two gyre become interconnected and the LIW exit the Levantine Sea without any recirculation. In the northern Ionian and in the southern Adriatic, the flow is cyclonic over the entire year. In the Levantine Sea the cyclonic gyre observed in the previous experiment occupies the center of the Basin, is less intense and east of Rhodes an anticyclone, similar to the Anaximander gyre of Fig. 4, is developed.

The circulation at 1200 m depth, Fig. 20, is more stable throughout the year, and shows marked differences with the results of experiment MED-1 in the WMED, where the circulation in the northwestern Basin does not reverse and remains cyclonic. In the Tyrrhenian Sea, dominated by a double gyre. In the EMED the circulation is still characterized by the cyclonic circulation encircling the whole Ionian Sea (fed by water of Adriatic origin) and by the cyclonic flow in the Levantine Sea.

The distribution of scalar properties and the transformation of water masses.

We describe now the temperature and salinity horizontal distribution, obtained in the last year of integration of the experiment MED-4. Fig. 21 shows the surface temperature distribution for the months of February and August. The WMED winter surface temperature ranges from minimum values slightly lower than 12° C, approximately in the center of the northern Balearic cyclonic cell, to maximum values slightly higher than 14° C (western Alboran Sea). Such values appear to be about 1° C colder with respect to the monthly climatologies published by *ENEA (1990)* . The tendency of the model to produce temperature values lower than the observed data in the WMED is more evident in summer where the difference between the model results and the abovementioned climatologies is about 2-3° C. However, the horizontal surface temperature distribution pattern in summer looks qualitatively similar to the observations. The minimum values are located approximately in the center of the cyclonic area of the northern Balearic Basin.

In the EMED the temperature surface values are closer to the observed data (*Anati, 1977, Ovchinnikov, 1984*). In winter the temperature increases west to east from 14° to 17° C. In the center of the Rhodes gyre the water temperature is about 15° C, a value corresponding to the LIW source water temperature. In summer, in the southern Ionian Sea and in the Cretan Passage (the area of the Ionian-Atlantic Stream) the isotherms are zonally oriented marking the MAW flow; the temperature decreases northward from 27° to 21° C. In the Levantine Sea, on the contrary, the isotherms tend to assume a meridional orientation.

The surface salinity fields for the same months are shown in Fig. 22. In the surface field the MAW inflow in the southern Balearic Basin is evident throughout the year as a progressive increase of the salinity value from west to east. However, from winter to summer the MAW inflow influences more the interior of the Balearic Basin, as indicated by the northward displacement of the isohalines, which tend to group in the area between the Balearic Islands and Sardinia, giving hints of the formation of a structure similar to the north Balearic front. To the north the salinity distribution reflects the cyclonic circulation already described.

As in the case of temperature, the surface salinity values of the WMED generated by the model do not match the observed data very well; the model values are 0.15 - 0.20 $^{o}/_{oo}$ lower, although the distribution is qualitatively similar to observed fields. Also in the EMED the surface salinity values increase from west to east reaching the maximum values (> 39.20 $^{o}/_{oo}$ in winter and > 39.60 $^{o}/_{oo}$ in summer) in the Levantine Sea. The isohalines have a predominantly meridional orientation. The transformation of the MAW salinity value under the effect of the surface forcing is, obviously, more rapid in summer than in winter; for example the salinity of the MAW entering the Levantine Sea in winter is about 38.50 $^{o}/_{oo}$, while in summer they have a value of about 39.00 $^{o}/_{oo}$.

The temperature and salinity horizontal distribution at 300 m depth in February and August (Fig. 23 and 24 respectively) reflects the circulation patterns described above; in particular the temperature field shows clearly the cyclonic circulation in the northern Balearic

Sea and the LIW outflow in the Cretan Passage, whereas the salinity fields reflects the anticyclonic circulation in the Ionian Sea. Fig. 24 also shows that, at 300 m depth the salinity values in the WMED are lower than reality, in particular in the southern Balearic Sea.

Fig.25 shows the location of several cross sections obtained by bivariate interpolation from the curvilinear grid and described below in order to illustrate the vertical distribution of water masses. Fig. 26. shows the February and August salinity distribution along the cross-section A. The discrepancy between the observed salinity data and those created by the model is particularly evident at depths between 300 and the 600 m, the LIW layer, where, in comparison with the nearby cross-sections by *Katz (1972)* and *ENEA (1990)*, the salinity is fresher by about 0.20 - 0.40 $^{o}/_{oo}$. The salinity decrease at intermediate depths occurs progressively throughout the integration time of every numerical experiment performed and it does not seem likely that such decrease is caused by the surface flux forcings. It is possible, however, that this freshening depends upon the anticyclonic circulation developed in the southern Balearic Basin at these depths and may be caused by excessive vertical mixing with water from the upper layers.

The salinity vertical distribution in Fig. 26 shows also that, despite such discrepancies, the model is successful in reproducing and maintaining one of the most important and typical features of the Mediterranean Sea thermohaline structure, the well known summer development of a subsurface salinity minimum marking the path of the MAW flowing into the Basin which is modified by the surface warming and fresh-water losses. The salinity minimum is clearly defined in the WMED at depths of about 30 - 50 m and it extends throughout the whole Basin, reaching the Strait of Sicily and developing also in the EMED at a depth of about 50 m (cross-section C, Fig.27) as far as the Cretan Passage and vanishing into the Levantine Sea. In both basin the salinity minimum is not developed in winter and appears only during the summer season throughout the entire integration time of the model.

In Fig. 27 we show also another important feature that the model reproduces, the presence of a LIW core with a salinity value greater than 38.80 $^{o}/_{oo}$, which occupies almost

all of the Levantine Sea and extends partially into the Ionian Sea through the Cretan Passage. The development of a LIW core led us to investigate the location of its source. The northern/central sector of the Levantine Sea (or Rhodes-Cyprus area) is a well investigated LIW source area (see, for instance *Ovchinnikov, 1984*) so that in Fig. 28 we show the winter distribution of potential temperature, salinity and sigma-θ along the meridional cross-section C, encompassing the whole Levantine Sea and crossing the Rhodes-Cyprus region. The temperature distribution shows the doming of the isotherms in the center of the section determined by the Rhodes cyclone circulation (*Anati, 1984*) and, overlying the dome, a layer of water with a thickness of about 300 m having homogeneous characteristics: potential temperature between 15.25 and 15.50° C, salinity greater than 39.05 $^{o}/_{oo}$ and a sigma-θ value comprised between 29.00 and 29.05. Such values are in close agreement with the values observed during LIW formation in the Rhodes gyre (*Ovchinnikov, 1984*). The general features of the thermohaline structure illustrated in the section indicate that two factors concurrently operate to break the surface water stratification and to form a relatively deep water layer with homogeneous properties: one is the divergence bringing dense water closer to the surface, the second are the thermal and the evaporative losses, which determine the winter buoyancy fluxes resulting in the increase of surface water density and convective mixing.

Lastly, we illustrate the model results relative to the formation of the deep water masses in the Adriatic Sea and in the northern Balearic Basin source areas. In Figs. 29 and 30 we show the potential temperature and sigma-θ winter distribution along section E, crossing the whole Adriatic Basin from the Gulf of Venice to the Strait of Otranto. The distribution of such properties is plotted at a 10 days interval for the period February 1 - February 30 of the climatological year. The potential temperature plots show the shallow northern Adriatic occupied by a cold water mass whose temperature increases to the south from ~11° to 13° C. The shapes of the isotherms indicate the flow of bottom water along the continental slope. The time evolution of the potential temperature distribution is clear evidence of the shelf deep

water formation process, i.e. the flow of cold waters along the continental shelf (*Artegiani and Salusti, 1987*) sliding into the southern deeper part of the Basin. In a time span of 30 days the greater part of the southern Adriatic water mass is cooled by about 0.25° C. Also the salinity distribution (not shown here) reflects the same patterns. The sigma-θ plots for the same period of time, confirm the existence of this process, but also give indications of a second deep-water formation process acting in the deeper southern Adriatic Sea. In fact the plot for the end of February (lower panel of Fig. 29) shows the formation of a surface layer whose sigma-θ value (29.25) equals the value of the underlying water mass, suggesting the potential for intensive convective mixing, developing according to a MEDOC like mechanism, as observed by *Ovchinnikov et. al. (1987)* in the southern Adriatic Sea. The newly formed dense water mass flows over the Otranto sill and spreads at depth to the whole EMED, as shown in fig 20.

Both processes are known to be dependent on air sea interactions, particularly wind related winter cooling and evaporation which determine the surface density increase and initiate the overturning and decay of the water column stratification (*Henderschott and Rizzoli, 1976*). In the southern Adriatic, a significant preconditioning role is also played by the permanent cyclonic circulation observed there (Fig. 18) that brings dense water closer to the surface as described previously in the case of LIW formation.

On the other hand, we were not able to find any significant evidence of intensive deep mixing of the water column in the northern Balearic Sea. Fig. 31 shows the salinity distribution along the cross section B in March. It can be noted that only a small and limited break in the stratification, extending from the surface to about 250 -300 m depth occurs in this period, during which deep water formation processes were observed; and the general distribution of salinity, density and temperature fields (not shown here) differ from those published by the *MEDOC group (1969), Stommel (1972) and Leaman and Schott (1991).* The different behaviour of the model in reproducing the deep water formation in the Adriatic Sea and in the Gulf of Lions is difficult to explain. The adjustment toward fresher salinity

values in the WMED, and the resulting surface water lighter than observed are probably playing an inhibiting role. Moreover, the coarse grid resolution is probably inadequate to capture the dynamic of the process and the use of climatological fluxes to force the model eliminates the strong wind (Mistral) bursts that start the deep water formation (*Bunker, 1972*), but these two factor are present also in the Adriatic Sea where the deep water is formed. We leave this apparent contradiction as an open question for further studies.

8: DISCUSSION AND CONCLUSIONS

The differences arising from the comparison of the results obtained from experiment MED-1 and MED-4 point out the relative importance of the seasonal wind stress and surface heat and salinity fluxes in modeling the general circulation of the Mediterranean Sea. In the WMED, both experiments provide a general picture of the surface circulation in the Balearic Basin characterized by a cyclonic circulation in the north and by the MAW inflow in the south which, in summer, generates mesoscale anticyclonic eddies originated by instabilities of the Almeria-Oran front/Algerian current system, and extends its influence farther north as defined by the position of the north Balearic front. The MAW flow in the WMED (as well as in the EMED) is characterized by the typical summer development of a salinity subsurface minimum. The substantial similarity between the two experiment, as well as the results of other modeling efforts (*Heburn, 1987; Pinardi and Navarra, 1991*), indicates that, in general, the wind-stress seasonality is a very important forcing factor. However, we have shown that the temporal and spatial variability in the surface salinity flux and the effect of fresh-water runoff are necessary to the maintenance of a realistic horizontal density gradient which drives the cyclonic circulation in the northern Balearic Basin. Moreover, the seasonal surface buoyancy flux seems to have an enhancing effect on the summer generation of the anticyclonic mesoscale eddies in the south and strengthens the seasonal reversal of the circulation in the Tyrrhenian Sea, which is extended in depth from the surface to the intermediate layers. This important seasonal change produces a variation in the LIW

circulation pattern, as the current reversal in the Tyrrhenian eliminates, or greatly reduces, the LIW flow into the Basin. Thus it seems that throughout the year the LIW circulation oscillates between a winter configuration similar to the hypothesis put forward by *Millot (1987b)*, involving the recirculation in the Tyrrhenian Sea and a summer configuration more in agreement with the interpretation given by *Katz (1972)* involving the direct flow of the LIW into the Balearic Basin along the western coast of Sardinia. This is obviously a topic requiring further observational and theoretical studies.

In the Ionian sea, the wind-stress and the surface buoyancy fluxes have a balancing effect on the seasonal variability of the Ionian-Atlantic stream, as the introduction of the surface fluxes in experiment MED-4 reduces the large northward shift of the stream occurring from winter to summer and the development of the broad anticyclonic gyre in the southern and central Ionian Sea. In the northern Ionian Sea, on the contrary, both experiments gave evidence of a weakening, in the transition from winter to summer conditions, of the observed cyclonic circulation. Thus the main forcing mechanism responsible for the weakening is the wind-stress.

An assessment of the leading forcing in the Levantine Sea is more problematic. The surface circulation is constituted of sub-regional gyres of both sign interconnected by the Mid-Mediterranean jet and the Asia Minor current. Both experiments reproduced the Rhodes gyre, the bifurcation of the Mid-Mediterranean jet east and west of Cyprus and the Asia Minor current. However, the Cretan cyclonic gyre, the Mersa-Matruh and Shikmona anticyclonic gyres appear better simulated in experiment MED-1 than in experiment MED-4. Such features appear very clearly in the geostrophic computations derived from the quasi-synoptical data collected during the POEM project *(Oszoy et al., 1989)*. The Mersa-Matruh gyre, in particular, constitutes the stronger signal observed. This evident discrepancy between models simulations and observations indicates a possible underestimation of the surface heat and salinity fluxes in the Levantine Sea area, whose effects on the circulation are probably counterbalanced by the wind-stress influence.

At intermediate depths the LIW outflow through the Strait of Sicily is reproduced well by the model. Their path across the EMED undergoes seasonal changes, particularly in the connecting flow between the Levantine and the Ionian Seas, across the Cretan Passage, which appears reduced in winter. The LIW current in the Ionian is entrained in the anticyclonic cell located in the center of the Basin and before entering the Strait of Sicily mixes furtherly with water coming from the northern Ionian Sea.

The water mass formation processes occurring in the Mediterranean Basin are strongly related to both the horizontal circulation and the surface fluxes. We have shown that the LIW and the deep water formation areas are coincident with horizontal cyclonic flows which cause causing doming of the underlying water and transport of dense water to the surface. On this structure, the surface fluxes create thermal and evaporative losses which lead to convective vertical mixing. The model results show that this mechanism is active in the Rhodes gyre region. An analogous, but more intense, situation responsible for the EMED deep water formation occurs in the southern Adriatic Sea. Intensive vertical mixing over the deeper part of the Basin and the shelf deep water formation are reproduced remarkably well by the model. However, the model did not produce realistically deep water formation in the WMED where in the northern Balearic Sea the model produces only a small and spatially limited homogeneous layer extending down to 200 m. We attribute this to the generalized adjustment of the WMED toward lower salinity values as well as, probably, to an insufficient horizontal resolution, but a precise assessment of the reason for the lack of deep water formation in the Gulf of Lions will require further studies.

Finally, we note that the use of climatological surface forcing fields eliminates completely from the model performance any influence on the circulation due to the interannual variability which in several areas of the Mediterranean Sea, such as the Adriatic, the Tyrrhenian Sea, the LIW and the deep water formation areas, can play a very important and significant role. The use of synoptic surface forcing fields together with a higher

resolution model will surely provide a better simulation and understanding of the circulation processes in the Mediterranean Sea.

9: ACKNOWLEDGMENTS

The support of the New Jersey Marine Science Consortium and the Agency for International Development under contract NEB-0158-G-SS-5192-00 *"A study of the circulation of the Levantine Basin"* and the support of NOAA's Geophysical Fluid Dynamics Laboratory are gratefully acknowledged. G.W. Heburn, S. Brenner and R.Slater kindly provided us with wind-stress, surface heat fluxes and precipitation data and I.A.Maiyza provided the annually averaged hydrological climatologies with which we initialized the model. Help and advice during the initial phase of this study were obtained from S.Levitus and M.Jackson.

10: REFERENCES

Anati D.A., 1977: Topics in the physics of the Mediterranean Seas. *Ph. D. Thesis, Weizmann Inst. Sci.*, 43 pp.

_____, 1984: A dome of cold water in the Levantine Basin. *Deep Sea Res.*, 31, 1251-1257.

Arnone R.A., D.A. Wiesenburg and K.D. Saunders, 1990: The origin and characteristics of the Algerian Current. *J. Geophys Res.*, 95, 1587-1598.

Artegiani A. and E. Salusti, 1987: Field observation of the flow of dense water on the bottom of the Adriatic Sea during the winter 1981. *Oceanol. Acta*, 10, 387-391.

Bethoux J.P., 1979: Budgets of the Mediterranean Sea. Their dependence on the local climate and on the characteristics of the Atlantic waters. *Oceanol. Acta*, 2, 157-163.

Blumberg A.F. and G.L. Mellor, 1983: Diagnostic and prognostic numerical circulation studies of the South Atlantic Bight, *J. Geophys. Res.*, 88, 4579-4592.

_____ and _____, 1985: A simulation of the circulation in the Gulf of Mexico. *Israel J. Earth Sci.*, 34, 122-144.

_____ and _____, 1987: A description of a three-dimensional coastal ocean circulation model. *Three-Dimensional Coastal Ocean Models, Coastal Estuarine Sci.*, 4, edited by N.S.Heaps, pp 1-16, AGU, Washington D.C., 1987.

Brenner S., Z. Rozentraub, J. Bishop and M. Krom, 1991: The mixed-layer/thermocline cycle of a persistent warm core eddy in the eastern Mediterranean. *Dyn. Atmos. Oceans*, 15, 457-476.

Bunker A., 1972: Wintertime interactions of the atmosphere with the Mediterranean Sea. *J. Phys. Oceanogr.*, 2, 225-238.

El-Din S. and Karam A., 1976: Geostrophic currents in the southeastern sector of the Mediterranean Sea. *Acta Adriatica*, 18, 221-235.

ENEA, 1990: *Climatological atlas of the western Mediterranean*. Santa Teresa Center for Energy and Environmental Research, 224 pp., La Spezia

Galperin B. and G.L. Mellor, 1990a: A time-dependent, three-dimensional model of the Delaware Bay and River. Part 1: Description of the model and tidal analysis. *Estuarine Coastal Shelf Sci.*, 31, 231-253.

_____ and _____, 1990b A time-dependent three-dimensional model of the Delaware Bay and River. Part 2: Three dimensional flow fields and residual circulation. *Estuarine Coastal Shelf Sci.*, 31, 255-281.

Green III D.W. and J.A. Price, 1991: Buoy tracks and circulation in the western Mediterranean. *Proc. Conf. MTS '91, New Orleans, November 10-14 1991*, 876-882.

Heburn G.W., 1987: The dynamics of the western Mediterranean Sea: A wind forced case study. *Ann. Geophys.*, 5B, 61-74.

_____ and P.E. La Violette, 1990: Variations in the structure of the anticyclonic gyres found in the Alboran Sea. *J. Geophys. Res.*, 95, 1599-1613.

Henderschott M.C. and Rizzoli P., 1976: The winter circulation of the Adriatic Sea. *Deep Sea Res.*, 23, 353-370.

Hopkins T.S., 1978: Physical processes in the Mediterranean basins.*Estuarine transport processes*, edited by B.Kjerfve, Univ. S. Carolina Press, pp. 269-310, Columbia, S. Carolina.

_____, 1985: Physics of the Sea.*Western Mediterranean*, edited by R. Margalef, Pergamon Press Publ., pp. 100-125, Oxford and N.Y.

Jaeger L., 1976: Monatskarte des niederschlags fur die ganze Erde, *Ber. Dtsch. Wetterdienstes*, Band 18, No1839.

Jerlov N.G., 1976: *Marine Optics*. Elsevier Sci. Pub., Amsterdam, 231 pp.

Katz E.J., 1972: The Levantine Intermediate water between the Strait of Sicily and the Strait of Gibraltar. *Deep Sea Res.*, 19, 507-520.

Kinder T.H. and G. Parrilla, 1987: Yes, some of the Mediterranean outflow does come from great depth. *J. Geophys. Res .*, 92, 2901-2906.

Krivosheya V.G. and I.M. Ovchinnikov, (1973): Peculiarities in the geostrophic circulation of the waters of the Tyrrhenian Sea. *Oceanology*, 12, 822-827.

Lacombe H. and P. Tchernia, 1960: Quelques trait generaux de l'hydrologie Méditerranéenne. *Cah. Oceanogr.*, 12, 525-547.

La Violette P.E., 1990: The Western Mediterranean Circulation Experiment: Introduction. *J. Geophys. Res.*, 95, 1511-1514.

Leaman K.D. and F.A. Schott, 1991: Hydrographic structure of the convection regime in the Gulf of Lions: winter 1987. *J. Phys. Oceanogr.*, 21, 575-598.

Malanotte-Rizzoli P. and A. Bergamasco, (1982): Hydrodynamics of the Adriatic Sea. *Hydrodynamics of semi-enclosed seas*, edited by J.C.Nihoul, pp. 177-186, Elsevier Sci. Pub., Amsterdam.

_____ and _____, 1989: The general circulation of the eastern Mediterranean. Part I: the barotropic wind-driven circulation. *Oceanol. Acta*, 12, 335-351.

_____ and _____, 1991: The wind and thermally driven circulation of the eastern Mediterranean Sea. Part II: the baroclinic case. *Dyn. Atmos. Oceans*, 15, 355-419.

_____ and A. Hecht, 1988: Large-scale properties of the eastern Mediterranean: a review. *Oceanol. Acta*, 11, 323-335.

May P.W., 1982: Climatological flux estimates in the Mediterranean Sea: Part I. Winds and wind stresses. *NORDA Techn. Rep.*, 54, 58 pp.

_____, 1986: A brief explanation of Mediterranean heat and momentum calculations, *unpublished*, 5 pp.

MEDOC Group, 1969: Observation of formation of deep water in the Mediterranean Sea., *Nature* , 227, 1037-1040.

Mellor G.L., 1991a: User's guide for a three dimensional, primitive equation, numerical ocean model.*Report AOS Program , Princeton Univ., Princeton NJ 08544-0710*, 34 pp.

_____, 1991b: An equation of state for numerical models of oceans and estuaries. *J. Atmos. Ocean Technol.*, 8, 609-611.

_____ and A.F. Blumberg, 1985: Modeling vertical and horizontal diffusivities with the sigma coordinate system. *Mon.Weather Rev.* , 113, 1279-1383.

_____ and T. Ezer, 1991: A Gulf Stream model and an altimetry assimilation scheme. *J. Geophys. Res.*, 96, 8779-8795.

_____ and T. Yamada, 1982: Development of a turbulent closure model for geophysical fluid problems. *Rev. Geophys.*, 20, 851-875.

Menzin A.B. and L.V. Moskalenko, 1982: Calculation of wind-driven currents in the Mediterranea Sea by the electrical simulation method (homogeneous model). *Oceanology*, 22, 537-540.

Millot C., 1985: Some features of the Algerian current. *J. Geophys. Res.*, 90, 7169-7176.

_____, 1987a: The circulation of the Levantine Intermediate Water in the Algerian Basin. *J. Geophys. Res.*, 92, 8265-8276.

_____, 1987b: Circulation in the western Mediterranean Sea. *Oceanol. Acta*. 10, 143-149.

_____, 1991: Mesoscale and seasonal variability of the circulation in the western Mediterranean. *Dyn. Atmos. Oceans*, 15, 179-214.

Morcos S.A., 1972: Sources of Mediterranean intermediate water in the Levantine Sea. *Studies in physical oceanography, a tribute to Georg Wust on his 80th birthday*, 2, edited by A.L. Gordon, pp 185-206, Gordon and Breach N.Y.

Oey L.-Y., G.L. Mellor and R.I. Hires, 1985a: A three-dimensional simulation of the Hudson Raritan estuary. Part I: Description of the Model and model simulations. *J. Phys. Oceanogr.*, 15, 1676-1692.

_____, _____ and _____, 1985b: A three-dimensional simulation of the Hudson Raritan estuary. Part II: Comparison with observations. *J. Phys. Oceanogr.*, 15, 1693-1709.

_____, _____ and _____, 1985c: A three-dimensional simulation of the Hudson Raritan estuary. Part III, Salt flux analysis. *J. Phys. Oceanogr.*, 15, 1711-1720.

Ovchinnikov I.M., 1966: Circulation in the surface and intermediate layers of the Mediterranean Sea. *Oceanology*, 6, 48-59.

_____, 1984: The formation of intermediate water in the Mediterranean. *Oceanology*, 24, 168-173.

_____ and A.F. Fedoseyev, 1965: The horizontal circulation of the water of the Mediterranean Sea during the winter and summer seasons. *Basic Features of the geological structure, hydrological regime and biology of the Mediterranean*, edited by L. M.Fomin, translation of the Institute for Modern Languages for the U.S. Navy oceanographic Office, 185-201.

_____, V.I. Zats, V.G. Krivosheya, M.S. Nemirosky, and A.I. Udodov 1987:, winter convection in the Adriatic and formation of deep eastern Mediterranean waters. *Ann. Geophys.*, 5B, 89-92.

Ozsoy E., A. Hecht and U. Unluata, 1989: Circulation and hydrography of the Levantine Basin. Results of the POEM coordinated experiments 1985-86. *Prog. Oceanog.*, 22, 125-170.

_____, _____, _____, S. Brenner, T. Oguz, J. Bishop, M.A. Latif and Z. Rozentraub, 1991: A review of the Levantine Basin circulation and its variability during 1985-1988. *Dyn. Atmos. Oceans*, 15, 421-456.

Pinardi N. and A. Navarra, 1991: Baroclinic wind adjustment processes in the Mediterranean Sea, *Submitted to J. Phys. Oceanogr.*

Pollak M.J., 1951: The sources of the deep waters of the eastern Mediterranean Sea. *J. Mar. Res.*, 10, 128-156.

Preller R.H., 1986: A numerical model study of the Alboran Sea gyre. *Progr. Oceanogr.*, 16, 113-146.

Robinson A.R., M. Golnaraghi M., W.G. Leslie, A. Artegiani, A. Hecht, E. Lazzoni, A. Michelato, E. Sansone, A. Theocaris and U. Unluata, 1991: The eastern Mediterranean general Circulation: features, structure and variability, *Dyn. Atmos. Oceans*, 15, 215-240.

Sankey T., 1973: The formation of deep water in the northwestern Mediterranean. *Progr. Oceanogr.*, 6, 159-179.

Stanev E.V., H.J. Friedrich and S. Botev, 1989: On the seasonal response of intermediate and deep water to surface forcing in the Mediterranean Sea. *Oceanol. Acta*, 12, 141-149.

Stommel H., 1972: Deep winter convection in the western Mediterranean Sea. *Studies in physical oceanography, a tribute to Georg Wust on his 80th birthday*, 2, edited by A.L. Gordon, pp 207-218, Gordon and Breach N.Y.

Tait R.I., 1984: The physical oceanography of the Tyrrhenian and Ligurian Seas. *Atti 6° Congr. Assoc. Ital. Oceanol. Limnol., Livorno, 12-14 Aprile 1984*, 48-84.

Tchernia P., 1980: *Descriptive regional oceanography*. Pergamon Press Publ., Oxford and N.Y., 253 pp.

Tintore J.D., P.E. La Violette, I. Blade and A. Cruzado, 1988: A study of an intense density front in the eastern Alboran Sea: The Almeria Oran front. *J. Phys. Oceanogr.*, 18, 1384-1397.

Tziperman E. and P.Malanotte-Rizzoli, 1991: The climatological seasonal circulation of the Mediterranean Sea. *J. Mar. Res.*, 49, 411-434.

UNEP, 1984: Pollutants from land-based sources in the Mediterranean. *UNEP regional seas reps. studies*, 32, 97 pp.

Wust G., 1961: On the vertical circulation of the Mediterranean Sea. *J. Geophys. Res.*, 66, 3261-3271.

Table 1: Characteristics of the numerical experiments.

EXPERIMENT	WIND-STRESS	THERMAL SURF. CONDITION	SALINITY SURF. CONDITION	RIVER RUNOFF
MED-1	Monthly	Surf. temperature equal to initial conditions	Surf. salinity equal to initial conditions	no
MED-2	Monthly	Monthly heat flux	Constant salinity flux	no
MED-3	Monthly	Monthly heat flux	Surf. salinity equal to initial conditions	no
MED-4	Monthly	Monthly heat flux	Monthly salinity flux	Annual

FIGURE CAPTIONS

Fig. 1: The Mediterranean Sea. Upper panel: Geographic features (adapted from *Hopkins. 1978*) lower panel: bathymetric map (source: U.S. Navy bathymetric data-bae). Contour interval is 250 m.

Fig.2: Schematic of the Mediterranean Sea water masses vertical distribution (adapted from *Hopkins. 1985*)

Fig.3: Schematic of the WMED circulation. Upper panel: MAW circulation, lower panel: LIW circulation (adapted from *Millot. 1987a*).

Fig.4: Schematic of the EMED circulation (adapted from *Robinson et al.. 1991*).

Fig.5: The model grid.

Fig.6: The model bathymetry. Contour interval is 250 m.

Fig.7: Annually averaged hydrological climatologies (model initial conditions). Upper panel: surface temperature. Contour interval is 1^{o} C, lower panel: surface salinity. Contour interval is $0.1^{o}/_{oo}$.

Fig.8: Total surface heat flux. Upper panel: February, lower panel: August. Contour interval is 10 $W*m^{-2}$. Not all the vectors are plotted

Fig.9: Wind-Stress. Upper panel: February, lower panel August. Units are $dyne*cm^{-2}$.

Fig.10: Surface fresh-water flux. Upper panel: February, lower panel: August. Contour interval is 10 mm.

Fig.11: Experiment MED-1: Surface elevation. Upper panel: February, lower panel: August. Contour interval is 2 cm.

Fig.12: Experiment MED-1: Velocity at 50 m depth. Upper panel:February, lower panel: August. Units are $m*s^{-1}$. In this picture, as well as the other velocity field picture, the vectors in the Gibraltar area are not plotted for clarity sake.

Fig.13:Experiment MED-1: Velocity at 300 m depth. Upper panel:February, lower panel: August. Units are $m*s^{-1}$.

Fig.14: Experiment MED-1: Velocity at 1200 m depth. Upper panel:February, lower panel: August. Units are $m*s^{-1}$.

Fig. 15: Experiment MED-2: Surface elevation. Upper panel: February, lower panel: August. Contour interval is 2 cm.

Fig.16. Temperature (left) and salinity (right) Basin average time history for experiment MED-4.

Fig.17: Experiment MED-4: Surface elevation. Upper panel: February, lower panel: August. Units are $m*s^{-1}$.

Fig.18: Experiment MED-4: Velocity at 50 m depth. Upper panel: February, lower panel: August. Units are $m*s^{-1}$.

Fig.19: Experiment MED-4: Velocity at 300 m depth. Upper panel: February, lower panel: August. Units are $m*s^{-1}$.

Fig.20: Experiment MED-4: Velocity at 1200 m depth. Upper panel: February, lower panel: August. Units are $m*s^{-1}$.

Fig.21: Location of the cross-section described in the text.

Fig.22: Experiment MED-4: Surface temperature distribution. Upper panel: February (contour interval is 0.5° C), lower panel: August (contour interval is 1.0° C).

Fig.23: Experiment MED-4: Surface salinity distribution. Upper panel: February (contour interval is 0.1‰), lower panel: August (contour interval is 0.2‰).

Fig.24: Experiment MED-4: Temperature distribution at 300 m depth. Upper panel: February, lower panel: August. contour interval is 0.2° C.

Fig.25: Experiment MED-4: Salinity distribution at 300 m depth. Upper panel: February, lower panel: August. Contour interval is 0.05 ‰.

Fig.26: Experiment MED-4: Salinity distribution along cross-section A in February (upper panel) and August (lower panel). Contour interval is 0.1 ‰.

Fig.27: Experiment MED-4: Salinity distribution along cross-section D in February (upper panel) and August (lower panel). Contour interval is 0.1 ‰.

Fig.28: Experiment MED-4: Cross-section C. Temperature (upper), salinity (middle) and sigma-θ distribution in February. Contour intervals are 0.25° C, 0.05 ‰ and 0.05 sigma-θ units.

Fig.29: Experiment MED-4: Cross-section E. Temperature distribution on February 10 (upper), 20 (middle) and 30 (lower) of the climatological year. Contour interval is 0.25°C.

Fig.30: Experiment MED-4: Cross-section E. Sigma-θ distribution on February 10 (upper), 20 (middle) and 30 (lower) of the climatological year. Contour interval is 0.05 sigma-θ units.

Fig.31: Experiment MED-4: Cross-section B: salinity distribution in March. Contour interval is 0.05 ‰.

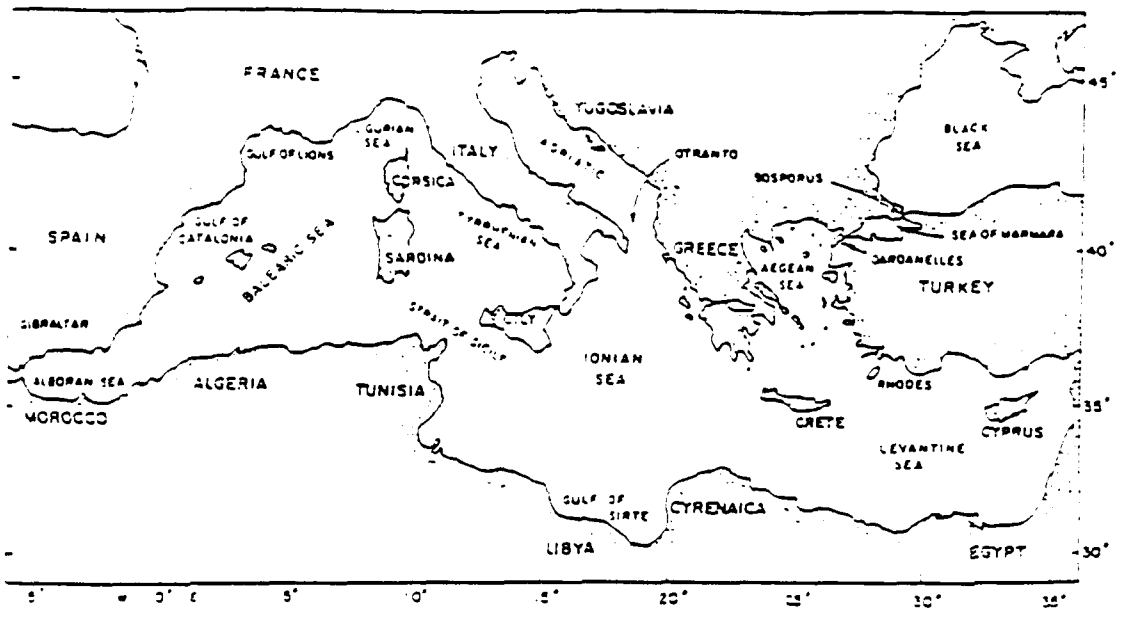
FRANCE
SPAIN
GULF OF LIONS
GULF OF CATALONIA
BALEARIC SEA
CORSICA
SARDINA
ITALY
TYRRHENIAN SEA
GIBRALTAR
ALBORAN SEA
MOROCCO
ALGERIA
TUNISIA
SICILY
IONIAN SEA
YUGOSLAVIA
OTRANTO
GREECE
AEGEAN SEA
BOSPORUS
BLACK SEA
SEA OF MARMARA
DARDANELLES
TURKEY
RHODES
CRETE
CYPRUS
LEVANTINE SEA
GULF OF SIRTE
CYRENAICA
LIBYA
EGYPT
45°
40°
35°
30°

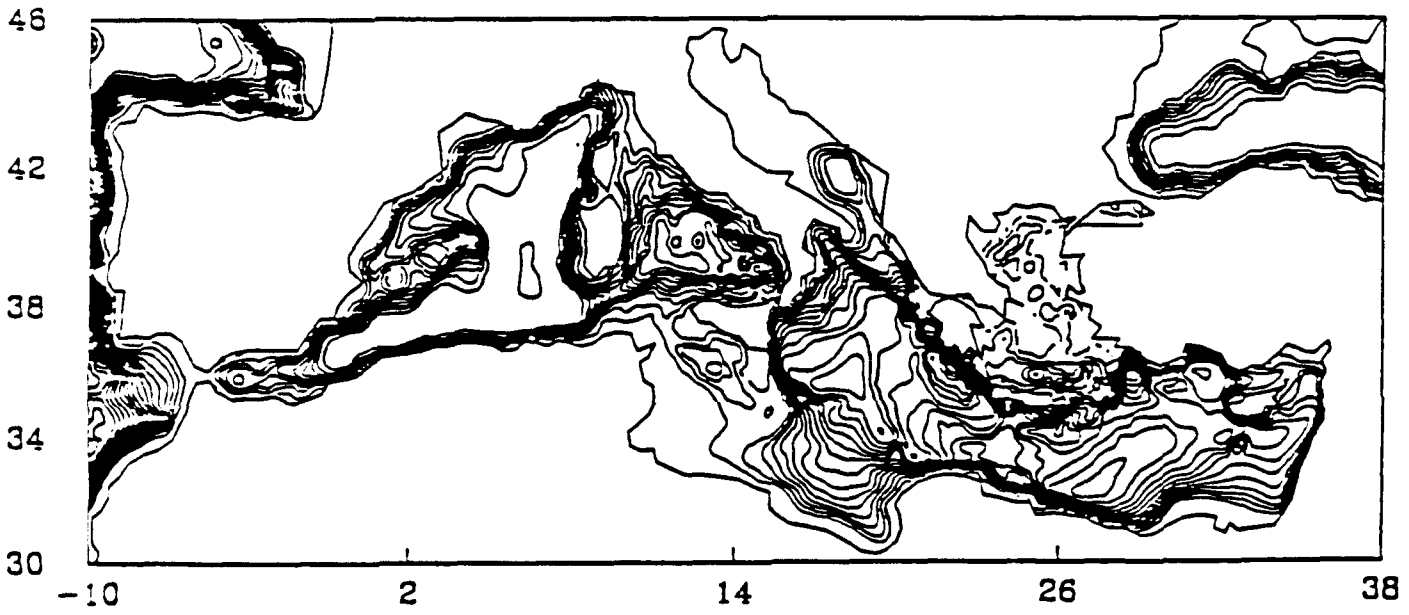
46
42
38
34
30
-10
2
14
26
38

FIGURE 1

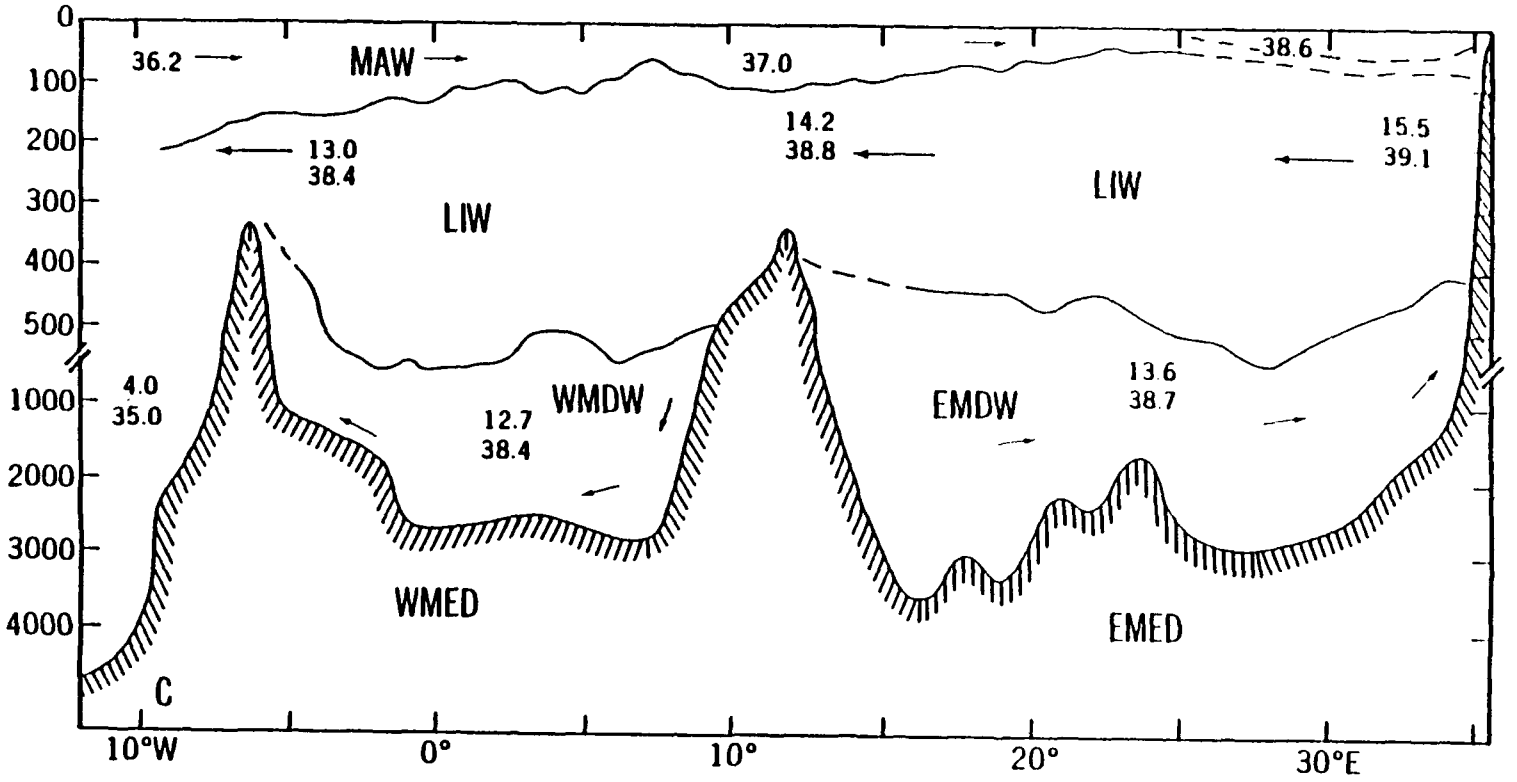
0
100
200
300
400
500
1000
2000
3000
4000
36.2
MAW
37.0
38.6
13.0
38.4
14.2
38.8
15.5
39.1
LIW
LIW
4.0
35.0
12.7
38.4
WMDW
EMDW
13.6
38.7
WMED
EMED
C
10°W
0°
10°
20°
30°E

FIGURE 2

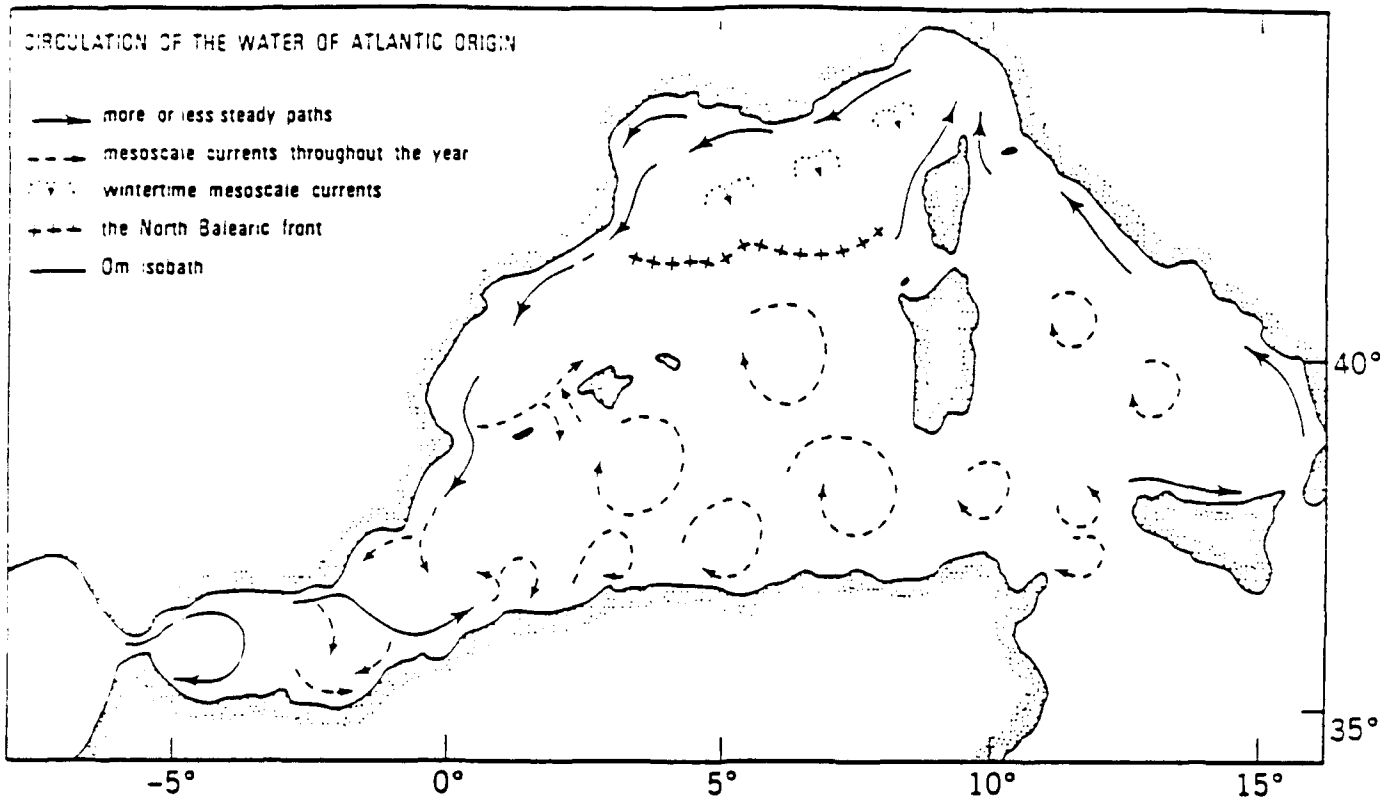
CIRCULATION OF THE WATER OF ATLANTIC ORIGIN
more or less steady paths
mesoscale currents throughout the year
wintertime mesoscale currents
the North Balearic front
0m isobath
40°
35°
-5°
0°
5°
10°
15°

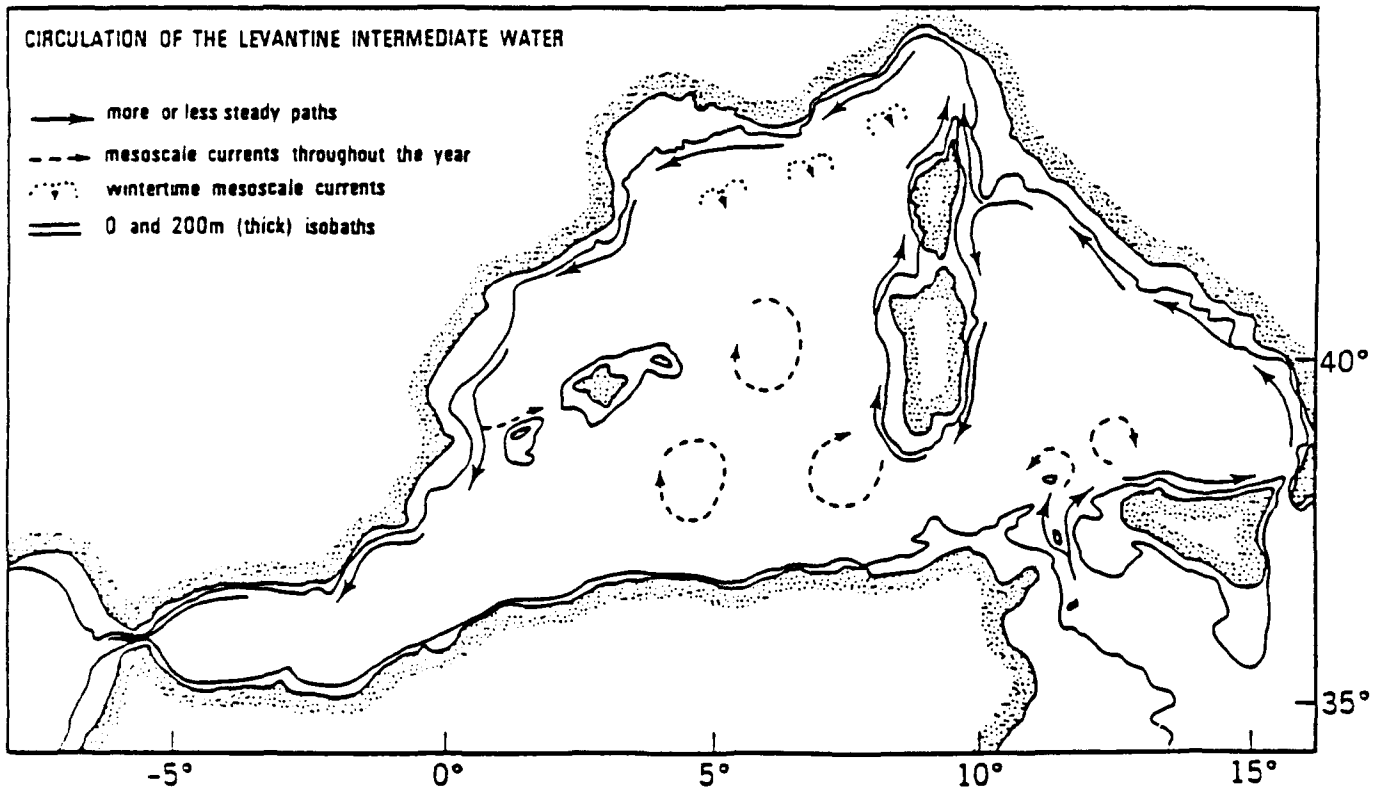
CIRCULATION OF THE LEVANTINE INTERMEDIATE WATER
more or less steady paths
mesoscale currents throughout the year
wintertime mesoscale currents
0 and 200m (thick) isobaths
40°
35°
-5°
0°
5°
10°
15°

FIGURE 3

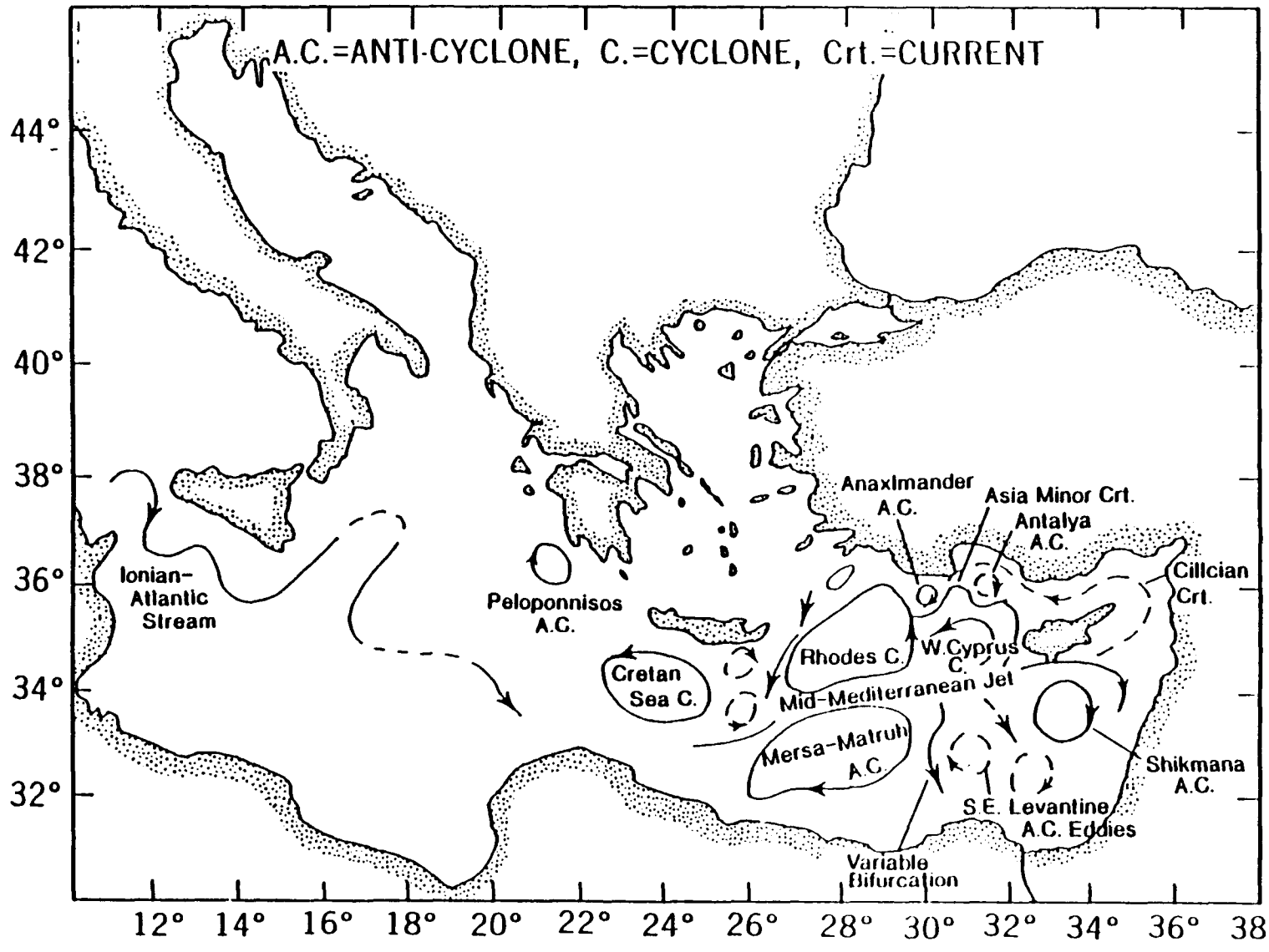
A.C.=ANTI-CYCLONE, C.=CYCLONE, Crt.=CURRENT
44°
42°
40°
38°
36°
34°
32°
12° 14° 16° 18° 20° 22° 24° 26° 28° 30° 32° 34° 36° 38°
Ionian-
Atlantic
Stream
Peloponnisos
A.C.
Anaximander
A.C.
Asia Minor Crt.
Antalya
A.C.
Cillcian
Crt.
Rhodes C.
W.Cyprus
C.
Cretan
Sea C.
Mid-Mediterranean Jet
Mersa-Matruh
A.C.
Shikmana
A.C.
S.E. Levantine
A.C. Eddies
Variable
Bifurcation

FIGURE 4

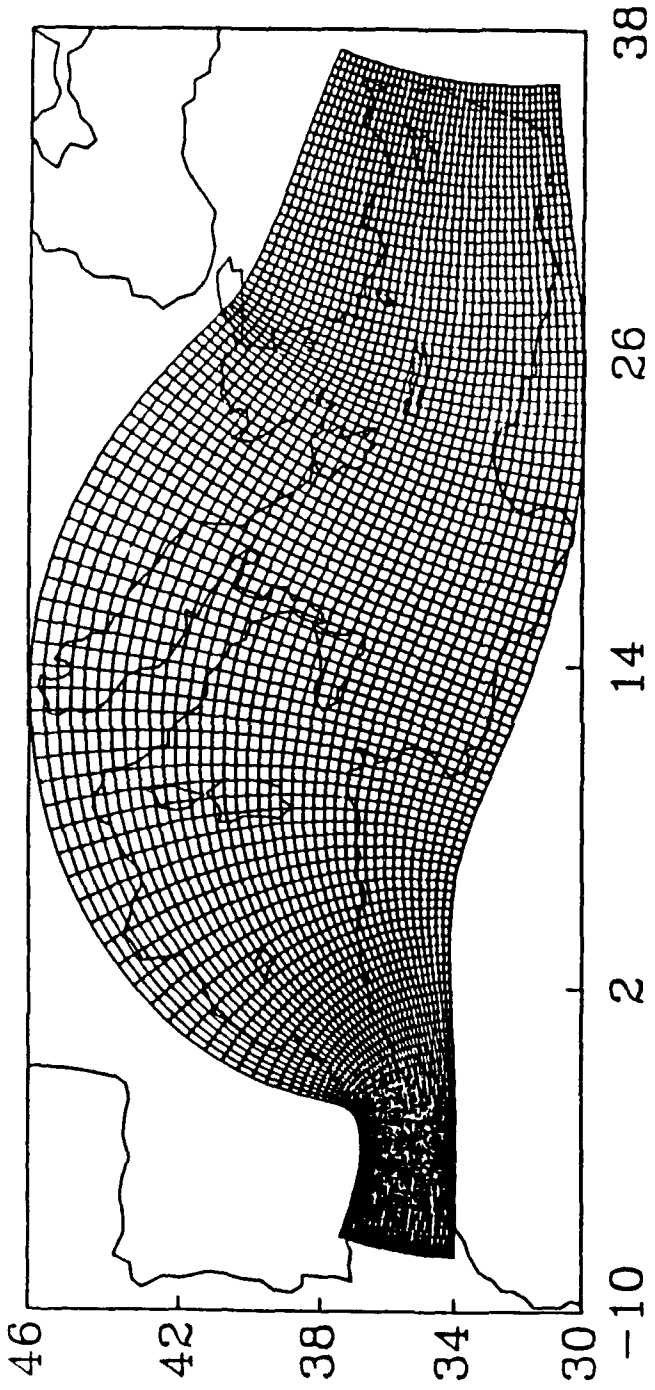

FIGURE 5

FIGURE 6

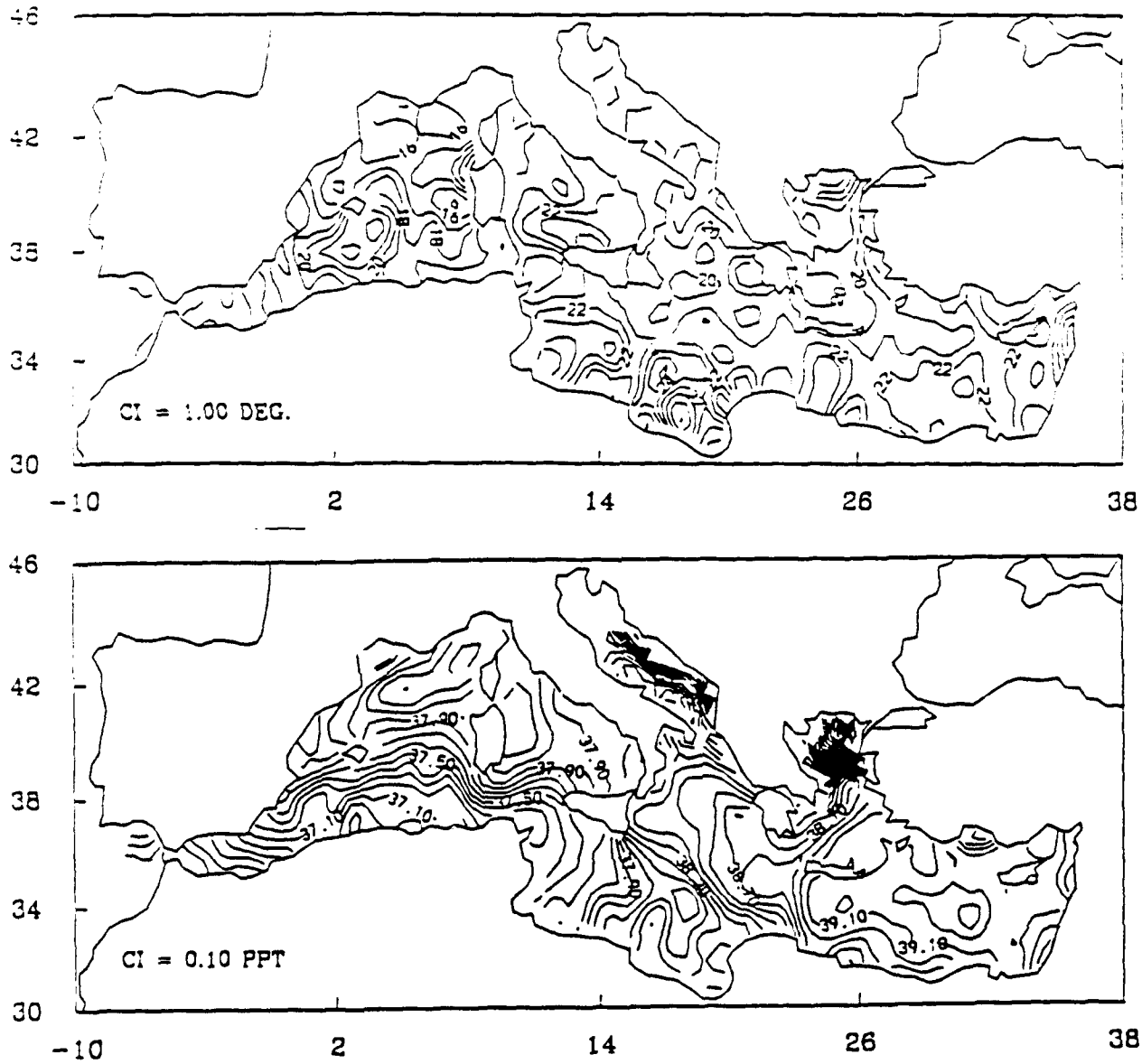
46
42
38
34
30
CI = 1.00 DEG.
-10
2
14
26
38
46
42
38
34
30
CI = 0.10 PPT
-10
2
14
26
38

FIGURE 7

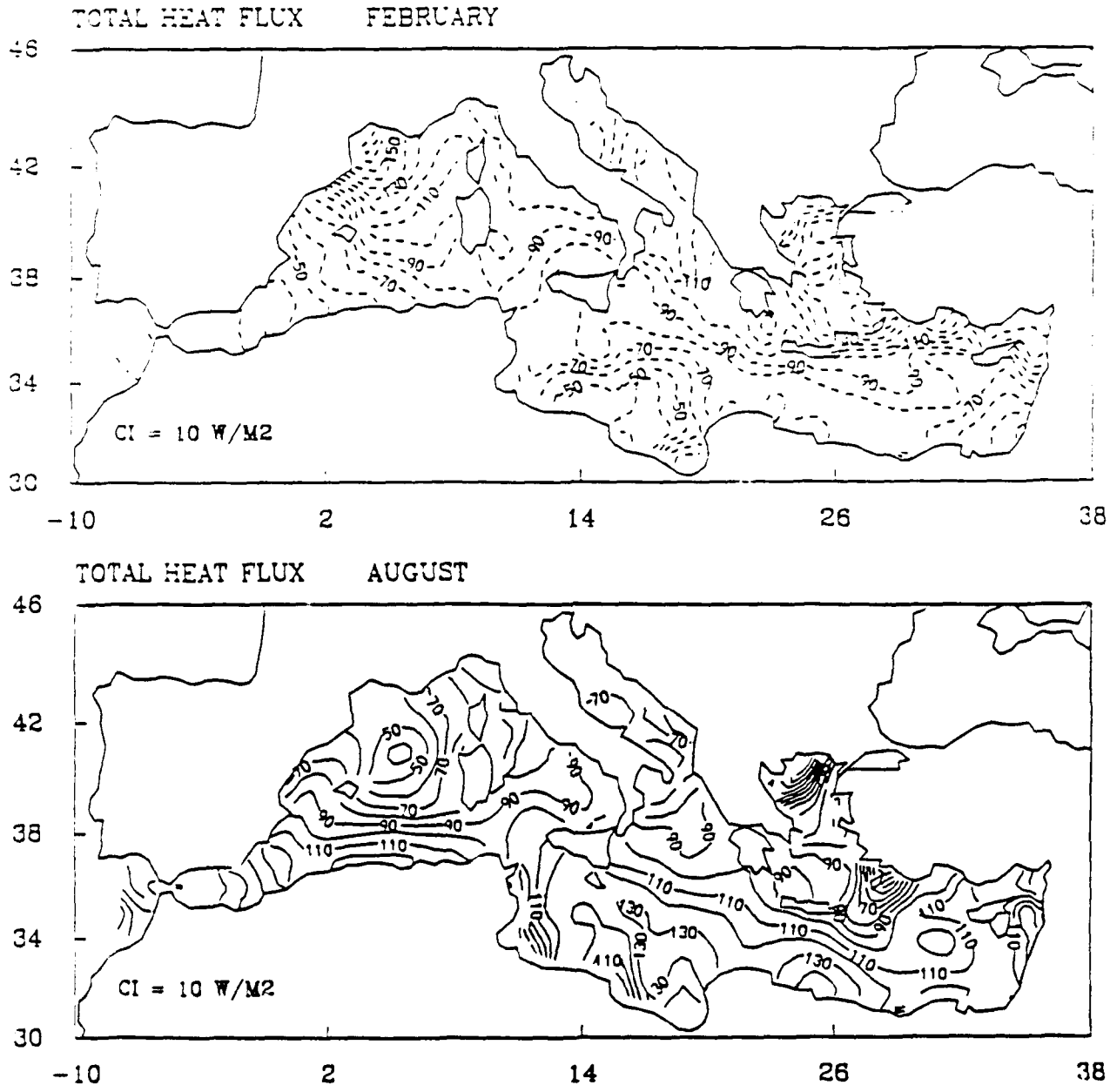
TOTAL HEAT FLUX FEBRUARY
CI = 10 W/M2
46
42
38
34
30
-10
2
14
26
38
TOTAL HEAT FLUX AUGUST
CI = 10 W/M2
46
42
38
34
30
-10
2
14
26
38

FIGURE 8

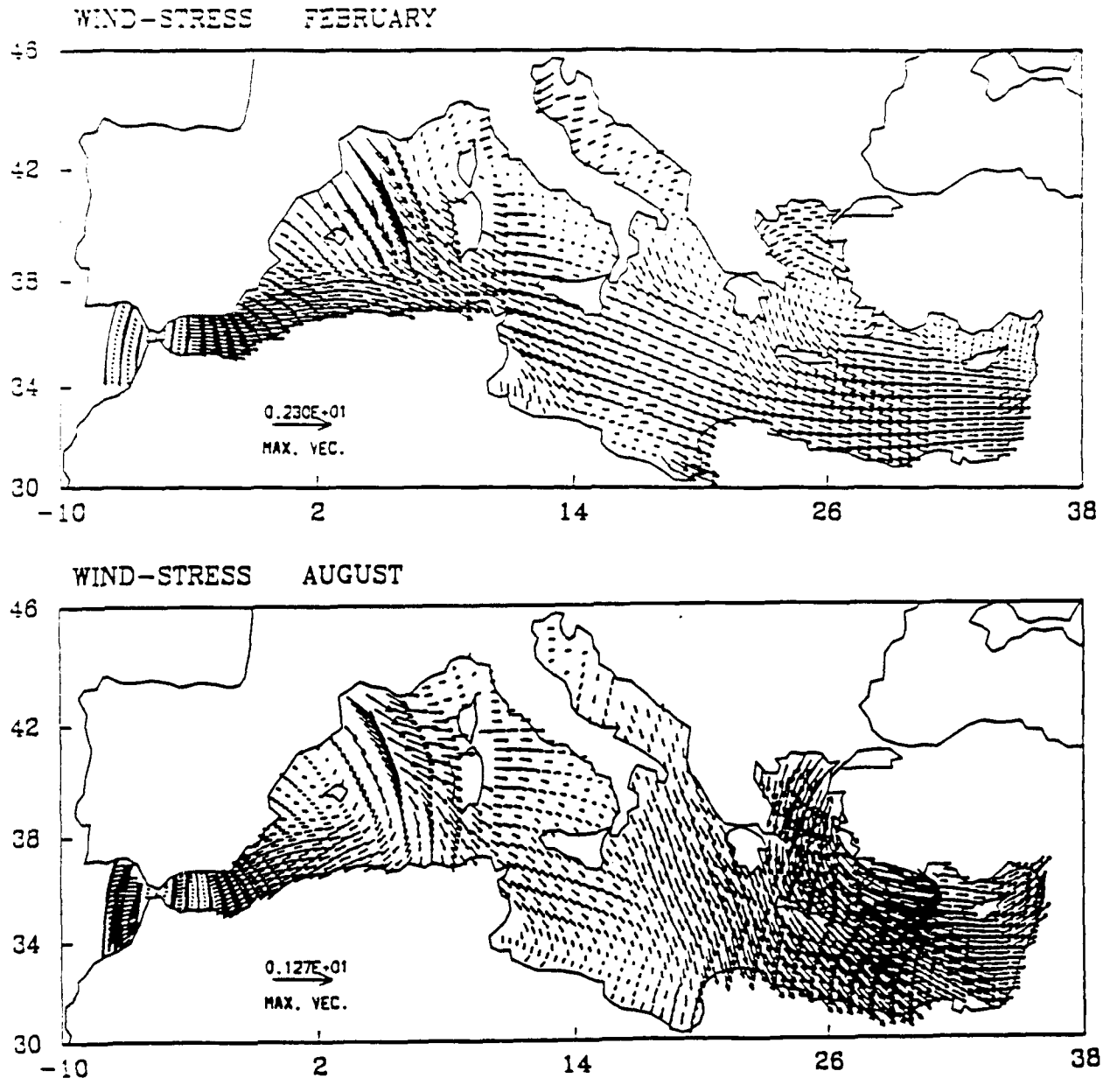
WIND-STRESS FEBRUARY
46
42
38
34
30
0.230E+01
MAX. VEC.
-10
2
14
26
38
WIND-STRESS AUGUST
46
42
38
34
30
0.127E+01
MAX. VEC.
-10
2
14
26
38

FIGURE 9

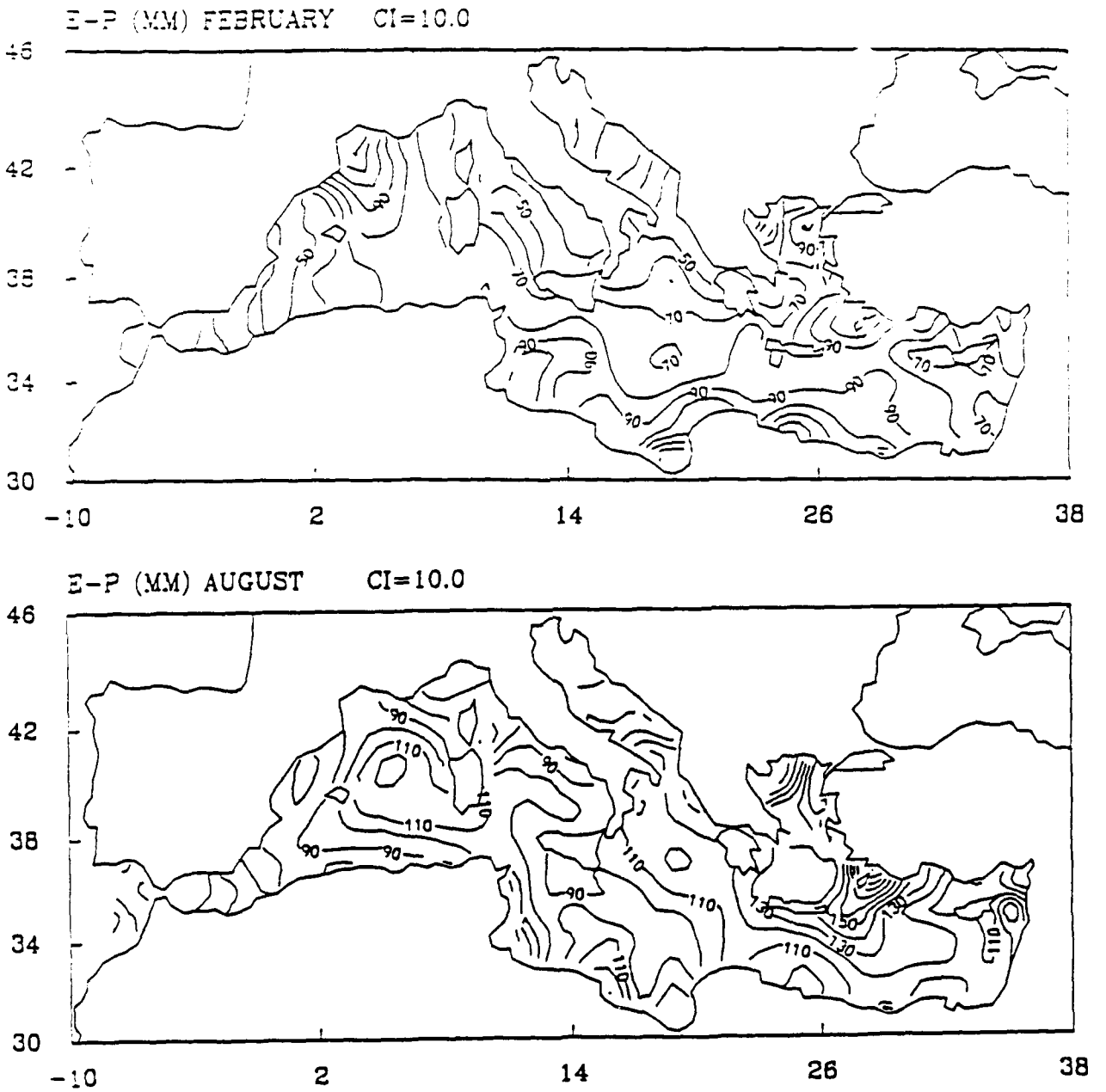
E-P (MM) FEBRUARY CI=10.0
46
42
38
34
30
-10
2
14
26
38
E-P (MM) AUGUST CI=10.0
46
42
38
34
30
-10
2
14
26
38

FIGURE 10

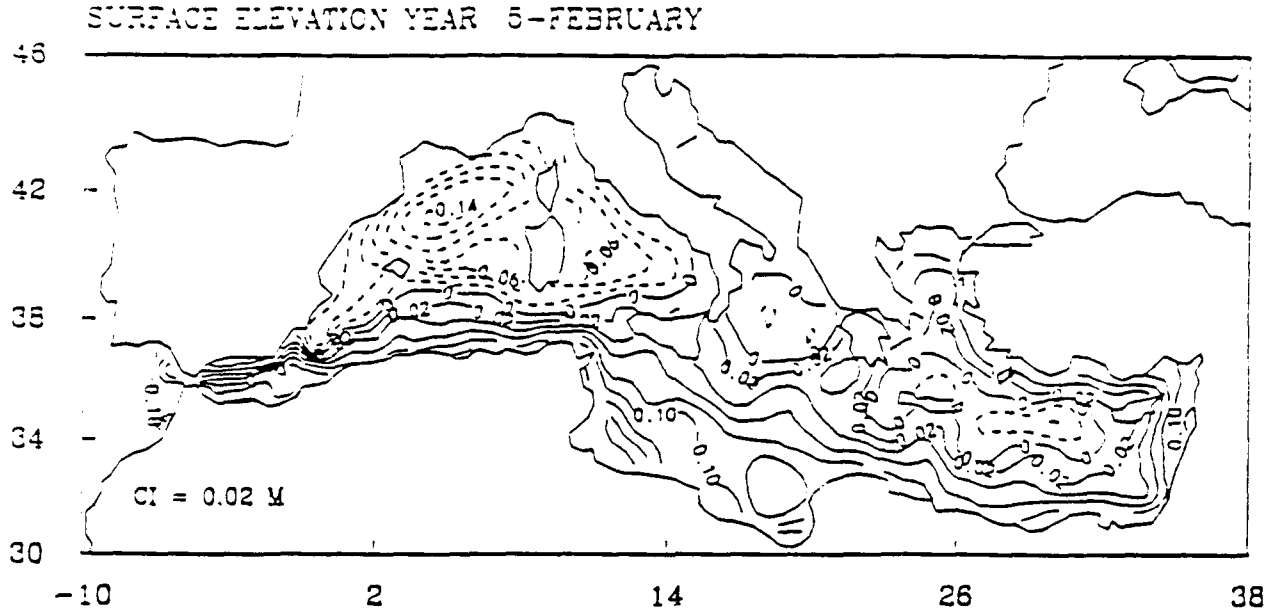
SURFACE ELEVATION YEAR 5-FEBRUARY
46
42
38
34
30
CI = 0.02 M
-10
2
14
26
38

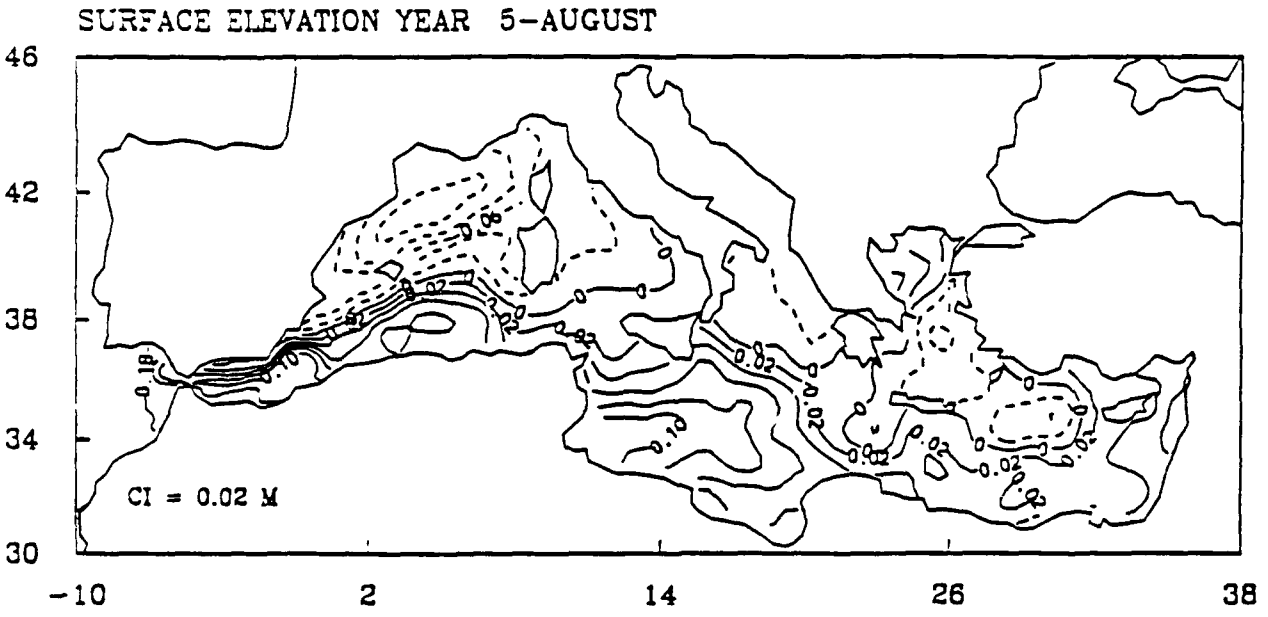
SURFACE ELEVATION YEAR 5-AUGUST
46
42
38
34
30
CI = 0.02 M
-10
2
14
26
38

FIGURE 11

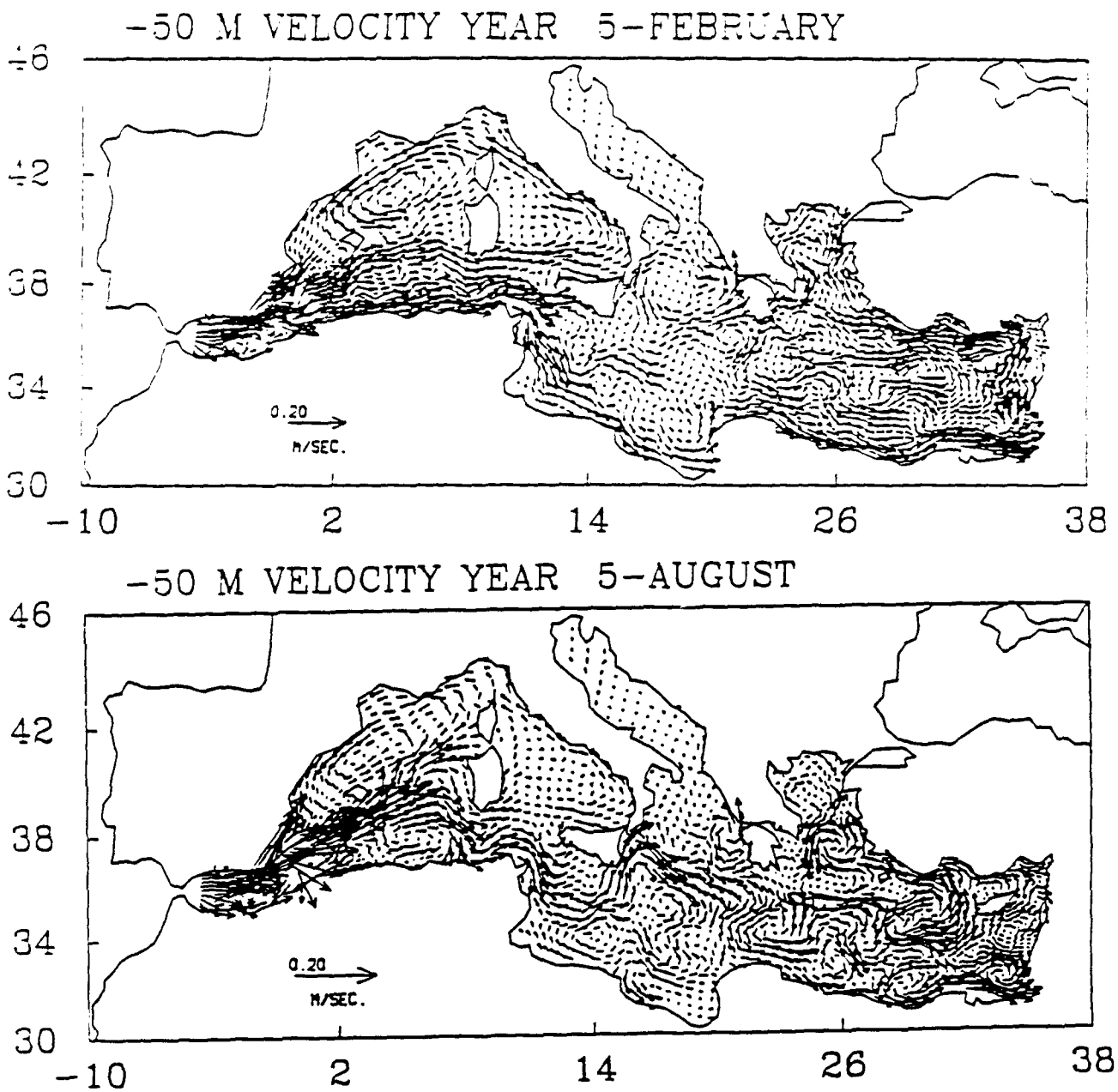
-50 M VELOCITY YEAR 5-FEBRUARY
46
42
38
34
30
-10
2
14
26
38
0.20
M/SEC.
-50 M VELOCITY YEAR 5-AUGUST
46
42
38
34
30
-10
2
14
26
38
0.20
M/SEC.

FIGURE 12

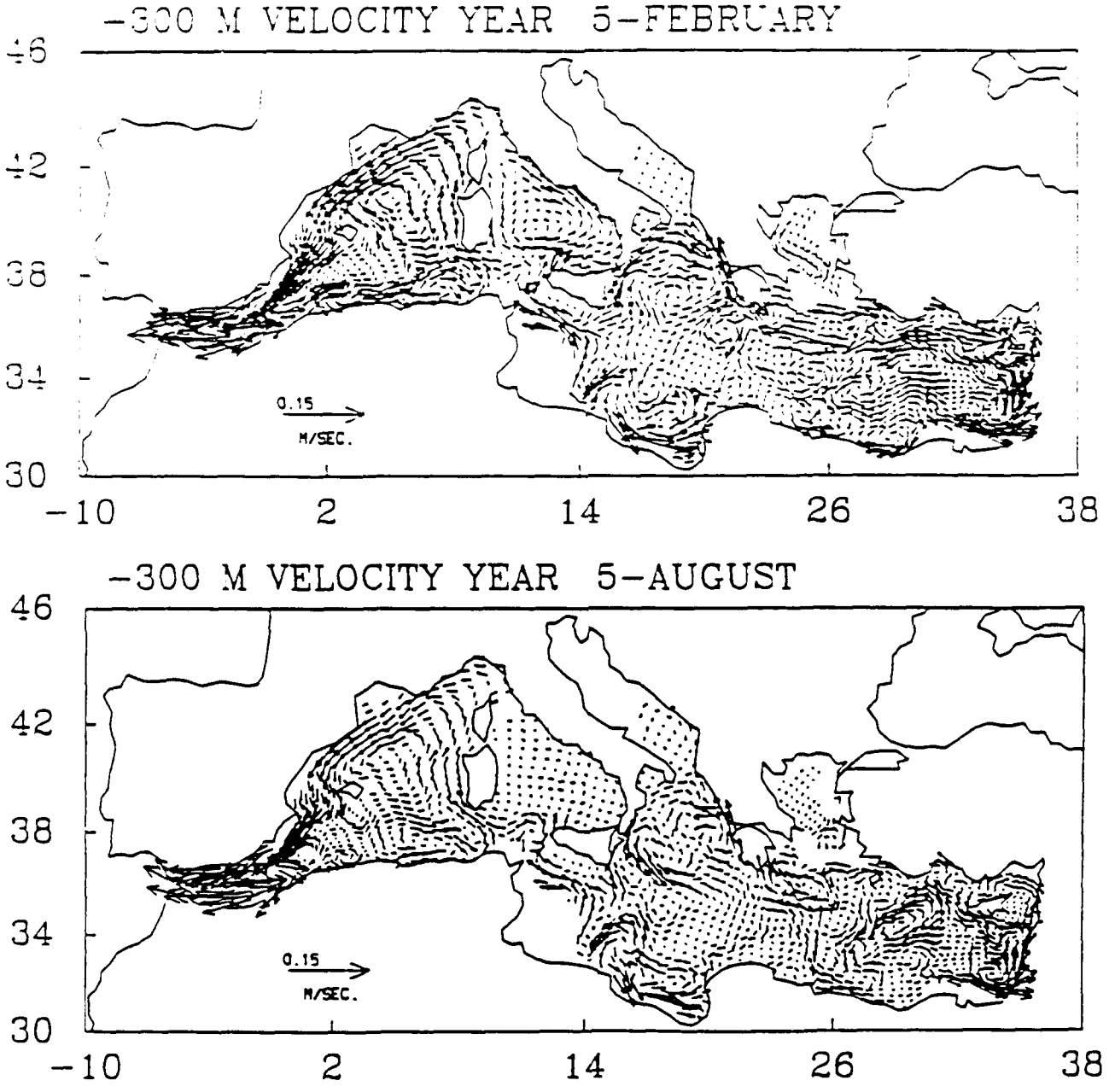
-300 M VELOCITY YEAR 5-FEBRUARY
46
42
38
34
30
-10
2
14
26
38
0.15
M/SEC.
-300 M VELOCITY YEAR 5-AUGUST
46
42
38
34
30
-10
2
14
26
38
0.15
M/SEC.

FIGURE 13

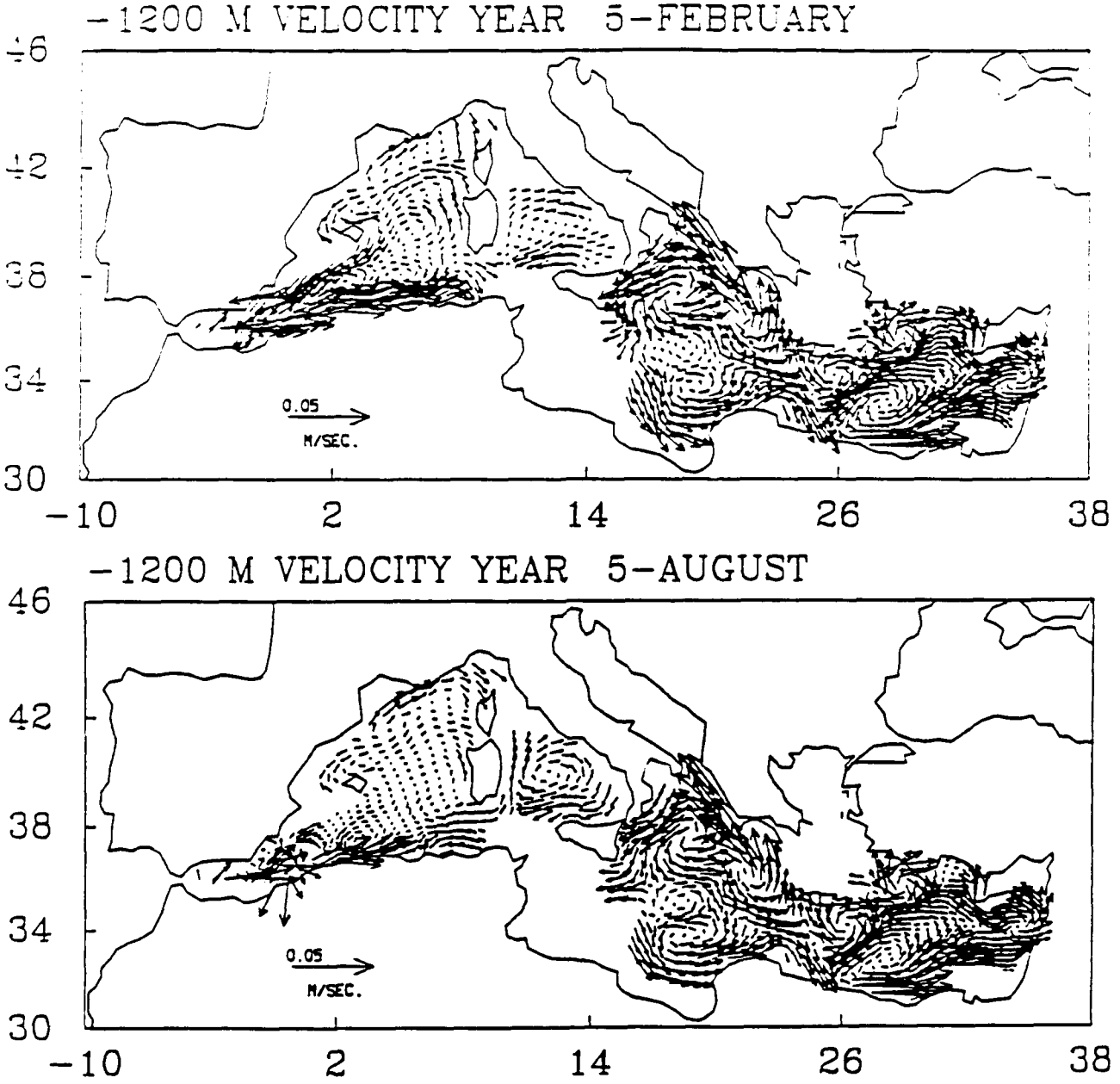
-1200 M VELOCITY YEAR 5-FEBRUARY
46
42
38
34
30
-10
2
14
26
38
0.05
M/SEC.
-1200 M VELOCITY YEAR 5-AUGUST
46
42
38
34
30
-10
2
14
26
38
0.05
M/SEC.

FIGURE 14

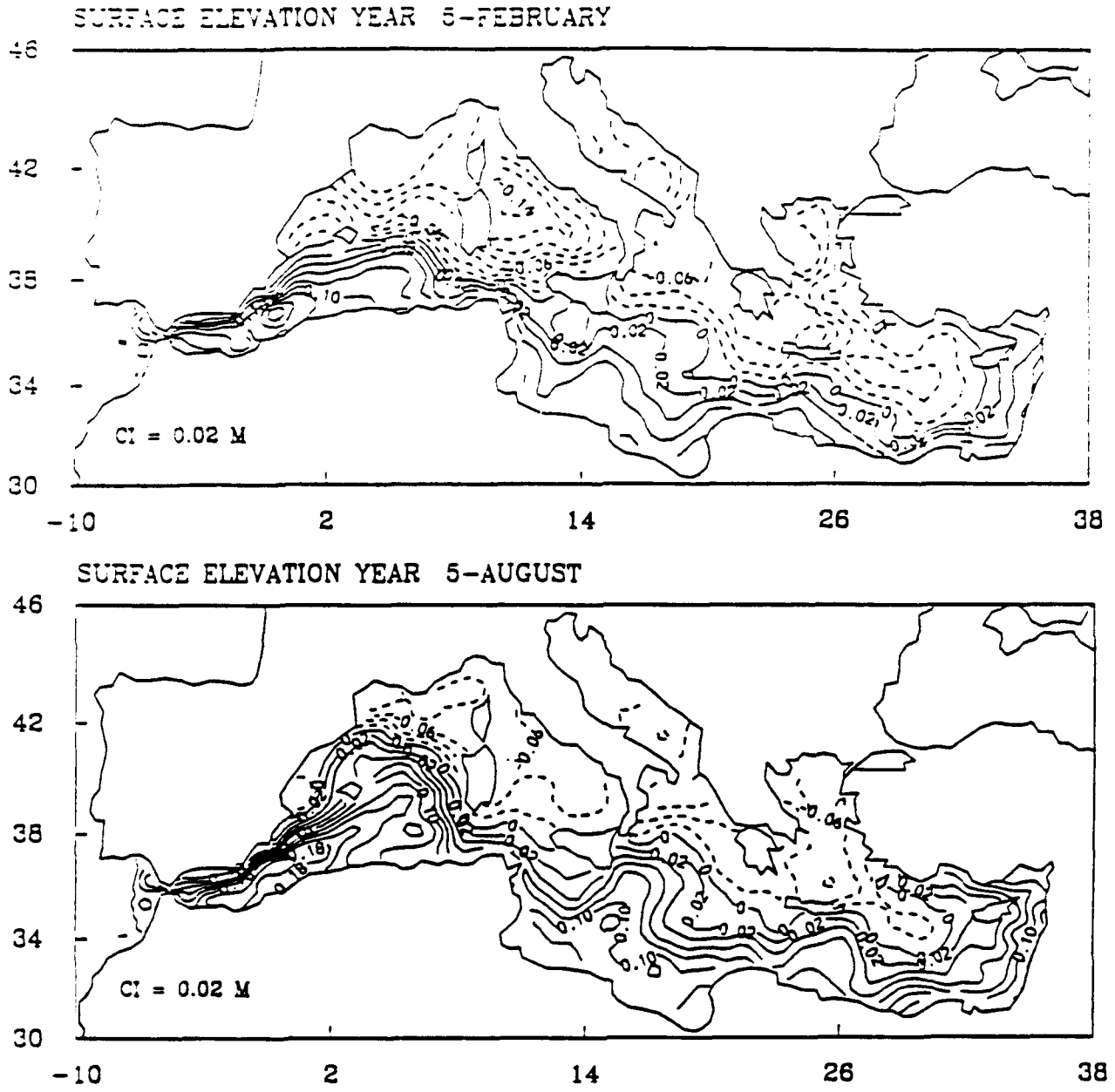
SURFACE ELEVATION YEAR 5-FEBRUARY
46
42
38
34
30
CI = 0.02 M
-10
2
14
26
38
SURFACE ELEVATION YEAR 5-AUGUST
46
42
38
34
30
CI = 0.02 M
-10
2
14
26
38

FIGURE 15

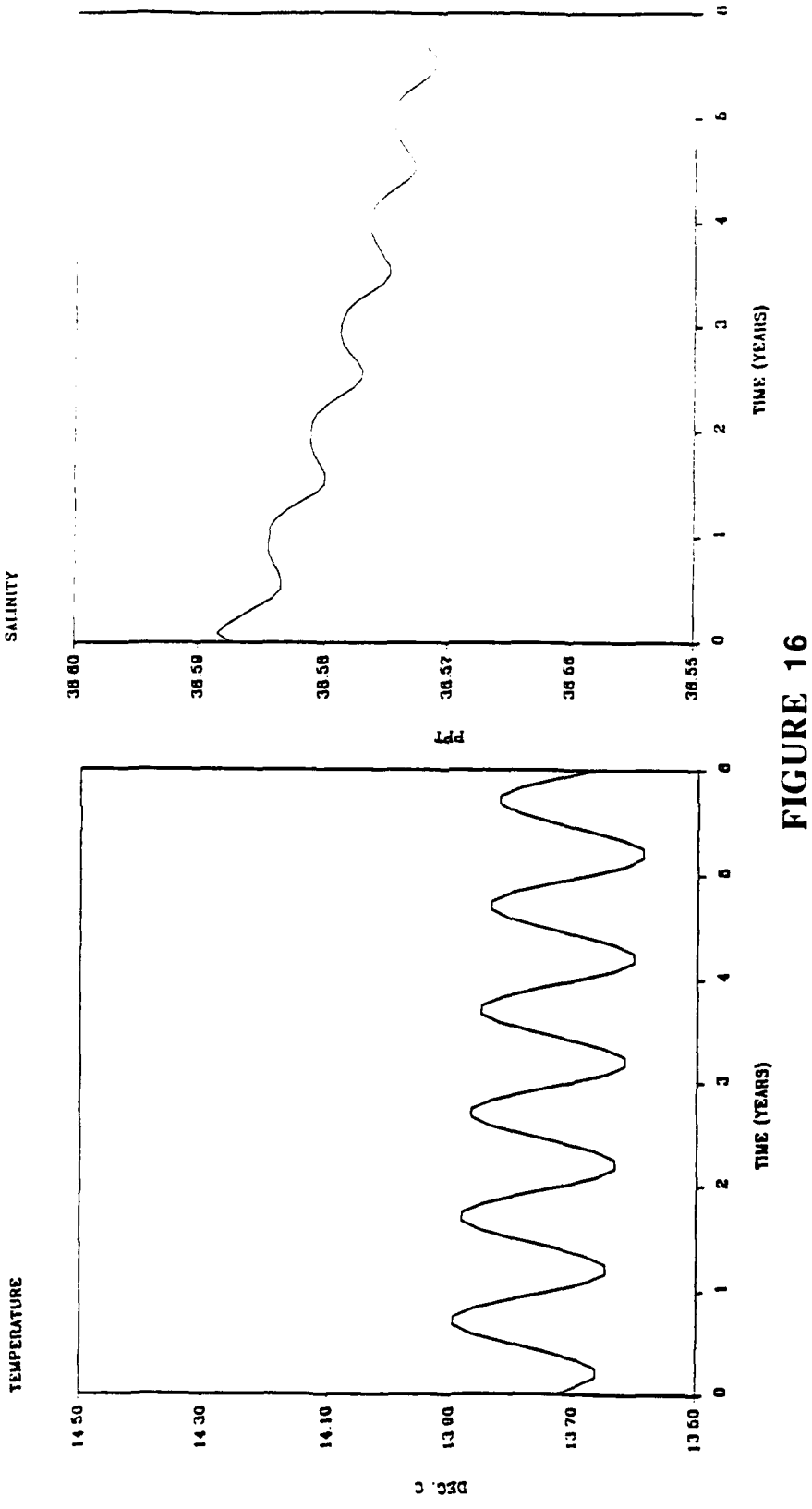
SALINITY
38.60
38.59
38.58
38.57
38.56
38.55
PPT
0
1
2
3
4
5
TIME (YEARS)
TEMPERATURE
14.50
14.30
14.10
13.90
13.70
13.50
DEG. C
0
1
2
3
4
5
6
TIME (YEARS)

FIGURE 16

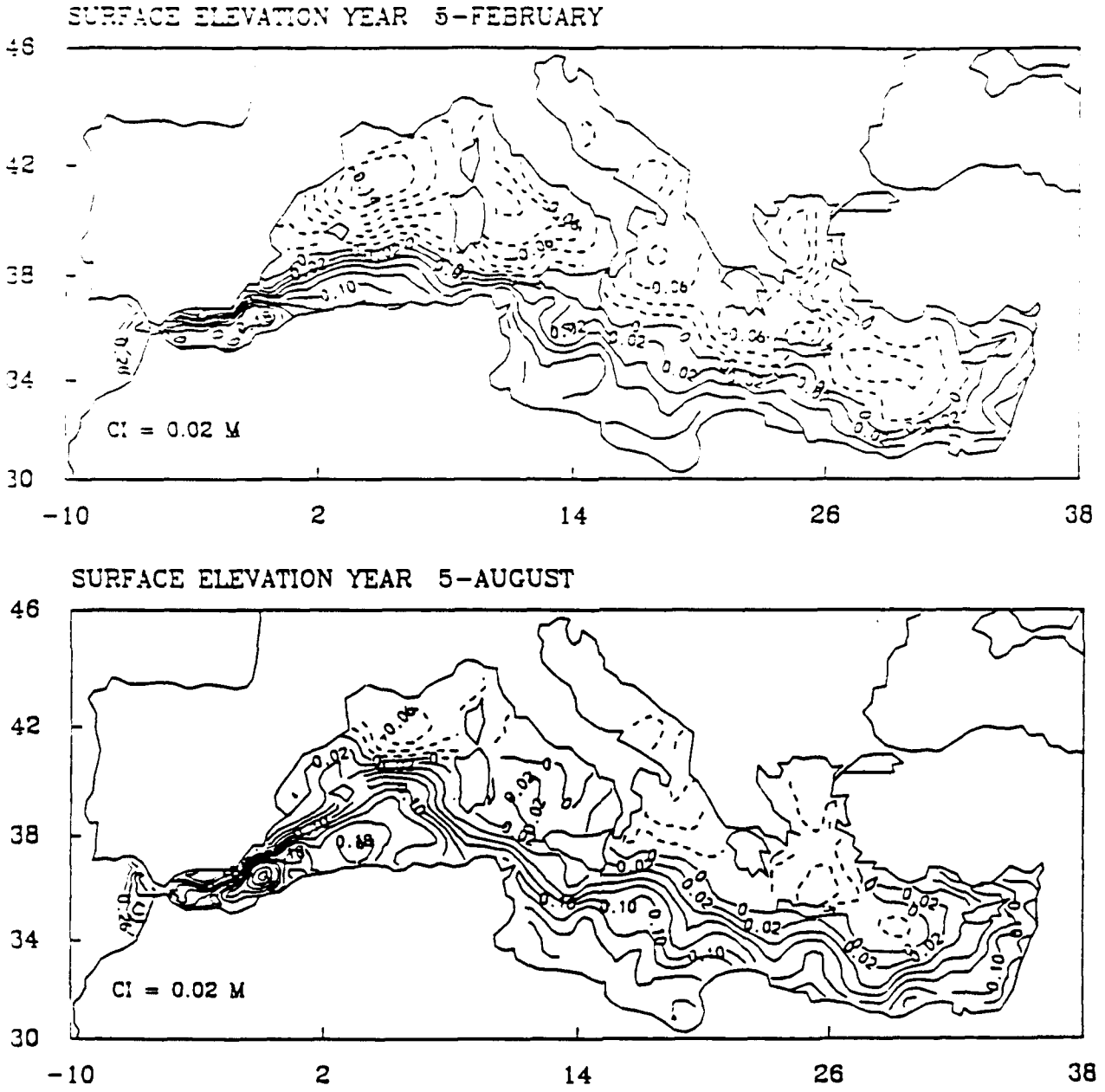
SURFACE ELEVATION YEAR 5-FEBRUARY
CI = 0.02 M
SURFACE ELEVATION YEAR 5-AUGUST
CI = 0.02 M
46
42
38
34
30
-10
2
14
26
38

FIGURE 17

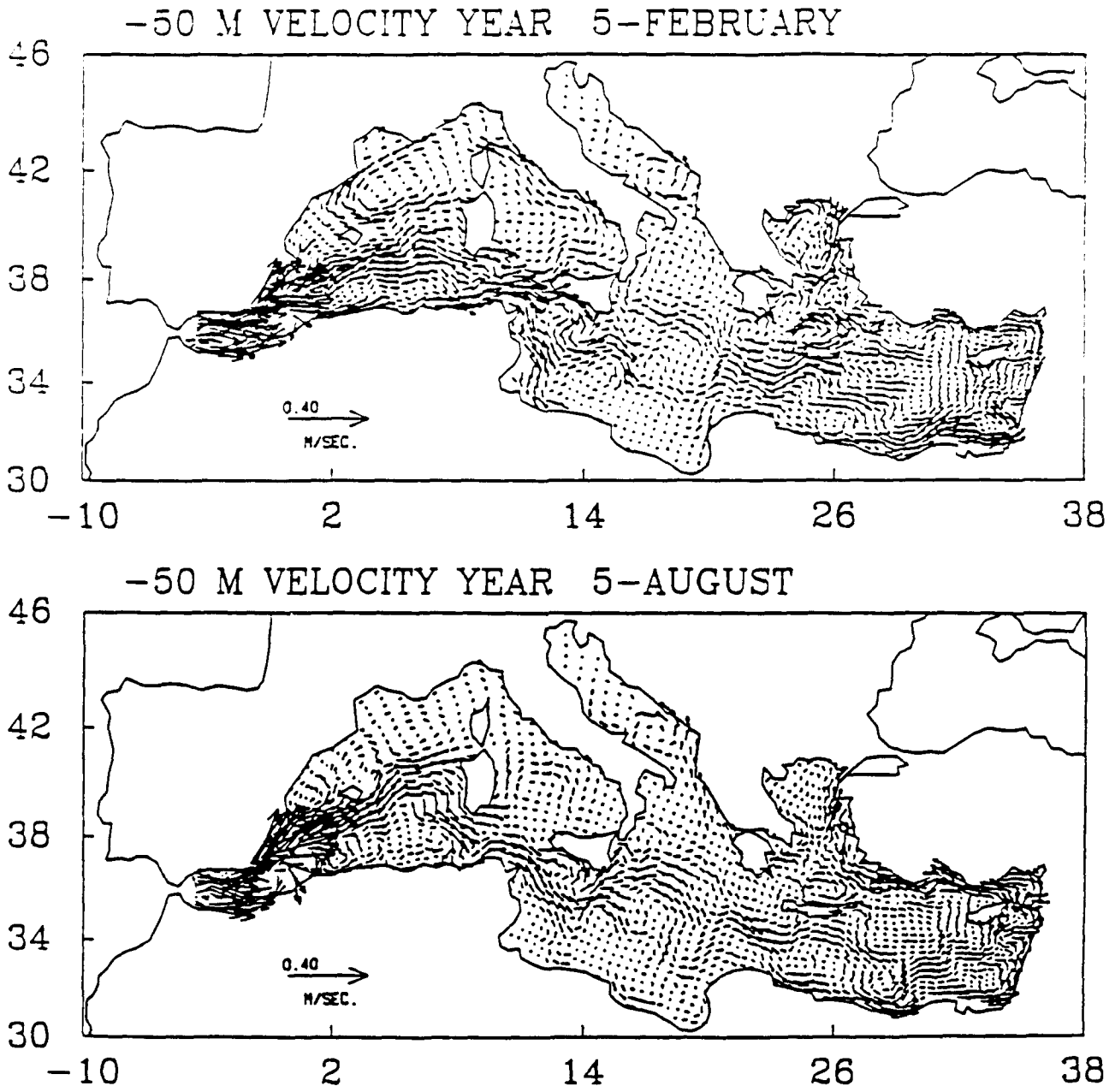
-50 M VELOCITY YEAR 5-FEBRUARY
46
42
38
34
30
-10
2
14
26
38
0.40
M/SEC.
-50 M VELOCITY YEAR 5-AUGUST
46
42
38
34
30
-10
2
14
26
38
0.40
M/SEC.

FIGURE 18

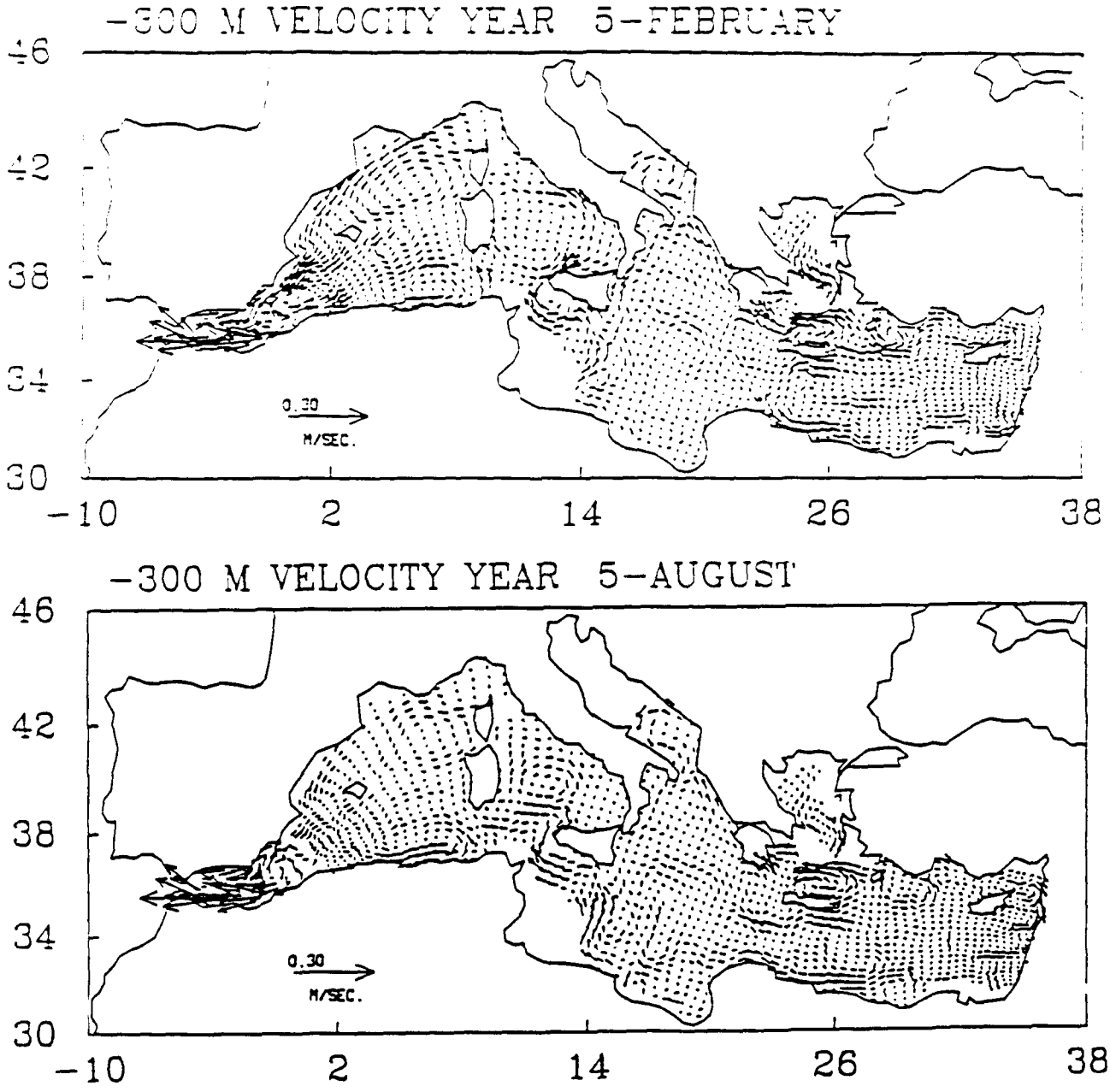
-300 M VELOCITY YEAR 5-FEBRUARY
46
42
38
34
30
0.30
M/SEC.
-10
2
14
26
38
-300 M VELOCITY YEAR 5-AUGUST
46
42
38
34
30
0.30
M/SEC.
-10
2
14
26
38

FIGURE 19

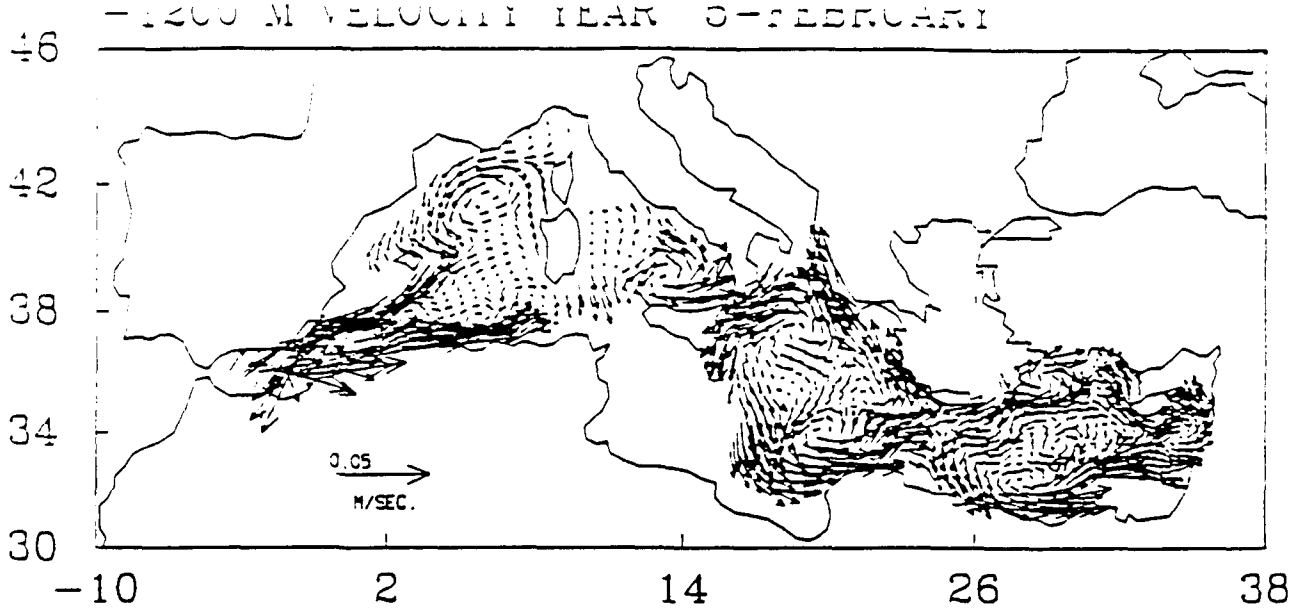
46
42
38
34
30
0.05
M/SEC.
-10
2
14
26
38

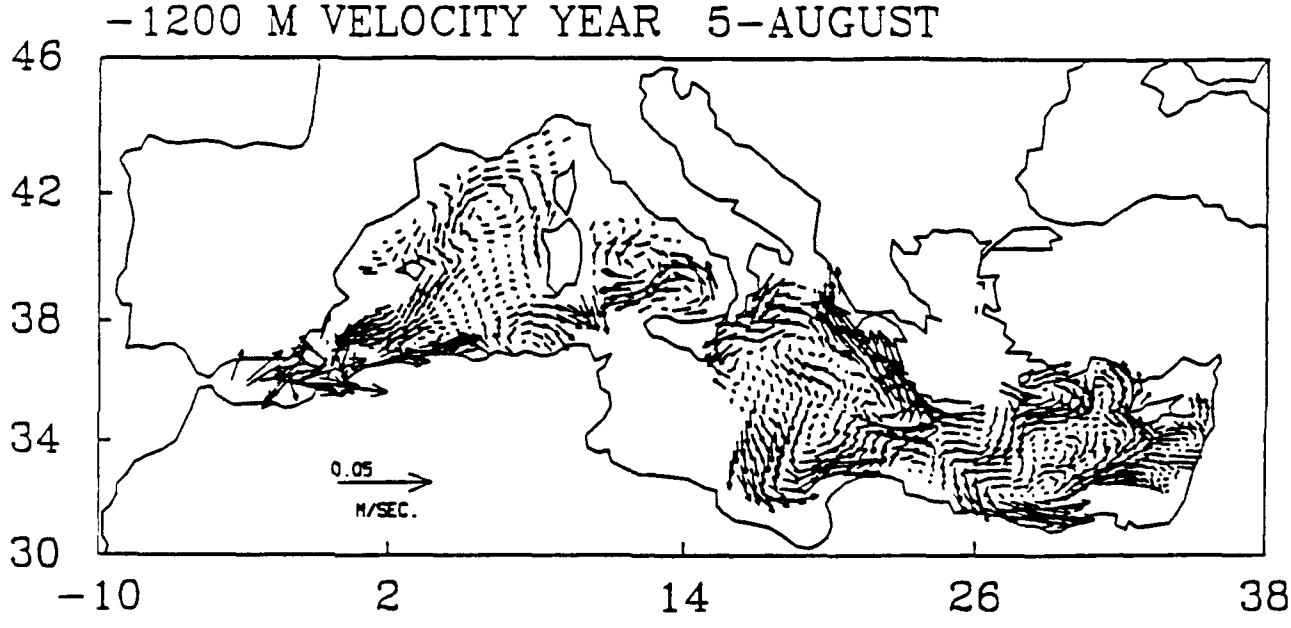
-1200 M VELOCITY YEAR 5-AUGUST
46
42
38
34
30
0.05
M/SEC.
-10
2
14
26
38

FIGURE 20

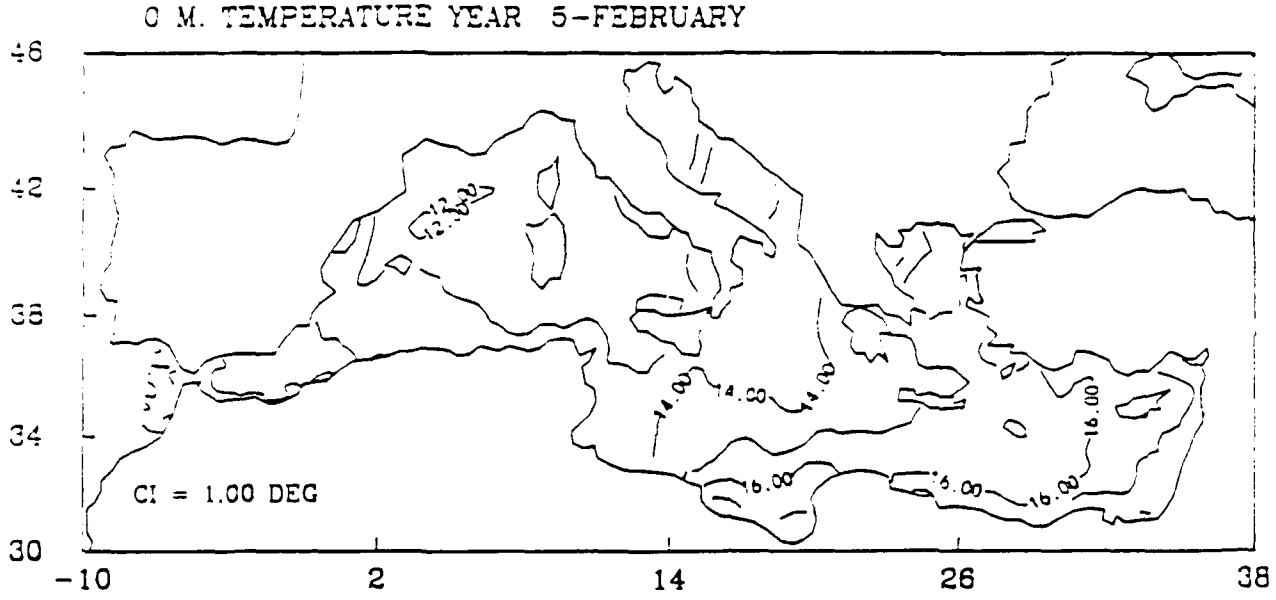
0 M. TEMPERATURE YEAR 5-FEBRUARY
46
42
38
34
30
CI = 1.00 DEG
14.00
16.00
-10
2
14
26
38

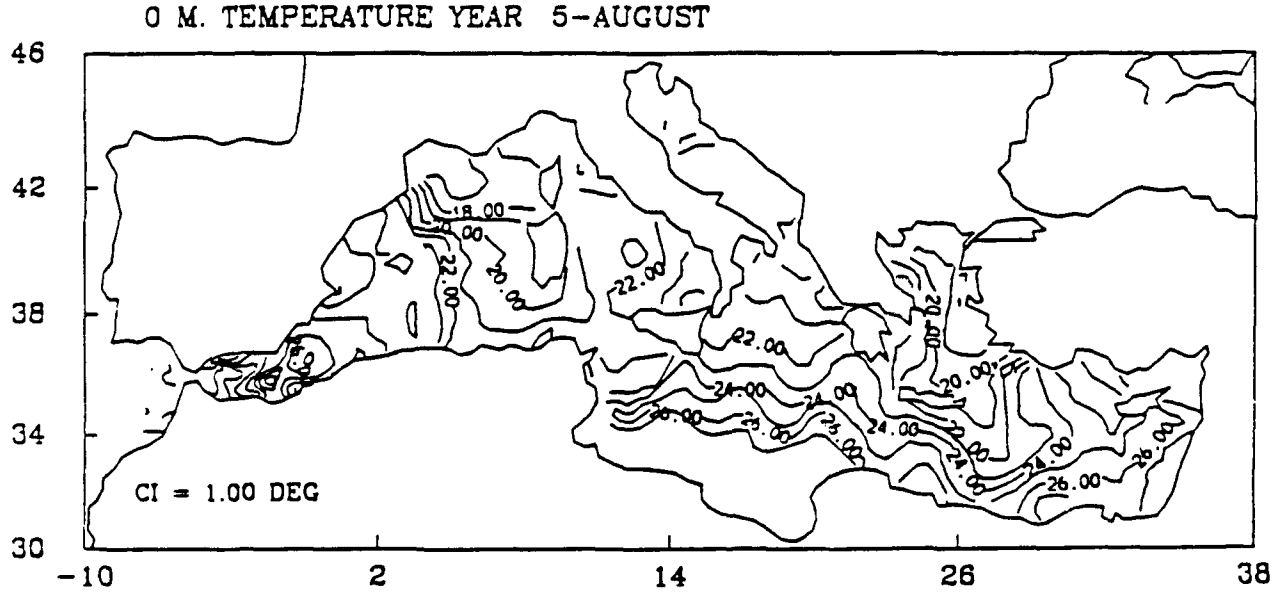
0 M. TEMPERATURE YEAR 5-AUGUST
46
42
38
34
30
CI = 1.00 DEG
18.00
20.00
22.00
24.00
26.00
-10
2
14
26
38

FIGURE 21

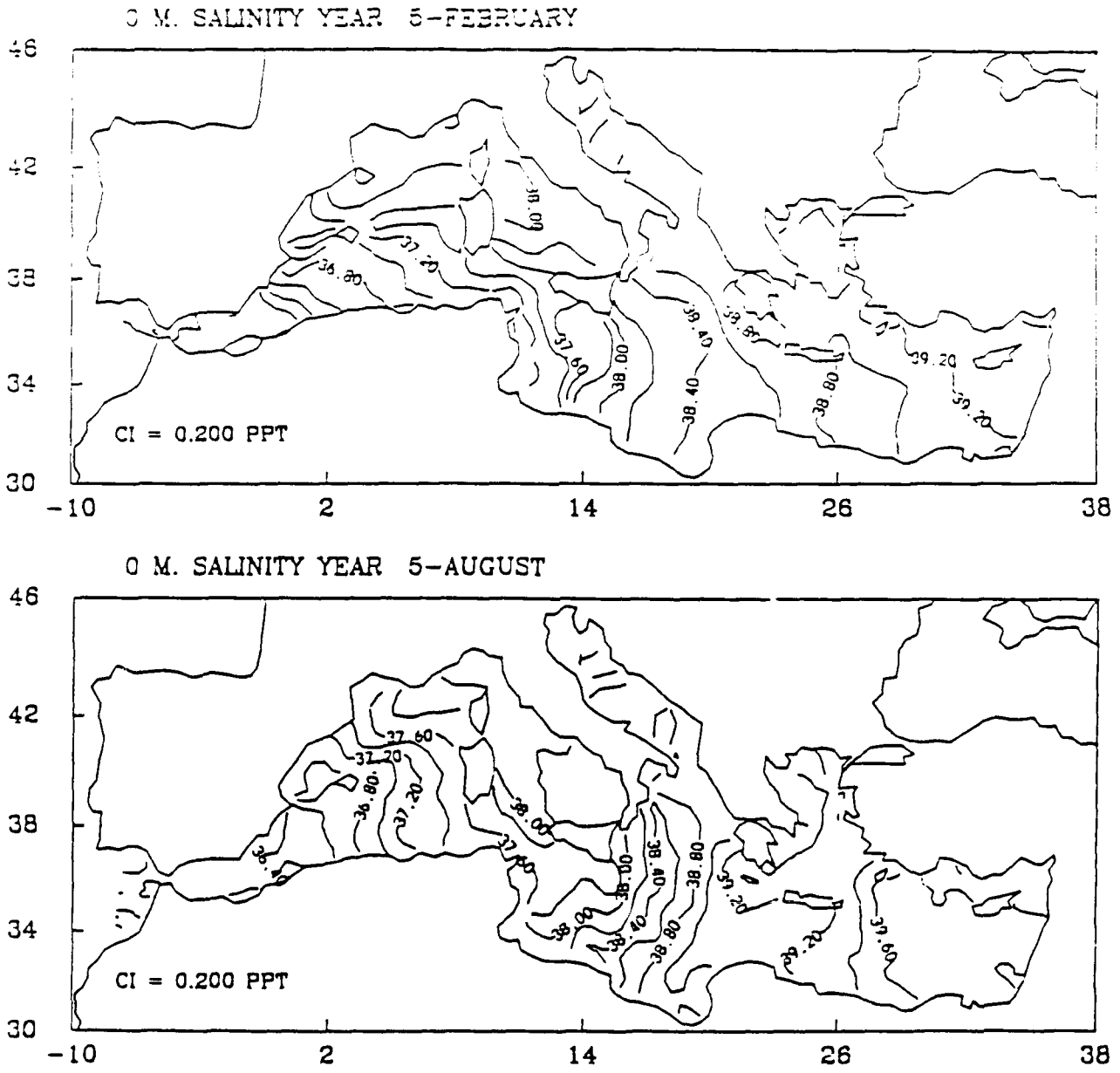
0 M. SALINITY YEAR 5-FEBRUARY
46
42
38
34
30
-10
2
14
26
38
CI = 0.200 PPT
0 M. SALINITY YEAR 5-AUGUST
CI = 0.200 PPT

FIGURE 22

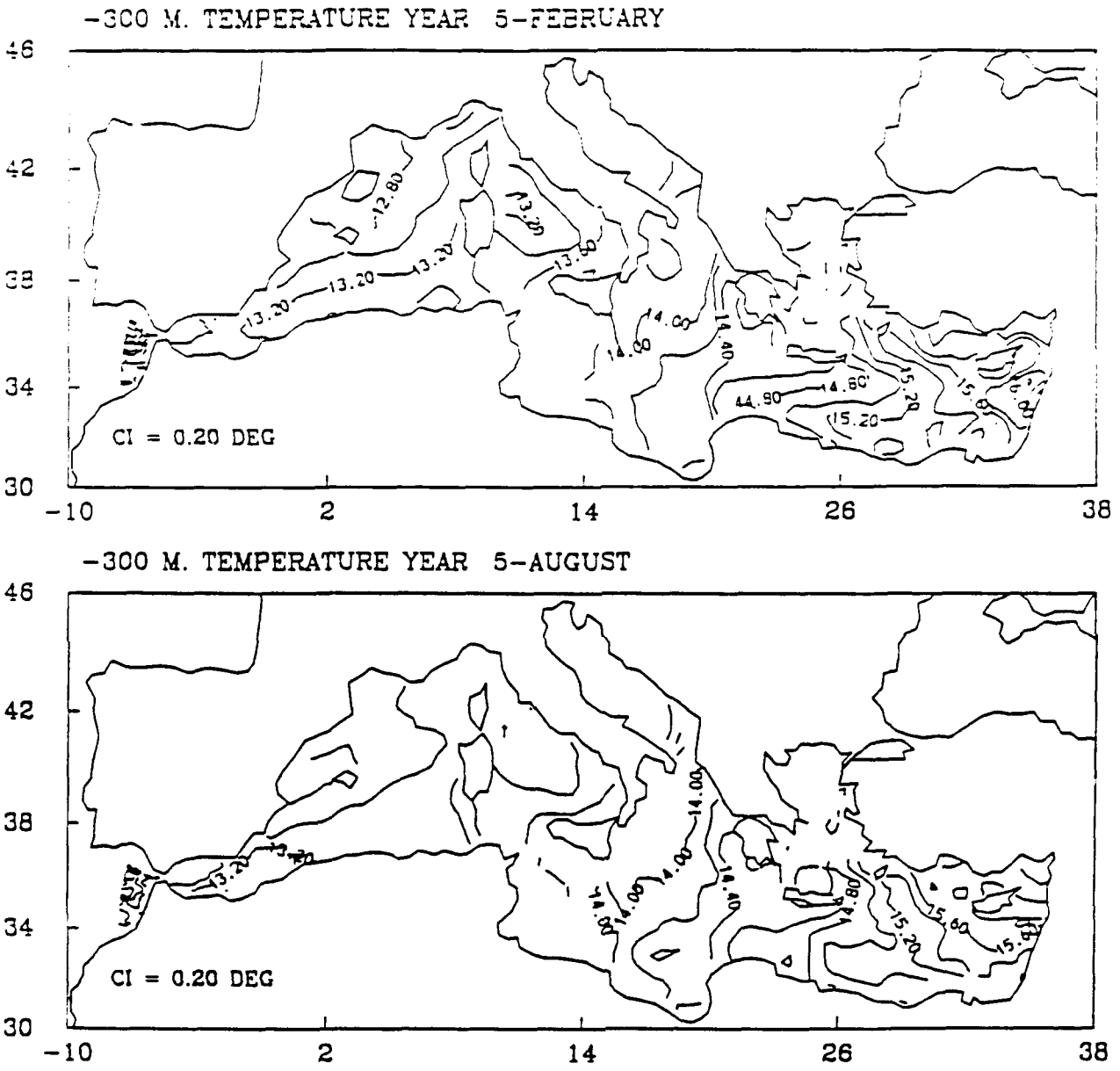
-300 M. TEMPERATURE YEAR 5-FEBRUARY
46
42
38
34
30
-10
2
14
26
38
CI = 0.20 DEG
-300 M. TEMPERATURE YEAR 5-AUGUST
CI = 0.20 DEG

FIGURE 23

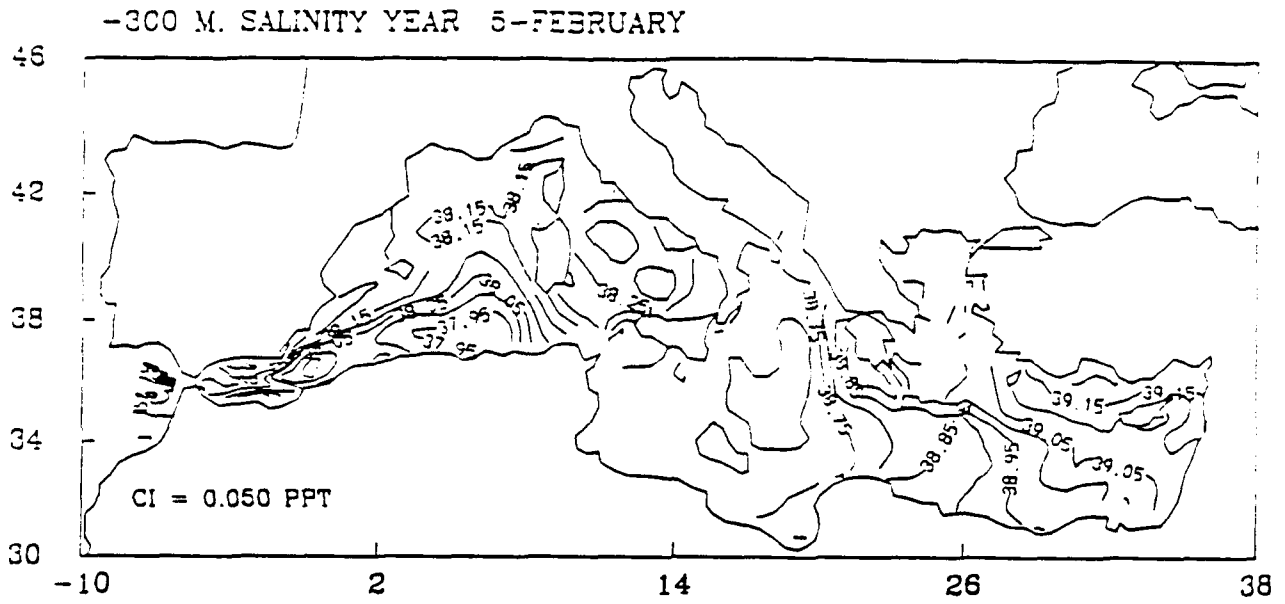
-300 M. SALINITY YEAR 5-FEBRUARY
46
42
38
34
30
-10
2
14
26
38
CI = 0.050 PPT

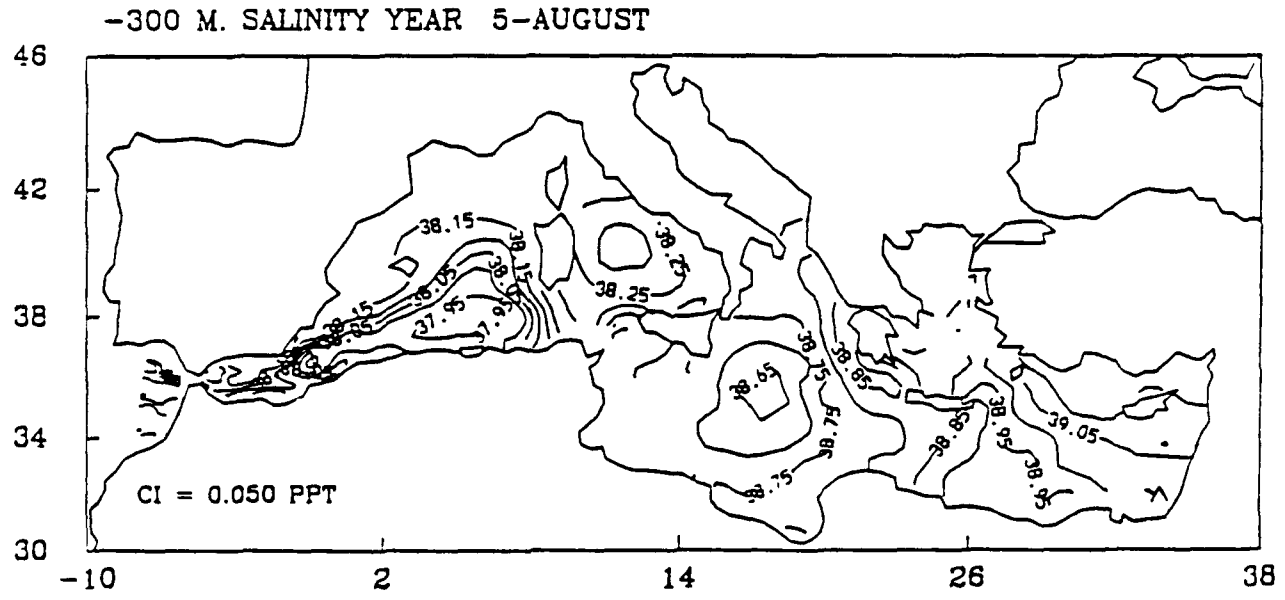
-300 M. SALINITY YEAR 5-AUGUST
46
42
38
34
30
-10
2
14
26
38
CI = 0.050 PPT

FIGURE 24

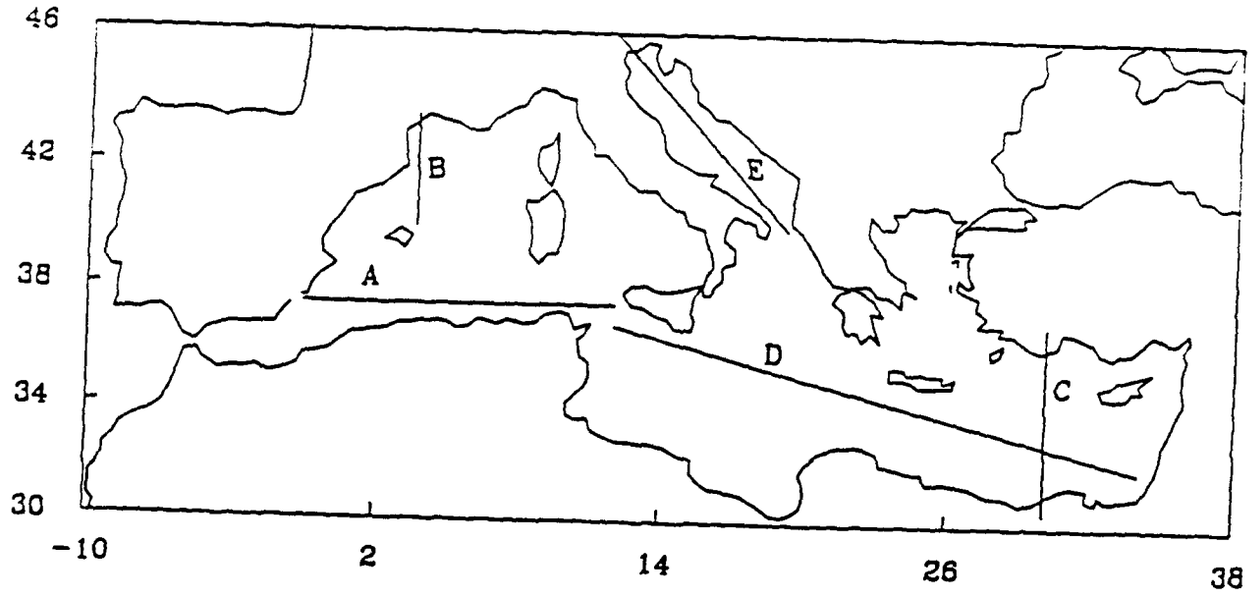

FIGURE 25

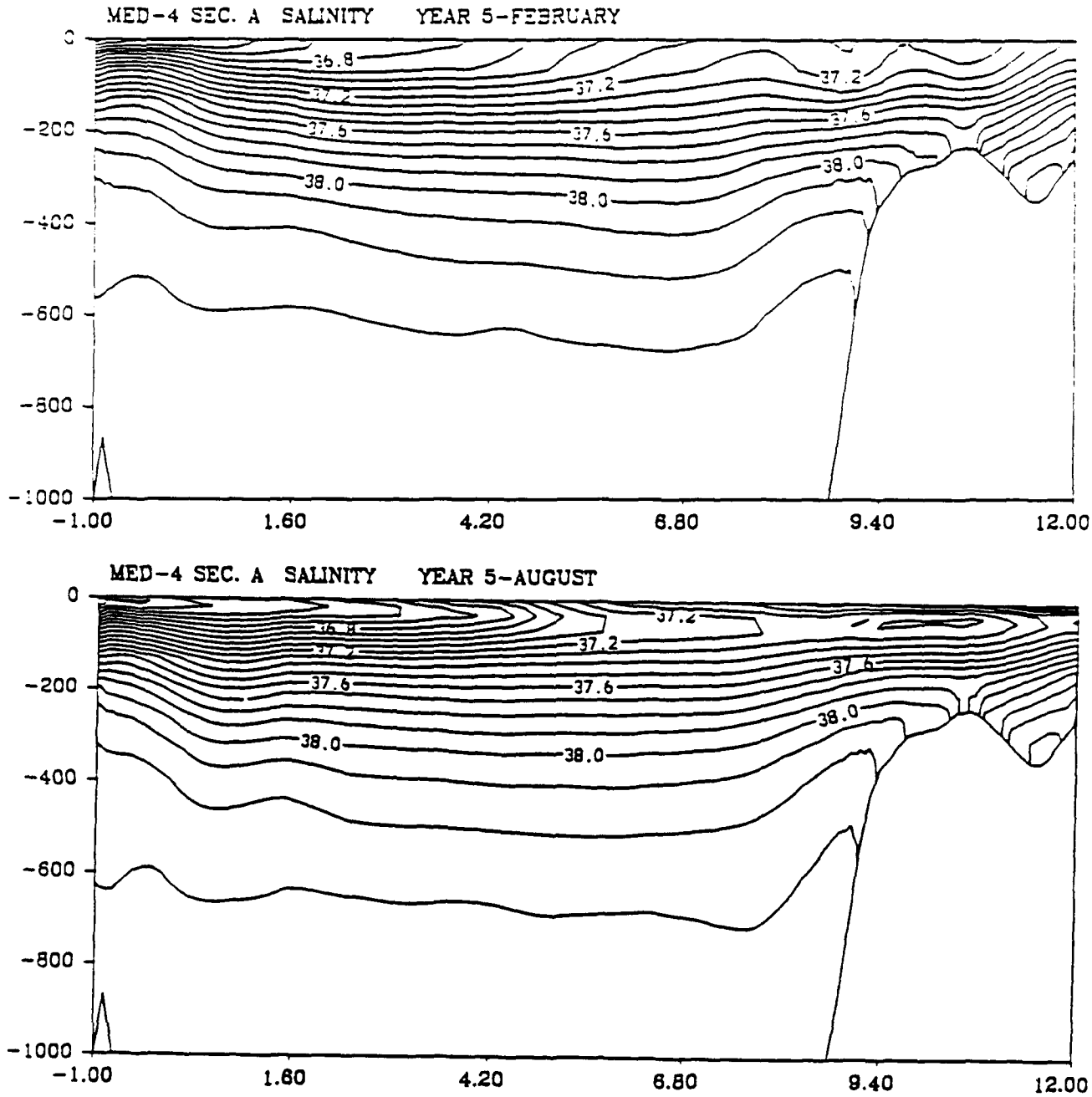
MED-4 SEC. A SALINITY YEAR 5-FEBRUARY
0
-200
-400
-600
-800
-1000
36.8
37.2
37.6
38.0
-1.00
1.60
4.20
6.80
9.40
12.00
MED-4 SEC. A SALINITY YEAR 5-AUGUST
0
-200
-400
-600
-800
-1000
37.2
37.6
38.0
-1.00
1.60
4.20
6.80
9.40
12.00

FIGURE 26

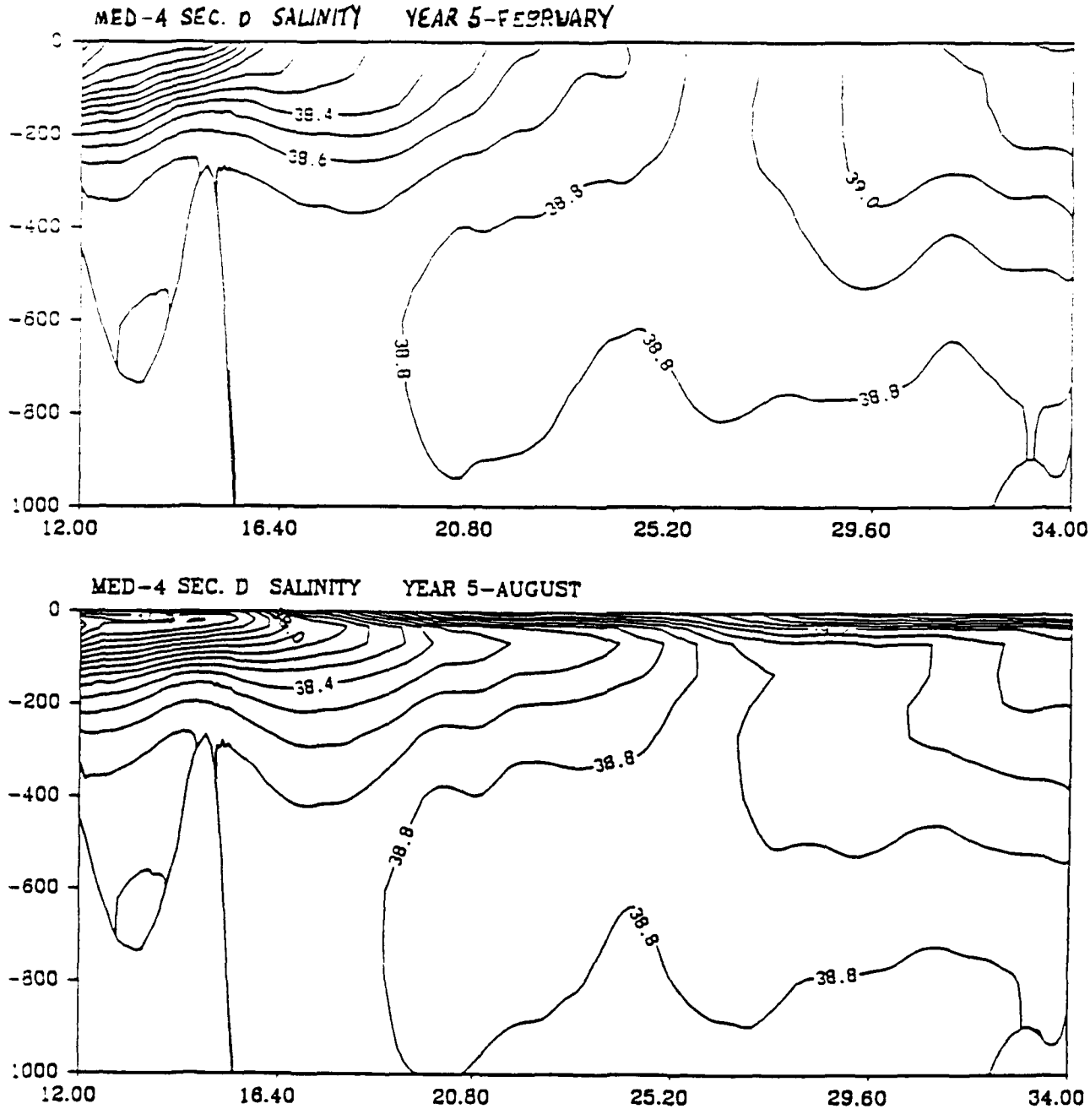
MED-4 SEC. D SALINITY YEAR 5-FEBRUARY
0
-200
-400
-600
-800
1000
38.4
38.6
38.8
38.8
38.8
38.8
38.8
12.00
16.40
20.80
25.20
29.60
34.00
MED-4 SEC. D SALINITY YEAR 5-AUGUST
0
-200
-400
-600
-800
1000
38.4
38.8
38.8
38.8
38.8
12.00
16.40
20.80
25.20
29.60
34.00

FIGURE 27

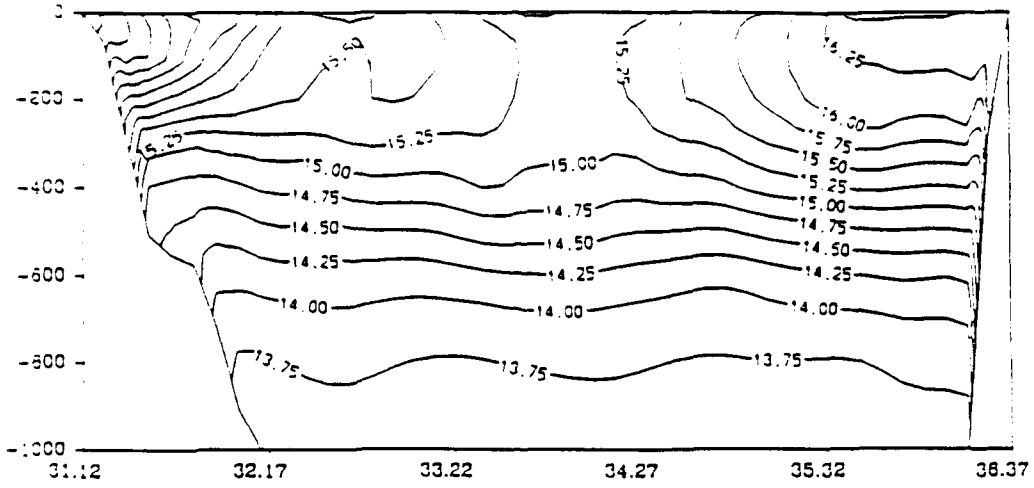
0
-200
-400
-600
-800
-1000
31.12
32.17
33.22
34.27
35.32
36.37
15.25
15.00
14.75
14.50
14.25
14.00
13.75

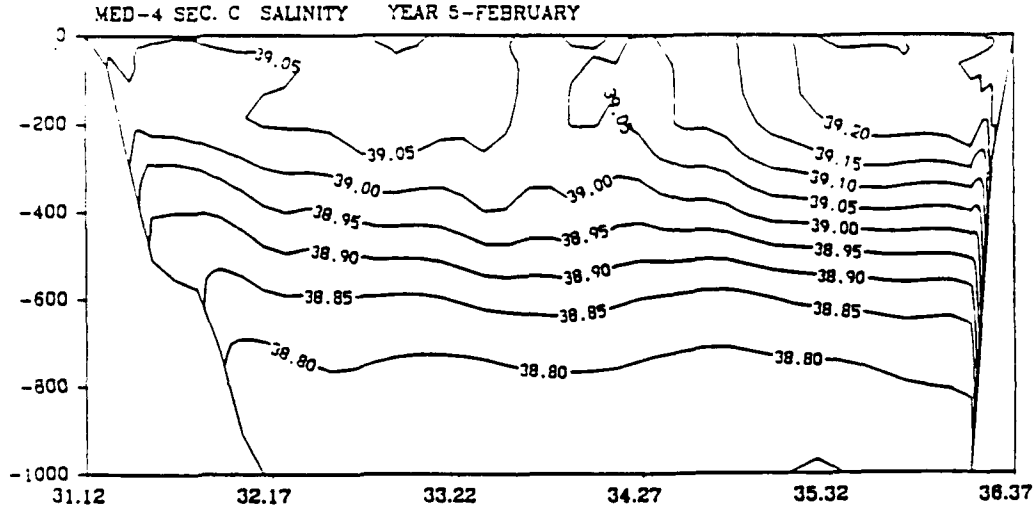
MED-4 SEC. C SALINITY YEAR 5-FEBRUARY
0
-200
-400
-600
-800
-1000
31.12
32.17
33.22
34.27
35.32
36.37
39.20
39.15
39.10
39.05
39.00
38.95
38.90
38.85
38.80

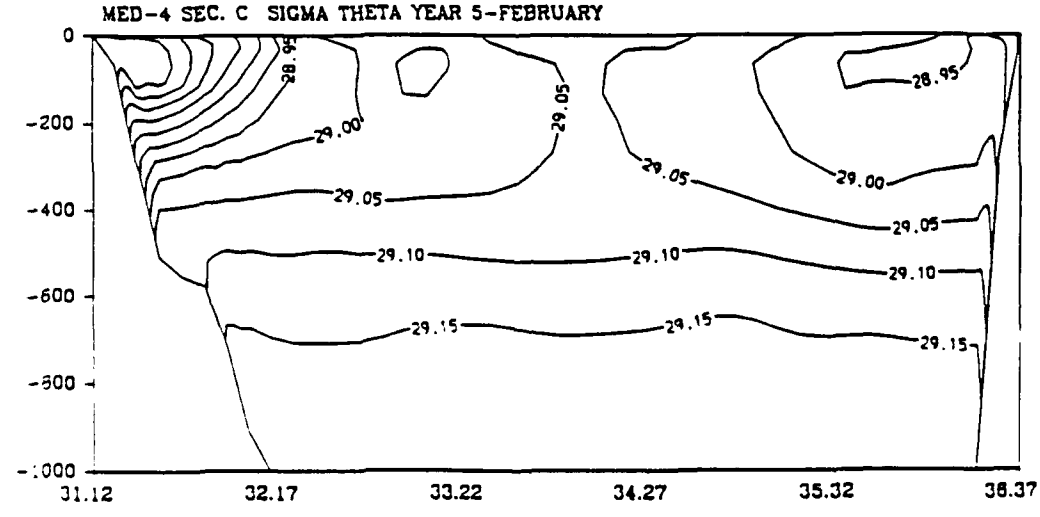
MED-4 SEC. C SIGMA THETA YEAR 5-FEBRUARY
0
-200
-400
-600
-800
-1000
31.12
32.17
33.22
34.27
35.32
36.37
28.95
29.00
29.05
29.10
29.15

FIGURE 28

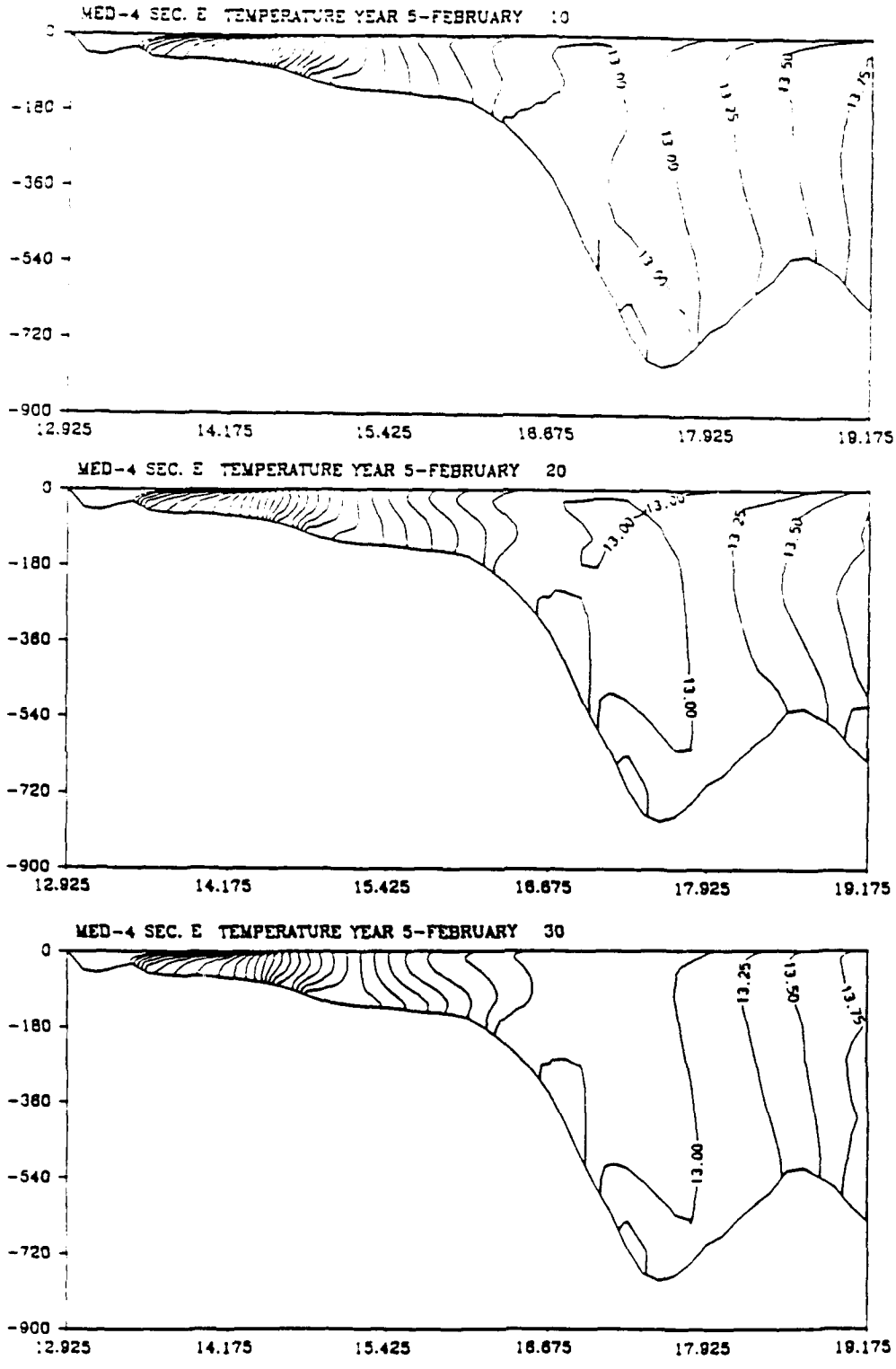
MED-4 SEC. E TEMPERATURE YEAR 5-FEBRUARY 10
0
-180
-360
-540
-720
-900
12.925
14.175
15.425
16.675
17.925
19.175
13.00
13.25
13.50
MED-4 SEC. E TEMPERATURE YEAR 5-FEBRUARY 20
0
-180
-360
-540
-720
-900
12.925
14.175
15.425
16.675
17.925
19.175
13.00
13.25
13.50
MED-4 SEC. E TEMPERATURE YEAR 5-FEBRUARY 30
0
-180
-360
-540
-720
-900
12.925
14.175
15.425
16.675
17.925
19.175
13.00
13.25
13.50
13.75

FIGURE 29

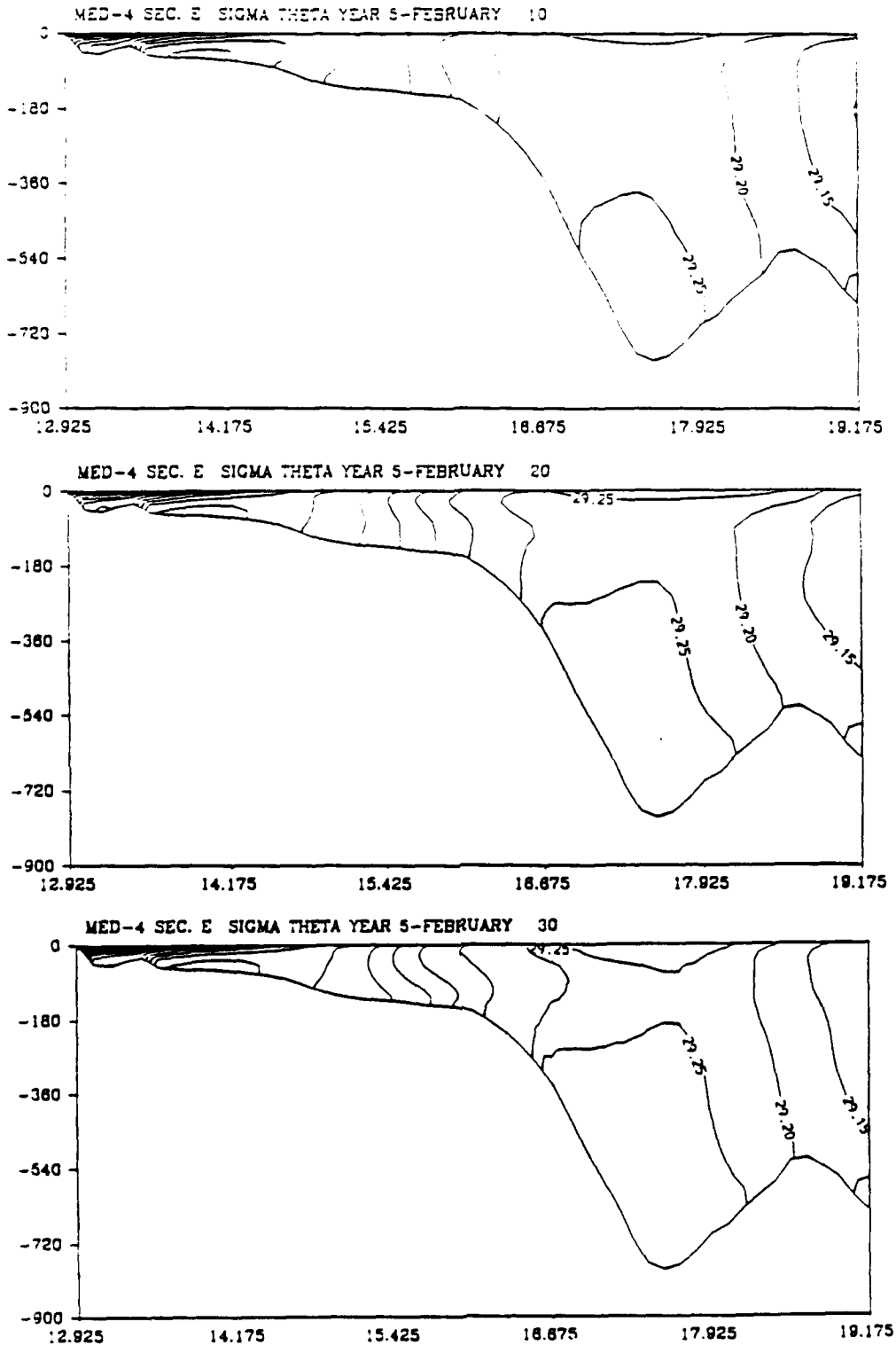
MED-4 SEC. E SIGMA THETA YEAR 5-FEBRUARY 10
0
-180
-360
-540
-720
-900
29.20
29.15
29.25
12.925
14.175
15.425
16.675
17.925
19.175
MED-4 SEC. E SIGMA THETA YEAR 5-FEBRUARY 20
0
-180
-360
-540
-720
-900
29.25
29.25
29.20
29.15
12.925
14.175
15.425
16.675
17.925
19.175
MED-4 SEC. E SIGMA THETA YEAR 5-FEBRUARY 30
0
-180
-360
-540
-720
-900
29.25
29.25
29.20
29.15
12.925
14.175
15.425
16.675
17.925
19.175

FIGURE 30

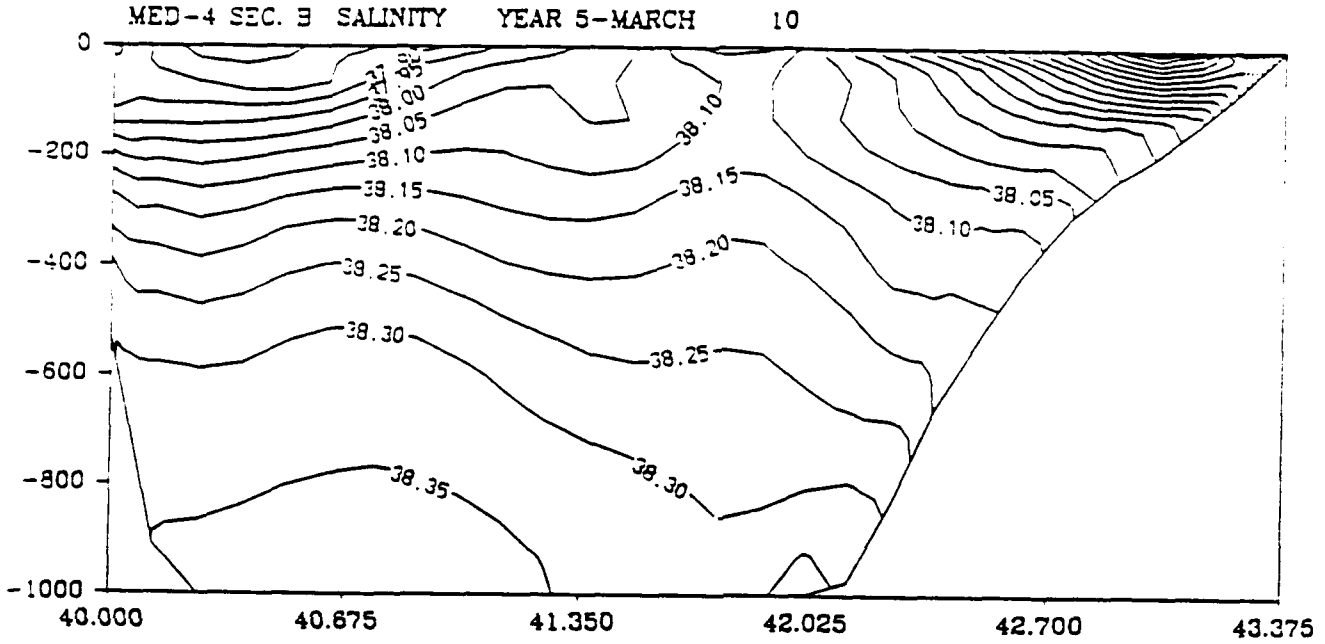
MED-4 SEC. B SALINITY YEAR 5-MARCH 10
0
-200
-400
-600
-800
-1000
38.00
38.05
38.10
38.15
38.20
38.25
38.30
38.35
38.10
38.15
38.20
38.25
38.30
38.05
38.10
40.000
40.675
41.350
42.025
42.700
43.375

FIGURE 31

THE NRL MEDITERRANEAN SEA MODEL
RECENT RESULTS

by
G.W. Heburn
Naval Research Laboratory
NRL Code 322
Stennis Space Center, MS 39529-5004

INTRODUCTION

The circulation in the Mediterranean Sea is extremely complex, consisting of numerous eddies and current meanders, particularly along the north African coast , in the Algerian basin and throughout the Ionian and Levantine basins. Satellite IR and CZCS imagery as well as recent hydrographic surveys (for example the POEM program) reveal a picture of the general circulation in the western and eastern Mediterranean consisting of sub-basin-scale gyres and interconnecting jets. There are many physical factors which exert an influence on the dynamics of the circulation of the Mediterranean Sea; wind stress, hydraulic controlled inflow/outflow through the Straits of Gibraltar and Sicily, intermediate and deep water formation, thermohaline forced circulation and topography.

Various versions of the NRL primitive equations ocean circulation model are used to systematically study the affects of these various forcing mechanisms, individually and in combination, on the circulation dynamics of the Mediterranean Sea. While the general results from various case studies involving wind, hydraulic, thermohaline and topographic forcing suggest that no one mechanism dominates the complex Mediterranean circulation and that non-linear interactions between the directly forced motions and internal flow instabilities play an important role, comparisons of model results from experiments using the ECMWF winds for the period 1981 to 1989 with observational data, both satellite IR and hydrographic, suggest that the winds play a major role in the evolution of the sub-basin-scale gyres seen in the Mediterranean Sea.

MODEL

The NRL multi-layer primitive equations ocean circulation model is a derivative of the Hurlburt and Thompson (1980) Gulf of Mexico model. For a full description of the basic model refer to Wallcraft (1991). The version used for most of the recent dynamical studies in the Mediterranean Sea is a three layer, finite depth, hydrodynamic, spherical coordinate version of the basic model. The model domain is presented in figure 1. The lateral boundaries for the model are taken at the 200m isobath. The initial layer thicknesses are take to be 200m for the upper layer representing the Modified Atlantic Water (MAW), 400m for the second layer representing the Levantine Intermediate Water (LIW) and the remainder in the third layer to the bottom topography representing the Mediterranean Deep Water (MDW). The inflow boundary condition was specified as a steady inflow of 1.2sv

through the Strait of Gibraltar in the upper layer with conpensating outflow in the second layer. The formation of LIW is parameterized as a steady detrainment for the upper layer to the second layer in the eastern Mediterranean basin.

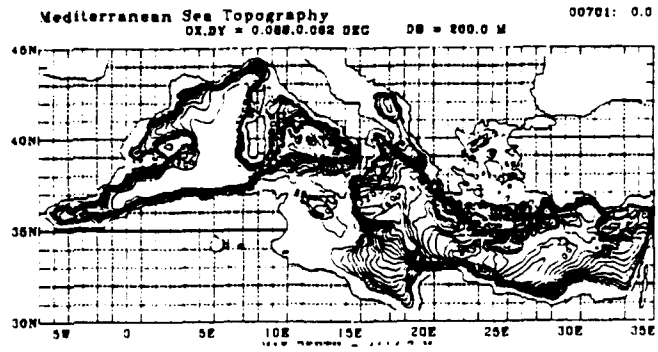

Figure 1: Mediterranean Sea Model Topography

The model was integrated to statical equilibrium using the Hellerman and Rosenstein monthly mean wind stress climatology and then integrated for a nine year period with a hybred wind stress data set using the annual mean from the Hellerman and Rosenstein climatology and the monthly mean annomallies from the ECMWF winds for the period from 1981 to 1989.

RESULTS

The results from the simulations using the hybred wind data set have been compared to satellite IR images for various time periods during the 1980s. The disappearance and reformation of the eastern Alboran gyre during July to August 1982 (Hebum and LaViolette, 1990) is well represented in the model simulation. The mean annual cycle of the transport of LIW through the Strait of Sicily is replicated in the model simulations using the climatological wind forcing as well as in the simlations using the hybred wind forcing data set. The simulations using the hybred data set also show considerable interannual varibility.

The complex series of sub-basin scales gyres and meandering currents observed in the eastern Mediterranean Sea are shown in the model simulations as well. These features also exibit considerable seasonal and interannual variability. The gyres in the Ionian basin appear to be primarily wind forced with a definite annual cycle.

REFERENCES

Hebum, G. W. and P. E. LaViolette (1990): Variations in the Structure of the Anticylonic Gyres Found in the Alboran Sea. JGR/Oceans, Vol. 95, No. C2, Pg. 1599-1613.

Hurlburt, H. E. and J. D. Thompson (1980): A Numerical Study of Loop Current Intrusions and Eddy Shedding. JPO Vol. 10, pg 1611-1651.

Wallcraft, A. J. (1991): The Navy Layered Ocean Model Users Guide. NOARL Report 35, pp 21.

MODELING THE GENERAL CIRCULATION OF THE MEDITERRANEAN SEA WITH EMPHASIS ON THE EASTERN BASIN

Paola Malanotte-Rizzoli

Department of Earth, Atmospheric, and Planetary Sciences
Massachusetts Institute of Technology
Cambridge, MA 02139

The modeling effort is the one undertaken by Malanotte-Rizzoli and collaborators in which three approaches have been used simultaneously. In the first study, Tziperman and Malanotte-Rizzoli (1991) use a simple inverse model to calculate the horizontal circulation of the upper 800 m of the entire Mediterranean Sea for a seasonal climatological hydrographic dataset. The inverse results were used to address three main aspects of the general Mediterranean circulation, namely the seasonality of the surface circulation; the shape of the general circulation of the Eastern basin and the shape of the deep circulation of the entire Mediterranean. Figure 1 shows the winter circulation (upper panel) and the summer one (lower panel) in the surface layer, at a depth of 10 m. A fairly steady yearly pattern of the surface circulation in the Western basin emerges from an examination of Figure 11. The seasonal signal is somewhat stronger in the Eastern basin and especially in the Ionian Sea where the jet of Atlantic water entering the Sicily Straits shoots southeastward in winter (Figure 11a) while forming an intense meander that protrudes into the Northern Ionian in summer (Figure 11b). Also, Figure 1 clearly shows the Eastern Mediterranean circulation to be constituted by a succession of subbasin scale gyres.

In a parallel study, Malanotte-Rizzoli and Bergamasco (1991) carried out an intensive series of numerical experiments investigating the wind-driven and thermohaline components of the Eastern Mediterranean circulation and the relative importance of the different forcing functions under climatological conditions in the different regions of the Eastern basin. They used a linearized, primitive equation level model with coarse resolution but with active thermodynamics, and realistic topography with the Sicily Straits open. The model is forced by the monthly climatological means of: wind stress; heat fluxes (incoming solar radiation, backscatter, latent and sensible heat); and evaporation minus precipitation fluxes. The inflow imposed at the Sicily Straits is derived from real data and

the hydrographic temperature and salinity dataset is the same used by Tziperman and Malanotte-Rizzoli (1991).

The numerical results indicate that the inflow at Sicily is the dominant driving mechanism in the Ionian Sea, with a strong seasonal modulation imposed by the change in polarity of the wind-stress curl from winter to summer over the Ionian. However, the thermohaline fluxes emerge to be the dominant driving mechanism for the circulation in the Eastern Levantine, where the seasonal signal is greatly attenuated. Figure 2 shows the total transport streamfunction in the Central Experiment, the one both wind and thermally forced in which all the fields are evaluated prognostically, respectively for January (upper panel) and September (lower panel). Examination of Figure 2 shows the circulation to be quasi-steady in the Eastern Levantine. In the Ionian Sea, the jet of Atlantic water entering through the Sicily Straits is deflected southward towards the African coast in winter (upper panel) while forming a big, northward protruding meander in summer (lower panel). The similarity of Figure 2 with the inverse results of Figure 1 is striking and also shows the importance of the barotropic, forced component of the circulation in the Eastern basin. A final result is that many of the persistent features found in the model circulation patterns can be related to the strong control exerted by the ambient potential vorticity (f/H) upon the circulation

In a final approach, the adjoint method of control theory is used to determine the seasonal circulations of the Eastern basin (Bergamasco *et al.*, 1992). The GFDL model, adapted to the Eastern basin, has been coupled with its adjoint developed by collaborators Long and Thacker. The prognostic model is forced with the climatological wind stress field and the hydrological data set of temperature and salinity is used to constrain the model predicted fields as part of the cost function of the adjoint. The cost function also includes terms penalizing the tendencies of the prognostic fields, i.e. horizontal velocities,

temperature and salinity. The GFDL model and its adjoint are used with 1/4° coarse resolution but with 17 vertical levels, thus allowing for a realistic topography in the Eastern basin. The Sicily Straits are also open with the same forcing inflow of Malanotte-Rizzoli and Bergamasco (1991). Thus, a seasonal circulation of the Eastern Mediterranean is reconstructed that is consistent both with the model dynamics and the climatological hydrographic dataset. A preliminary result in Figure 3 shows the circulation pattern in the surface layer, 1 to 50 m depth, for the winter season. Again, the similarity is striking between the winter circulation and the corresponding patterns obtained through the independent inverse method (Figure 1a) and the prognostic calculations (Figure 2a).

References

(1) Bergamasco, A., P. Malanotte-Rizzoli, R.B. Long, and W.C. Thacker. The seasonal circulation of the Eastern Mediterranean investigated with the adjoint method. In preparation, 1992.

(2) Malanotte-Rizzoli, P., and A. Bergamasco. The wind and thermally-driven circulation of the Eastern Mediterranean Sea, *Dynam. of Atmos. & Oceans, 15*, 355-420, 1991.

(3) Tziperman, E., and P. Malanotte-Rizzoli. The climatological seasonal circulation of the Mediterranean Sea, *J. Marine Res., 49*, 1-25, 1991.

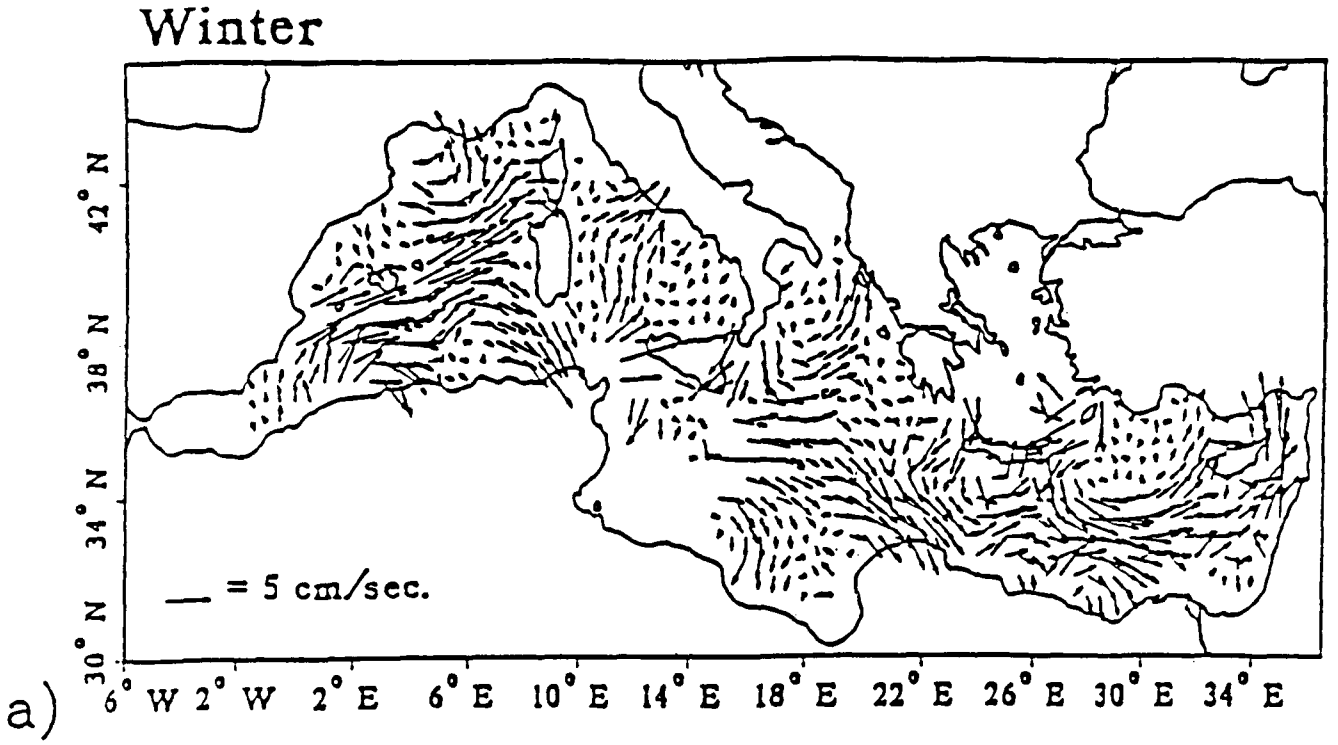
Winter
42° N
38° N
34° N
30° N
— = 5 cm/sec.
a)
6° W 2° W 2° E 6° E 10° E 14° E 18° E 22° E 26° E 30° E 34° E

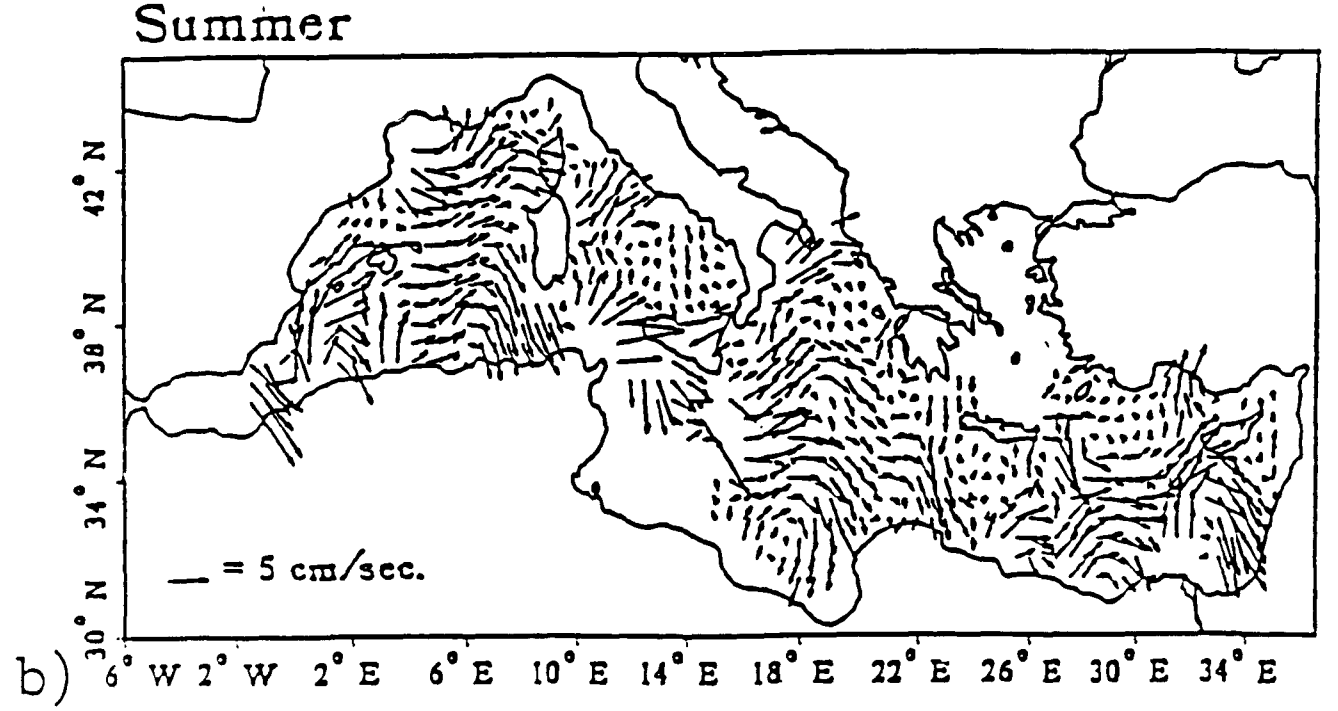
Summer
42° N
38° N
34° N
30° N
— = 5 cm/sec.
b)
6° W 2° W 2° E 6° E 10° E 14° E 18° E 22° E 26° E 30° E 34° E

FIGURE 1

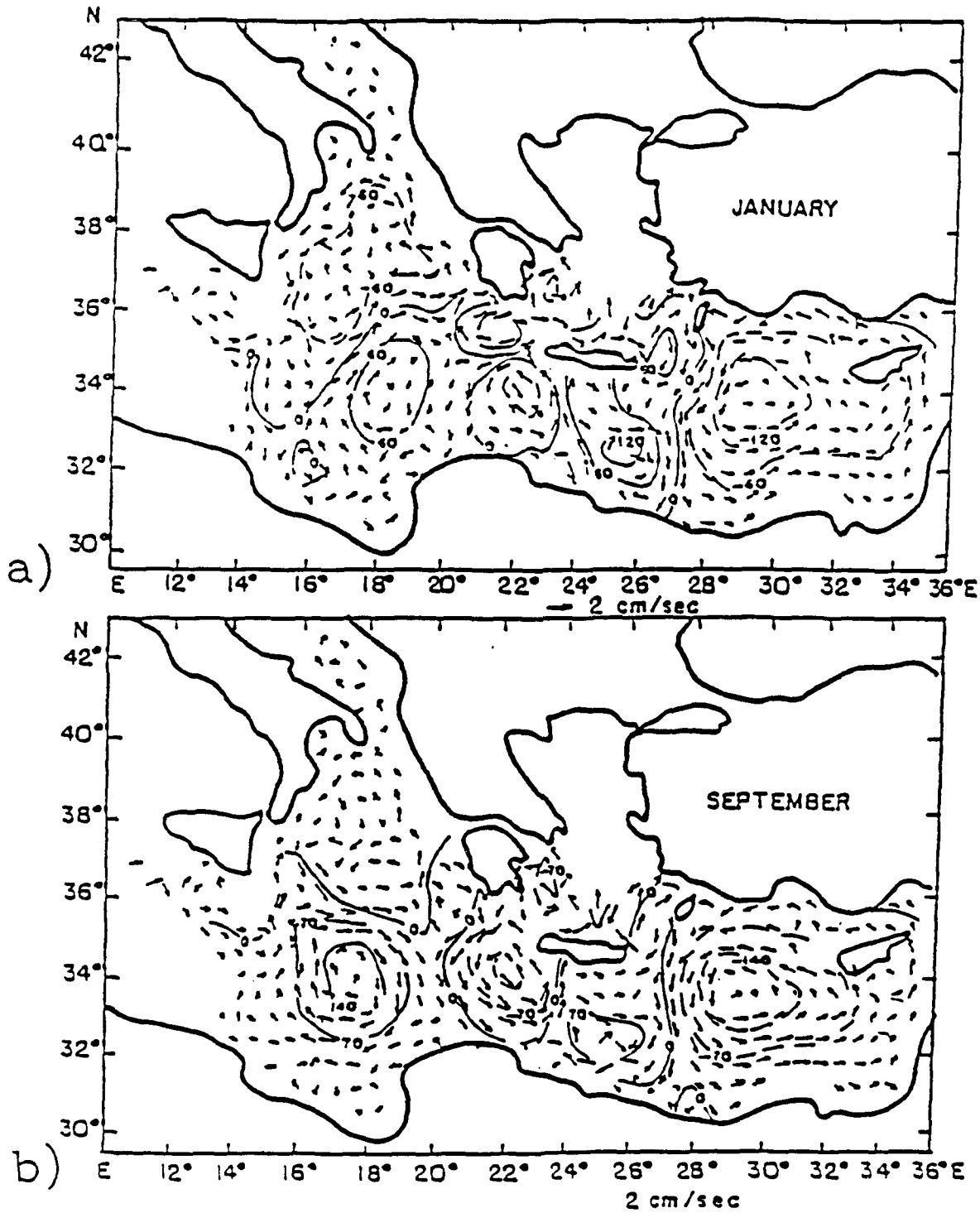
a)
N
42°
40°
38°
36°
34°
32°
30°
JANUARY
E 12° 14° 16° 18° 20° 22° 24° 26° 28° 30° 32° 34° 36°E
2 cm/sec
b)
N
42°
40°
38°
36°
34°
32°
30°
SEPTEMBER
E 12° 14° 16° 18° 20° 22° 24° 26° 28° 30° 32° 34° 36°E
2 cm/sec

FIGURE 2

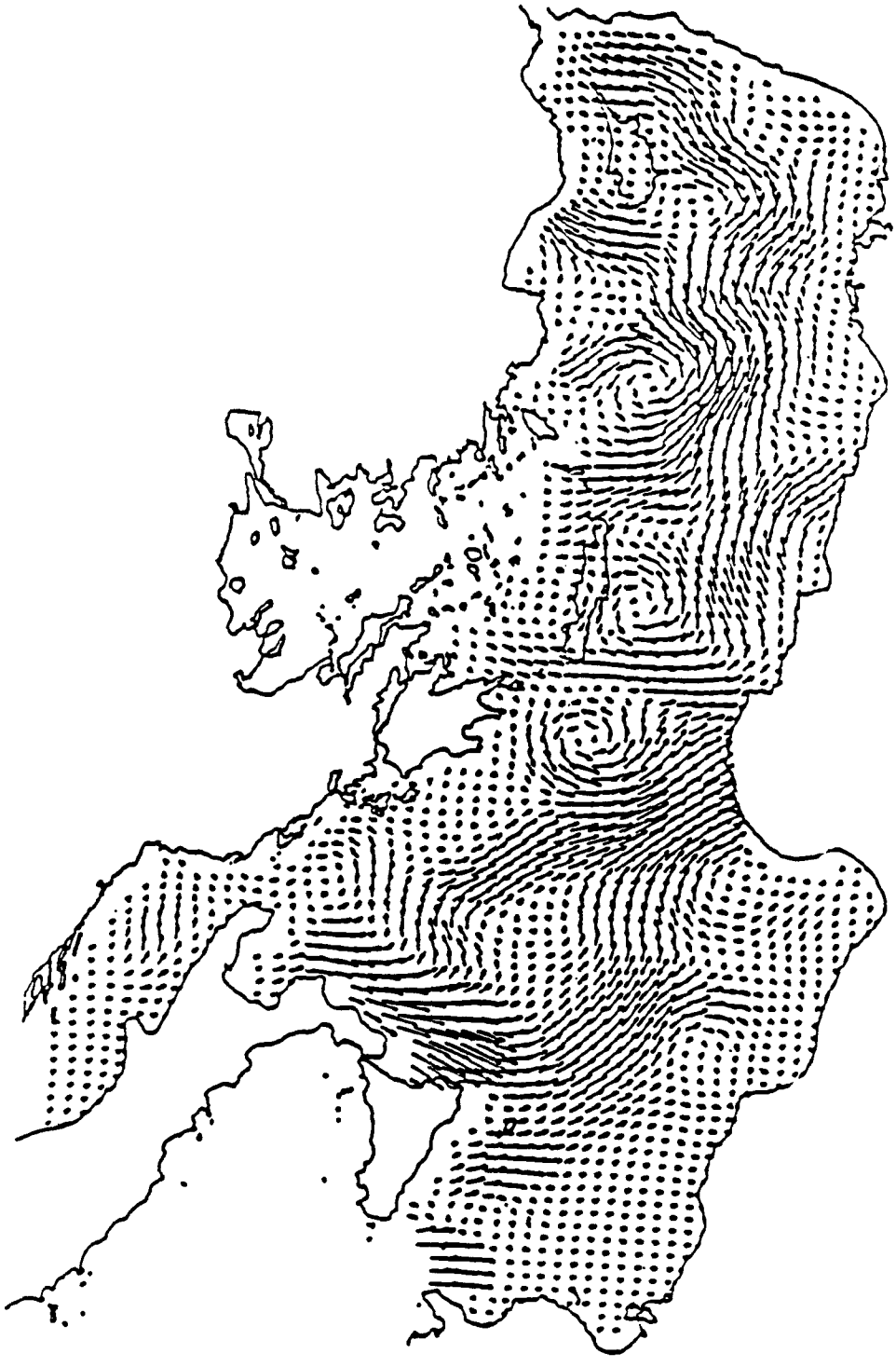

FIGURE 3

A "CLOSE TO OPTIMAL" SUB-OPTIMAL FILTER FOR DATA ASSIMILATION INTO LINEAR MODELS

Ziv Sirkes

Given a System Model:

$$x_k = A_{k-1}x_{k-1} + B_{k-1}u_{k-1} + G_{k-1}w_{k-1} \tag{1}$$

where:
x_k is the $[N \times 1]$ system state vector at time t_k,
A_k is the $[N \times N]$ state transition matrix at time t_k,
B_k is the $[N \times L]$ forcing matrix at time t_k,
u_k is the $[L \times 1]$ forcing vector at time t_k,
G_k is the $[N \times N]$ error transition matrix at time t_k,
w_k is the $[N \times 1]$ vector of model error (assumed to be Gaussian with 0 mean and Q covariance matrix).

and a measurement Model:

$$z_k = H_k x_k + v_k \tag{2}$$

where:
z_k is the $[M \times 1]$ measurement vector at time t_k.
H_k is the $[M \times N]$ matrix giving the interpolation from the state vector to the measurement points.
v_k is the $[M \times 1]$ vector of measurement error (assumed to be Gaussian with 0 mean and R covariance matrix).

One can predict the state estimate as:

$$\hat{x}_{k,k-1} = A_{k-1}\hat{x}_{k-1,k-1} + B_{k-1}u_{k-1} \tag{3}$$

where:
$\hat{x}_{k,k-1}$ ist the estimate of the state vector at time t_k, using measurements up to time t_{k-1}

with an error covariance:

$$P_{k,k-1} = A_{k-1}P_{k-1,k-1}A_{k-1}^T + G_{k-1}Q_{k-1}G_{k-1}^T. \quad (4)$$

Using measurements (data) at time t_k one can update the state estimate :

$$\hat{x}_{k,k} = \hat{x}_{k,k-1} + K_k(z_k - H_k\hat{x}_{k,k-1}) \quad (5)$$

where:
K_k is the filter gain

and the error covariance :

$$P_{k,k} = (I - K_kH_k)P_{k,k-1}(I - K_kH_k)^T + K_kR_kK_k^T. \quad (6)$$

If one wants to minimize the elements along the diagonal of the error covariance $P_{k,k}$, giving an optimal filter, then the filter gain becomes:

$$K_{k_{opt}} = P_{k,k-1}H_k^T(H_kP_{k,k-1}H_k^T + R_k)^{-1}. \quad (7)$$

The error covariance for the optimal filter can be simplified to:

$$P_{k,k_{opt}} = (I - K_{k_{opt}}H_k)P_{k,k-1}. \quad (8)$$

The two main problems with this recursive procedure (Kalman filter) are:

1. The covariance matrix is very big ($[N \times N]$).

2. Equation 4 requires 1.5 matrix multiplications.

Equations 8 and 4 can be combined into one equation, called the "Discrete Ricatti Equation":

$$\begin{aligned} P_{k+1,k} &= A_k\left(P_{k,k-1} - P_{k,k-1}H_k^T\left(H_kP_{k,k-1}H_k^T + R_k\right)^{-1}H_k^TP_{k,k-1}\right)A_k^T \\ &\quad + G_kQ_kG_k^T. \end{aligned} \quad (9)$$

For a time invariant case (where A, B, G, Q, H, R do not change with time) the DRE reduces to:

$$P_{k+1,k} = A\left(P_{k,k-1} - P_{k,k-1}H^T\left(HP_{k,k-1}H^T + R\right)^{-1}H^T P_{k,k-1}\right)A^T + GQG^T. \qquad (10)$$

Using a doubling algorithm one can calculate $P_{2k+1,2k}$ from $P_{2k,2k-1}$ by performing 11.5 matrix multiplications. This is more expensive than the 1.5 multiplications in eq. 4, however the progression in time is exponential.

If we use a startegy of calculating $P_{2k+1,2k}$ with the doubling algorithm, and use a constatnt K_k until the next update of the error covariance matrix, we will have to perform less matrix multiplications over the long run , while applying a suboptimal filter. This filter will be very close to optimal, since it will be updated very often at the beginning ($t = 1, 2, 4, 8, 16, ...$) when the error covariance matrix is changing relatively fast, and will be changed less and less frequent as time passes (and as the error covariance matrix approaches a steady state).

For an experiment with $2^{10} = 1024$ assimilation cycles one would have to perform 115 multiplications using this method (compared to 1536 multiplications for the regular Kalman filter).

PLENARY GROUP DISCUSSION

David Dietrich

The question of baroclinic pressure gradient accuracy was declared to be a non-issue, based on recent improvements of initialization procedures reported by George Mellor, and on recent vertical resolution sensitivity results reported by Charles Horton. George also noted that the energy conservation issue (i.e., that, unlike level vertical coordinates, the truncation errors lead to non-conservation of available potential plus kinetic energy) is not a major problem. Perhaps geophysical modelers have previously put too much emphasis on energy conservation, when overall accuracy is the ultimate goal. Also, Tom Rosmond had noted earlier that the widely publicized baroclinic pressure gradient issue in sigma coordinates was not a major issue.

In particular, George noted that, in the case of exactly stratified initial flow, the erroneous baroclinic pressure gradient associated with truncation errors can be compensated by a slight adjustment of the initial density field. In particular, the initial density field can be adjusted such that the initial baroclinic pressure gradient is exactly zero, as calculated in sigma coordinates. To be useful, such adjustment must be small compared to the local density fluctuations that normally occur. Charles Horton reported results which suggest that, with about 20 vertical levels and 10 km horizontal resolution, and with real Mediterranean bathymetry and realistic stratification, this adjustment is sufficiently small (equivalent to a geostrophic baroclinic velocity change of less than 10 cm/sec). Presumably, this kind of adjustment could also be made when realistic nonzero initial horizontal density gradients occur.

One question that remains is whether the effects of the initial numerical density redistribution can be "unravelled" after a calculation, so that the Navy has a sufficiently accurate density field for its intended applications. Because the baroclinic pressure gradient issue relates strictly to truncation error effects, the rapporteur believes that a systematic resolution sensitivity study should be done for a small basin (i.e., with dimensions about 500 km) with bottom slopes and horizontal and vertical density gradients comparable to those in the Mediterranean. If this is done, no serious CFD scientist should question the applicability of sigma coordinates to ocean problems, but, until this is done, some geophysical modelers who are not intimately involved with the details of initialization using sigma coordinates, might be skeptical. George noted that it seemed reasonable to have a z-level model also involved in the Mediterranean studies. It was also noted that the only model recognized by the Navy for use by INO in such studies is his (the Princeton) model. Sigma coordinates are a good choice when buoyancy effects do

not strongly dominate over boundary layer effects, such as in shallow continental shelf regions. However, they are not as accurate or robust as corresponding z-level models in deep water regions, especially near the edge of continental shelves, where buoyancy effects dominate, in spite of the excellent job being done by the Princeton model developers in improving its application to such regions. In such deep water regions, z-level coordinates are closer to solution adaptive (density contour following) grids. It was decided that it is very difficult to represent two very small scale phenomena, that are also probably significant, using present turbulence closure schemes. These are coastal scales (tides, diurnal wind effects, boundary currents) and "chimneys" of rapidly sinking dense water. The former can probably be adequately addressed by using boundary-fitted coastal models, which are currently under development, but might require very robust numerics (because, as suggested by Dietrich's recent results, realistic modeling of the interaction between boundary and interior flows might require very high Reynolds number calculations). The latter require process studies to determine how they might be addressed in the Mediterranean. Both of these phenomena are considered important in ocean modeling. It was decided that the software functionalities that should be included in the ECMOP system depend on the expressed needs of individual scientists. New needs will probably evolve, such as those specific to boundary-fitted coastal models. Free surface effects are considered important enough that they should be addressed. Although they are not strongly coupled to ocean general circulations on short time scales, George observed that free surface models have the advantage that they are massively parallelizable, because the rigid-lid approximation leads to some pressure solver operations that are parallelizable only in one dimension, unless relatively slow SOR-like solvers are used. (The degree of SOR convergence required again raises the perhaps over-emphasized energy conservation issue.) The rapporteur notes that such SOR solvers still require much fewer operations than the barotropic free-surface mode requires, and that a question remains: does the interaction between free-surface and internal waves somehow limit the "long" time step used by sigma coordinate models for the internal modes? Different kinds of data that will be useful for assimilation for modeling the Mediterranean were discussed. Wind and heat flux data are available from atmospheric models, but probably will have to be modified to higher resolution for Mediterranean modeling. Basic research is needed to get better relations among winds, wind-wave interactions, wind stresses, and surface heat fluxes. Satellite data sets are available for sea-surface heights and temperatures, but the temperatures probably require correction for air humidity because of the low amplitude temperature signal in the Mediterranean. Model-predicted sea surface temperature can be used to distribute atmospheric model and satellite heat exchange data appropriately to small Mediterranean scales. The new high-resolution NORAPS data will be most welcome. Meantime, existing multi-year data sets from ECMWF can be used. Drifters are more useful for model validation than for assimilation.

Professor Joe Thompson
Engineering Research Center
Mississippi State University

The use of numerically-generated curvilinear coordinate systems in partial differential equation (PDE) solutions allows finite difference methods to treat irregular boundaries without interpolation or stair-stepping, since some coordinate surface will be coincident with each boundary segment. This allows difference representations and boundary conditions to be implemented easily, regardless of the shape of the boundaries of the region. The entire problem is, in fact, converted to one that is logically rectangular, i.e., a solution on an equally-spaced Cartesian grid on a region composed of rectangular blocks.

Thus, solution algorithms can operate on an equally-spaced rectangular grid, regardless of the shape of the region. It is also possible to vary the distribution of the grid lines in order to reduce the spacing in regions of large solution variation, either statically beforehand or through dynamic coupling with the developing solution.

The price to be paid in the use of such block-structured grids is that the PDE's acquire additional terms, and all directional components in the equations are coupled. For instance, the first derivative becomes, in two dimensions,

$$f_\chi = \frac{f_\varepsilon\, y_\eta - f_\eta\, y_\varepsilon}{\chi_\varepsilon\, y_\eta - \chi_\eta\, y_\varepsilon}$$

Stencils that are 5-point in 2-D on orthogonal grids become 9–point on general nonorthogonal systems. Similarly, 7-point stencils in 3-D become 27–point.

Also, any advantage taken of the χ-momentum equation being dependent only on the χ-component of the pressure gradient, as in some staggered–grid approaches, is lost in the general curvilinear system, since in 2–D the χ–momentum equation will contain both p_ε and p_η. Such staggered-grid codes are not directly convertible to use the general curvilinear systems. However, other codes can be converted without unreasonable effort, since all that is really involved is the addition of terms to the expressions and some data handling.

The principal advantages of general curvilinear systems come into play when (1) boundary shape is important to the solution, or (2) there is the need to resolve strong gradients. A third consideration can be storage, since all points are utilized and none are outside the boundary.

The Engineering Research Center at Mississippi State University has experience in converting and developing codes for general curvilinear systems and can assist code developers in the effort.

APPENDIX B

Descriptive Oceanography

This appendix includes a list of some of the relevant dynamical considerations in the Mediterranean.

1. North African current baroclinically unstable. ~1.2 Sv inflow.

2. Ligurian Sea flow: τ - driven.

3. Straits of Sicily divides basins, modified Atlantic water penetrates to the east.

4. Topographic control $\left(\frac{f}{h}\right)$ important everywhere.

5. $(V \times \tau)_z$ probably important in Ionian Basin and west.

6. ~ 1.0 Sv of thermohaline circulation exits Gibraltar at intermediate depths; 0.2 Sv evaporates.

7. Bottom water formation occurs in South Adriatic. Does it also occur in Ligurian or Tyrrhenian? How to capture in models?

8. Interactions between basins, sub-basins, and mesoscale flows.

9. Surface exchanges (waves, etc.).

APPENDIX C

Attendees

The attendees were:

Name	Organization	E-Mail
Bob Willems	INO	Willems@jupiter.ino.ucar.edu
John R. Apel	INO	OMNET J.APEL
Ranjit M. Passi	INO	Passi@jupiter.ino.ucar.edu
Jim Corbin	INO	Corbin@jupiter.ino.ucar.edu
Tom Rosmond	NRL, Monterey	Rosmond@pops.navo.navy.mil
Patricia A. Phoebus	NRL, Monterey	OMNET P.PHOEBUS
Jim Goerss	NRL, Monterey	
George Mellor	Princeton Univ.	G.MELLOR/gem@splash
Patrick C. Gallagher	NRL, SSC	P.GALLAGHER/gallagher@ mt-hood.princeton.edu
Richard M. Hodur	NRL, Monterey	hodur@pops.navy.mil noarl.navy.mil
Charles W. Horton	NAVOCEANO	horton@spop.navo.navy.mil
Melody A. Clifford	NAVOCEANO	clifford@spop.navo.navy.mil
Andy Johnson	NAVOCEANO	OMNET A.JOHNSON.JR
George W. Heburn	NRL, SSC	OMNET G.HEBURN/heburn@ Lexington, NOARL, navy.mil
Germana Peggion	INO	peggion@jupiter.ino.ucar.edu
Paola M. Rizzoli	MIT	OMNET R.RIZZOLI
Aaron Lai	INO	aaron@jupiter.ino.ucar.edu
Dong-Shan Ko	INO	ko@jupiter.ino.ucar.edu
David Dietrich	INO	dietrich@jupiter.ino.ucar.edu
Louise Perkins	INO	perkins@jupiter.ino.ucar.edu
Ziv Sirkes	INO	sirkes@golem.ino.ucar.edu
Allan R. Robinson	Harvard	OMNET A.ROBINSON/ Robinson@Pacific.Harvard.Edu
Joe Thompson	Miss. State	Joe@ERC.MSSTATE.EDU
Le Ngoc Ly	INO	Ly@jupiter.ino.ucar.edu

DISTRIBUTION LIST

1. Office of Naval Research
   Code 1242 (10 copies)
   800 North Quincy Street
   Arlington, VA 22217-5000

2. Director, Atmospheric Sciences Directorate
   NRL West (Code 400)
   Monterey, CA 93943-5000

3. Commanding Officer
   Fleet Numerical Oceanography Office
   Monterey, CA 93943-5000

4. Commanding Officer
   Naval Oceanographic Office
   Stennis Space Center, MS 39529

5. Technical Director
   CNOC (Code OOT)
   Stennis Space Center, MS 39529

6. Officer In Charge
   NRL (Code 100)
   Stennis Space Center, MS 39529

7. Technical Director
   NRL (Code 110)
   Stennis Space Center, MS 39529

8. Director, Ocean Sciences Directorate
   NRL (Code 300)
   Stennis Space Center, MS 39529

9. Dr. A. D. Kirwan, Jr.
   College of Sciences
   Dept. of Oceanography
   Old Dominion University
   Norfolk, VA 23529-0276

10. Head, Ocean Sensing and Prediction Division
    NRL (Code 320)
    Stennis Space Center, MS 39529

11. Library (3 copies)
    NRL (Code 125)
    Stennis Space Center, MS 39529

12. Dr. William Holland
    National Center for Atmospheric Research
    P.O. Box 3000
    Boulder, CO 80307

13. UCAR Library
    P.O. Box 3000
    Boulder, CO 80307

14. Dr. Albert W. Green, Jr.
    NRL, Code 330
    Building 1105
    Stennis Space Center, MS 39529

15. Professor George L. Mellor
    Princeton University
    P.O. Box CN710, Sayre Hall
    Princeton, NJ 08544-0710

16. Dr. John R. Apel
    Applied Physics Laboratory
    Johns Hopkins University
    Laurel, MD 20723

17. Dr. J. Dana Thompson
    NRL, Code 320
    Stennis Space Center, MS 39529

18. Dr. William J. Schmitz
Dept. of Physical Oceanography
Woods Hole Oceanographic
Institution
Woods Hole, MA 02543

19. Dr. Edward L. Barker
NRL, Code 440
Monterey, CA 93943-5006

20. Professor Otis B. Brown
Division of Meteorology &
Physical Oceanography
RSMAS, University of Miami
4600 Rickenbacker Causeway
Miami, FL 33149

21. Dr. Richard W. Miksad, Chairman
Dept. of Aerospace Engineering
and Engineering Mechanics
The University of Texas at Austin
Austin, TX 78712-1085

22. Professor Allan R. Robinson
Center for Earth &
Planetary Physics
Harvard University, Pierce Hall
29 Oxford Street, Room 100D
Cambridge, MA 02138

23. Dr. Ron McPherson, Director
National Meteorological Center
World Weather Building
5200 Auth Road
Camp Springs, MD 20746

24. Workshop Attendees

REPORT DOCUMENTATION PAGE

Form Approved
OMB No. 0704-0188

1. Agency Use Only *(Leave blank).*	2. Report Date.	3. Report Type and Dates Covered.
	JULY 1992	Special Report

4. Title and Subtitle.
Proceedings of the Data Assimilation in Coupled Air-Sea Nowcast/Forecast Systems Workshop
An INO-Sponsored Workshop

5. Funding Numbers.

Program Element No.	61153N
Project No.	R310300
Task No.	801
Accession No.	DN250022

6. Author(s).
A. Louise Perkins

7. Performing Organization Name(s) and Address(es).
Institute for Naval Oceanography
Building 1103, Room 233
Stennis Space Center
SSC, MS 39529

8. Performing Organization Report Number.
SP-8

9. Sponsoring/Monitoring Agency Name(s) and Address(es).
Naval Research Laboratory
Stennis Space Center
SSC, MS 39529

10. Sponsoring/Monitoring Agency Report Number.

11. Supplementary Notes.

12a. Distribution/Availability Statement.
Approved for public release; distribution is unlimited.

12b. Distribution Code.

13. Abstract *(Maximum 200 words).*

The Institute for Naval Oceanography (INO) sponsored Workshop on Data Assimilation in Coupled Air–Sea Nowcast/Forecast Systems was held February 27 and 28, 1992, to promote discussions and develop a strategy for research and development of data assimilation techniques in coupled atmospheric/ocean nowcast/forecast modeling systems for the Mediterranean Sea. The motivation for the workshop, in terms of INO's program, is the changing priority of Navy program sponsors to an emphasis in coastal and semi-enclosed seas research and development efforts. Within this area, the Mediterranean Sea has been specifically identified by the Navy as priority.

14. Subject Terms. (U) NAOPS (U) SPEM (U) PRINCETON (U) INO (U) NOGUFS (U) MODEL (U) PREDICTION (U) HARVARD (U) DART (U) HYPER

15. Number of Pages. 179

16. Price Code.

17. Security Classification of Report.	18. Security Classification of This Page.	19. Security Classification of Abstract.	20. Limitation of Abstract.
UNCLASSIFIED	UNCLASSIFIED	UNCLASSIFIED	SAR